The University Of Sheffield.

Investigating genetic mechanisms of blood vessel formation and function in the zebrafish: The roles of Foxc transcription factors and Calcrl

Z Jiang

A thesis submitted in partial fulfilment of the requirements for the degree of Doctor of Philosophy

The University of Sheffield

Faculty of Medicine, Dentistry & Health

Department of Infection, Immunity & Cardiovascular Disease

January 2018

Investigating genetic mechanisms of blood vessel formation and function in the zebrafish: The roles of Foxc transcription factors and Calcrl

Zhen Jiang

A thesis submitted in partial fulfilment of the requirements for the degree of Doctor of Philosophy

The University of Sheffield

Faculty of Medicine, Dentistry & Health

Department of Infection, Immunity & Cardiovascular Disease

January 2018

Acknowledgements

Tuesday, 27th March 2013 was the first day I started in the Wilkinson lab. After 1,803 days, I have finally finished my beginner's scientific journey. It has been a wonderful 5 years as a member of the Wilkinson lab and there are so many people I would like to thank.

First of all, I would like to spend this entire paragraph to thank my supervisor/ friend Dr Robert Wilkinson during my MSc and PhD. I am very proud to be the first master student as well as the first PhD student to graduate from the Wilkinson lab. It is hard to believe that Rob was kindly and patient enough to put up with me (Quoting Rob: The annoying Jane) for the past 5 years. I was lucky enough to get his first independent master project despite the fact I wasn't good enough to arrange an interview first and also to receive an enormous amount of day to day supervision from him. Looking back, science is certainly not the only thing that I will miss from the Wilkinson lab; there was also workday pubbing, weekend pubbing, Sheffield pub-crawl and the amazing peak district pub-crawl. And hopefully, I did not make 'THE' mistake in this acknowledgement.

Speaking of pubbing, I would like to thank my amazing PhD/ drinking buddy, Dr Aaron Savage. Not only just beer, but also milk tea. Thank you for keeping me company for the last 3 years and half. You really did make it easier for me as we were sharing stress, pressure and other enjoyable moments together. Thank you for teaching me my very first British swear 'bloody hell' and thank you for always being there.

I would like to thank Yan Chen and *Philippa Carr*, who are lovely members of the daily caramel coffee group. Thanks to you guys, my third year was not as hard and stressful as I imagined.

In addition, I would like to thank all PIs and members of the Chico, van Eeden and Noël groups and everyone else from the lovely C06 big family. Karishma, Eli, Karen, Davide, Hannah, Eric, Chris, Rosemary, Eleanor, Stone, Rings, Matt, Julia, Lisa and Marcus. Thank you for all the help, laughs and fun both in the lab and office for the past 5 years.

Thanks to my best friends, April and Paweł, who were always there during my 'mental time'.

Finally, I would like to thank the junior software developer Dr Ben Webster for your friendship and company during my ups and downs for the past year and half. Thank you for being the 5th person, who would ever read my thesis thoroughly and proofreading my acknowledgements now.

Table of Contents

List of Tables

List of Figures

Abbreviations

+/+	Wild-type
+/-	Heterozygous mutant
-/-	Homozygous mutant
7TM-2	7 transmembrane receptor
AJ	Adherens junction
AA'	Aortic arches
AA1	First aortic arch
ALPM	Anterior lateral plate mesoderm
AM	Adrenomedullin
Ang1	Angiopoietin 1
Ang2	Angiopoietin 2
AVC	Arterial-venous connection
BA	Basilar artery
BBB	Blood brain barrier
BLEC	Brain lymphatic endothelial cell
BMP4	Bone morphogenic protein 4
Calcrl	Calcitonin receptor-like receptor
CCV	Common cardinal vein
CGRP	Calcitonin gene-related peptide
CHT	Caudal haematopoietic tissue

CNS	Central nervous system
CoA	Coactivator
CRISPR	Clustered Regularly Interspaced Short Palindromic Repeats
CtA	Central artery
CVP	Caudal vein plexus
DA	Dorsal aorta
DLAV	Dorsal longitudinal anastomotic vessel
Dll4	Delta-like 4
DLLV	Dorsal longitudinal lymphatic vessel
dpf	Days post fertilisation
EC	Endothelial cell
ECM	Extracellular matrix
ERK	Extracellular signal regulated kinase kinase
FGF2	Fibroblast growth factor 2
FLS	Facial lymphatic sprout
Fox	Forkhead Box
GPCR	G-protein receptor
HBSS	Hank's Balanced salt solution
H	Hypochord
Hh	Hedgehog
hpf	Hours post fertilisation
HRM	hormone receptor domain

HSC	Haematopoietic stem cell
IMD/ AM2	Intermedin
ISLV	Intersegmental lymphatic vessel
ISV	Intersegmental vessel
JLV	Jugular lymphatic vessel
K	Kidney
KD	Knock-down
KO	Knock-out
LAA	Lymphatic branchial arch
LDA	Lateral dorsal aorta
LEC	lymphatic endothelial cell
LFL	Lateral facial lymphatic
LPM	lateral plate mesoderm
MAB	Maleic acid buffer
MAM	Mastermind
MAPK	Mitogen-activated protein kinase
MCeV	Middle cerebral vein
MFL	Medial facial lymphatic
mFlt1	Membrane binding Flt1
mib	*mind bomb*
Mo	Morpholino
MOC	Midbrain organising centre
MsV	Mesencephalic vein

NICD	Notch intracellular domain
NC	Notochord
NS	Not significant
NT	Neural tube
Nrp1	Neuropilin-1
Nrp2	Neuropilin-12
OLV	Otolithic lymphatic vessel
PBI	Posterior blood island
PBS	Phosphate buffered solution
PCV	Posterior cardinal vein
PDGF	Platelet-derived growth factor
PHBC	Primordial hindbrain channel
PHS	Primary head sinus
PI3K	Phosphatidylinositol 3-kinase
PLC-γ	Phospholipase C-gamma
PLPM	Posterior lateral plate mesoderm
PMBC	Primordial midbrain channel
Prox1	Prospero homeobox 1
Ptc1	Patched-1
RA	Retinoic acid
RAMP	receptor activity-modifying protein
ROC	Rostral organising centre
SC	Stalk cell

SeA	Segmental artery
SeV	Segmental vein
sFlt1	Soluble Flt1
Shh	Sonic hedgehog
SIV	Sub-intestinal vein
Sox18	Sex determining region Y box 18
Sox7	Sex determining region Y box 7
SoxF	SRY-related high mobility group box superfamily F-subgroup
T	Thymus
TAMRA	Tetramethylrhodamine
TC	Tip cells
TD	Thoracic duct
TJ	Tight junction
VEGF	Vascular endothelial growth factor
VEGFR	Vascular endothelial growth factor receptor
vSMC	Vascular smooth muscle cell
VVO	Vesiculo-vascuolar organelle
Y	Yolk
WT	Wild-type
Xirp	Xin-actin-binding repeat-containing protein

Abstract

In this thesis, we perform detailed analysis of novel *foxc1a*, *foxc1b, calcrla* and *calcrlb* zebrafish mutants and determine their function during vascular development and haematopoietic stem cell (HSC) formation. Overall, our data indicate a requirement for *foxc1a* and *foxc1b* during angiogenesis and HSC formation, whereas *calcrla* and *calcrlb* genetically interact to promote vascular integrity and lymphangiogenesis.

The Forkhead box transcription factors *Foxc1* and *Foxc2* are essential to establish intact vascular networks in mammals. How these genes interact with endothelial signalling pathways to exert their functions remains incompletely understood. We have generated novel zebrafish mutants in *foxc1a* and *foxc1b,* the zebrafish orthologues of mammalian *Foxc1,* to determine their function during angiogenesis. *foxc1a* mutants display abnormal formation of cranial veins including the primordial hindbrain channels (PHBC), reduced Vascular endothelial growth factor (Vegf) receptor expression in these and loss of central arteries. *foxc1b* mutants are normal, whereas *foxc1a*; *foxc1b* double mutants exhibit ectopic angiogenesis from trunk segmental arteries. Dll4/Notch signalling is reduced in *foxc1a; foxc1b* double mutant arteries and ectopic angiogenesis can be suppressed by induction of Notch or inhibition of Vegfc signalling. We conclude that *foxc1a* and *foxc1b* play compensatory and context-dependent roles to co-ordinate angiogenesis by promoting venous sprouting via induction of Vegf receptor expression whilst antagonising arterial sprouting by inducing Dll4/ Notch signalling. *foxc1a*/ *b*-mediated induction of both pro- and anti-angiogenic axes of Vegf-Dll4/ Notch negative feedback imparts competition to balance arterial and venous angiogenesis within developing vascular beds. Furthermore, we also demonstrate that *foxc1a* and *foxc1b* promote HSC formation via positively regulating expression of Notch ligands which mediate cell-autonomous and non-cell-autonomous induction of HSC gene expression.

In *calcrla*/ *calcrlb* zebrafish mutants, abnormal trunk lymphatic development and increased vascular permeability were observed. By performing detailed analysis, we demonstrate that *calcrla* is dispensable for embryonic development and *calcrlb* is dispensable for blood vessel formation. However, *calcrlb* plays a key role in promoting trunk lymphatic development and vascular integrity. In addition, our data also provide the first evidence of the genetic compensation between *calcrla* and *calcrlb*, which contributes to these processes in zebrafish.

CHAPTER 1

Introduction

1.1 Blood vessel formation

The cardiovascular system is the first system to form in embryogenesis, and is essential for metabolic exchange and nutrient transport to facilitate growth and to link all organ systems in the body. The first descriptive record of difference between arteries and veins was made two millennia ago (Historically reviewed in (Lawson and Weinstein, 2002a)), yet, the functional definitions of these were not established until nearly 400 years ago by William Harvey, who provided a meticulous description of blood circulation of vertebrates and proposed that arteries carry blood away from the heart, whereas veins do the opposite (Lawson and Weinstein, 2002a). Theodor Schwann first provided evidence that vertebrate vessels showed different layers composed of cells (Schwann, 1993). The inner layer of cells that contact blood directly were identified as endothelium and these specialised cells were then termed endothelial cells (ECs) (Historically reviewed in (Bikfalvi, 2017)). The internal surfaces of newly formed blood vessels are covered by a monolayer of ECs (Giannotta et al., 2013). Various congenital and acquired diseases are related to abnormalities in blood vessel formation (Folkman, 1995). Two of the leading causes of death worldwide, cardiovascular disease and cancer (World Health Organization, 2018), are linked to abnormalities in the structure and function of blood vessels. Tumours hijack the signals and mechanisms which promote blood vessel formation to create their own blood supply, leading to tumour growth and subsequent metastasis. Targeting the tumour blood supply is therefore a major therapeutic goal. Conversely, during cardiovascular disease the ability to promote angiogenesis and allow the circulation to bypass blockages in vessels would be advantageous. Therefore, understanding how blood vessel growth is regulated *in vivo* is essential to achieve these therapeutic goals.

During these pathological cases, abnormally regulated signalling pathways have been identified, and these pathways are similar to those detected during embryogenesis (Lawson and Weinstein, 2002a). Studies in blood vessel formation during embryonic development has therefore became an attractive translational subject (Lawson and Weinstein, 2002a). There are 3 key steps involved in embryonic blood vessel formation in vertebrates (Lawson and Weinstein, 2002a): (1) Vasculogenesis; the *de novo* formation of main vessels from angioblasts (Fig. 1.1 C) (Pardanaud et al., 1989, Poole and Coffin, 1989), (2) Angiogenesis; the formation of new blood vessels from pre-existing blood vessels (Fig. 1.1 D) (Pardanaud et al., 1989, Poole and Coffin, 1989) and (3) Blood vessel maturation, recruitment of non-endothelial cells including pericytes and vascular smooth muscle cells (vSMC) to provide support and stabilise the vascular network (Gaengel et al.,

2009, Jain, 2003). Haematopoietic stem cells (HSC) are vital but rare cells that are capable of self-renewal and generating all adult blood lineages throughout the adulthood of vertebrates (Medvinsky et al., 2011). HSCs are derived from the haemogenic endothelium of the aorta-gonad-mesonephros (AGM), therefore intact and functional blood vessel formation is necessary for HSC formation (Burns et al., 2005, Gering and Patient, 2005, Bertrand et al., 2010).

Zebrafish have become an attractive animal model organism for many aspects of embryonic development, particularly for blood vessel formation (reviewed in (Dahm and Geisler, 2006, Lawson and Weinstein, 2002a)). Over 70% of human genes showed identifiable orthologues in zebrafish (Howe et al., 2013). In addition, zebrafish has undergone partial genome duplication, which facilitates the *in vivo* study of lethal mammalian genes which often result in prenatal death (Isogai et al., 2001, Haffter et al., 1996, Driever et al., 1996). The zebrafish develops primary vasculature with functional blood circulation from 26 hours post fertilisation (hpf) followed by secondary remodelling of the primary vasculature (Gore et al., 2012). Vascular development and the signalling pathways which govern this process are highly conserved among zebrafish, mammalian models and humans (Hasso and Chan, 2011). Zebrafish can be genetically manipulated easily, their small and translucent embryos facilitating experimental procedures such as cell labelling to allow cell- and tissue-tracking during development. Furthermore, various genome editing strategies have been developed including Zinc Finger Nuclease (Sander et al., 2011), Transcription Activator-Like Effector Nuclease (TALEN) (Cermak et al., 2011) and Clustered Regularly Interspaced Short Palindromic Repeats (CRISPR)/Cas system (Hwang et al., 2013) to introduce mutations and to generate stable zebrafish mutant lines. Their small size and oxygen-rich environment permit zebrafish embryos to develop normally without blood circulation for up to 9 days due to passive diffusion of oxygen from the water (Sarmah and Marrs, 2016). This makes zebrafish an advantageous animal model to visualise and study blood vessel formation and its interactions with other developmental processes *in vivo*. In this introduction, we will discuss embryonic development of blood vessel formation, haematopoiesis and review recent works related to these essential processes in different species. In particular, we focus on the key signalling pathways that control these processes.

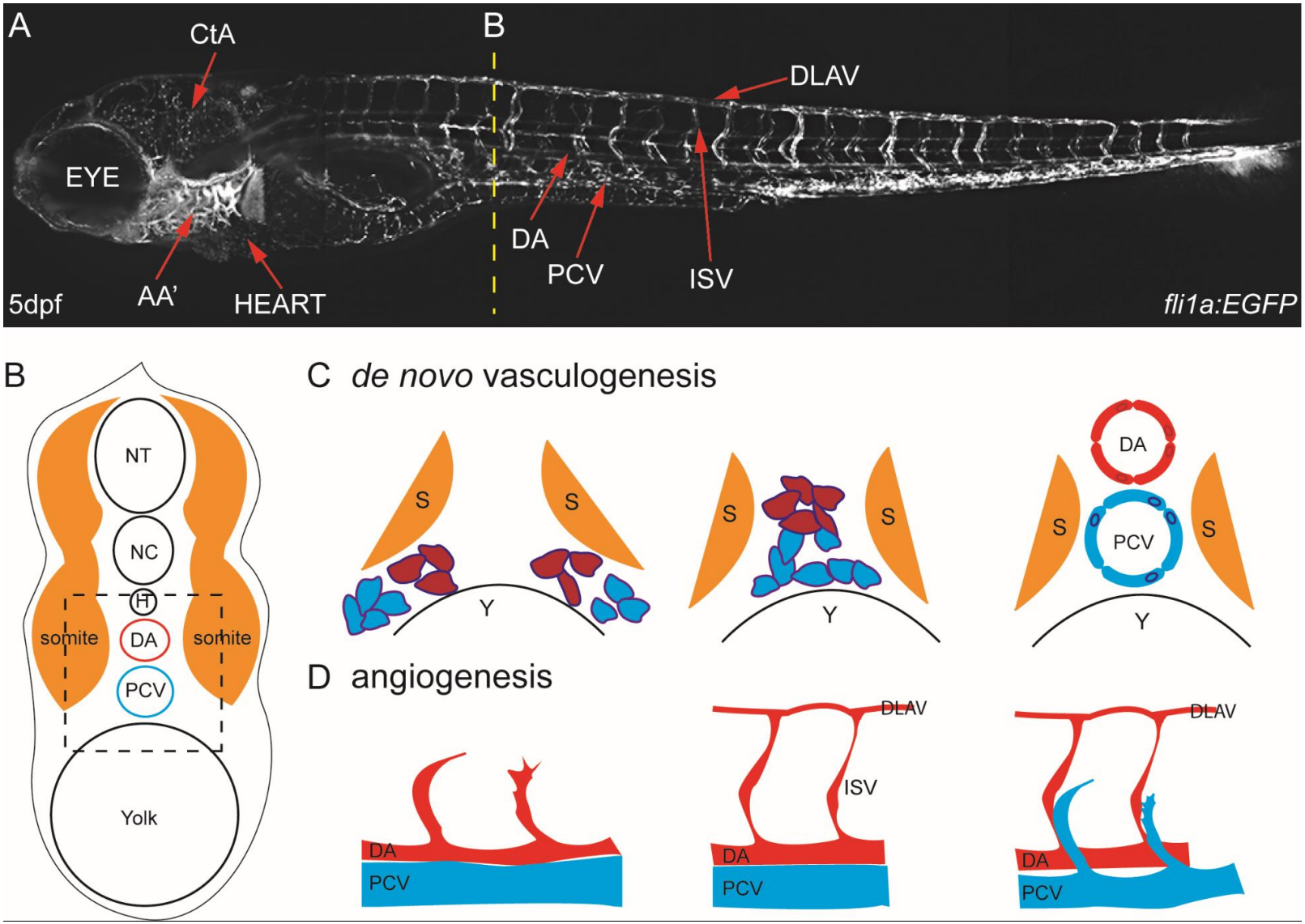
A
CtA
B
DLAV
EYE
DA
PCV
ISV
AA'
HEART
5dpf
fli1a:EGFP
B
NT
NC
H
somite
DA
somite
PCV
Yolk
C de novo vasculogenesis
S
S
Y
S
S
Y
DA
S
PCV
S
Y
D angiogenesis
DA
PCV
DLAV
ISV
DA
PCV
DLAV
DA
PCV

Figure 1.1 Vasculature formation in zebrafish

(A) Lateral view of 5dpf vasculature in WT embryo with *Tg(fli1a:EGFP)* background. (B) Illustration of transverse section of zebrafish trunk from panel A (yellow dotted line). (C) Illustration of the process of *de novo* vasculogenesis of dotted boxed area in panel B. Arterial angioblasts (red cells with purple outline) and venous angioblasts (blue cells with purple outline) are generated from the lateral plate mesoderm, migrate to the midline and form the intermediate cell mass, which then differentiates into the DA and PCV. (D) Illustration of the process of angiogenesis. Arterial sprouts form from the DA and migrate dorsally to form the ISV and DLAV; secondary angiogenesis initiates at 32hpf with venous sprouts emerging from the PCV. CtA, central artery; AA', aortic arch; DA, dorsal aorta; PCV, posterior cardinal vein; ISV, intersegmental vessel; DLAV, dorsal longitudinal anastomosing vessel; NT, neural tube; NC, notochord; H, hypochord; Y, yolk.

1.2 Vasculogenesis

1.2.1 *de novo* vasculogenesis

Vasculogenesis describes the process of vessel formation from free migratory endothelial precursor cells termed angioblasts. In vertebrates, angioblasts are derived from the lateral plate mesoderm (LPM) (Fouquet et al., 1997). The LPM is situated bilaterally in the embryo and both tissues migrate towards the midline during early embryonic specification (Fouquet et al., 1997, Zovein et al., 2010). After arriving at the midline, angioblasts, in association with haematopoietic progenitors and bipotential haemangioblasts form blood islands, which subsequently contribute to the primary capillary plexus formation in the extra-embryonic yolk sac in mammals or the intermediate cell mass in teleosts (Fig. 1.1 C) (Adams and Alitalo, 2007, Warga et al., 2009, Tam and Behringer, 1997).

The avascular zebrafish *cloche* mutants were characterised over two decades ago and the potential gene that is responsible for this mutation has been shown to be essential for EC formation and haematopoiesis (Stainier et al., 1995). It was not until recently that the *cloche* gene was successfully isolated and identified as a basic-helix-loop-helix-PAS gene called *npas4l* (Reischauer et al., 2016). *npas4l* is a master regulator for endothelial lineage specification (Reischauer et al., 2016) that functions upstream of *etv2* (previously known as *etsrp*, *er71 and etsrp71*) and *scl/tal1*, which are early markers of endothelial lineages (Kennedy et al., 1997, Lugus et al., 2007). The angioblast migration requires *etv2* (Sumanas and Lin, 2006, Lee et al., 2008). Completely abolished blood vessel formation was observed in *Etv2*-depleted mice (Lee et al., 2008). Similarly, *etv2* zebrafish morphants display reduced medial migration of angioblasts, which in turn results in significantly reduced blood vessel formation (Sumanas and Lin, 2006). Multiple signalling pathways have been reported to play essential roles during establishment of this primitive vascular network. Bone morphogenetic protein 4 (BMP4) and fibroblast growth factor 2 (FGF2) are both important for primitive mesoderm formation from which blood and endothelium derive (Winnier et al., 1995, Saxton and Pawson, 1999). Failure in mesoderm development was observed in the absence of *Bmp4* in mice (Winnier et al., 1995). In the absence of the murine receptor for FGF2, *Fgfr1*, accumulated mesodermal precursors failed to migrate through the primitive streak and therefore failed to form the mesoderm (Saxton and Pawson, 1999). Vascular endothelial growth factor (VEGF) and its receptor (VEGFRs) have also been shown to play essential roles during many aspects of vascular development (Ferrara et al., 1996, Shalaby

et al., 1995, Carmeliet et al., 1996, Fong et al., 1999, Lawson et al., 2002, Coultas et al., 2010, Takashima et al., 2002). During *de novo* vasculogenesis, loss of function of *Vegfr2* (also known as *Flk1/Kdr*) in mice resulted in reduced EC number and absent blood island in the yolk sac (Shalaby et al., 1995). Furthermore, in the absence of both murine VEGF co-receptors, Neuropilin-1 (*Nrp1)* and Neuropilin-2 (*Nrp2)*, completely abolished vasculature formation within both the embryo and yolk sac (Takashima et al., 2002). Consistent with these vital functions of the VEGF pathway, zebrafish mutants of *vegfa* failed to establish the arterial identity resulting in a single 'vein-like' axial vessel, which suggests vasculogenesis was abnormal (Rossi et al., 2016). Expression of *aplnra* and *aplnrb*, which encode the receptors for Elabela/Toddler, were observed in endothelial precursors (Helker et al., 2015). Elabela is a short hormonal peptide which functions as an attractant located in the midline to guide angioblast migration (Helker et al., 2015). Zebrafish Elabela-deficient mutants showed significantly impaired angioblast migration (Helker et al., 2015).

1.2.2 Arterial-venous specification

During the *de novo* formation of endothelial cords via vasculogenesis, endothelial progenitors are specified as arterial- and venous- progenitors via processes of segregation and differentiation. In zebrafish embryos, two distinct populations of angioblasts which are specified to form arteries or veins are derived from the LPM (Fig. 1.1 C) (Kohli et al., 2013). The migration of Notch-positive arterial angioblasts initiates 3 hours earlier than the migration of the venous angioblasts (Fig. 1.1 C) (Quillien et al., 2014, Kohli et al., 2013, Zhong et al., 2001, Zhong et al., 2000). Arterial or venous fate in the primary blood island is determined by a complex signalling network (Fig. 1.2 A). The Hedgehog (Hh)-VEGF-Notch signalling axis was first identified as a key regulator of *de novo* vasculogenesis and arterial-venous differentiation in zebrafish and subsequently demonstrated to be conserved in mammals (Lawson et al., 2002, Coultas et al., 2010, Lawson et al., 2001). At the top of this hierarchy is Sonic Hedgehog (Shh), which acts through its receptor Patched-1 (Ptc1) to induce expression of Vegfa, which promotes arterial specification (Le Bras et al., 2010, Vokes et al., 2004, Jia et al., 2004b). Interestingly, Nicoli *et al.* proposed that the calcitonin receptor-like receptor (Calcrl) functions upstream of Vegf signalling and is required for arterial-venous specification in zebrafish (Nicoli et al., 2008). However, *in vitro* data suggests CALCRL and VEGF do not function as a linear pathway (Fernandez-Sauze et al., 2004). Consistent with this, in zebrafish, *calcrl* has been shown to signal in parallel to Vegf to promote arterial differentiation via induction of Notch signalling (Wilkinson et al., 2012).

In mammals, 5 VEGF ligands (VEGFA-E) and 3 VEGF receptors (VEGFR1-3) have been identified (Fig. 1.2 B) (Takahashi and Shibuya, 2005). A partial genome duplication in zebrafish has resulted in two zebrafish orthologues of mammalian *VEGFA*, namely *vegfaa* and *vegfab* (Bahary et al., 2007). The *vegfd* (orthologue of mammalian *VEGFB* (Song et al., 2007, van Rooijen et al., 2010)) and *vegfc* ligand (Ober et al., 2004) are also present in zebrafish. These four zebrafish Vegf ligands selectively bind to 4 cognate Vegf receptors (Vegfr1-4) (Bussmann et al., 2008) to induce specific cellular responses (Fig. 1.2 B). VEGFA-mediated signalling activates phospholipase C-gamma (PLC-γ) and the mitogen-activated protein kinase (MAPK)/extracellular signal regulated kinase kinase (ERK) signalling, whereas VEGFD activates the phosphatidylinositol 3-kinase (PI3K)/protein kinase AKT pathway (Jia et al., 2004a). VEGFC-mediated signalling is essential to induce both MAPK and AKT pathways (Makinen et al., 2001). Zebrafish studies have demonstrated that the PLC-γ/ERK pathway positively regulates arterial EC formation (Lawson et al., 2003b, Takahashi et al., 2001), whereas PI3K/AKT signalling inhibits PLC-γ/ERK-mediated arterial specification *in vivo* and *in vitro* (Hong et al., 2006). In addition, there is an additional level of control for VEGF activity. During arterial-venous differentiation, Neuropilin-1 (NRP1) stimulates VEGFR2 to increase its affinity to bind VEGFA, which is essential for arterial differentiation (Fig. 1.2 A) (Mukouyama et al., 2005).

A characteristic feature of an EC to adopt an arterial fate is the activation of the Notch pathway (Fig. 1.2 A; Fig. 1.3) (Quillien et al., 2014). In mammals, the Notch signalling pathway is composed of 4 Notch receptors (Notch1-4) and 5 Notch ligands (Delta-like 1, 3, 4 and Jag1-2). Notch signalling functions through interactions between Notch receptors and Notch ligands (Fig. 1.3), which subsequently induce two cleavages via ADAMs and γ-secretase to release the Notch intracellular domain (NICD) (Fig. 1.3). The NICD then enters the nucleus and binds to transcription factor CSL (also known as RBPJ) along with other accessory proteins including coactivators (CoA) and Mastermind (MAM, the co-activator of CSL) (Fig. 1.3), which is essential for transcription of the Notch target genes including the *Hes* and the *Hey* genes (Radtke et al., 2005).

Lost function of Notch signalling leads to failure in arterial specification in both mammals and teleosts (Lawson et al., 2001, Krebs et al., 2004, Krebs et al., 2000, Duarte et al., 2004, Gale et al., 2004). The expression of arterial marker, EphrinB2, is controlled by Notch signalling (Wang et al., 1998, Adams et al., 1999), whereas the expression of EphB4 (cognate receptor of ephrinB2) is venous-restricted (Fig. 1.2 A) (Wang et al., 1998, Adams et al., 1999). This Ephrin-Eph interaction was suggested to play an important role in maintaining arterial/venous identity (Wang et al., 1998, Adams et al., 1999, Moyon et al., 2001). It was postulated that venous fate was a default state during embryonic development and that induction of Shh/Vegf/Notch signalling functioned

as a switch to divert EC differentiation from venous to arterial fate (Thurston and Yancopoulos, 2001). This hypothesis was refuted when active venous signalling was identified which inhibited arterialising signals (You et al., 2005). Such a factor, COUP-TFII (NR2F2) was identified as a positive regulator of venous specification (Fig. 1.2 A) (You et al., 2005). Overexpression of COUP-TFII negatively regulates Delta-like 4 (Dll4) and NRP1 expression to antagonise arterial specification (You et al., 2005). Furthermore, Forkhead box (Fox) transcription factors including Foxc1 and Foxc2 promote arterial vessel formation via direct activation of Notch signalling pathway (Fig. 1.2 A) (Hayashi and Kume, 2008b, Seo et al., 2006). Interestingly, *in vitro* data suggests that COUP-TFII inhibits expression of FOXC1 in HUVECs (Chen et al., 2012). Taken together, COUP-TFII antagonises the Notch signalling pathway via direct suppression of FOXC1 to regulate arterial-venous development (Fig. 1.2 A) (Chen et al., 2012).

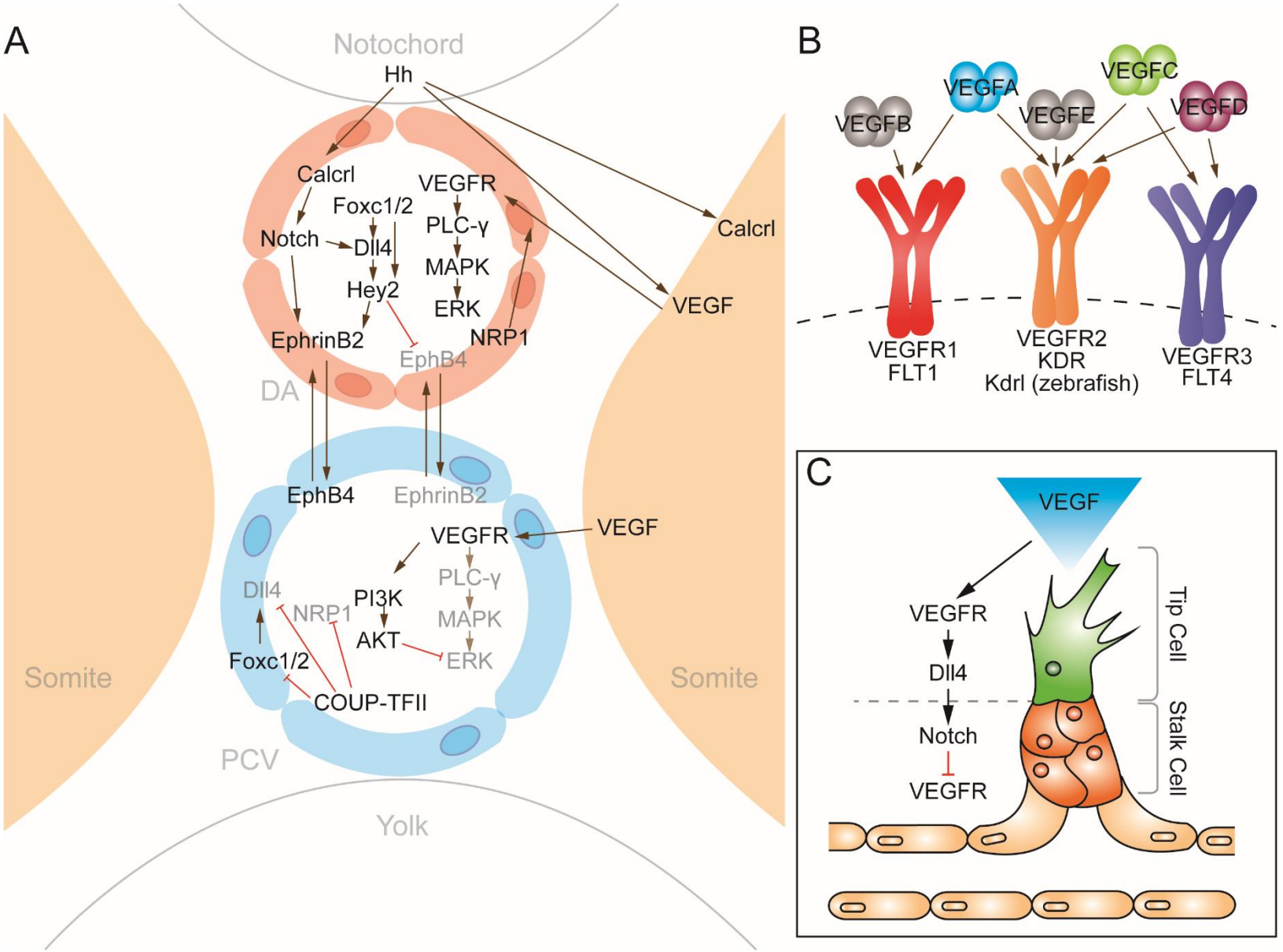
A
Notochord
Hh
Calcrl
Foxc1/2
Notch
Dll4
Hey2
EphrinB2
EphB4
VEGFR
PLC-γ
MAPK
ERK
NRP1
Calcrl
VEGF
DA
EphB4
EphrinB2
VEGF
VEGFR
PLC-γ
Dll4
NRP1
PI3K
MAPK
AKT
ERK
Foxc1/2
COUP-TFII
PCV
Somite
Somite
Yolk
B
VEGFA
VEGFB
VEGFC
VEGFD
VEGFE
VEGFR1
FLT1
VEGFR2
KDR
Kdrl (zebrafish)
VEGFR3
FLT4
C
VEGF
VEGFR
Dll4
Notch
VEGFR
Tip Cell
Stalk Cell

Figure 1.2 Molecular control during vascular development

(A) Illustration of simplified signalling pathways involved in *de novo* vasculogenesis and arterial-venous specification. Adapted from (Wilkinson and van Eeden, 2014) (B) Illustration of VEGF ligand-receptor interactions. (C) Illustration of lateral inhibition. Adapted from (Herbert and Stainier, 2011). DA, dorsal aorta; PCV, posterior cardinal vein.

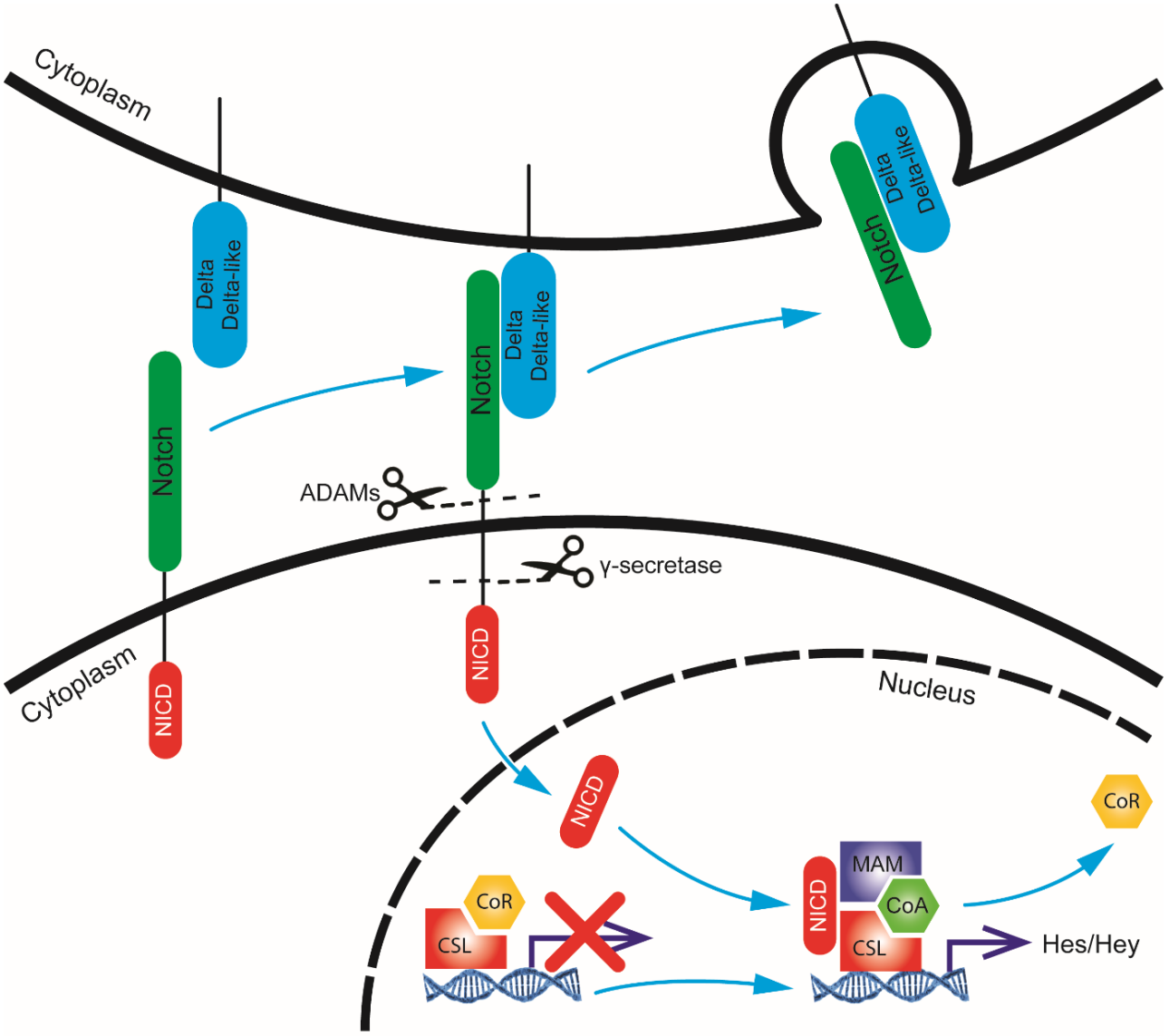
Cytoplasm
Delta
Delta-like
Notch
ADAMs
γ-secretase
NICD
Cytoplasm
Nucleus
NICD
CoR
CSL
MAM
CoA
NICD
CSL
CoR
Hes/Hey

Figure 1.3 Notch signalling pathway

Illustration of Notch signalling pathway. Adapted from (Radtke et al., 2005). The interactions between Notch ligands and receptors can induce two cleavages including ADAMs and γ-secretase, which will in turn release NICD. After entering the nucleus, NICD will bind accessory proteins including MAM, CLS, CoA and transcribe the Notch downstream gene targets including the *Hes* and *Hey* genes.

1.2.3 Cranial vasculogenesis

Similar to trunk vasculogenesis, which originates from the posterior LPM (PLPM), angioblasts derived from the anterior lateral plate mesoderm (ALPM) contribute to the zebrafish cranial vasculature (Fig. 1.4 A) (Lieschke et al., 2002, Warga et al., 2009). Instead of migrating medially, ALPM angioblasts retain their bilateral position (Proulx et al., 2010), which is not surprising since major cranial vessels including the primordial hindbrain channel (PHBC) and lateral dorsal aorta (LDA) are located bilaterally in the head (Fig. 1.4 B). In zebrafish, the common cardinal vein (CCV) is the major vein that transports all venous blood to the heart (Fig. 1.4 B) (Helker et al., 2013). It forms from a sub-population of angioblasts from the ALPM (Fig. 1.4 A) (Helker et al., 2013).

In addition to angioblasts, the ALPM also generates endocardial and myeloid progenitors (Fig. 1.4 A) (Bussmann et al., 2007, Schoenebeck et al., 2007). Unlike the cranial angioblasts, ALPM-derived endocardial precursors will migrate towards the midline from the 12 somite stage (s) (15hpf) onwards in zebrafish (Bussmann et al., 2007, Schoenebeck et al., 2007). Siekmann *et al.* provided the first evidence of distinct EC populations giving rise to different arteries in the head and trunk (Siekmann et al., 2009). Subsequent generation of the *Tg(etsrp:EGFP)* transgenic line facilitated a comprehensive description of cranial vasculogenesis in zebrafish (Proulx et al., 2010). *Etv2/etsrp*, as previously described, is essential for vasculogenesis and also myelopoiesis in vertebrates (Ferdous et al., 2009, Lee et al., 2008, Pham et al., 2007, Sumanas et al., 2008, Sumanas and Lin, 2006, Liu et al., 2012, Liu et al., 2015). Cranial blood vessels form via a combination of vasculogenesis and angiogenesis (Proulx et al., 2010). Cranial vasculogenesis originates from two separate clusters of endothelial progenitors termed the rostral organising centre (ROC) and midbrain organising centre (MOC) (Fig. 1.4 A) (Proulx et al., 2010). Endocardial progenitors derived from the MOC give rise to the first aortic arch (AA1) and the heart. Both clusters give rise to arteries and veins, which suggest unlike trunk vasculogenesis, where angioblasts acquire arterial/venous identity before migration (Kohli et al., 2013), cranial vasculogenesis may have less defined arterial/venous identity prior to initiation of blood circulation (Fig. 1.4 A) (Proulx et al., 2010).

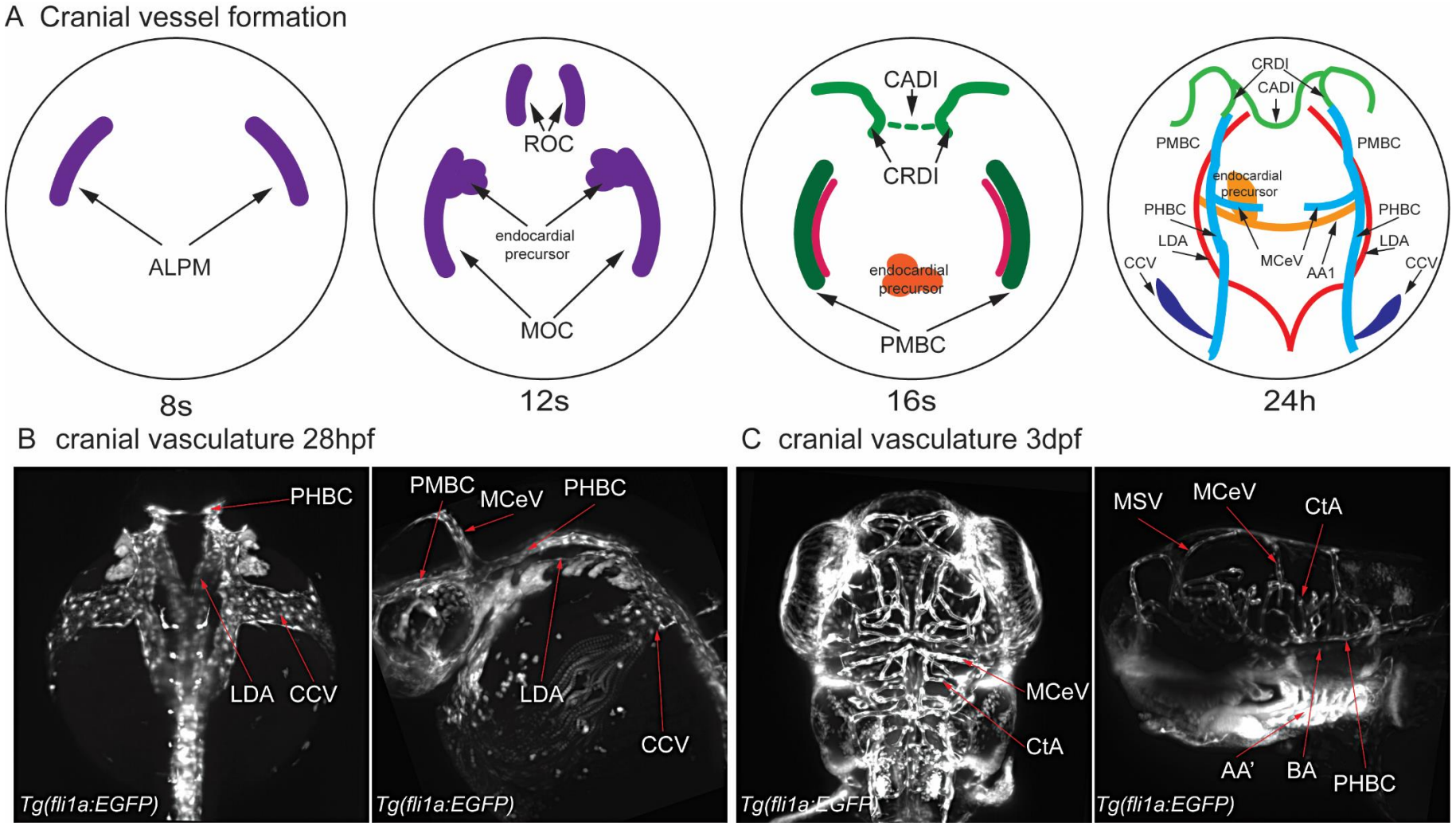
A Cranial vessel formation
ALPM
8s
ROC
endocardial precursor
MOC
12s
CADI
CRDI
endocardial precursor
PMBC
16s
CRDI
CADI
PMBC
PMBC
endocardial precursor
PHBC
PHBC
LDA
LDA
MCeV
AA1
CCV
CCV
24h
B cranial vasculature 28hpf
PHBC
LDA
CCV
Tg(fli1a:EGFP)
PMBC
MCeV
PHBC
LDA
CCV
Tg(fli1a:EGFP)
C cranial vasculature 3dpf
MCeV
CtA
Tg(fli1a:EGFP)
MSV
MCeV
CtA
AA'
BA
PHBC
Tg(fli1a:EGFP)

Figure 1.4 Cranial blood vessel formation

(A) Illustration of simplified process of cranial vasculature development. Adapted from (Proulx et al., 2010). Angioblasts derived from the ALPM retain their bilateral position and then differentiate into multiple cranial vessels including PMBC, PHBC and LDA, whereas endocardial precursors specified from the MOC migrate to the midline and differentiate into the AA1 and heart. Angioblasts from ROC develop into anterior cranial vessels including CRDI and CADI. A sub-population of angioblasts derived from the MOC will differentiate into CCV. (B) Dorsal and lateral view of cranial vessels in WT embryos with *Tg(fli1a:EGFP)* background at 28hpf. (C) Dorsal and lateral view of cranial vessels in WT embryos with *Tg(fli1a:EGFP)* background at 3dpf. ALPM, anterior lateral plate mesoderm; ROC, rostral organising centre; MOC, midbrain organising centre; PMBC, primordial midbrain channel; CRDI, cranial division of internal carotid artery; CADI, caudal division of internal carotid artery; AA1, first aortic arch; PHBC, primordial hindbrain channel, LDA, lateral dorsal aorta; CCV, common cardinal vein; MCeV, middle cerebral vein; MSV, mesencephalic vein; BA, basilar artery; CtA, central artery; AA', aortic arch.

1.3 Angiogenesis

1.3.1 Angiogenesis and vascular patterning

Angiogenesis refers to the formation of new blood vessels from pre-existing vessels by a process of remodelling. Angiogenesis is an essential step to facilitate blood transportation into developing organs and increase exchange of metabolic products in the blood (Adams and Alitalo, 2007). The formation of segmental arteries (SeA) within the zebrafish trunk has been developed as a stereotypical model to study primary sprouting angiogenesis. Primary angiogenic sprouts in zebrafish originate from the dorsal wall of the dorsal aorta (DA), in contrast to haematopoietic stem cells (HSCs) which arise from the ventral wall (Bertrand et al., 2010, Boisset et al., 2010, Kissa and Herbomel, 2010). Primary sprouts migrate dorsally to form the SeA until they reach their dorsal migration limit and begin sprouting laterally, forming a T-branch along the roof of the neural tube where they form long filopodia to reach rostrally and caudally to connect with adjacent sprouts. This dorsal vessel is called the dorsal longitudinal anastomotic vessels (DLAV) (Fig. 1.1 A, D) (Isogai et al., 2003).

During angiogenesis, a small proportion of ECs will be selected as endothelial tip cells (TC), which have highly dynamic filopodia and lead the sprouting of angiogenic vessels (Gerhardt et al., 2003). The cells following the lead of TCs are termed stalk cells (SC), which are less mobile and also contribute to the developing vessels (Fig. 1.2 C) (Adams and Alitalo, 2007). Tip versus stalk cell selection is regulated by the interactions between VEGF and Notch signalling. VEGF induces and guides the leading TC, which in turn induces expression of a Notch ligand, *delta-like 4* (*dll4*) within the TC (Fig. 1.2 C) (Gerhardt et al., 2003, Hellstrom et al., 2007). Conversely, Notch signalling is elevated in the SCs, in which TC fate is suppressed by Notch-mediated inhibition of VEGFR expression, thereby inhibiting the ability of SCs to respond to VEGF and thus controlling the number of TCs within a sprouting vessel (Fig. 1.2 C) (Lobov et al., 2007).

VEGFR2 is the major VEGF receptor expressed in TCs, especially in filopodia (Gerhardt et al., 2003). VEGFR2 binds to VEGFA and provides guidance for migrating ECs (Fig. 1.2 B) (Ruhrberg et al., 2002, Gerhardt et al., 2003). Expression of matrix-binding VEGFA (murine VEGF164 and human VEGF165) was shown to exhibit spatial gradients, and act as chemoattractant to lead TC filopodia elongation and therefore sprout formation (Ruhrberg et al., 2002, Gerhardt et al., 2003). Other isoforms of VEGFA which do not possess a heparin-binding motif (murine VEGF120 and human VEGF121) facilitate EC proliferation (Ruhrberg et al., 2002, Gerhardt et al., 2003). *In vitro*

data further demonstrate that matrix-binding VEGFA induces prolonged activation of VEGFR2, whereas other isoforms of VEGFA without an extracellular matrix binding domain do not exert this effect (Chen et al., 2010). In addition, VEGF co-receptor NRP1 binds to matrix-bound VEGFA (VEGF164/ VEGFA165) but not soluble VEGFA (VEGF120/ VEGF121), and this interaction was shown to contribute to angiogenesis (Pan et al., 2007, Mamluk et al., 2002, Lee et al., 2002). Mild abnormalities were observed in *Nrp1* knock-out (KO) mice, however, which indicates other VEGFRs may possess more important roles in angiogenesis than NRP1 alone (Ruhrberg et al., 2002, Gerhardt et al., 2004).

The decoy VEGFR (termed VEGFR1/Flt1) also interacts with VEGFA (Fig. 1.2 B) (Hiratsuka et al., 2005) and exhibits higher affinity for VEGFA than VEGFR2 (Hiratsuka et al., 2005). In zebrafish, *vegfr1/sflt1* has been shown to function as an anti-angiogenic factor (Krueger et al., 2011). Membrane binding FLT1 (mFLT1) and soluble Flt1 (sFLT1) were identified as major isoforms of VEGFR1 (Krueger et al., 2011). Knock-down (KD) of *flt1* in zebrafish embryos induces hypersprouting in the trunk (Krueger et al., 2011). sFLT1 also contributes to vascular development by binding free VEGFA and acting as a sink which efficiently limits VEGFA-VEGFR2 signalling-induced angiogenic activity (Gerhardt et al., 2003, Ambati et al., 2006, Roberts et al., 2004). Very recently, studies utilising zebrafish mutants with loss of function of isoform-specific *flt1* indicate that *sflt1* plays a more important role in negative regulation of angiogenesis than *mflt1* (Wild et al., 2017). Furthermore, *sflt1* zebrafish mutants display ectopic angiogenesis from veins but not arteries, overexpression of both neuronal *sflt1* and endothelial *sflt1* could rescue this ectopic angiogenesis (Wild et al., 2017, Matsuoka et al., 2016). However, it remains unclear in which cells *sflt1* functions to antagonise angiogenesis.

The balance between Notch and VEGF signalling pathways is essential to maintain normal patterning of the vasculature. Activation of the Notch signalling pathway limits VEGF-VEGFR-induced angiogenesis (Siekmann and Lawson, 2007). Reduced Notch signalling in *dll4* morphants (Leslie et al., 2007), *mind bomb* (*mib*) mutants (Lawson and Weinstein, 2002a, Lawson et al., 2001) and DAPT (γ-secretase inhibitor)-treated embryos (Geudens et al., 2010) display ectopic angiogenesis. Furthermore, Dll4-mediated suppression of Flt4/Vegfc signalling negatively regulates arterial angiogenesis (Le Guen et al., 2014, Villefranc et al., 2013, Hogan et al., 2009b, Lobov et al., 2007).

1.3.2 Secondary angiogenesis and lymphangiogenesis

Zebrafish lymphatic endothelial cells (LECs) derive from the venous axial vessels, posterior cardinal vein (PCV) (Fig. 1.1 D) (Karpanen and Schulte-Merker, 2011). Segmental vein (SeV) sprout from the PCV at 32hpf, via a process termed secondary angiogenesis, following which, these venous sprouts will adapt to one of two fates: (1) Connect to existing SeA and remodel to become a SeV; (2) Migrate to the horizontal myoseptum and become parachordal lymphangioblasts. Around half of these venous sprouts will follow the latter lymphatic fate. Normally, parachordal lymphangioblasts form at 50hpf (Karpanen and Schulte-Merker, 2011, Hogan et al., 2009a). In a process which takes approximately 10 hours, parachordal lymphangioblasts will migrate along the ISVs either dorsally to form the longitudinal lymphatic vessel (DLLV) or ventrally to form the thoracic duct (TD). Formation of DLLV is similar to the formation of the DLAV, however the DLLV is located ventral to the DLAV (Hogan et al., 2009a). When forming the TD, lymphangioblast migration beneath the DA at 3dpf is followed by extensions of filopodia from lymphangioblasts horizontally along the DA to connect with other lymphangioblasts to form a continuous TD (Kuchler et al., 2006). At 5dpf, the trunk lymphatic system including TD, DLLV and intersegmental lymphatic vessels (ISLV) will become functional (Karpanen and Schulte-Merker, 2011).

The VEGF pathway also plays key roles in lymphangiogenesis (Jeltsch et al., 2003). Unlike arteries, in which Flt4/Vegfc expression is suppressed by Dll4/Notch signalling (Le Guen et al., 2014, Villefranc et al., 2013, Hogan et al., 2009b, Lobov et al., 2007), in veins, Flt4/Vegfc signalling is absolutely required to promote secondary angiogenesis and lymphangiogenesis (Gordon et al., 2013, Le Guen et al., 2014, Villefranc et al., 2013). Zebrafish *vegfc* mutants and *flt4* mutants share similar phenotypes including lymphoedema and completely abolished lymphatic development due to a failure of LEC specification (Gordon et al., 2013, Le Guen et al., 2014, Villefranc et al., 2013). Interestingly, *full-of-fluid* mutant zebrafish do not undergo venous angiogenesis and lymphangiogenesis, and the responsible locus was later isolated and identified as *ccbe1* (Alders et al., 2009, Hogan et al., 2009a). Ccbe1 was shown to be essential for Vegfc maturation and activation and thus important to facilitate binding between Vegfc and Flt4 (Alders et al., 2009, Hogan et al., 2009a, Le Guen et al., 2014, Roukens et al., 2015).

Murine Prospero homeobox 1 (*Prox1*) is a transcription factor which is also critical for lymphangiogenesis (Wigle and Oliver, 1999, Wigle et al., 2002). *Prox1* mutant mice do not undergo lymphangiogenesis (Wigle and Oliver, 1999, Wigle et al., 2002). *In vitro* studies of human oral squamous cell carcinoma cells further suggested that *PROX1* promotes lymphatic development via positive regulation of the expression of *VEGFC* (Sasahira et al., 2014). Furthermore, *FOXC2* is an upstream activator of *PROX1* in oral squamous cell carcinoma (Sasahira et al., 2014). In section 1.2.2 we described how

COUP-TFII plays an essential role in establishment of venous fate during vasculogenesis (You et al., 2005). Since lymphangiogenesis has a venous origin, it is not surprising that COUP-TFII is also vital for lymphatic development (Lee et al., 2009, Yamazaki et al., 2009). Indeed, murine and human cell culture studies have demonstrated that COUP-TFII physically interacts with PROX1 to form a protein complex essential for LEC specification via positive regulation of VEGFC/FLT4 signalling (Lee et al., 2009, Yamazaki et al., 2009). In addition, the dosage of PROX1 is important for activation of *Flt4* expression, but activation of VEGFC/FLT4 signalling also promotes the expression of *Prox1* and its downstream functions via positive feedback (Srinivasan et al., 2014).

Sex determining region Y box 18 (Sox18) is a transcription factor also implicated in lymphatic formation (Irrthum et al., 2003, Francois et al., 2008) since *Sox18* null mice showed arrested LEC specification and overexpression of *Sox18* induces lymphatic marker expression including *Prox1* (Francois et al., 2008). Zebrafish injected with a sub-phenotypic dose of both *sox18* and *vegfc* morpholinos (Mo) induce abnormal lymphatic formation, indicating a genetic interaction between *sox18* and *vegfc* during lymphatic development (Cermenati et al., 2013). Zebrafish mutants with depleted *prox1a* function (orthologue of mammalian *Prox1*) showed significantly reduced trunk LEC numbers (Koltowska et al., 2015), whereas *prox1b* (orthologue of mammalian *Prox1*) alone was shown to be dispensable for lymphangiogenesis (Tao et al., 2011). *prox1a* is expressed prior to secondary angiogenesis and lymphangiogenesis in zebrafish, which suggests LEC fate is established before lymphatic sprouting (Shin et al., 2016b, Nicenboim et al., 2015, Koltowska et al., 2015). A ventral-to-dorsal movement of ECs, which are *lyve1*-positive (lymphatic endothelial marker (Okuda et al., 2012)), occurs at 24hpf within the zebrafish PCV (Nicenboim et al., 2015). These pre-specified LECs within the ventral PCV were suggested to form the future trunk lymphatic system (Nicenboim et al., 2015). However, later zebrafish studies proposed the induction of Prox1 expression after this ventral-to-dorsal migration from 30-32hpf establishes the LEC fate of these ECs within the dorsal PCV (Koltowska et al., 2015, Shin et al., 2016b). These dorsal LEC precursors then proliferate prior to secondary angiogenesis, which further contribute to lymphatic development (Koltowska et al., 2015). It still remains unclear, which cell population represents the true LEC precursor.

1.3.3 Cranial angiogenesis and lymphangiogenesis

As introduced in section 1.2.3, cranial vascular development in zebrafish occurs via a combination of vasculogenesis and angiogenesis (Proulx et al., 2010). The first angiogenic sprout is detected around 12-16s (15-16hpf) from the ROC, and migrate posteriorly to form cranial division of internal carotid artery and eventually connect with the primordial midbrain channel (PMBC), which is derived from the MOC via

vasculogenesis (Fig. 1.4 A) (Proulx et al., 2010). Major cranial vessels in zebrafish that contribute to the blood brain barrier (BBB) including the PHBC, LDA and central arteries (CtAs), form via a complicated morphogenetic mechanism (Fig. 1.4) (Isogai et al., 2001). The formation of CtAs via angiogenesis has become an attractive area for studying the formation and function of the BBB in the past decade. Similar to trunk angiogenic development, the formation of CtAs requires balanced Vegf-Notch signalling, since *dll4* morphants and DAPT treated zebrafish embryos display ectopic formation of CtAs (Bussmann et al., 2011). In addition, Vegfa (including Vegfaa and Vegfab) signalling through Kdrl is essential for CtA sprouts (Bussmann et al., 2011). Zebrafish *vegfaa* mutants and *vegfaa*; *vegfab* double mutants display an absence of CtAs (Rossi et al., 2016).

A zebrafish mutant screen isolated the *no food for thought* mutant (Shaw et al., 2006), which were subsequently identified as *reck* mutants, displaying an absence of CtA formation but retaining trunk angiogenesis (Ulrich et al., 2016, Vanhollebeke et al., 2015). Ulrich *et al.* further proposed that Reck, a Glycosylphosphatidylinositol-anchored membrane protein, positively regulates the canonical Wnt signalling pathway to contribute to intracerebral vessel formation (Ulrich et al., 2016). Gpr124 functions to promote angiogenesis in the murine central nervous system (CNS) by positively regulating the Wnt/β-catenin pathway (Kuhnert et al., 2010, Zhou and Nathans, 2014). Reck and Gpr124 have been shown to interact with each other and positively regulate CtA sprout formation in a cell-autonomous manner (Vanhollebeke et al., 2015). Chemokines have also been proposed to guide CtA sprouting, since increased CtA interconnections were observed in *cxcrl12b* and *cxcr4a* zebrafish mutants (Bussmann et al., 2011). Blood flow is also essential for cranial vessel patterning as reduced blood circulation induces increased angiogenic activity in CtAs (Bussmann et al., 2011). However, this conclusion conflicts with another zebrafish study, which showed that lack of blood circulation induced by *tnnt2*-KD did not affect CtA patterning (Fujita et al., 2011).

The basilar artery (BA), located medially to the bilateral PHBCs within the hindbrain, forms via angiogenesis from the PHBC from 28hpf (Ulrich et al., 2011). Similar to CtAs, BA formation is dependent upon Vegfa/Kdrl signalling. *vegfaa; vegfab* double mutants and *kdrl* mutant zebrafish display similar absent BA formation (Bussmann et al., 2011, Rossi et al., 2016). During BA formation the connections formed between BA and PHBC are called arterial-venous connections (AVC), which normally regress via pruning after BA establishment at 48hpf (Ulrich et al., 2011). Blood flow has been shown to be important for this AVC pruning process and in *silent-heart* zebrafish mutants, which do not exhibit blood circulation, increased AVCs are present (Ulrich et al., 2016).

The facial lymphatic system represents the major cranial lymphatic system in zebrafish, and this originates from the CCV sprouts, which are termed facial lymphatic sprout (FLS) (Helker et al., 2013). At 1.5dpf, facial

lymphatic sprouts undergo further migration and remodelling to form the facial lymphatic network including lateral facial lymphatic (LFL); lymphatic branchial arches (LAA); medial facial lymphatic (MFL) and otolithic lymphatic vessel (OLV) (Helker et al., 2013). At 5dpf, the posterior extension of the facial lymphatics specifies the jugular lymphatic vessel (JLV) from LFL, which connects to the TD and forms an intact lymphatic system throughout the body (Helker et al., 2013). Angioblasts specified from the primary head sinus (PHS) also contribute to the LFL (Helker et al., 2013). Similar to trunk lymphatic development, facial lymphatic formation is also largely controlled by Vegfc/Flt4 signalling (Okuda et al., 2012). In addition, zebrafish morpholino studies have suggested that knocking down of neither *vegfc* nor *vegfd* alone can completely arrest facial lymphatic development and that these 2 genes co-operate to promote facial lymphatics formation (Astin et al., 2014). Zebrafish *vegfc*; *vegfd* double mutants display more severe defects in facial lymphatics formation when compared with either *vegfc* or *vegfd* single mutants thereby demonstrating interaction between *vegfc* and *vegfd* (Duong et al., 2014).

In addition to the facial lymphatic network, brain lymphatic endothelial cells (BLECs) have been recently identified which potentially contribute to tissue drainage (van Lessen et al., 2017, Venero Galanternik et al., 2017). Brain lymphatic endothelial cells originate from venous sprouts from the PMBC which subsequently migrate along the mesencephalic vein (MsV) to form two stereotypical loop structures bilaterally behind the eyes in the forebrain (van Lessen et al., 2017). In *ccbe1* null zebrafish, BLEC formation was abrogated, indicating the Ccbe1-mediated Vegfc/Flt4 pathway is required for BLEC specification (van Lessen et al., 2017).

1.4 Vascular Maturation

Newly formed blood vessels consist of a fragile monolayer of ECs. During later development these single-layered blood vessels recruit non-endothelial mural cells (MC) including pericytes and vascular smooth muscle cells (vSMCs), which helps maintain vessel stability and regulate vasomotor tone during subsequent development and throughout adult life (Whitesell et al., 2014, Wilkinson and van Eeden, 2014, Dejana, 1997, Dejana et al., 1997). Vessel leakage caused by hyperpermeability is responsible for many cardiovascular diseases including myocardial infraction, diabetes and also cancer (reviewed in (Claesson-Welsh, 2015)). Fluid and macromolecules that leak from vessels can cause oedema and subsequently lead to organ failure or even death. Therefore understanding the mechanisms which regulate vascular permeability may hold the key to solve many blood vascular diseases.

1.4.1 Vascular permeability

Vascular permeability describes the capability of the vasculature to allow solutes and molecules to travel through (Claesson-Welsh, 2015). Molecules under 40kDa are subject to spontaneous extravasation (Egawa et al., 2013). However, larger molecules may require distinct mechanisms to extravasate. There are three major mechanisms involved in extravasation including fenestrae, transcellular gaps and paracellular gaps (Fig. 1.5) (Claesson-Welsh, 2015). These three extravasation mechanisms vary in different tissues and organs, and also largely depend on the nature of the cargo undergoing extravasation (Fig. 1.5) (Claesson-Welsh, 2015). Fenestrae occur in the endothelium of the kidney glomerulus to facilitate rapid exchange and filtration of molecules (Tse and Stan, 2010). Transcellular gaps including the vesiculo-vascuolar organelle (VVO) (Dvorak and Feng, 2001) facilitate transcytosis, which is characterised as the major pathway for transportation of macromolecules and inflammatory cells (Claesson-Welsh, 2015, Kohn et al., 1992). Paracellular gaps also support macromolecule extravasation. The VVOs were observed mainly by electron microscopy previously, and were shown to be present in normal vasculature and also in tumour vasculature (Dvorak and Feng, 2001). The VVO has been described as the dominant transcellular pathway for transportation of macromolecules (Kohn et al., 1992) but has not been studied in a living organism (Claesson-Welsh, 2015).

Two types of junctions that connect ECs are tight junctions (TJ) and adherens junctions (AJ). Among these junctions, AJ can be targeted by specific signalling pathways and lead to modulation of vascular permeability paracellularly (Corada et al., 1999, Dejana, 2012). One special cadherin which is specific to ECs is vascular endothelial cadherin/ Cdh5 (Dejana et al., 2009). Starved ECs *in vitro* display very low phosphorylation of Cdh5, however, under permeability-increasing stimuli, Cdh5 phosphorylation was

increased dramatically (Esser et al., 1998, Allingham et al., 2007, Turowski et al., 2008). Interestingly, continuous phosphorylation of Cdh5 was detected only in veins but not in arteries *in vivo* without treatment of permeability-increasing agents (Orsenigo et al., 2012). Therefore, this venous vascular endothelial cadherin phosphorylation is not sufficient to increase vascular permeability. However, it is possible that this continuous phosphorylation of Cdh5 in veins but not arteries can sensitise the effects caused by permeability-increasing agents, which is consistent with previous observations that veins are the primary target of inflammatory agents (Orsenigo et al., 2012). Oxidative stress, inflammation and EC apoptosis are believed to be the main causes for microvascular dysfunction and vessel leakage. In addition, ageing is also a common cause for hyperpermeability (Oakley and Tharakan, 2014).

Angiopoietin 1 (Ang1), is a well-known antagonist of hyperpermeability, which maintains vascular permeability by blocking endocytosis (Dejana, 2012). Angiopoietin 2 (Ang2) is an antagonist of Ang1 and plays a contradictory role, and disrupts vessel formation by promoting vessel permeability during embryonic development (Maisonpierre et al., 1997, Pitera et al., 2004). In addition, Adrenomedullin (AM) is a well-known vasodilator, whose expression has been reported to increase during multiple cardiovascular conditions (reviewed in (Gibbons et al., 2007)). The Calcitonin receptor-like receptor (CALCRL, formerly known as CLR and CRLR) is a 7-transmembrane G-protein receptor (GPCR) which binds to numerous receptor activity-modifying proteins (RAMPs) to regulate downstream signalling (Sexton et al., 2006, McLatchie et al., 1998). In mammals, RAMP1 and CALCRL comprise the receptor for the calcitonin gene-related peptide (CGRP), whereas RAMP2-CALCRL and RAMP3-CALCRL are the receptor complexes for AM (McLatchie et al., 1998). This AM signalling pathway promotes angiogenesis, maintains blood vessel integrity, and guides arterial differentiation (Hippenstiel et al., 2002, Nicoli et al., 2008, Nikitenko et al., 2006), and will be further discussed in Chapter 5.

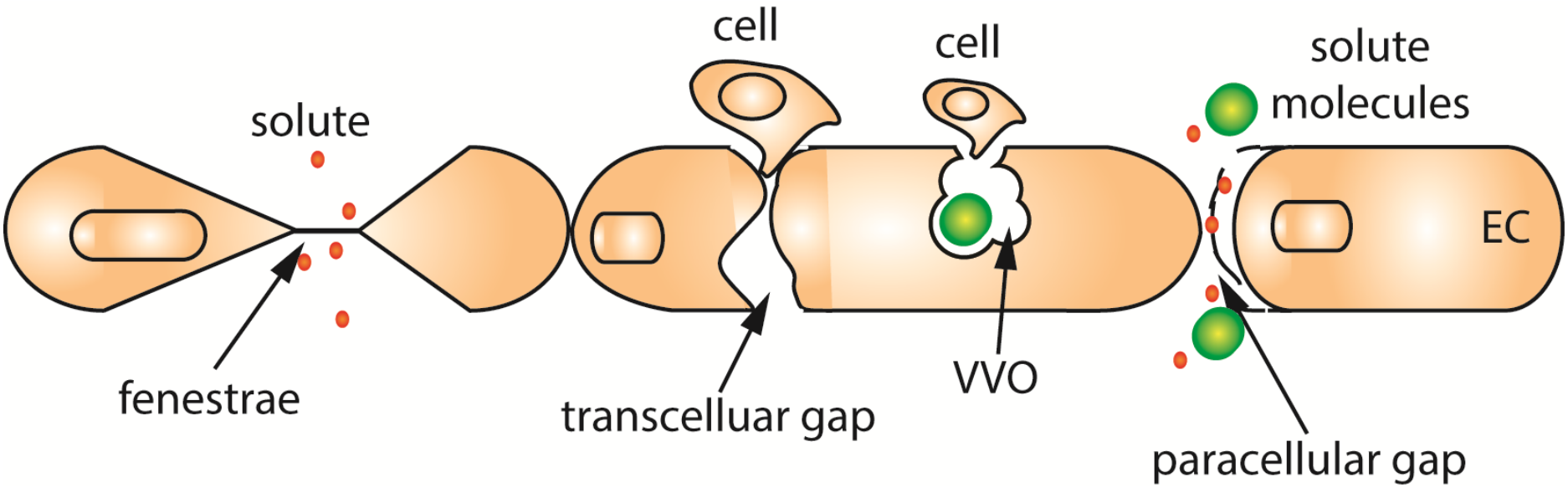

Figure 1.5 Major mechanisms of extravasation

Illustration of three major mechanisms involved in extravasation including fenestrae, transcellular gap and paracellular gap. Fenestrae mainly facilitate the extravasation for solutes. Transcellular gaps including the VVOs are the dominant mechanisms for extravasation of macromolecules and cells in the brain. Paracellular gaps also facilitate macromolecule extravasation. VVO, vesiculo-vascuolar organelle.

1.4.2 Vascular stability

Vascular maturation involves MC recruitment including vSMC and pericytes. These periendothelial cells form extravascular layers and provide physical support to stabilise the formed vasculature (Whitesell et al., 2014, Wilkinson and van Eeden, 2014, Dejana, 1997, Dejana et al., 1997). In zebrafish, vSMCs have only recently been characterised (Whitesell et al., 2014). Using a transgenic line which highlights cells expressing *acta2*, it was demonstrated that vSMCs develop post initiation of blood circulation from around 72hpf (Whitesell et al., 2014). The platelet-derived growth factor (PDGFB) and its receptor (PDGFRβ) are pericyte markers and this signalling pathway plays an essential role in pericyte recruitment (Ohlsson et al., 1999, Olson and Soriano, 2011, Wang et al., 2014). Recently, *TgBAC(pdgfrb:EGFP)* was generated by Ando *et al.* to visualise the MC recruitment and coverage *in vivo*, which showed arterial preference of MC coverage during vascular development (Ando et al., 2016). Interestingly, the avascular *cloche* mutants (Stainier et al., 1995) displayed transgelin-positive MCs, which are located in the corresponding DA position (Santoro et al., 2009). On the contrary, *hand* mutants with abnormally developed LPM exhibit complete loss of perivascular MCs (Santoro et al., 2009, Yelon et al., 2000). Taken together, these findings suggest MCs are derived from LPM rather than from ECs (Santoro et al., 2009). However, in mammals, vSMC derived from multiple tissues (reviewed in (Majesky, 2007)). Similarly in zebrafish, cranial vSMCs are derived from the neural crest, while posterior vSMCs emerge from the mesothelial tissues (reviewed in (Majesky, 2007)). A recent zebrafish study described that vSMCs, which cover the DA, are derived from the adjacent sclerotome (Stratman et al., 2017).

Multiple signalling pathways including TGFβ and Notch have been reported to be required for the differentiation and recruitment of MCs (Wang et al., 2014, Krymskaya et al., 1997). Recent zebrafish studies have provided evidence suggesting that blood flow promotes the recruitment of vSMCs (Chen et al., 2017). This will be further discussed in Chapter 3 and Chapter 4.

1.4.3 The blood brain barrier

The blood brain barrier (BBB) is important for the brain to maintain its tightly enclosed construction (Claesson-Welsh, 2015). In addition to TJs and AJs, the brain vasculature is also composed of vascular basement membrane, which further facilitates the high-resistance barrier function (Claesson-Welsh, 2015, Paolinelli et al., 2011). The BBB is also constructed with perivascular cells including pericytes, vSMC and astrocytes (Paolinelli et al., 2011). Transcytosis-mediated by the VVO is recognised as the major pathway for extravasation in the brain (Armulik et al., 2010, Claesson-Welsh, 2015). Murine *Pdgfb* mutants showed reduced pericyte coverage, with increased transcytosis-mediated BBB hyperpermeability (Armulik et al., 2010). Extracellular matrix (ECM) proteins are essential for BBB formation and also to maintain its

integrity since reduced ECM expression induces brain vascular hyperpermeability (Gould et al., 2005, Gustafsson et al., 2013). Interestingly, KDs of *foxc1* genes in zebrafish induce disorganised basement membrane formation (Skarie and Link, 2009). Further discussion of the role of the Foxc1 pathway in BBB formation will be provided in Chapter 3.

1.5 Haematopoiesis

Haematopoiesis is the process by which all blood cellular components are made. Haematopoiesis occurs concomitant with the development of the vasculature. There are two waves of haematopoiesis in vertebrates, the first being a transient primitive wave, or embryonic haematopoiesis, followed by a definitive, or adult wave of haematopoiesis. The primitive wave gives rise to haemangioblasts, primitive erythrocytes and erythromyeloid progenitors from the LPM, intermediate cell mass and posterior blood island (PBI), whereas the definitive wave occurs in the aorta-gonad-mesonephros (AGM), which gives rise to haematopoietic stem cells (HSCs) (Chen and Zon, 2009). During mammalian embryogenesis, embryonic globin synthesis in primitive blood is essential for development of the organism before the definitive wave is established (Palis et al., 1999). Conversely, zebrafish can survive without any primitive blood (Chen and Zon, 2009, Goessling and North, 2011). Definitive haematopoiesis is initiated with the emergence of HSCs. HSCs are vital but rare cells capable of self-renewal and generate all adult blood lineages throughout the life of organisms. After definitive haematopoiesis initiates, primitive blood cells are gradually replaced by the definitive blood, which will maintain the blood supply during adulthood (Medvinsky et al., 2011).

1.5.1 Haematopoiesis overview and haematopoietic stem cell origins

Studies on haematopoiesis have been performed using various animal models including chick, mouse, amphibian and zebrafish. However, our understanding of the mechanisms which control haematopoiesis remain incomplete (reviewed in (Medvinsky et al., 2011, Ciau-Uitz and Patient, 2016)).

In mammals, the first haematopoietic organ is the yolk sac, which contributes to primitive haematopoiesis extra-embryonically (Fig. 1.6) (Moore and Metcalf, 1970). The intra-embryonic haematopoietic origin, termed AGM (Fig. 1.6 B, C), was first identified in chick-quail chimeras (Dieterlen-Lievre, 1975), and has been proposed to be the dominant haematopoietic site for definitive blood lineages (Medvinsky and Dzierzak, 1996, Muller et al., 1994). Additional haematopoietic sites involved in haematopoietic development have been identified, which include the fetal liver, thymus, spleen and bone marrow (Fig. 1.6 C). The exact contributions of these haematopoietic organs still remain debatable (Medvinsky et al., 2011). Disagreement exists about whether mammalian definitive haematopoiesis initiates in the placenta (Gekas et al., 2005, Ottersbach and Dzierzak, 2005, Robin et al., 2009, Medvinsky et al., 2011). The placenta has been

shown to be the niche for definitive HSCs in many studies (Robin et al., 2009, Gekas et al., 2005, Ottersbach and Dzierzak, 2005). However, the possibility that definitive HSCs derive from the internal AGM and then colonise the placenta to contribute to the subsequent proliferation of these cells cannot be excluded (Medvinsky et al., 2011).

The very first definitive haematopoietic activity was detected in the AGM (Medvinsky and Dzierzak, 1996), however, the possibility that the mammalian yolk sac contributes to definitive haematopoiesis has not been excluded (Medvinsky et al., 2011). Several studies have defined the origin of the HSC within the ventral wall of the DA (Bertrand et al., 2010, Boisset et al., 2010, Kissa and Herbomel, 2010). The ECs with the potential of giving rise to HSCs are called haemogenic endothelium (Lancrin et al., 2009). After HSCs enter the blood circulation, they colonise haematopoietic niches, firstly, the fetal liver, prior to undergoing further differentiation and proliferation (Fig. 1.6 C) (Cumano and Godin, 2007). HSCs will subsequently seed the thymus followed by the bone marrow where they reside throughout the life of the organism (Orkin and Zon, 2008, Medvinsky et al., 2011, Cumano and Godin, 2007). In zebrafish, as in mammals, HSCs are derived from the ventral wall of the DA (Fig. 1.7 A1) (Bertrand et al., 2010). After entering the blood circulation, HSCs seed the caudal haematopoietic tissue (CHT) at around 36hpf (Fig. 1.7 A2) (Murayama et al., 2006, Tamplin et al., 2015). In zebrafish, this represents an intermediate vascular niche for HSC proliferation and maturation and is equivalent to the mammalian fetal liver (Fig. 1.6 C) (Murayama et al., 2006). Subsequently, zebrafish HSCs will colonise the thymus and then the kidney, which is equivalent to the mammalian bone marrow (Fig. 1.7 A3, 1.6 C) (Murayama et al., 2006, Medvinsky et al., 2011).

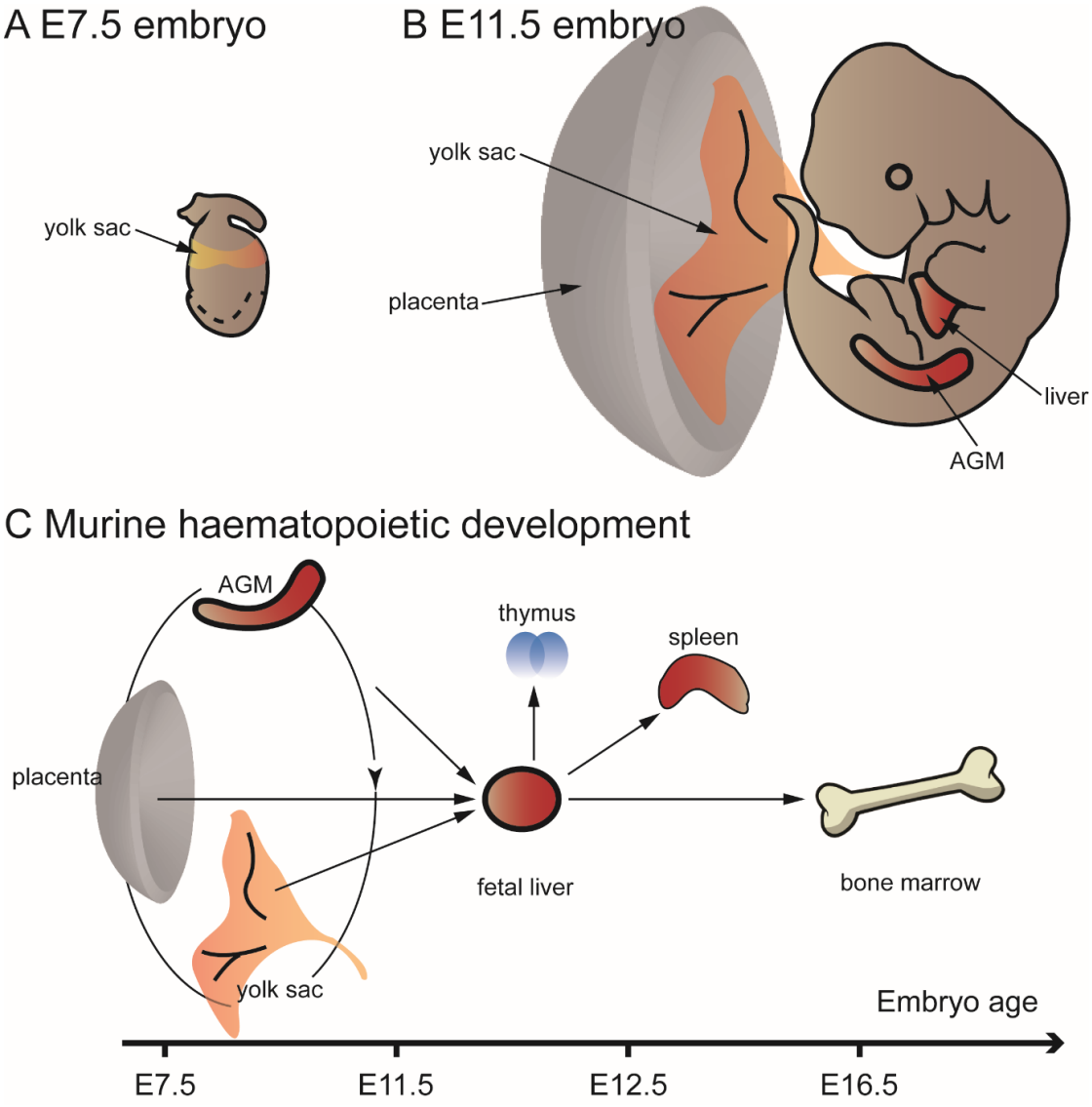

Figure 1.6 Murine haematopoietic development

Illustration of murine haematopoietic development, adapted from (Medvinsky et al., 2011). (A) Illustration of E7.5 murine embryo (anterior to the left). (B) Illustration of E11.5 murine embryo. (C) Illustration of murine haematopoietic development timeline. AGM, aorta-gonad-mesonephros.

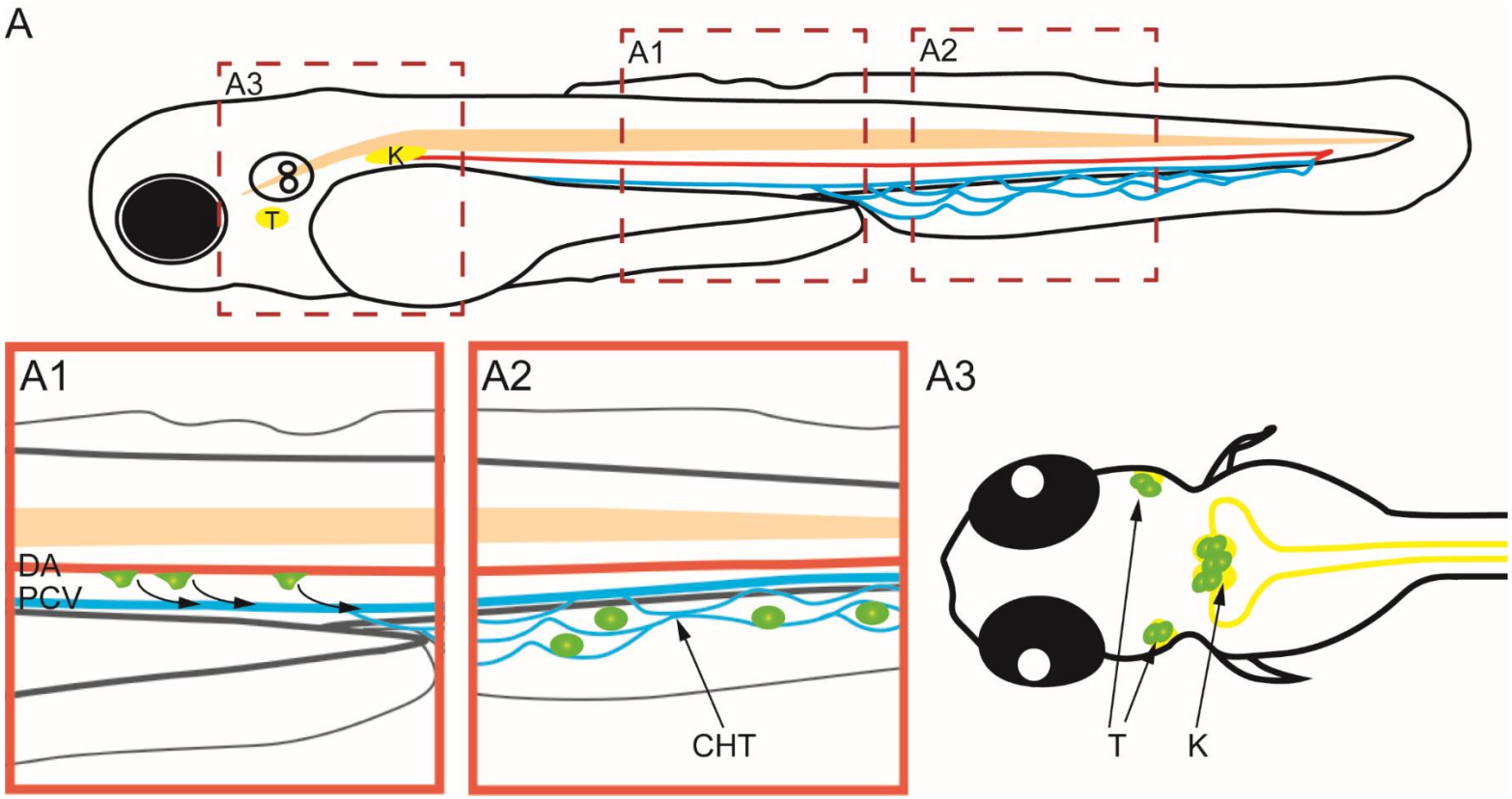

Figure 1.7 Haematopoiesis in zebrafish

(A) Illustration of lateral view of multiple haematopoietic tissues in zebrafish. (A1) Illustration of how HSCs (green cells) derive from the ventral wall of the DA and enter blood circulation. (A2) Illustration of HSC seeding the CHT at 36hpf followed by proliferation of HSCs. (A3) Illustration shows HSCs migrating and colonising the thymus and kidney, which will provide all kinds of blood lineages through adulthood. T, thymus; K, kidney; DA, dorsal aorta; PCV, posterior cardinal vein; CHT, caudal haematopoietic tissue.

1.5.2 Notch signalling and haematopoiesis

The requirement for Notch signalling in HSC formation is well established (Caolo et al., 2012, Kumano et al., 2003). In zebrafish, Notch-deficient *mib* mutants, show failure in HSC specification (Burns et al., 2005, Bertrand et al., 2010). Similar abnormalities have also been observed in mammalian *mib* mutants (Yoon et al., 2008). Signalling pathways upstream of Notch including Shh (Wilkinson et al., 2009, Lawson et al., 2002, Gering and Patient, 2005) and VEGF (Gering and Patient, 2005, Rowlinson and Gering, 2010) are essential to promote Notch expression in arteries and thus induce HSC emergence. In addition, Bmp4 signalling contributes to induction of HSC gene expression programs independently of arterial fate in zebrafish and mammals (Wilkinson et al., 2009, Kobayashi et al., 2014, Souilhol et al., 2016). Induction of *tgfb1a*/ *b* by Vegfa-Kdrl/ Kdr signalling is important to specify HSCs within haemogenic endothelium (Monteiro et al., 2016).

The Notch1 receptor is a major regulator of HSC specification (Kumano et al., 2003, Hadland et al., 2004). Murine and zebrafish *Notch1* mutants display reduced HSC formation (Kumano et al., 2003, Hadland et al., 2004, Kim et al., 2014), whereas *Notch2* appears to be dispensable for this process (Kim et al., 2014, Kumano et al., 2003). Recently, the Notch1-medicated Foxc2 pathway was proposed as a novel signalling pathway for HSC formation in mice (Jang et al., 2015). This will be further described in Chapter 4.

In addition to the cell-autonomous Notch pathway which specifies HSCs, Notch signalling is also involved in HSC emergence via a non-cell-autonomous manner in zebrafish (Clements et al., 2011). In zebrafish, there are 5 homologues of the mammalian Delta/ Delta-like ligands, namely *dla, -b, -c, -d* and *dll4*. Non-canonical Wnt (*wnt16*) signals within the developing somites to induce *dlc*/ *dld* expression, which further contribute to Notch signalling activation in migrating angioblasts and promote their HSC potential during vasculogenesis and haematopoiesis (Clements et al., 2011). This elegant Notch transduction between the somite and angioblast is facilitated by the interaction between Jam1a and Jam2a, which are junctional adhesion molecules (Kobayashi et al., 2014). Further evidence provided by the Traver lab suggests Notch3 functions downstream of the Wnt16-Dlc/ Dld pathway to specify HSCs (Kim et al., 2014). However, it remains unclear how this Notch3 somitic pathway functions to contribute to haematopoiesis (Kim et al., 2014). Recently, R-spondin 1 has been shown to function upstream of both Wnt16-Dlc/ Dld and Vegfa-TGFβ pathways, thus also positively regulating HSC formation (Genthe and Clements, 2017).

1.6 Aims and Objectives

The aims of this project were to determine the mechanism by which *foxc1a* and *foxc1b* control blood vessel formation and how the GPCR Calcrl controls blood vessel formation and function. In the following chapters we will address the following questions:

1. How do *foxc1a* and *foxc1b* control angiogenesis?

2. With which cell signalling pathways do *foxc1a* and *foxc1b* interact to regulate angiogenesis?

3. How does *calcrl* regulate the formation and function of blood vessels in zebrafish?

4. Is *calcrl* function important for normal lymphangiogenesis and/ or vascular integrity?

By understanding the regulatory roles of both Foxc1 and Calcrl pathways *in vivo*, we will gain novel insights into blood vessel formation which may ultimately be exploited for therapeutic benefit.

CHAPTER 2

Materials & Methods

2.1 Materials

2.1.1 Zebrafish husbandry

All fish were kept between 24°C and 30°C, at pH7.5. The aquarium system operated on a 14-hour light and 10-hour dark cycle. Zebrafish were fed with artemia. Breeding was performed by either pair mating or by group-laying (marbling). Zebrafish husbandry was undertaken by the NACWO team of The University of Sheffield. All zebrafish experiments were performed in accordance with UK home office guidelines.

2.1.2 Wild-type strains

AB, LWT and Nacre strains were used.

2.1.3 Transgenic lines

Transgenic lines used in this thesis are listed below.

Transgenic lines	Tissue labelling	References
Tg(fli1a:EGFP)^{y1}	Endothelial GFP	(Lawson and Weinstein, 2002b)
Tg(-0.8flt1:enhRFP)^{hu5333}	Arterial RFP	(Bussmann et al., 2010)
Tg(gata1a:DsRed)	Erythrocyte RFP	(Traver et al., 2003)
Tg(gfi1aa:GFP)^{Qmc551}	Haematopoietic stem cells and progenitor cells GFP	(Thambyrajah et al., 2016)
Tg(fli1a:LifeACT-mClover)^{sh467}	Endothelial filopodia GFP	Generated by Mr Aaron Savage
Tg(kdrl:HRAS-mCherry)	Vascular membrane RFP	(Hogan et al., 2009a)
Tg(sm22ab:mcherry)	Smooth muscle RFP	Generated by Dr Robert Wilkinson
Tg(flk1: EGFP-NLS)^{zf109}	Nuclei localised endothelial GFP	(Zygmunt et al., 2011)

Tg(dll4in3:GFP)	Arterial endothelial cell specific GFP	(Sacilotto et al., 2013)
Tg(hs:Gal4; UAS-NICD)	Heat-shock induced gain of function of notch signalling	(Scheer and Campos-Ortega, 1999)

Table 2.1: Transgenic line information.

2.1.4 Mutant lines

Mutant lines used in this thesis are listed below, homozygotes lethal mutants were generated by heterozygotes incross.

Mutants lines	Mutation	Generated by	Mutagenesis Approach
foxc1a^{sh356}	4bp insertion	Dr Robert Wilkinson	TALENs
foxc1b^{sh408}	13bp deletion	Dr Robert Wilkinson	CODA ZFNs
foxc1b^{sh409}	7bp deletion	Dr Robert Wilkinson	CODA ZFNs
calcrla^{sh404}	1bp deletion	Dr Robert Wilkinson	TALEN
calcrla^{sh405}	1bp deletion	Dr Robert Wilkinson	TALEN
calcrlb^{sh468}	8bp insertion 7bp deletion	Ms Zhen Jiang	CRISPR/CAS9
calcrlb^{sh469}	4bp deletion 10bp insertion	Ms Zhen Jiang	CRISPR/CAS9
calcrlb^{sh487}	7bp deletion 3bp insertion	Ms Zhen Jiang	CRISPR/CAS9

Table 2.2: Mutant allele information.

2.1.5 Mutant Genotyping

Mutants lines	Enzyme used	WT band size	Mutant band size
foxc1a^{sh356}	NsiI	186bp	119bp + 71bp
foxc1b^{sh408}	NdeI	130bp + 98bp	215bp
foxc1b^{sh409}	NdeI	130bp + 98bp	221bp

calcrla^{sh404}	DrdI	71bp + 78bp	149bp
calcrla^{sh405}	DrdI	71bp + 78bp	149bp
calcrlb^{sh468}	BslI	333bp + 68bp	402bp
calcrlb^{sh469}	BslI	333bp + 68bp	407bp
calcrlb^{sh487}	BslI	333bp + 68bp	397bp

Table 2.3: Mutant genotyping information

2.1.6 Solution and buffers

All chemicals were from Sigma-Aldrich®, unless otherwise stated.

Solutions and buffers	Ingredients
20X SSC	300mM Na3Citrate; 3M NaCl.
1X E3	5mM NaCl, 0.17mM KCl, 0.33mM CaCl2, 0.33mM MgSO4, 10-5 % Methylene Blue
4% Paraformaldehyde	4% PFA in 1X PBS
1X TAE	40mM Tris-Cl, 20mM Acetate and 1mM EDTA
BCL buffer III	100mM Tris-Cl pH:9.5; 50mM MgCl2; 100mM NaCl; 0.1% Tween 20
Hybridisation buffer +/+	50% Formamide; 5X SSC; 50µg/ml Heparin; 500µg/ml tRNA; 0.1% Tween 20
Hybridisation buffer -/-	50% Formamide; 5X SSC; 0.1% Tween 20
Maleic acid buffer (MAB)	For 500mL stock: 5.8g maleic acid, 1.5M NaCl, pH: 7.5,
Blocking reagent	MABtw containing 2% block reagent (from Roche)
Blocking with antibody	0.02% Anti-Digoxigenin-AP in MABtw containing 2% blocking reagent (from Roche)
Bleaching solution	0.5X SSC, 5% formamide, 1% H2O2

0.5M EDTA	For 500mL stock: 93.06g disodium EDTA in milliQ water, pH:8.0
Phosphate buffered solution (PBS)	Made up from the 10X stock (from Thermo Fisher)
Linker buffer	50mM Tris-Cl pH8.0, 100mM NaCl, 1mM EDTA
1% low melting point agarose gel for lightsheet mounting	1% Low melting point agarose gel in 1X E3 without methylene blue.
1% agarose gel	1% agarose gel in 1X TAE buffer containing 0.2-0.5µg/mL ethidium bromide.
3% agarose gel	1.5% agarose gel, 1.5% Metaphor agarose gel in 1X TAE buffer containing 0.2-0.5µg/mL ethidium bromide.
Pronase	1 in 10 dilution of 20mg/mL stock pronase
Proteinase K	10µg/mL proteinase K in PBStw
TE buffer	10mM Tris-Cl pH:8.0; 1mM EDTA
TES	10mM Tris-Cl pH:8.0; 1mM EDTA; 0.1M NaCl

Table 2.4: Solution and buffers

2.1.7 Probes for *in situ* hybridisation

Probes	template	Made by	Reference
calcrlb-both	PCR	Ms Zhen Jiang	This thesis
calcrlb-long	PCR	Ms Zhen Jiang	This thesis
cdh5	PCR	Dr Robert Wilkinson	Unpublished
cmyb	Plasmid	Dr Robert Wilkinson	(Thompson et al., 1998)
cxcl12b		Mr. Christopher Mayo	Unpublished
cxcr4a	Plasmid	Dr Sheng-Wei Chong	

dlc	Plasmid	Dr Robert Wilkinson	(Lawson et al., 2001)
dld	Plasmid	Dr Robert Wilkinson	
dll4	Plasmid	Dr Robert Wilkinson	
ephrinb2a	Plasmid	Dr Robert Wilkinson	(Lawson et al., 2001)
flt4	Plasmid	Dr Robert Wilkinson	(Thompson et al., 1998)
foxc1a	Plasmid	Dr Robert Wilkinson	IMAGE:6789584
foxc1b	Plasmid	Dr Robert Wilkinson	IMAGE:5601888
grl	Plasmid	Dr Martin Gering	
gata2a	Plasmid	Dr Robert Wilkinson	(Butko et al., 2015)
gata2b	Plasmid	Mr. Jack Adams	(Butko et al., 2015)
her12	PCR	Dr Robert Wilkinson	IMAGE: 6904047
mflt1	Plasmid	Dr Jenna Krueger	(Krueger et al., 2011)
msr	Plasmid	Dr Ellen van Rooijen	IMAGE: 6795347
notch1b	Plasmid	Dr Martin Gering	(Butko et al., 2015)
notch3	Plasmid	Dr Robert Wilkinson	
pax1a	Plasmid	Dr Wilson Clements	(Clements et al., 2011)
pax9	Plasmid	Dr Wilson Clements	(Clements et al., 2011)
pdgfrb	Plasmid	Dr Yuying Wang	(Wang et al., 2014)
rag1	Plasmid	Dr Robert Wilkinson	(Wilkinson et al., 2009)
runx1	Plasmid	Dr Robert Wilkinson	(Kalev-Zylinska et al., 2002)
sflt1	Plasmid	Dr Jenna Krueger	(Krueger et al., 2011)
snai1b	Plasmid	Dr Wilson Clements	(Clements et al., 2011)

snai2	Plasmid	Dr Wilson Clements	(Clements et al., 2011)
sox18	PCR	Dr Robert Wilkinson	Unpublished
sox7	PCR	Dr Robert Wilkinson	IMAGE: 7045912
tbx20	plasmid	Dr Robert Wilkinson	(Wilkinson et al., 2012)
twist1b	plasmid	Dr Wilson Clements	(Clements et al., 2011)
twist2	Plasmid	Dr Wilson Clements	(Clements et al., 2011)
vegfc	Plasmid	Dr Robert Wilkinson	(Hogan et al., 2009b)
wnt16	PCR	Dr Robert Wilkinson	(Wilkinson et al., 2012)
wnt5b		Dr Montserrat Garcia Romero	(Montserrat Garcia Romero, PhD thesis, University of Sheffield)
xirp1	Plasmid	Dr Cecille Otten	(Otten et al., 2012)
xirp2a	Plasmid	Dr Cecille Otten	(Otten et al., 2012)

Table 2.5： Probes for *in situ* hybridisation

2.1.8 Primers used

Primer name	Sequences
CRISPR-F	5’- GCGTAATACGACTCACTATAG-3’
CRISPR-R	5’-AAAGCACCGACTCGGTGCCAC-3’
calcrlb-both-F	5’-ACTGTTGGCAACCTCTGAGT-3’
calcrlb-both-R	5’-ACATGAGGTGCTTCTCT-3’
calcrlb-ex4-bslIF	5’-TGCACTAATTCGGGCCATTG-3’
calcrlb-ex4-bslIR	5’-CATCATTGTGGGCTCAAGATCA-3’
calcrlb-FL-F	5’-GGATCCATGGATAGATGCTGCATTACC-3’

calcrlb-FL-R	5’-CTCGAGTCACATGTACAGGTTGTCTG-3’
calcrlb-large-F	5’-CCTGCATTCATCCACGCAAT-3’
calcrlb-large-R	5’-CATGTGACCGTCAATGCTGT-3’
foxc1a-F	5’-TACATCAGCGACCAAAG-3’
foxc1a-R	5’- GTAGCTGTACGGGGGTTTCA-3’
foxc1b-F	5’-GCCTTATATCCCCGGAGACC-3’
foxc1b-R	5’-TCGGATGAGTTCTGGATGGC-3’
sox18-FL-F BamHI	5’-GGATCCATGAATATATCTGAGTCTAGTTGC-3’
sox18-FL-R ClaI	5’-ATCGATTTATCCTGTAATGCAGGC-3’
sox7-FL-F ClaI	5’-ATCGATATGGCGGCTCTGATAAGTG-3’
sox7-FL-R XhoI	5’-CTCGAGTTATGAAATGCTGTAGTTGTTC-3’

Table 2.6： Primers used

2.1.9 Tested CRISPR and Morpholino

Name	CRISPR targeting sequence	Designed by	Additional info
calcrlb-ex2-1	CTCTCAGAGAACAGCACTGGAGG	Ms Zhen Jiang	
calcrlb-ex4-2	GGAGTAATTACACCGACTGTAGG	Ms Zhen Jiang	
ramp2b ex5-mwoI	CCG GCATTGCAGGCTGCTTTTAC	Dr Marcus Keatinge	
ramp2b ex5-BslI	CTTTTACCCAAACCATGTGGTGG	Dr Marcus Keatinge	
foxc1a new 1	AAATACGGTGGACTCTGTGGTGG	Ms Zhen Jiang	Not working with CRISPRi

foxc1a new 2	AACTTCTAAACGCTAAGCATCGG	Ms Zhen Jiang	Not working with CRISPRi
foxc1a new 3	ATGCGCGCTCCGAGAGAAAGAGG	Ms Zhen Jiang	Not working with CRISPRi
foxc1a CRISPR 5'UTR-MwoI:	AGAGGAGGCGCATTTCAAGCAGG	Ms Zhen Jiang	Not working with CRISPRi
foxc1a CRISPR 1-BsrI:	GTCTCCAGTCCCAACTCGCTGGG	Ms Zhen Jiang	Not working
foxc1a CRISPR 2-BslI:	GCCGCCGGAGGGGGGTACACCGG	Ms Zhen Jiang	Not working
Ramp2b-ex4-1	GTACTATCGACGAGCAGAACTGG	Ms Zhen Jiang	Not working
Ramp2b-ex4-2	GAACTGGTGTGTTATGGAGGTGG	Ms Zhen Jiang	Not working
foxc1a-cilia paper	GGGTGGAAGGGATGCTGTGCGG	(Chen et al., 2017)	Not working with CRISPRi
foxc1b-cilia paper	GGCGGCATGGCTCGCGCATAGG	(Chen et al., 2017)	Not working with CRISPRi
vegfc-ATG-Mo	GAAAATCCAAATAAGTGCATTTTAG	(Hogan et al., 2009a)	0.4ng was injected
tnnt2 blocking Mo	CATGTTTGCTCTGACTTGACACGCA	(Sehnert and Stainier, 2002)	4ng was injected
Standard control Mo	CCTCTTACCTCAGTTACAATTTATA	(Lee et al., 2002)	

Table 2.7: Tested CRISPR and morpholinos

2.2 Methodology

2.2.1 Preparation of DNA

2.2.1.1 Genomic DNA extraction

Genomic DNA was extracted using 50mM NaOH. Tissue sample or embryos were incubated with 20-50µL 50mM NaOH at 95°C for 10mins in PCR machine. After incubation, samples were neutralised by 10% of total volume of 1M Tris-Cl pH 8.0 (Wilkinson et al., 2013).

2.2.1.2 Bacterial transformation and culture

50µL NEB10β chemically competent *Escherichia coli* were thawed on ice for 10mins prior to transformation. 1-3µL plasmid sample was added to competent cells followed by gentle mixing. The mixture was then cooled on ice for 30mins before 30s heatshock at 42°C followed by 5mins cooling on ice. 950µL LB was added into mixture directly with gentle mixing. This was then cultured in shaking incubator for at least 1 hour before plating out on LB agar plates, which contained corresponding anti-biotics. LB agar plates were incubated overnight at 37°C.

2.2.1.3 Mini and midi prep isolation of plasmid DNA

Plasmid DNA extraction from culture was performed with QIAGEN® mini Kit or Nucleobond® Plasmid midi Kit for small or medium scale culture respectively. Experiments were performed according to manufacturer's instructions.

2.2.2 Manipulation of DNA

2.2.2.1 DNA sequencing

All Sanger DNA sequencing was performed by the Medical School sequencing facility of the University of Sheffield. For purification of PCR products, see section 2.2.2.5.

2.2.2.2 Restriction enzyme digestion

All enzymes and digestion buffers were from New England Biolabs (NEB), unless otherwise stated. Restriction enzyme digestion was set up according to manufacturer's instructions, with exception of mutant genotyping where digestions were performed within PCR Reddymix™.

2.2.2.3 Preparation of total RNA extracted from zebrafish embryos

TRIZOL® Reagent was used to extract total RNA from 24hpf zebrafish embryos according to manufacturer's instructions.

2.2.2.4 PCR and electrophoresis

PCR was performed in a total reaction volume of 20µL, containing 10µL 2x Reddymix™ PCR Master Mix (Thermo), 1µL 10µM forward primer, 1µL 10µM reverse primer, 1-2µL gDNA template and milliQ water.

Standard cycling parameters were as follows: 94°C for 3mins, (94°C for 30s, 55°C for 30s, 72°C for 30s) (bracketed steps were repeated for 35 cycles), 72°C for 3mins and 12°C hold. The annealing and extension temperature and period may vary for different primer sets.

PCR products were verified for size by electrophoresis on 1% agarose under 120V with 1X TAE buffer containing ethidium bromide.

2.2.2.5 PCR purification prior to sequencing

PCR products were ExoI/SAP purified prior to sequencing using the following protocol:

Reaction Mix: 5µL PCR product, 1µL SAP, 0.25µL ExoI, 3.95µL milliQ water. Reaction was incubated at 37°C for 45mins followed by 80°C incubation for 15mins within a PCR machine.

2.2.2.6 PCR purification using QIAquick® PCR Purification Kit

PCR purification was carried out using QIAquick® PCR Purification Kit according to manufacturer's instructions.

2.2.2.7 PCR gel extraction using QIAquick® Gel Extraction Kit

PCR gel extraction was carried out by using the QIAquick® gel extraction Kit according to manufacturer's instructions.

2.2.2.8 Construction of *in situ* probes from plasmid

a. Plasmid linearisation and precipitation

Probe name	vector	antibiotic	antisense linearisation	antisense polymerase
calcrlb-both	PGEMT-easy	Amp	SacII	SP6
calcrlb-long	PGEMT-easy	Amp	SacI	T7
pax1a	PCRII	Amp+Kan	HindIII	T7
pax9	PCR4	Amp	XbaI	T7
pdgfrb	PCS2	Amp	smaI	T7
snai1b	PCRII	Amp+Kan	NotI	SP6
snai2	PCRII	Amp+Kan	NotI	SP6
twist1b	PCRII	Amp+Kan	NotI	SP6
twist2	PCRII	Amp+Kan	BamHI	SP6
xirp1	PGEM-TEasy	Amp	SalII	Sp6
xirp2a	PGEM-TEasy	Amp	NsiI	T7

Table 2.8: Plasmids used to synthesise probes

After linearisation, the digestion mixture was made up to 400µL with milliQ water. Plasmid DNA was then extracted by 400µL phenol:chloroform:soamylalcohol (25:24:1) and 400µL chloroform:isoamylalcohol (24:1) successively. After 5mins centrifuge spinning at max speed, supernatant was transferred to a fresh tube. 40µL 3M NaAC or 10M NH_4AC and 1mL 100% Ethanol were added into the supernatant to precipitate DNA. The mixture was vortexed thoroughly, followed by incubation for 30mins at -20°C. To pellet the DNA, samples were centrifuged for 30mins at maximum speed. After removal of supernatant, DNA pellets were washed with 70% ethanol followed by 5mins centrifugation at maximum speed. DNA pellets were then air dried and re-suspended in 20µL milliQ water and stored at -20°C for future usage.

b. *In vitro* transcription

Transcription was performed in a 20µL reaction volume containing 2µL linearised plasmid DNA template, 4µL 5x transcription buffer, 2µL 10X Anti-Digoxigenin-labelling, 0.5µL rRNAse-inhibitor,

1µL corresponding RNA polymerase (See table 2.8) and MilliQ water. Reaction mixtures were incubated in 37°C water bath for at least 2 hours prior to precipitation (See section 2.2.2.8.c).

c. Probe RNA precipitation

After transcription, 1µL DNAse was added into the sample followed by 15mins incubation at 37°C in a water bath to digest the DNA template. To stop the reaction, 1µL of 0.5M EDTA and 80µL milliQ water were added into the mixture followed by addition of 33µL 10M NH_4AC or 3M NaAC and 350µL ice cold 100% ethanol. Mixture was vortexed well prior to chilling at -20°C for 2 hours to precipitate RNA followed by 30mins centrifugation at maximum speed at 4°C. After removal of supernatant, RNA pellet was washed with 70% ethanol followed by 10mins centrifugation at maximum speed at 4°C. Resulting pellets were air dried and re-suspended in 100µL milliQ water and stored at -20°C for future use.

2.2.2.9 Construction of *in situ* probes from PCR templates

a. RT-PCR

SuperScript™III One-Step RT-PCR System from Invitrogen was used for RT-PCR according to manufacturer's instructions, in a 20µL volume with 2µL RNA template (See section 2.2.2.3).

b. Gel extraction

See section 2.2.2.7

c. Transcription

See section 2.2.2.8.c

2.2.2.10 In vitro synthesis of full length mRNA

a. RT-PCR

See section 2.2.2.9.a

b. Gel extraction

See section 2.2.2.7

c. DNA ligation into pGEM®-T Easy vector

pGEM®-T Easy vector system was used. DNA ligation was set up according to manufacturer's instructions. Ligation was performed either at room temperature for 2 hours or 4°C overnight.

d. DNA ligation into pCS2+

Ligation into pCS2+ expression vector was performed in a 20µL reaction volume containing pCS2+ vector: insert DNA in a 1:3 ratio, 1µL T4 ligase, 2µL 10X T4 ligase buffer and MilliQ water.

e. Transformation and plasmid DNA extraction

See section 2.2.1.2 and 2.2.1.3. Prior to ligation into pCS2+ vector, insert DNA was excised from pGEM®-T with corresponding enzymes and purified with QIAquick® Gel Extraction Kit (See section 2.2.2.7).

f. *In vitro* transcription of full-length mRNA

Prior to transcription, the PCS2+ plasmid containing DNA insert was linearised with NotI, after complete linearisation, the linearised plasmid was extracted with phenol/chloroform extraction (See section 2.2.2.8.a/ b).

Transcription of full length mRNA was performed with mMESSAGE mMACHINE® Transcription Kit according to manufacturer's instructions.

g. Phenol/ chloroform extraction of full-length mRNA

After transcription 115µL milliQ water and 15µL 10M NH_4AC were added into the mixture to stop the reaction. RNA was successively extracted by same volume of phenol:chloroform:isoamylalcohol (25:24:1) and chloroform:isoamylalcohol (24:1). After recovery of equeoss phase, supernatant was transferred to fresh tube. RNA was then precipitated by adding 1 volume of isopropanol and mixed throughly. The mixture was then chilled at -20°C for 15mins and followed by 15mins centrifugation at maximum speed to pellet RNA. The supernatant was carefully removed before air drying and then resuspended with 20µL milliQ water.

2.2.2.11 Construction of multisite Gateway® constructs

Multisite gateway LR reaction was set up with 10 fmoles of each entry clone, 20 fmoles of destination vector and 2µL of LR Clonase™ II Plus enzyme mix. This reaction mix was made up

with TE buffer to 10µL followed by overnight incubation at 25°C. To terminate the reaction, 1µL of the Proteinase K was added into the solution and incubated at 37°C for 10mins. Resulting reactions were transformed into chemically competent *E.coli* as described in section 2.2.1.2.

2.2.3 Manipulation of zebrafish embryos

2.2.3.1 Microinjection

a. Normal injection

Mo, full length mRNA, CRISPR and construct were directly injected into embryos at one cell stage.

b. Rhodamine Dextran injections

20µg dextran tetramethylrhodamine dextran (2,000,000 molecular weight) was injected directly into the common cardinal vein at both 2dpf and 3dpf or into the posterior cardinal vein at 3dpf.

2.2.3.2 Dechorionation of zebrafish embryos

Pronase treatment was used to dechorionate large batches of embryos, 1mL of stock pronase (20mg/mL) was diluted with 9mL E3, embryos were treated with pronase solution for 10-15mins before washed into E3. Manual dechorionation was also employed for both small batches of embryos and also young embryos.

2.2.3.3 Fixation and preparation of zebrafish embryos for *in situ* hybridisation

Embryos were fixed in 4% PFA in PBS either overnight at 4°C or at room temperature for 3 hours (embryos up to 15 somite stage were fixed in chorions and dechorionated prior to *in situ* hybridisation). After fixation, embryos were washed with PBStw 3X5mins followed by 25%, 50%, 75% and 100% methanol in PBStw wash 5mins each. Embryos were then stored at -20°C at least overnight.

2.2.3.4 Whole–mount *in situ* hybridisation

Whole–mount *In situ* hybridisation was performed as described previously (Thambyrajah et al., 2016, Wilkinson et al., 2012).

a. Day one

Dehydrated embryos were rehydrated through 75%, 50%, 25% Methanol in PBStw followed by 100% PBStw wash 4X5mins.

If embryos were older than 24hpf, they were treated with 10µg/ml Proteinase K for 20-45mins according to different stages. Proteinase K treatment was stopped by 2mg/ml glycine in PBStw wash 2X5mins followed by refixing in 4% PFA in PBStw for 20mins at room temperature. Embryos were then rinsed with PBStw 5X5mins with gentle agitation before washing with 50%PBStw;50% Hybe+/+ for 5mins. For pre-hybridisation, embryos were incubated in 100% Hybe+/+ for at least 1hour at 65°C. The pre-hybridisation solution was then be replaced by Hybe+/+ containing a 1:200 dilution of Probe, embryos were then incubated at 65°C overnight.

b. Day two

Hybe+/+ containing probe was removed from the sample, which can be re-used up to 6 times. Samples were then washed through 100%, 75%, 50%, 25% Hybe-/- in 2XSSC 10mins each followed by a 10mins 2XSSC wash and 0.2XSSC wash 4X15mins successively. All above washes were done at 65°C. Embryos were then be washed through 75%, 50%, 25% 0.2XSSC in MABtw, 5mins each at room temperature. 100% MABtw wash was applied to embryos before blocking with 2% Boehringer Blocking Reagent™ (Roche) in MAB for 1 hour with gentle agitation at room temperature. Block was then replace with anti-Digoxigenin antibody diluted in 2% Boehringer Blocking Reagent™ (Roche) in MAB and incubate at 4°C overnight with gentle agitation.

c. Day three

Embryos were further incubated in anti-Digoxigenin antibody diluted in 2% Boehringer Blocking ReagentTM (Roche) in MAB for 1 hour at room temperature, followed by MABtw wash 8X15mins at room temperature with gentle agitation. Samples were then washed with BCLIII buffer 3X5mins. Embryos were then washed into 50% BMpurple ™ (Roche);50% BCLIII for staining in dark. (Staining duration depends on the probe efficiency). After staining was properly developed, the reaction was stopped by 5mins BCLIII wash and then refixed with 4%PFA at room temperature for 3 hours or at 4°C overnight followed by PBStw wash 3X5mins in the dark.

Bleaching step was only applied to embryos with pigmentation by incubating embryos with bleaching solution at room temperature for 1-1.5 hour depends on the embryos stage, followed by PBStw wash 4X5mins. Embryos were long-term stored in 80% glycerol in PBS at room temperature in the dark.

2.2.3.5 Fluorescence-*in situ* hybridisation and immunostaining

a. Day one

See section 2.2.3.4.a.

b. Day two

Hybe+/+ containing probe was removed from samples, samples were then washed through 100%, 75%, 50%, 25% Hybe-/- in 2XSSC 30mins each followed by a 30mins 2XSSC wash and 0.2XSSC wash 2X30mins successively. All above washes were done at 70°C. Embryos were then washed through 75%, 50%, 25% 0.2XSSC in MABtw, 5mins each at room temperature with gentle agitation. 100% MABtw wash was applied to embryos before blocking with 2% Boehringer Blocking Reagent™ (Roche) in MAB for 1 hour with gentle agitation at room temperature. Block was then replaced with 1 in 400 diluted anti-Digoxigenin POD in 2% Boehringer Blocking Reagent™ (Roche) in MAB and 1 in 1000 diluted anti-GFP (Torrey Pines Biolabs), which was then incubated at 4°C overnight with gentle agitation.

c. Day three

Embryos were further incubated with MABtw wash 7X15mins and one 15mins PBStw washed successively at room temperature with gentle agitation. Samples were then stained with 100µL of 1:25 diluted Cy3 tyramide in amplification buffer (Perkin Elmer) for 30mins at room temperature, and then briefly washed with PBStw prior to PBStw 4X30mins wash.

For subsequent immunostaining. Embryos were treated with PBDT for 20mins and then incubated with 1 in 500 diluted anti-Rabbit Alexa 488 secondary antibody in PBDT for 2h (or overnight incubation at 4°C) with gentle agitation. Stained embryos were then washed through PBStw 4X15mins before 4% PFA fixation and another PBStw 4X5mins wash. Embryos with Fluorescence-*in situ* hybridisation and immunostaining were stored in PBStw at 4°C for a short period prior to imaging.

2.2.3.6 Fin clipping

Fin clipping was used to identify the genotype of adult zebrafish. A small amount of tissue was biopsied from the caudal fin. Zebrafish were maintained under light anaesthesia (4.2% Tricaine in aquarium water). After clipping, the processed fish was kept in an isolated tank until fully recovered.

2.2.3.7 Adult zebrafish wax sections

Adult fish were culled by overdose of anaesthetic (4.2% Tricaine in aquarium water) under schedule 1. After the onset of rigor mortis, zebrafish were transferred into 15mL freshly made 4% PFA for fixation at room temperature for 48h, followed by 15mL 0.5M EDTA decalcification at room temperature for 48h. Paraffin embedded tissue section were performed by Ms Fiona Wright of the core histology service, University of Sheffield.

2.2.3.8 Hematoxylin and eosin stain

Slides were dewaxed thoroughly in 2 changes of xylene 20mins each, followed by rehydration through graded alcohols 2X 100% ethanol 5mins; 1X 95% ethanol 5mins; 1X70% ethanol 5mins; running water 5mins. Slides were then stained with 50% haematoxylin for 3mins and then rinsed under running water until all residual staining solution was removed. Slides were then rinsed quickly in 0.1M TBS pH8 to 'blue' the nuclei. Prior to 30mins eosin staining, slides were rinsed well under running tap water. After removal of the residual staining solution by a quick rinse in water, slides were dehydrated quickly back through the graded alcohols 1X70% ethanol 3 dips; 1X95% ethanol 3 dips; 2X100% ethanol 3 dips, followed by 2X xylene wash 2mins each. Stained tissue slides were mounted with a xylene based mounting media.

2.2.3.9 Heat shock induction of UAS-NICD

Heat shock was performed at 18s by incubating embryos with pre-warmed E3 at 37°C for 30mins. Embryos were maintained at 28.5°C following heat shock prior to imaging.

2.2.3.10 Drug treatment

DAPT stock solution (10mM) was made up to 50µM with E3. Embryos were incubated in DAPT solution from budding stage (10hpf) up to 30hpf prior to image taking. Same concentration of DMSO was used as control treatment.

AV951 stock solution (10mM) was made up to 250nM with E3. Embryos were incubated in AV951 solution at budding stage (10hpf) up to 28hpf prior to image taking. Same concentration of DMSO was used as control treatment.

2.2.3.11 Mounting embryos prior to imaging

a. Flat mount *in situ* embryos

Early stage embryos were mounted on the tissue slide. Prior to the mounting, the yolk was removed gently using forceps. Embryos were then mounted in 80% glycerol.

b. Spinning disc confocal microscopy

Embryos were mounted in 0.7% or 1% Low melting point agarose gel in 1X E3 with 4.2% tricaine on coverslide.

c. Light sheet microscopy

Embryos were mounted in 1% Low melting point agarose gel in 1X E3 without methylene blue in capillary tube.

2.2.3.12 Imaging of zebrafish embryos

Microscopic imaging was performed using spinning disk (Leica DM IRE2 microscope) and ZEISS Lightsheet Z.1. Images were analysed using Velocity Version 6.0.1 (PerkinElmer) and ZEN respectively. Images of embryos following *in situ* hybridisation and using epifluorescence were taken using a Leica M165FC and Leica DFC and imaged using Leica Application Suite software (LAS v4.3.0).

2.2.3.13 Preparation of figures

Figure preparation was done using Adobe Photoshop CS6 and Adobe Illustration CS6.

2.2.4 CRISPR

2.2.4.1 CRISPR design

CRISPR design was performed using online tools http://crispr.mit.edu/ and http://chopchop.cbu.uib.no/

DNA ultramers were ordered from integrated DNA technologies according to protocols described previously (Hruscha et al., 2013).

2.2.4.2 CRISPR gRNA synthesise

CRISPR ultramers were amplified with CRISPR-gRNA primer set (sequences are provided in section 2.1.7) with 2µL Ultramer (100µM) template. PCR programme was set to 40cycles with 60°C annealing temperature. PCR products were then purified with QIAquick® PCR Purification Kit and eluted with 20µL EB buffer before checking on 1% agarose gel.

Transcription reactions were performed using MEGAshortscript™ T7 Transcription Kit, reaction was set up according to manufacturer's instructions with 1µL amplified Ultramer (>30ng), reaction mixture incubated at 37°C for at least 2 hours prior to 30mins DNAse purification at 37°C.

After transcription, the mixture was made up to 100µL with RNAse free water, and then ice cold 350µL ethanol and 33µL 10M NH_4AC were added. The mixture was vortexed and chilled at -20°C for 2 hours followed by 30mins centrifugation at 4°C at maximum speed. Pellet was washed with ice cold 70% ethanol before air drying and then resuspended with 7µL RNAse free water.

2.2.5 Genetic synteny analysis

Genetic synteny analysis was performed by our collaborators Dr Teri Evans and Dr Matt Loose, The University of Nottingham.

2.2.6 Statistical analysis

Statistical analysis was performed Using GraphPad Prism 6.

CHAPTER 3

Investigating the Role of *foxc1a* and *foxc1b* Transcription Factors in Cranial Blood Vessel Formation

3.1 Introduction

The Fork Head Proteins (previously known as Hepatocyte Nuclear Factor 3/ Winged Helix Proteins) were first identified as transcription factors by Weigel *et al.* in *Drosophila* (Weigel et al., 1989). More than 80 Forkhead box (*FOX*) genes have been identified in mammals (Kaufmann and Knochel, 1996). These proteins possess a highly conserved Forkhead DNA binding domain (Lai et al., 1993, Kaufmann and Knochel, 1996). In humans, *FOXC1* (previously known as *FKHL7*), located on chromosome 6p25, is mutated in cerebral small vessel disease which leads to stroke (French et al., 2014) and Axenfeld-Rieger syndrome, which results in skeletal defects and iris hypoplasia (Smith et al., 2000, Winnier et al., 1999, Mears et al., 1996, Nishimura et al., 1998). *FOXC1* has also been considered as a key therapeutic target for various types of breast cancer (Han et al., 2015, Han et al., 2017). *FOXC2* (previously known as *FKHL14*), on chromosome 16p22-24, is mutated in Lymphoedema distichiasis syndrome, which results in primary lymphoedema (Mellor et al., 2011, Kaestner et al., 1996, Miura et al., 1997). Therefore, understanding how these Fox transcription factors function is essential for future therapeutic benefits.

While many murine studies have shown that *Foxc1* and *Foxc2* are both required for cardiovascular development, the regulatory mechanisms remain largely unknown. Due to the limits of the viability of the mouse model, it has been difficult to gain information during embryonic development in real time. Zebrafish can survive without a functional cardiovascular system for up to 7 days, which makes it an excellent animal model to study blood vessel formation in real time *in vivo* (Sarmah and Marrs, 2016). Two *Foxc1* orthologues have been identified in zebrafish, *foxc1a* and *foxc1b*, while no orthologues for mammalian *Foxc2* exist in zebrafish based on sequence analysis (Topczewska et al., 2001b). In the literature the genetic/ functional orthology regarding *foxc1a* and *foxc1b* when compared to mammalian *Foxc1* or *Foxc2* remains unclear and inconsistent (Topczewska et al., 2001b, Veldman and Lin, 2012, Jang et al., 2015, Chen et al., 2017). Therefore, this project is designed to understand: (1) The genetic/ functional conservations between zebrafish *foxc1a*/ *foxc1b* and the mammalian *Foxc1*/ *Foxc2*. (2) The mechanisms by which *foxc1a* and *foxc1b* regulate different aspects of embryogenesis with a particular focus on blood vessel formation.

3.1.1 The role of mammalian *Foxc1* and *Foxc2* during blood vessel formation

Studies in mice have shown *Foxc1* is required for many aspects of blood vessel formation, including arteriovenous specification and early lymphatic development (Winnier et al., 1999, Siegenthaler et al., 2013, Seo et al., 2012, Haldipur et al., 2014, Kume et al., 2001). Rodent *Foxc1* expression can be detected in endothelial cells (EC) of the cardiovascular system, mesoderm and brain pericytes (Winnier et al., 1999, Siegenthaler et al., 2013). In *Foxc1* homozygous null mutants, cardiovascular abnormalities including interruption and coarctation of aortic arches and dysplasia of semilunar valves were observed, which contribute to their pre or perinatal death (Winnier et al., 1999). *Foxc1* has been demonstrated to be required for angiogenesis in the mouse fetal brain (Siegenthaler et al., 2013). Interestingly, the EC-conditional *Foxc1* knock-out (KO) mice are homozygous viable, no severe abnormal vasculature development was observed (Hayashi and Kume, 2008a). This data suggests that murine *Foxc1* is required for vascular development via a non-cell-autonomous manner. In addition to this pro-angiogenic function of *Foxc1*, another anti-angiogenic function was also identified in mice cornea (Koo and Kume, 2013, Schultz et al., 2013, Seo et al., 2012). Elegant experiments were performed to demonstrate that *Foxc1* secreted from the neural crest increases the expression of both matrix metalloproteases and the anti-angiogenic *sflt1* to inhibit angiogenesis in the cornea; Whereas the EC contribution of *Foxc1* does not affect cornea angiogenesis (Koo and Kume, 2013, Schultz et al., 2013, Seo et al., 2012). Taken together these data indicate that the different regulatory roles of murine *Foxc1* in blood vessel formation are non-cell-autonomous and cell type-dependent. Conditional KO of *Foxc1* in pericytes and vascular smooth muscle cells (vSMC) in mice resulted in an increased proliferation of both pericytes and vSMCs in the brain, which further led to cerebral haemorrhages and EC hyperplasia (Siegenthaler et al., 2013). This data suggests an important role of rodent *Foxc1* in maintaining or establishing blood vessel integrity.

Foxc2 also plays an essential role during cardiovascular development (Winnier et al., 1997, Iida et al., 1997), which shares largely overlapped expression with *Foxc1* in the paraxial mesoderm, mesenchyme and ECs of blood vessels (Winnier et al., 1999, Winnier et al., 1997). *Foxc2* homozygous null mutants exhibit pre or perinatal lethality with skeletal and cardiovascular defects including loss of intersegmental vessel (ISV) and defects in blood vessel maturation resulting in variable blood pooling, which could account for the lethality in *Foxc2* homozygous mutants (Winnier et al., 1997). These observations indicate that *Foxc2* is required for blood vessel formation and skeletogenesis during embryonic stage in mice (Winnier et al., 1997, Iida et al., 1997). Furthermore, *Foxc2* positively regulates tumour angiogenesis potentially via regulating the

matrix metalloproteases and VEGF signalling, which is opposite to the reported *Foxc1* function in mouse cornea (Sano et al., 2010, Koo and Kume, 2013, Schultz et al., 2013, Seo et al., 2012). *Foxc2* is also required for different aspects of lymphatic vessel formation (Liebl et al., 2015, Norrmen et al., 2009, Mellor et al., 2011, Ivanov et al., 2013, Sasahira et al., 2014). An *in vitro* study suggests that *Foxc2* increases the expression of *Prox1* to induce angiogenesis and lymphangiogenesis in human oral squamous cell carcinoma (Sasahira et al., 2014). In *Foxc2* homozygous mice, maturation of formed lymphatic vessels was affected (Norrmen et al., 2009). Norrmen *et al.* further demonstrated the interaction between murine *Foxc2* and *NFATc1* during this process (Norrmen et al., 2009). *Foxc2* potentially acts downstream of CDK5, which phosphorylates Foxc2 and positively regulates lymphatic vessel formation and valve formation (Liebl et al., 2015, Ivanov et al., 2013). Interestingly, unlike the expression of *Foxc1*, murine *Foxc2* cannot be detected in brain ECs at E14.5 (Siegenthaler et al., 2013). This difference in spatiotemporal expression between *Foxc1* and *Foxc2* was also reported in murine heart (Winnier et al., 1999), indicating a selective requirement of these two genes during different aspects of vascular development.

3.1.2 Interaction of *Foxc1* and *Foxc2* in blood vessel formation

The genetic interaction between mammalian *Foxc1* and *Foxc2* has been reported during various aspects of embryonic development (Winnier et al., 1999, Kume et al., 2000, Kume et al., 2001). Comparison between phenotypes of *Foxc1; Foxc2* compound heterozygotes and *Foxc1* heterozygotes revealed an interaction between *Foxc1* and *Foxc2* during cardiovascular development (Winnier et al., 1999, Kume et al., 2000). *Foxc1; Foxc2* double mutant mice exhibit similar phenotypes to *Foxc1* homozygous mutants but with much more pronounced abnormalities in cardiovascular system development (Kume et al., 2001, Seo et al., 2006). These data indicate that *Foxc1* and *Foxc2* work synergistically during these processes. Furthermore, *Foxc1* and *Foxc2* have identical DNA-binding domains and target specificities (van Dongen et al., 2000, Seo et al., 2006, Kume et al., 2000). These observations suggest that murine *Foxc1* and *Foxc2* have similar functions during cardiovascular development. Interestingly, Kume *et al.* further compared the phenotypes between *Foxc1*-/-; *Foxc2*+/- and *Foxc1*+/-; *Foxc2*-/-. Their data showed that *Foxc1* and *Foxc2* do not share the exact same gene functions (Kume et al., 2001), which could potentially be explained by the spatiotemporal difference in their expression patterns as mentioned in an earlier section (Winnier et al., 1999, Kume et al., 2001). *Foxc1*; *Foxc2* compound mutant mice also exhibited ectopic lymphangiogenesis, which was potentially caused by *Foxc1/ Foxc2* deficiency-mediated elevated ERK activity (Seo et al., 2006, Fatima et al., 2016). Interestingly, a novel vascular-restricted enhancer was discovered previously, which showed that

FOXC proteins co-operate with ETS transcription factors to induce endothelial-specific gene expression during various aspects of blood vessel formation (De Val et al., 2008). *In vitro* studies also showed that FOXC1 and FOXC2 directly activate the Dll4 and Hey2 promoters in cultured murine endothelial cells during blood vessel formation (Hayashi and Kume, 2008b, Seo et al., 2006). Taken together, these data provide evidence that *Foxc* genes regulate vasculature development cell-autonomously, which conflicts with previous murine data (Koo and Kume, 2013, Schultz et al., 2013, Seo et al., 2012).

3.1.3 Zebrafish *foxc1a* and *foxc1b* in blood vessel formation

Whole mount *in situ* hybridisation of *foxc1a* and *foxc1b* in zebrafish embryos showed an overlapping expression pattern in the paraxial mesoderm, presomitic mesoderm and vasculature during early embryonic development (Topczewska et al., 2001b, Skarie and Link, 2009). Early zebrafish studies of *foxc1a* and *foxc1b* were limited by using identical morpholinos (Mo) (Topczewska et al., 2001a, De Val et al., 2008, Skarie and Link, 2009, O'Brien et al., 2011, Veldman and Lin, 2012, Jang et al., 2015). However, the reported *foxc1a/ foxc1b* morphants' phenotypes are variable and inconsistent between studies due to dosage variability and Mo toxicity (Topczewska et al., 2001a, O'Brien et al., 2011, Veldman and Lin, 2012, Jang et al., 2015). Nevertheless, KD of *foxc1a* showed reduced ISV formation (De Val et al., 2008) and haemorrhages (Skarie and Link, 2009), indicating the *foxc1a* is required for blood vessel formation and maintaining vessel integrity and/ or stability. On the contrary, *foxc1b* morphants showed no obvious or a less profound phenotype when compared with *foxc1a* single morphants (De Val et al., 2008, Skarie and Link, 2009). Interestingly, in *foxc1a*; *foxc1b* double zebrafish morphants, disrupted arterial-venous specification, reduced trunk angiogenesis, haemorrhages and disorganised hyaloid vessels were observed (De Val et al., 2008, Skarie and Link, 2009). *foxc1a*; *foxc1b* double morphants showed more substantial abnormalities than those observed in *foxc1a* single morphants (De Val et al., 2008, Skarie and Link, 2009), which are similar to the phenotypes following loss of mammalian *Foxc1* and *Foxc2*, indicating there is functional conservation of these *Foxc* genes between mammals and zebrafish (Kume et al., 2001, Seo et al., 2006). Collectively, these data suggest functional redundancy between *foxc1a* and *foxc1b* during vasculature development.

During this project, several studies were published using independent zebrafish *foxc1a* mutants which report that *foxc1a* is required for anterior somite formation (Hsu et al., 2015, Li et al., 2015) and neural circuit development (Banerjee et al., 2015), which is in line with previous Mo studies

(Topczewska et al., 2001a). Similar phenotypes in *foxc1a* mutants (Hsu et al., 2015, Banerjee et al., 2015, Li et al., 2015) to *foxc1a* morphants were reported with smaller eyes, pericardial oedema and variable blood circulation defects but without haemorrhages (Skarie and Link, 2009). While several studies have shed light on *foxc1a* functions using mutant zebrafish (Hsu et al., 2015, Banerjee et al., 2015, Li et al., 2015), neither the genetic interaction between *foxc1a* and *foxc1b* nor their roles in vascular development have been addressed in *foxc1a* mutant backgrounds. In addition, many Mo studies reported variable and dose-dependent phenotypes suggesting the possibility of off-target effects caused by the published Mos (Topczewska et al., 2001a, De Val et al., 2008, Skarie and Link, 2009, O'Brien et al., 2011, Veldman and Lin, 2012, Jang et al., 2015).

3.1.4 Objectives

The aim of this project was to generate and utilise novel zebrafish mutants of *foxc1a* and *foxc1b* to determine: (1) how these genes transcriptionally regulate blood vessel formation; (2) to understand the conserved genetic functions of *Foxc* genes between mammals and teleosts during evolution.

This chapter will focus on the signalling pathways that are involved during cranial blood vessel formation and how *foxc1a*/ *foxc1b* interact with these to regulate angiogenesis within the developing brain. Here we report that *foxc1a* is required for both cranial vasculogenesis and angiogenesis by regulating the expression of different *vegf* receptors. In addition, our data also suggest a regulation of *sox7* and *sox18* by *foxc1a*/ *foxc1b* during cranial blood vessel formation and cranial lymphangiogenesis. While *foxc1a* is required for cranial angiogenesis, *foxc1b* is dispensable for this. Interestingly, *foxc1b* cooperates with *foxc1a* to contribute to major vessel formation in the head, suggesting that *foxc1a* but not *foxc1b* is a master regulator of cranial blood vessel formation in zebrafish. Furthermore, our observations suggest that the level of VEGF signalling perceived by endothelial cells within developing cranial vessels is critical to promote cranial angiogenesis.

3.2 Results

3.2.1 Generation of *foxc1a*^{sh356}, *foxc1b*^{sh408} and *foxc1b*^{sh409} mutant alleles

Unlike mammals, who possess two FOXC genes, zebrafish have two *Foxc1* orthologues (*foxc1a* and *foxc1b*) (Topczewska et al., 2001b), whereas no identifiable *Foxc2* orthologues exist in zebrafish (Fig. 3.1, 3.2). This data is in line with previously published sequence alignment of *foxc1a/ b* (Topczewska et al., 2001b), but contrary to report which claim *foxc1a* and *foxc1b* are orthologues of *Foxc2* (Jang et al., 2015).

foxc1a and *foxc1b* are single exon genes and encode proteins containing 476 and 433 amino acids respectively (Fig. 3.3) (Topczewska et al., 2001b). To investigate the function of zebrafish *foxc1a* and *foxc1b* during vascular development, *foxc1a* and *foxc1b* mutants were generated by Dr Robert Wilkinson using genome editing via Zinc Finger Nuclease and Transcription activator-like effector nuclease (TALEN) technologies respectively before I joined his lab. The *foxc1a*^{sh356} allele has a 4bp insertion at position 169 (CATG), which is predicted to retain the first 56 amino acids of wildtype (WT) Foxc1a before shifting frame (Fig. 3.3 A, B Boxed area), inducing a premature stop codon at amino acid position 71 after 14 incorrect amino acids (Fig. 3.3 A Red asterisk indicates stop codon). The *foxc1b*^{sh408} allele is predicted to contain the first 58 WT amino acids, then shifts frame due to a 13bp deletion (ΔCGCGCATATGGGC at position 172) (Fig. 3.3 C, D Boxed area), 10 incorrect amino acids and a termination codon were induced after this point, before the conserved Forkhead DNA binding domain (Fig. 3.3 C Red asterisk). *foxc1b*^{sh409} allele has a 7bp deletion (ΔGCATATG at positon 175) (Fig. 3.3 E, F Boxed area). *foxc1b*^{sh409} allele contains the first 58 amino acids of WT Foxc1b, then frame shifts truncating 12 amino acids after this point, before the conserved DNA binding domain (Fig. 3.3 E). The conserved Forkhead DNA binding domain is predicted to be lost in all *foxc1a*^{sh356}, *foxc1b*^{sh408} and *foxc1b*^{sh409} alleles, therefore these alleles are likely to represent severe loss of function or null mutations. All data in Chapter 3 and 4 were generated with *foxc1a*^{sh356} and *foxc1b*^{sh408} alleles, hereafter referred to as *foxc1a* and *foxc1b*, unless otherwise stated.

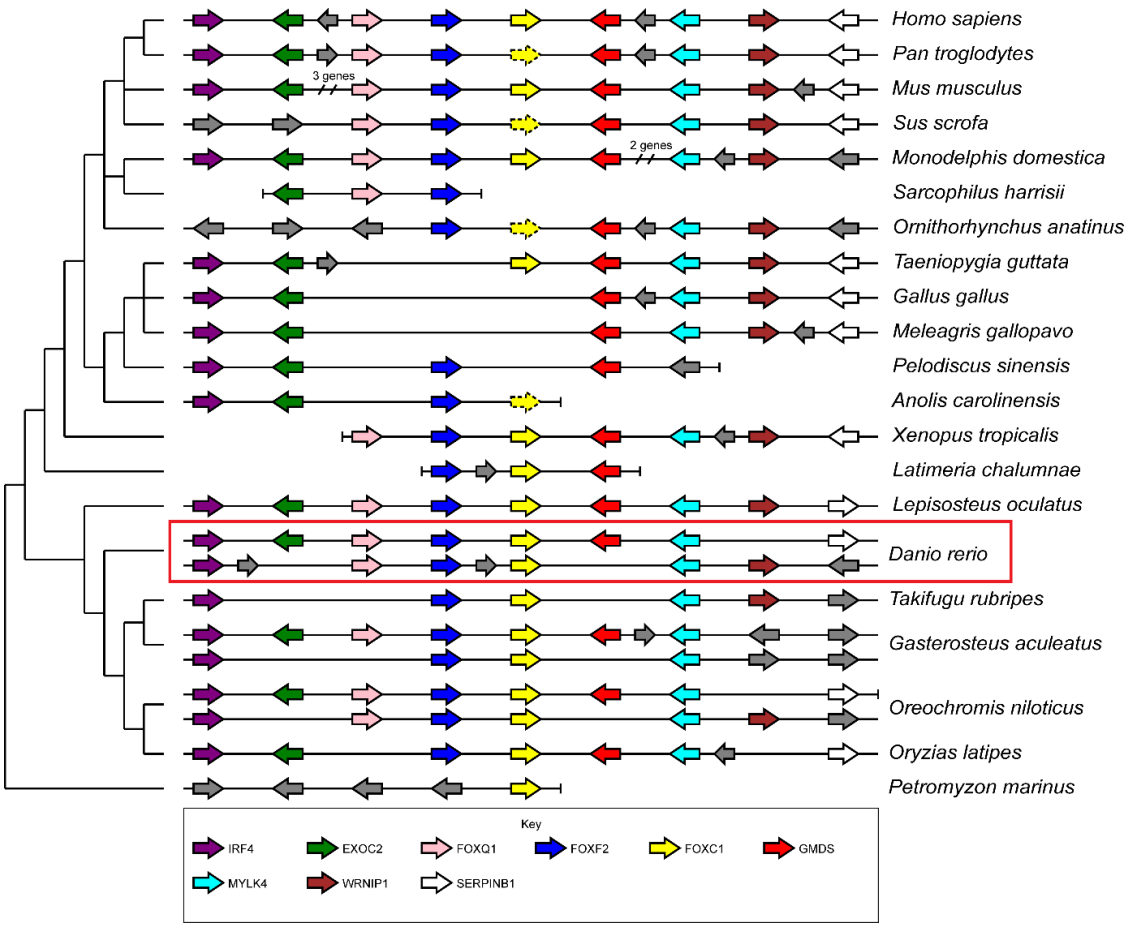

Figure 3.1 FOXC1 Synteny

The genomic region containing *Foxc1* has undergone duplication in teleost lineages, generating two orthologues of mammalian *Foxc1*, *foxc1a* and *foxc1b*. Arrow directions indicate corresponding DNA strand, predicted genes are represented as dotted arrows. At left are scaffold lines showing the relatedness of the individual species. Grey arrowheads represent non-conserved genes. Zebrafish lineage is shown in red boxed area. Data kindly provided by Dr Teri Evans, University of Nottingham.

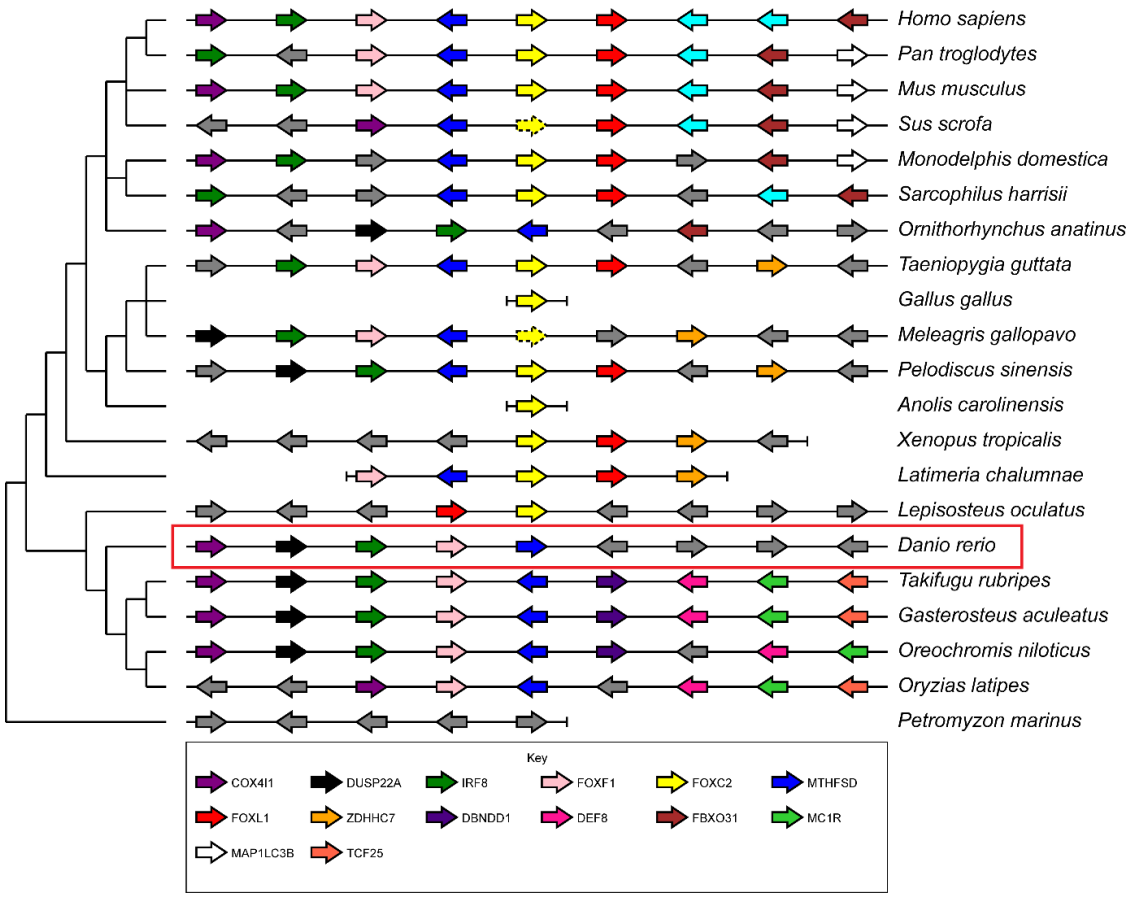

Figure 3.2 FOXC2 Synteny

The genomic region containing *Foxc2* has been lost in teleost lineages. Arrow directions indicate corresponding DNA strand, predicted genes are represented as dotted arrows. At left are scaffold lines showing the relatedness of the individual species. Zebrafish lineage is shown in red boxed area. Data kindly provided by Dr Teri Evans, University of Nottingham.

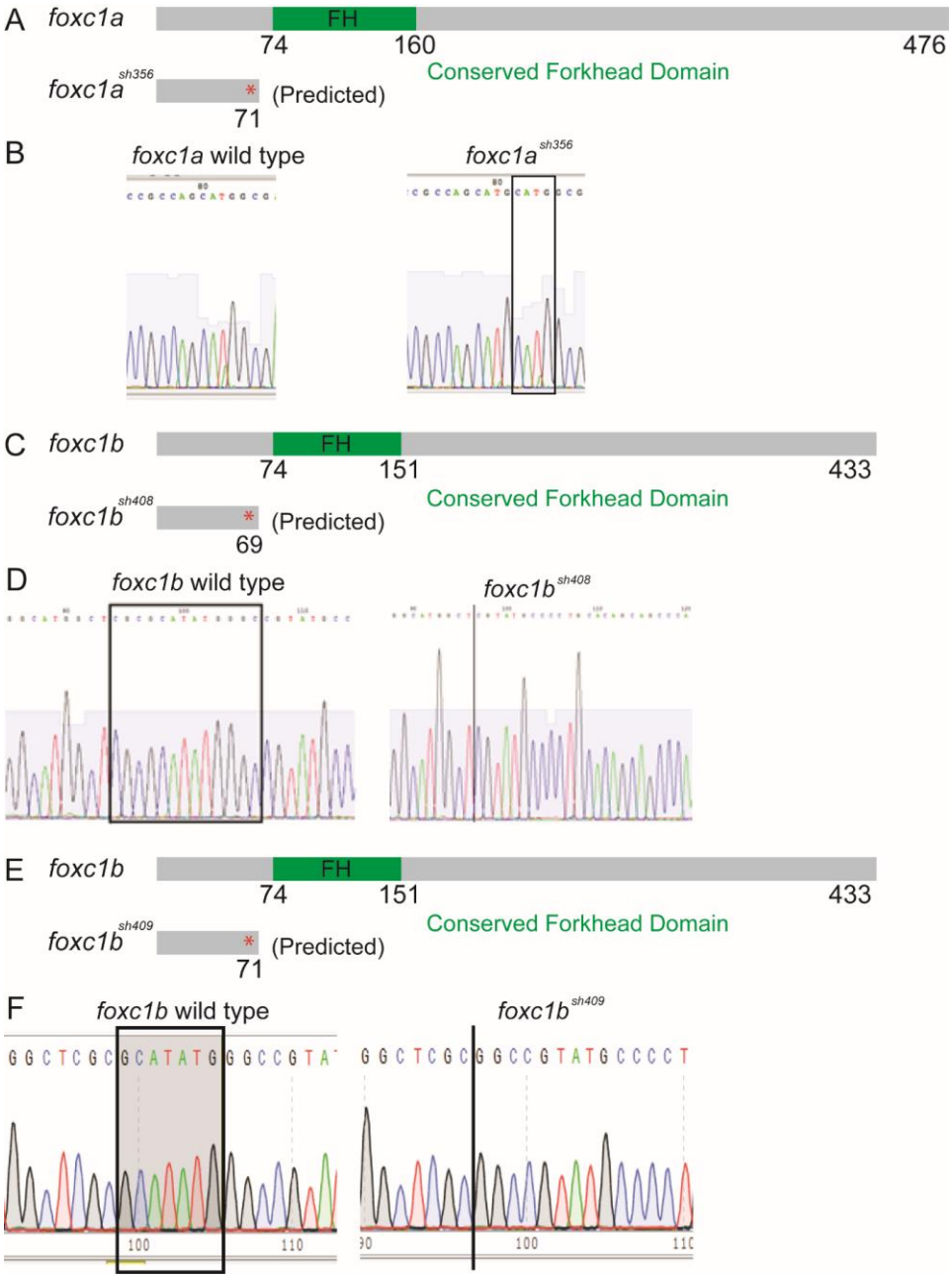

Figure 3.3 Generation of *foxc1a*^{sh356}, *foxc1b*^{sh408} and *foxc1b*^{sh409} alleles

(A) Schematic representation of the WT *foxc1a* and *foxc1a*^{sh356} allele with premature stop codon after amino acid 70 (red asterisk). (B) WT *foxc1a* coding sequence and *foxc1a*^{sh356} allele contains 4bp insertion at boxed region. (C) Schematic representation of WT *foxc1b* and *foxc1b*^{sh408} allele with premature stop codon after amino acid 68 (red asterisk). (D) WT *foxc1b* coding sequence, 13bp boxed region is deleted in the *foxc1b*^{sh408} allele. (E) Schematic representation of WT *foxc1b* and *foxc1b*^{sh409} allele with premature stop codon after amino acid 70 (red asterisk). Green box indicates the conserved Forkhead (FH) Domain. (F) WT *foxc1b* coding sequence, 7bp boxed region is deleted in the *foxc1b*^{sh409} allele.

3.2.2 *foxc1a* single mutants and *foxc1a*; *foxc1b* double mutants exhibit reduced blood circulation within the trunk

Zebrafish *foxc1a* mutants displayed absent or substantially reduced blood circulation within the developing trunk (Fig. 3.4 C, E), variable blood pooling in the caudal vein plexus (CVP) (Fig. 3.4 C Black arrowhead, E) and severe pericardial oedema in comparison to WT siblings (Fig. 3.4 A, C Red arrowhead). However, some *foxc1a* mutants retained the anterior cranial circulatory loop, comprised of the heart, ventral aorta, lateral dorsal aorta (LDA), primitive internal carotid artery, basilar artery (BA), primordial hindbrain channel (PHBC) and common cardinal vein (CCV) (Fig. 3.4 C Red dotted line; E Orange colour coded). Overall, around 25% of pooled embryos from multiple *foxc1a* heterozygous incrosses showed disrupted blood circulation (Fig. 3.4 E). These embryos with reduced blood flow were later proved to be *foxc1a* mutants, whereas the embryos with WT phenotype were siblings (data not shown). This observation fits with Mendelian ratios. By contrast, *foxc1b* homozygous mutants were morphologically normal, viable and fertile (Fig. 3.4 B). The morphology of *foxc1a*; *foxc1b* double mutants was similar to that observed in *foxc1a* single mutants (Fig. 3.4 C, D) with disrupted blood flow (Fig. 3.4 D Red dash line), pericardial oedema and variable blood pooling in the CVP (Fig. 3.4 D Red and black arrowheads respectively). However, *foxc1a*; *foxc1b* double mutants displayed more severe vascular abnormalities, which will be introduced in the following sections.

3.2.3 *foxc1a* single mutants and *foxc1a; foxc1b* double mutants display abnormal vasculature

Since *foxc1a* single mutants and *foxc1a; foxc1b* double mutants displayed reduced blood circulation, we employed the pan endothelial cell transgenic line *Tg(fli1a:EGFP)* to analyse the vasculature in both WT and mutant embryos. At 3 days post fertilisation (dpf), PHBC formation was irregular in *foxc1a*; *foxc1b* double mutants (Fig. 3.5 C Blue arrowhead) but not in *foxc1a* single mutants (Fig. 3.5 B Blue arrowhead). Under normal circumstances, the PHBC forms via vasculogenesis (Gore et al., 2012). This data suggests *foxc1a* and *foxc1b* might interact genetically during PHBC formation.

Central artery (CtA) formation was significantly reduced in *foxc1a* single mutants with almost total loss of cranial angiogenic sprouts (Fig. 3.5 B Red arrowheads, D) at 3dpf. In *foxc1b* single mutants, all vasculature was normal when compared to the WT embryos at 3dpf (Fig. 3.6 A-D). In addition, CtA formation in the *foxc1a*; *foxc1b* double mutants was similar to *foxc1a* single mutants (Fig. 3.5

B, C Red arrowheads, D). This suggests that the reduced CtA formation displayed in *foxc1a; foxc1b* double mutants is more likely due to loss of *foxc1a* alone.

The axial vasculature (*i.e.* dorsal aorta and posterior cardinal vein) was patented and specified normally, however, *foxc1a* single mutants and *foxc1a*; *foxc1b* double mutants exhibited reduced diameter of the DA (Fig. 3.5 B, C Red bar), which may have been due to absent trunk blood circulation. In addition, in both *foxc1a* single mutants and *foxc1a*; *foxc1b* double mutants, more leading tip cells were observed within the developing sub-intestinal vein. This is also likely caused by disrupted blood circulation in the mutants (Unpublished observations, Ms Yan Chen, Wilkinson lab).

Interestingly, in *foxc1a*; *foxc1b* double mutants, we observed vascular hypersprouting (Fig. 3.5 C Yellow arrowheads), suggesting a genetic interaction between *foxc1a* and *foxc1b* during trunk intersegmental vessel (ISV) formation. Further analysis of trunk angiogenesis in *foxc1a*; *foxc1b* double mutants will be described in chapter 4.

Taken together, we report almost complete loss of cranial angiogenesis in the absence of *foxc1a*, suggesting *foxc1a* is required for normal CtA formation, whereas *foxc1b* is dispensable for cranial angiogenesis (Fig. 3.6). These data indicate that *foxc1a* and *foxc1b* genetically interact during zebrafish blood vessel formation.

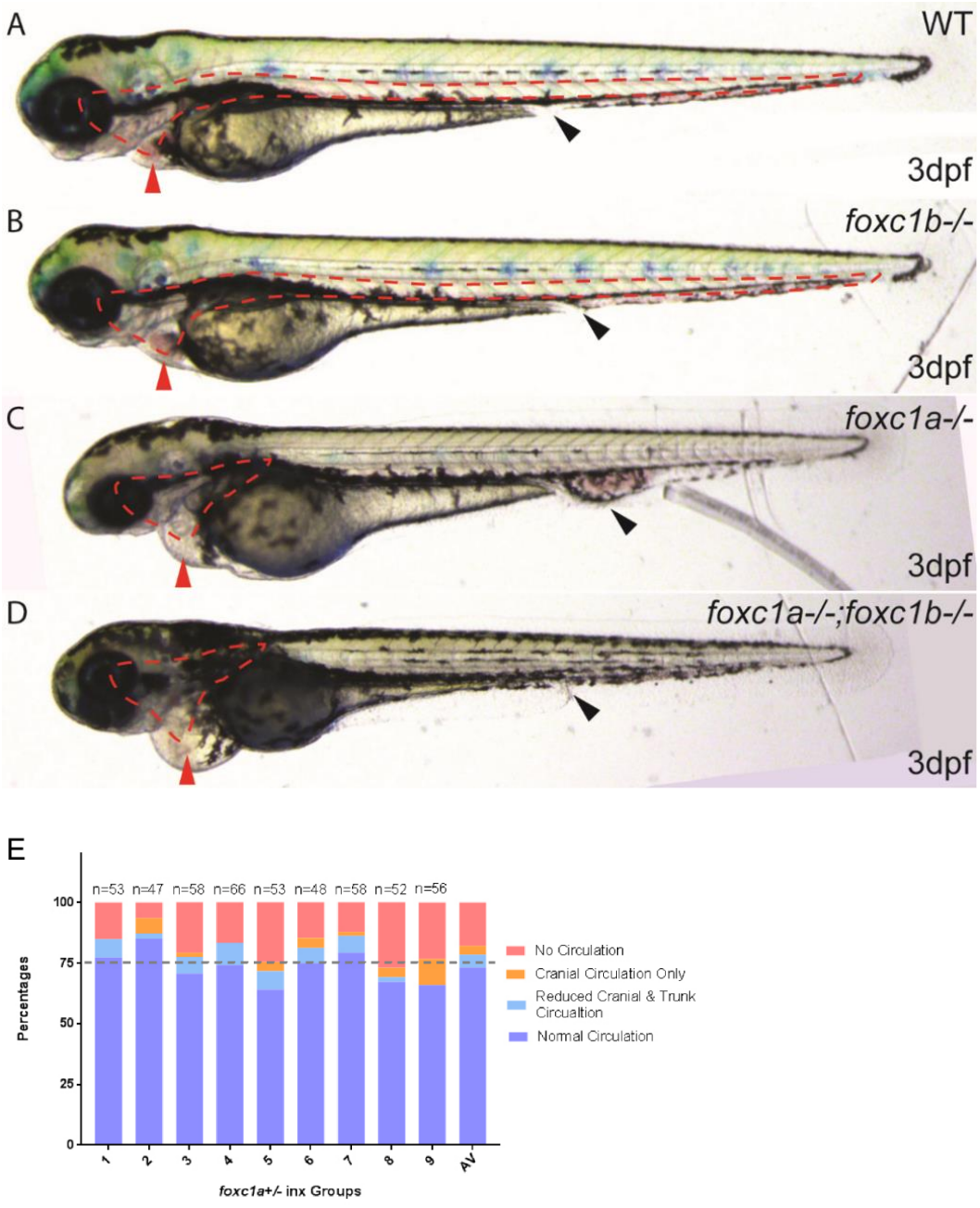

Figure 3.4 *foxc1a* single and *foxc1a*; *foxc1b* double mutants display defective blood circulation, leading to variable blood pooling and pericardial oedema

(A, B) WT sibling and *foxc1b* single mutants (B) show normal morphology, whereas *foxc1a* single mutants (C), and *foxc1a*; *foxc1b* double mutants (D) display disrupted blood circulation (highlighted by red dotted line). Red arrowheads highlight presence of pericardial oedema; black arrowheads highlight variable caudal blood pooling. (E) Quantification of variable circulation defects in *foxc1a* heterozygous incrossed embryos. 491 embryos were analysed. Each number on the X-axis represent an independent *foxc1a* heterozygous incross, AV represents average data of 9 individual incrosses.

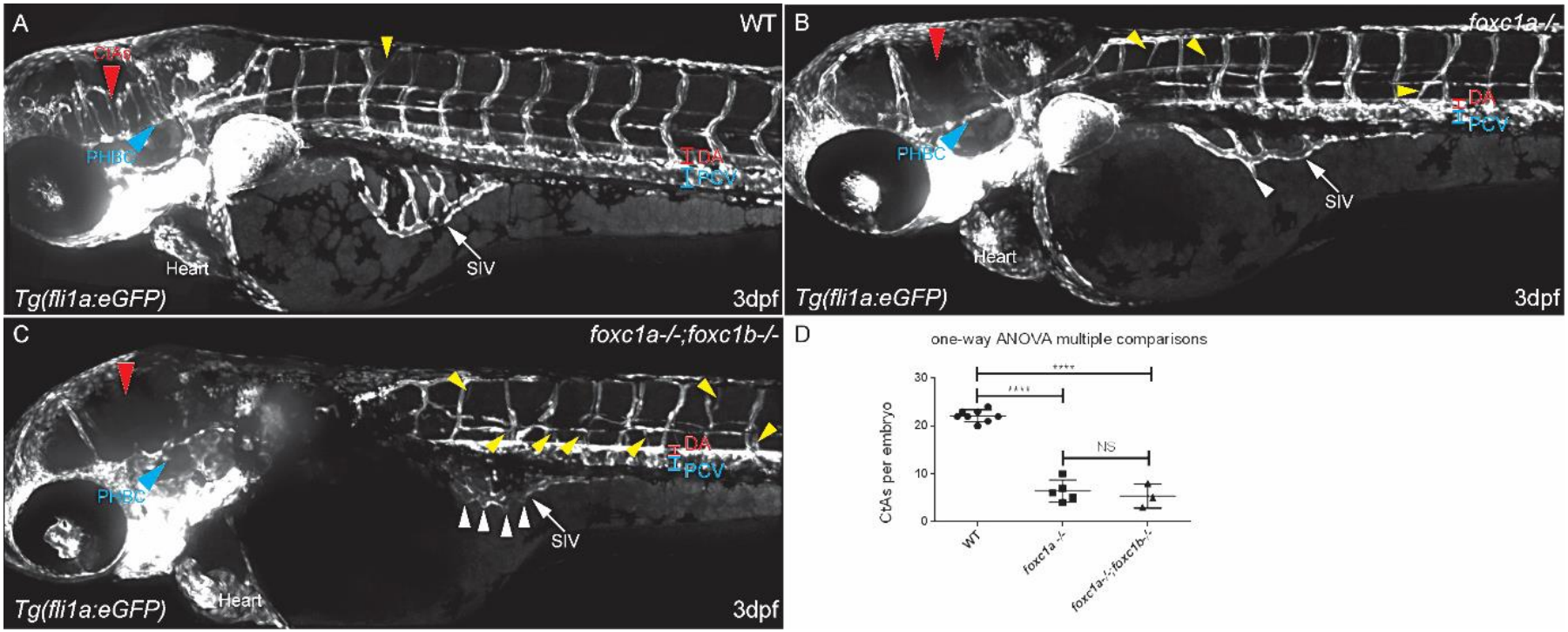

Figure 3.5 *foxc1a* single mutants and *foxc1a*; *foxc1b* double mutants display abnormal vasculature

(A-C) Lateral view of confocal microscopy images in 3dpf *Tg(fli1a:EGFP)* WT sibling (A), *foxc1a* single mutants (B) and *foxc1a*; *foxc1b* double mutants (C). Red arrowheads point to CtAs; blue arrowheads indicate PHBC; yellow arrowheads denote ectopic ISVs; blue bar points to PCV and Red bar denotes the DA. (D) Number of CtAs per embryo at 2.5dpf of WT embryos (n=8), *foxc1a* single mutants (n=5) and *foxc1a*; *foxc1b* double mutants (n=3). One-way ANOVA multiple comparisons. ****<0.0001, NS: not significant. CtA: central artery; ISV, intersegmental vessel; PHBC, primordial hindbrain channel; DA, dorsal aorta; PCV, posterior cardinal vein; SIV, sub-intestinal vein.

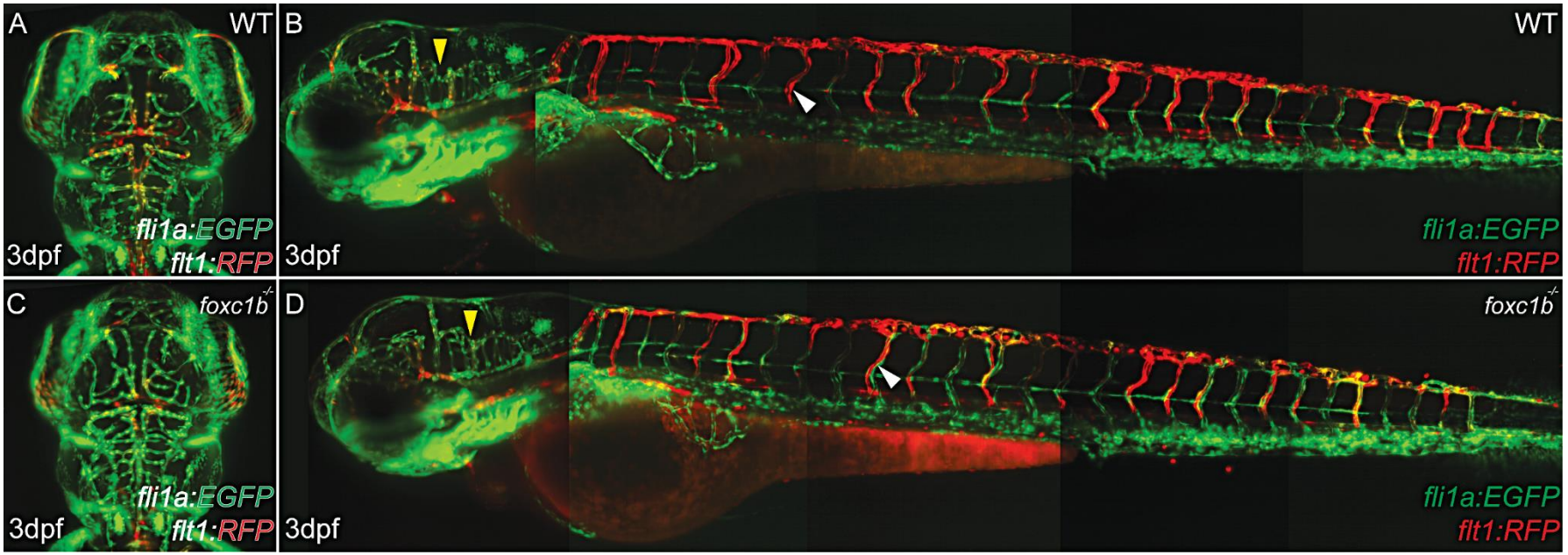

Figure 3.6 *foxc1b* single mutants display normal vasculature

(A, C) Dorsal view of the head in WT (A) and *foxc1b* single mutants (C). (B, D) Lateral view of WT and *foxc1b* single mutants show normal vessel formation. Yellow arrowheads highlight CtAs, white arrowheads indicate ISVs. CtA: central arteries; ISV: intersegmental vessel.

3.2.4 *foxc1a* is required for formation of zebrafish lateral dorsal aorta

foxc1a single mutants displayed abnormal LDA formation by 3dpf, which was variable in severity. This LDA defect might be responsible, at least partially, for the variable trunk blood circulation defects that was displayed in the mutants (Fig. 3.5 B). The LDA is the main artery in the head (Gore et al., 2012, Hermkens et al., 2015). In WT embryos, the LDA formed a stereotypical 'V' shape to connect the cranial blood circulation with the posterior circulation via the dorsal aorta (DA). There are two aortic arches (AA') located and connected bilaterally with the posterior LDA (Fig. 3.7 A, A'). In *foxc1a* single mutants, this structure was disrupted with abnormal LDA vessel patterning and absent AA' connections (Fig. 3.7 B-D'). Three examples of abnormal LDA formation are highlighted in the illustration in Fig. 3.7: (1) Connections between LDA and DA were present in *foxc1a* mutants, but with reduced diameters, which may contribute to the disrupted blood circulation (Fig. 3.7 B, B'); (2) LDA patterning was disrupted with abnormal connection to the DA in the trunk, which could potentially result in retention of cranial blood circulation but absence of trunk circulation (Fig. 3.7 C, C'); (3) Connections between LDA and DA were severely mispatterned with missing connections between LDA and DA (Fig. 3.7 D, D'). This mispatterned LDA was likely to account for the failure in trunk circulation in *foxc1a* single mutants and indicate that *foxc1a* is required for normal LDA formation.

3.2.5 *foxc1a* is required for formation of facial and brain lymphatic vessels

Mammalian *Foxc1* and *Foxc2* have been reported to play important roles in lymphangiogenesis (Kume et al., 2001, Hayashi and Kume, 2008a, Seo et al., 2006). In addition, since *foxc1a* mutants displayed variable oedema, we examined formation of the lymphatic system in the head (Fig. 3.8). We utilised the pan endothelial cell marker *Tg(fli1a:LifeACT-mClover)* (Savage *et al*. 2018 in revision) and *Tg(kdrl:mcherry)* because expression of *Tg(kdrl:mcherry)* is excluded from lymphatic ECs (Hogan et al., 2009a). Therefore, ECs which express *fli1a:LifeACT-mClover* alone could be identified as lymphatic endothelial cells (LECs). At 5dpf facial lymphatic formation was abnormal in *foxc1a* single mutants with dilated otolithic lymphatic vessel (OLV), absent medial facial lymphatic (MFL) vessel and lymphatic branchial arch (LAA) (Fig. 3.8 B, B' Blue dotted line and asterisks). These lymphatic abnormalities could potentially contribute to the severe cranial oedema observed in *foxc1a* single mutants post day 4 (data not shown).

The brain lymphatic EC (BLEC) is a recently identified unique type of venous endothelium derived LEC in the head (van Lessen et al., 2017, Venero Galanternik et al., 2017). Its discovery provided

a novel use of zebrafish to study the function of the brain. We analysed BLEC formation in *foxc1a* mutants using the *Tg(fli1a:LifeACT-mClove; kdrl:mcherry)* transgenes (Fig. 3.9). As described previously (van Lessen et al., 2017), at 56hpf, BLECs with weak *kdrl* expression began to sprout alongside the mesencephalic vein (MsV) from the primordial midbrain channel (PMBC) in WT embryos (Fig. 3.9 A-A'' Blue arrowheads). No BLEC sprouts could be detected in *foxc1a* single mutants (Fig. 3.9 B-B'') at 56hpf, which could be due to delayed BLEC development and/ or defective BLEC specification. The morphology of the MsV and PMBC were different in *foxc1a* single mutants when compared with the WT embryos (Fig. 3.9 A-B''), suggesting loss of function of *foxc1a* disrupted formation of these blood vessels.

At 5dpf, BLECs normally finish sprouting alongside the MsV and form two stereotypical loop structures bilaterally behind the eyes in the forebrain (Fig. 3.10 A-A'' Blue arrowheads)(van Lessen et al., 2017). In *foxc1a* mutants, BLECs could still be detected, but the stereotypical loop structure no longer existed (Fig. 3.10 B-B'' Blue arrowheads). These observations indicate that *foxc1a* is required for normal facial lymphatic formation and BLEC sprouting and migration.

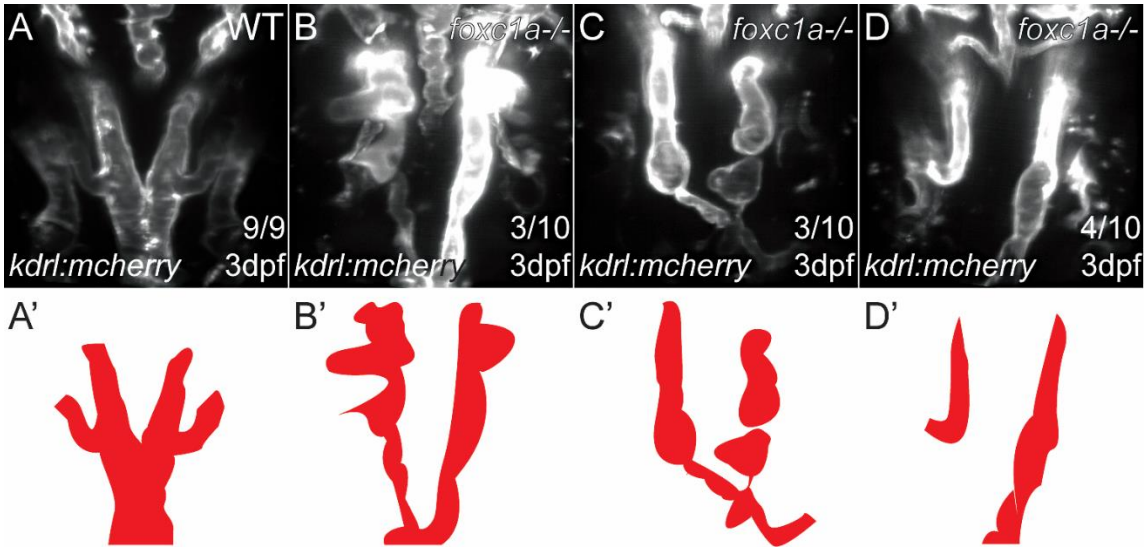

Figure 3.7 *foxc1a* is required for formation of the lateral dorsal aorta

(A-A') Dorsal view of LDA and illustrations (A') at 3dpf in *Tg(Kdrl:mcherry)* of WT embryos. (B-D') Dorsal view of LDA and illustrations (B'-D') show variable deformed LDA at 3dpf in *Tg(Kdrl:mcherry)* of *foxc1a* single mutant embryos. LDA, lateral dorsal aorta; DA, dorsal aorta; AA', aortic arches.

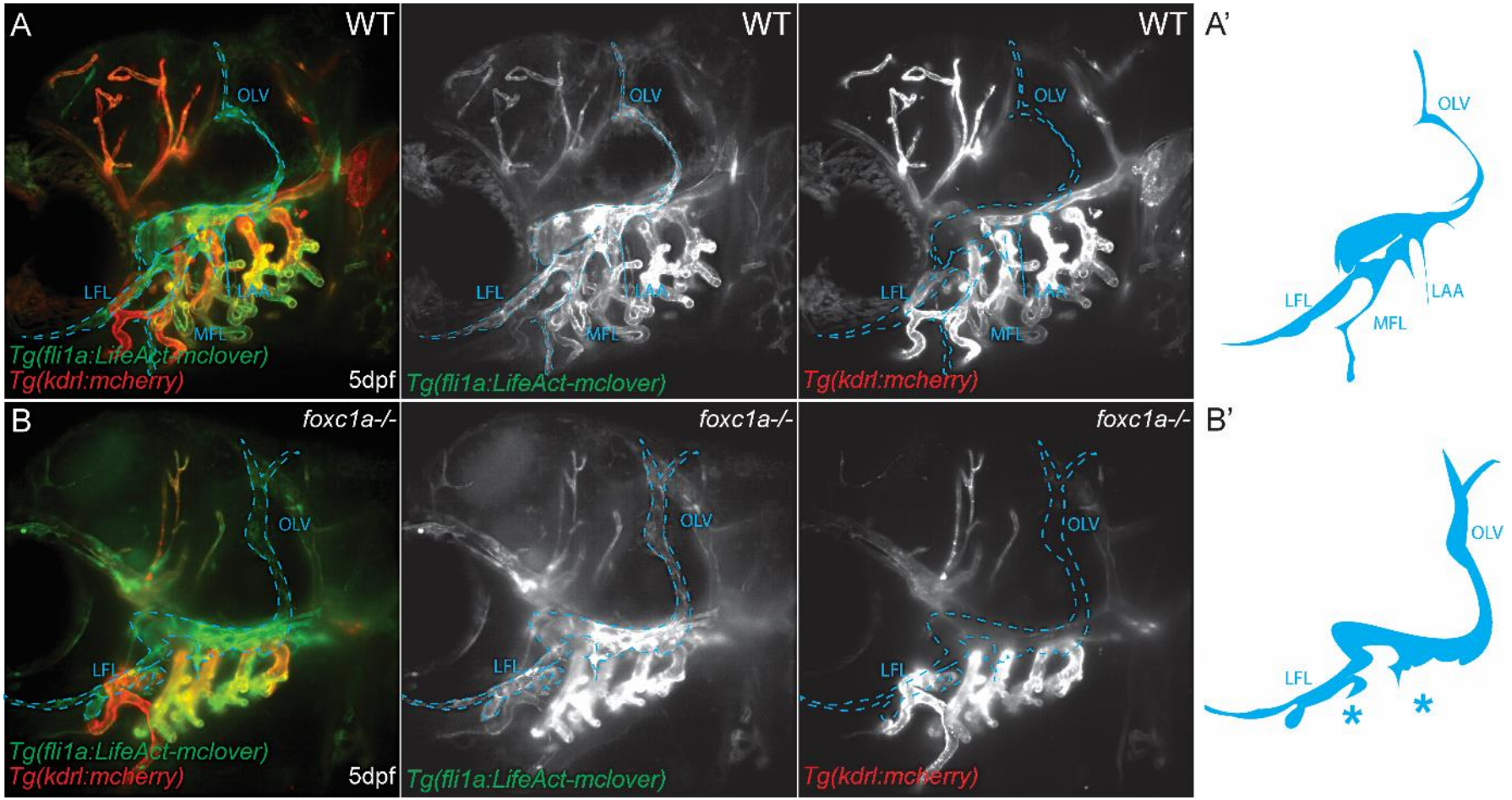
A
WT
OLV
LFL
LAA
MFL
Tg(fli1a:LifeAct-mclover)
Tg(kdrl:mcherry)
5dpf
WT
OLV
LFL
LAA
MFL
Tg(fli1a:LifeAct-mclover)
WT
OLV
LFL
LAA
MFL
Tg(kdrl:mcherry)
A'
OLV
LFL
LAA
MFL
B
foxc1a-/-
OLV
LFL
Tg(fli1a:LifeAct-mclover)
Tg(kdrl:mcherry)
5dpf
foxc1a-/-
OLV
LFL
Tg(fli1a:LifeAct-mclover)
foxc1a-/-
OLV
LFL
Tg(kdrl:mcherry)
B'
OLV
LFL

Figure 3.8 *foxc1a* is required for formation of facial lymphatic vessels

(A-A') Lateral view of facial lymphatics with illustration in WT embryos with *Tg(fli1a:LifeACT-mClover; kdrl:mcherry)* at 5dpf. (B-B') Lateral view of defectively formed facial lymphatics and illustration in *foxc1a* single mutants with dilated OLV, absent MFL and LAA (blue asterisks). LFL, lateral facial lymphatic; MFL, medial facial lymphatic; OLV, otolithic lymphatic vessel; LAA, lymphatic branchial arche.

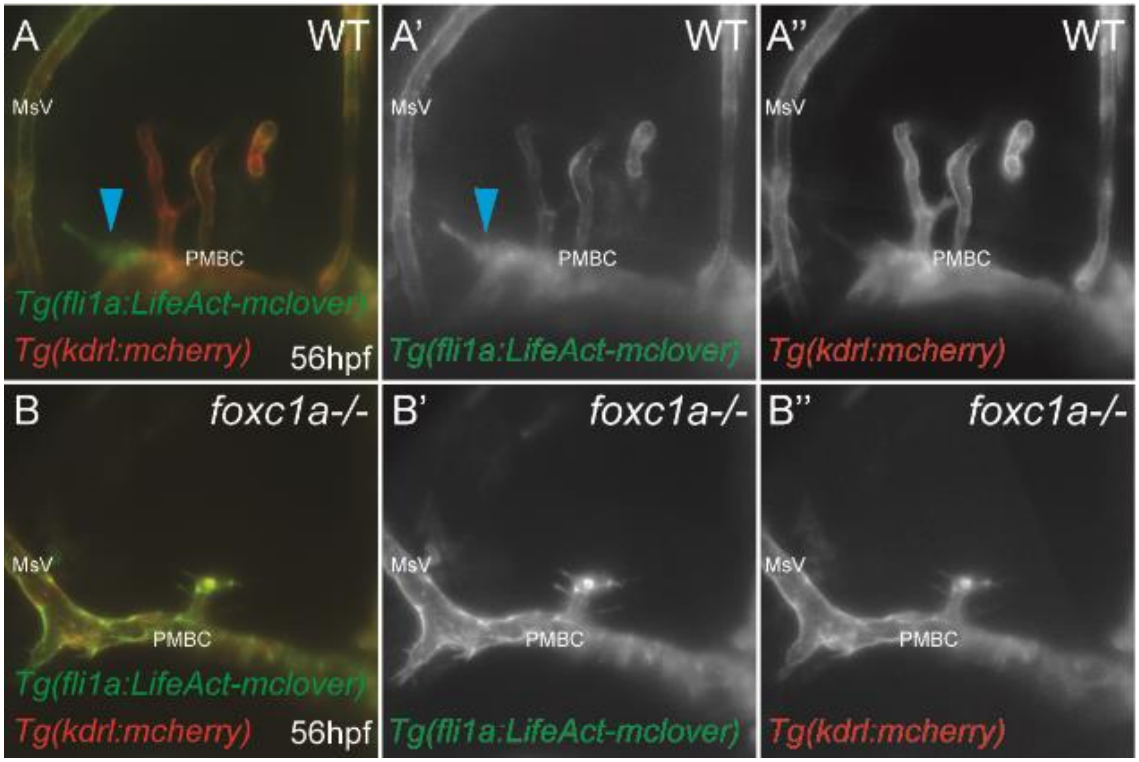

Figure 3.9 *foxc1a* is required for brain lymphatic endothelial cell sprouting

(A-A'') Lateral view of forehead in WT embryos with *Tg(fli1a:LifeACT-mClover; kdrl:mcherry)* background. Blue arrowheads indicate the initiation of BLECs sprouting with high *fli1a:LifeACT-mChlover* expression and low *kdrl:mcherry* expression from the PMBC in WT embryos at 56hpf. (B-B'') Lateral view of forehead in *foxc1a* single mutants show absent BLECs sprouting at 56hpf. PMBC, primordial midbrain channel; MsV, mesencephalic vein.

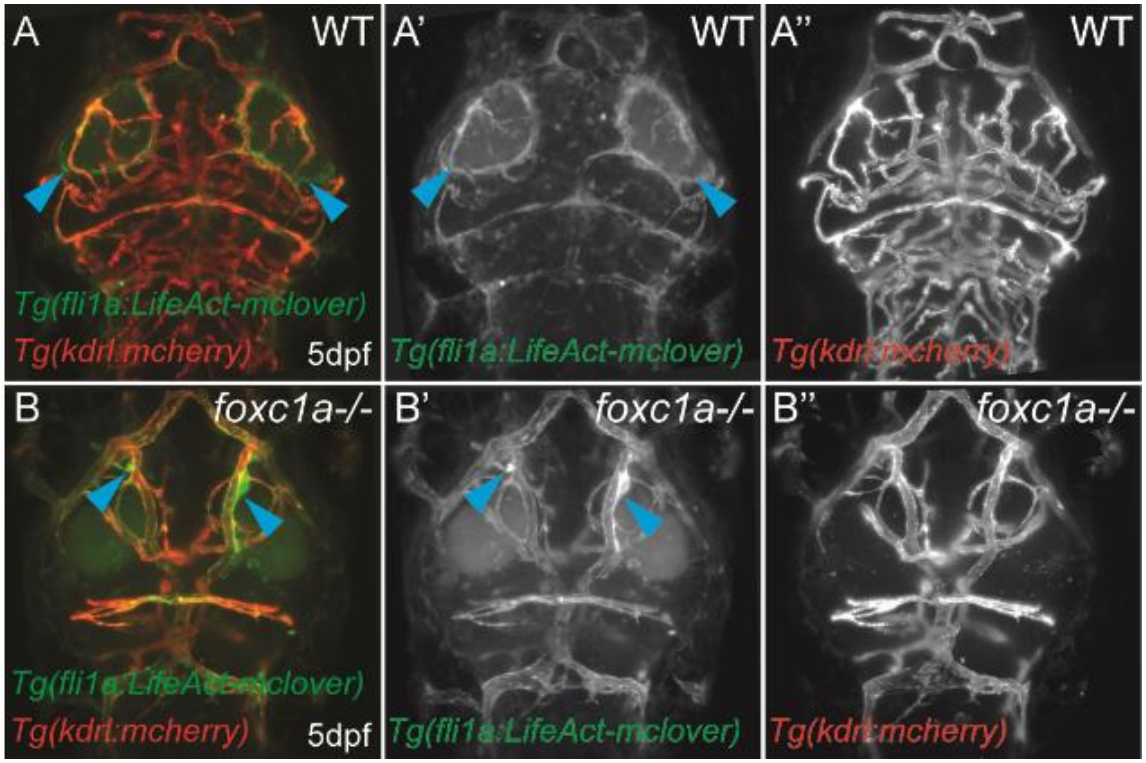

Figure 3.10 *foxc1a* is required for migration of brain lymphatic endothelial cells

(A-A'') Dorsal view of head in WT embryos with *Tg(fli1a:LifeACT-mClover; kdrl:mcherry)* background shows normal formed BLEC loops located bilaterally in the forebrain (blue arrowheads) at 5dpf. (B-B'') Dorsal view of head in *foxc1a* single mutants with head circulation show abnormal BLEC migration (blue arrowheads).

3.2.6 *foxc1a* and *foxc1b* are required for cranial basal vessel formation

The major vessels in the hindbrain represent the junction which links rostral and posterior blood circulation (Isogai et al., 2001). Therefore, to further investigate the cause of reduced trunk blood circulation and abnormal CtAs formation, we analysed cranial vasculogenesis at 22hpf, which establishes the basal vessels, namely PHBC, LDA and CCV, in the hindbrain and other major vessels in the head. At 22hpf, the CCV was not detectable in either *foxc1a* or *foxc1a*; *foxc1b* double mutants (Fig. 3.11 B, C Yellow asterisks), whereas these were correctly formed in WT embryos (Fig. 3.11 A Yellow arrowheads). In WT, the LDA was able to form the stereotypical V-shape beneath the PHBC at 22hpf, but in *foxc1a* mutants, LDA was not properly lumenised at this stage (Fig. 3.11 B White arrows). In addition, formation of the PHBCs commenced by 22hpf in WT embryos (Fig. 3.11 A Red arrowheads), however, we could not detect initiation of PHBC formation at this stage (Fig 3.11 B, C Red asterisks) in either *foxc1a* single mutants or *foxc1a*; *foxc1b* double mutants. In addition, in the absence of both *foxc1a* and *foxc1b* the delay in formation of major cranial vessels were more pronounced than those observed in *foxc1a* single mutants. Formation of middle cerebral vein (MCeV) and LDA were not detectable in *foxc1a*; *foxc1b* double mutants at 22hpf (Fig. 3.11 C Blue and white asterisks respectively). These observations indicate that *foxc1a* and *foxc1b* function co-operatively during cranial vasculogenesis.

3.2.7 *foxc1a* is required for common cardinal vein formation

Formation of CCVs was abnormal in *foxc1a* single mutants at 28hpf (Fig. 3.12 C). *foxc1a*; *foxc1b* double mutants also showed disrupted CCV formation, which was similar to the phenotype displayed in *foxc1a* single mutants (data not shown). We employed the *Tg(fli1a:LifeACT-mClover)* transgenic line to label filopodia in ECs, which allowed us to observe CCV formation more clearly. As opposed to the WT embryo, in which the CCVs formed evenly outgrowing EC sheets with tightly connected cell-cell junctions (Fig. 3.12 B, D), the CCVs in *foxc1a* single mutants were significantly disrupted (Fig. 3.12 C, E). At 28hpf, the initiation of EC collective migration to form the CCV was not detectable in *foxc1a* single mutants (Fig. 3.12 C blue arrowheads)(Helker et al., 2013) and by 56hpf, the CCVs were thinner in *foxc1a* single mutants than observed in WT siblings (Fig. 3.12 D, E Blue dotted line). Disrupted CCV formation would also inhibit blood circulation and may therefore contribute to reduced circulation in *foxc1a* mutants.

Given CCV formation was abnormal in *foxc1a* single mutants and *foxc1a; foxc1b* double mutants, we analysed expression of *foxc1a* and *foxc1b* using fluorescent *in situ* hybridization (See section

2.2.3.5), which provides better resolution than traditional chromogenic *in situ* hybridisation. Expression of *foxc1a* and *foxc1b* were detected by fluorescent *in situ* hybridisation with Cy3 tyramide (Red channel), endothelial GFP in *Tg(fli1:EGFP)* was detected by immunofluorescence with α-GFP antibody (Green channel) as vessel reference (See section 2.2.3.5). *foxc1a* Cy3 tyramide staining could be detected in the pharyngeal arches adjacent to the CCV (Fig. 3.13 A, A' Purple arrowheads) and also the ECs within the CCVs (Fig. 3.13 A' white and blue arrowheads). Interestingly, *foxc1a* was expressed at higher levels in ECs of the posterior CCV (Fig. 3.13 A' blue arrowheads) than in the anterior migratory CCV ECs (Fig. 3.13 A' white arrowheads). *foxc1b* expression was not detectable in either developing CCV or adjacent mesenchyme (Fig. 3.13 B').

Collectively, *foxc1a* is expressed in the developing CCV and is required for CCV formation, suggesting a potential cell-autonomous role, whereas, *foxc1b* is excluded from the developing CCV and is dispensable for CCV formation.

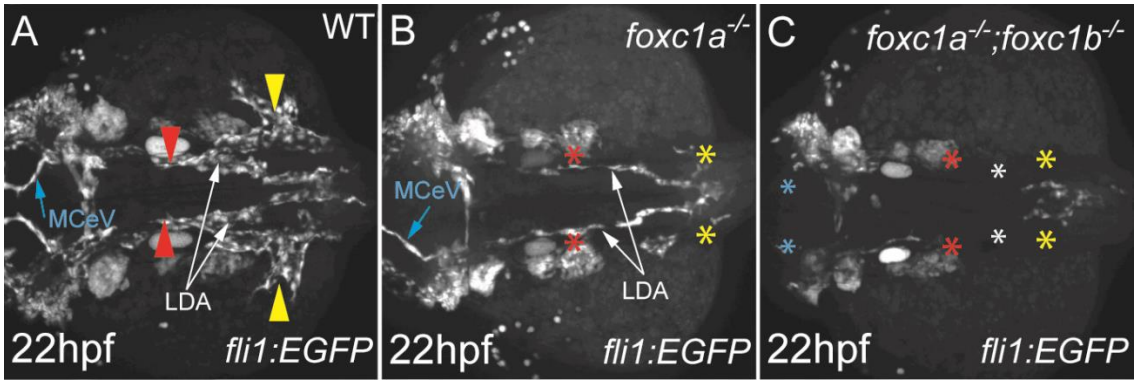

Figure 3.11 *foxc1a* and *foxc1b* function co-operatively during cranial vasculogenesis

(A) Dorsal view of WT hindbrain at 22hpf. Red arrowheads indicate PHBCs, yellow arrowheads point to CCVs. (B) *foxc1a* single mutants show delayed PHBC (red asterisks) and MCeV formation, absent CCVs (yellow asterisks) and defective LDA formation. (C) *foxc1a*; *foxc1b* double mutants show more pronounced delay in PHBC (red asterisks) and MCeV (blue asterisks) formation with absent CCV (yellow asterisks) and LDA (white arrowheads) at 22hpf. PHBC: primordial hindbrain channel; CCV: common cardinal vein; LDA: lateral dorsal aorta; MCeV: middle cerebral vein.

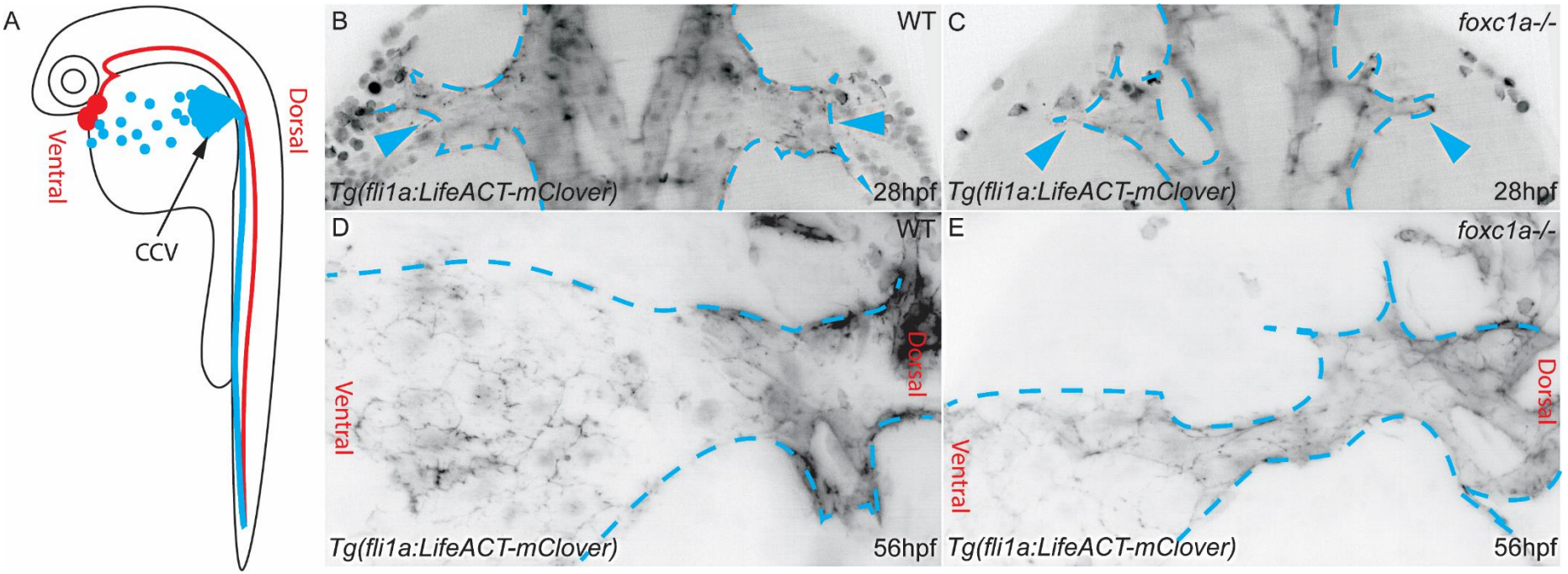

Figure 3.12 *foxc1a* is required for common cardinal vein formation

(A) Schematic representation of CCV formation in zebrafish embryo with lateral view. (B) Dorsal view of WT embryos show normal CCVs (blue arrowheads and dotted lines) located bilaterally above the yolk in *Tg(fli1a:LifeACT-mClover)*. (B) *foxc1a* single mutant embryo shows abnormal CCV formation (blue arrowheads and dotted lines) at 28hpf. (C, D) Lateral view of CCV formation at 56hpf in WT embryos (C) and *foxc1a* single mutants (D). Blue dotted lines map the CCV outline. CCV, common cardinal vein.

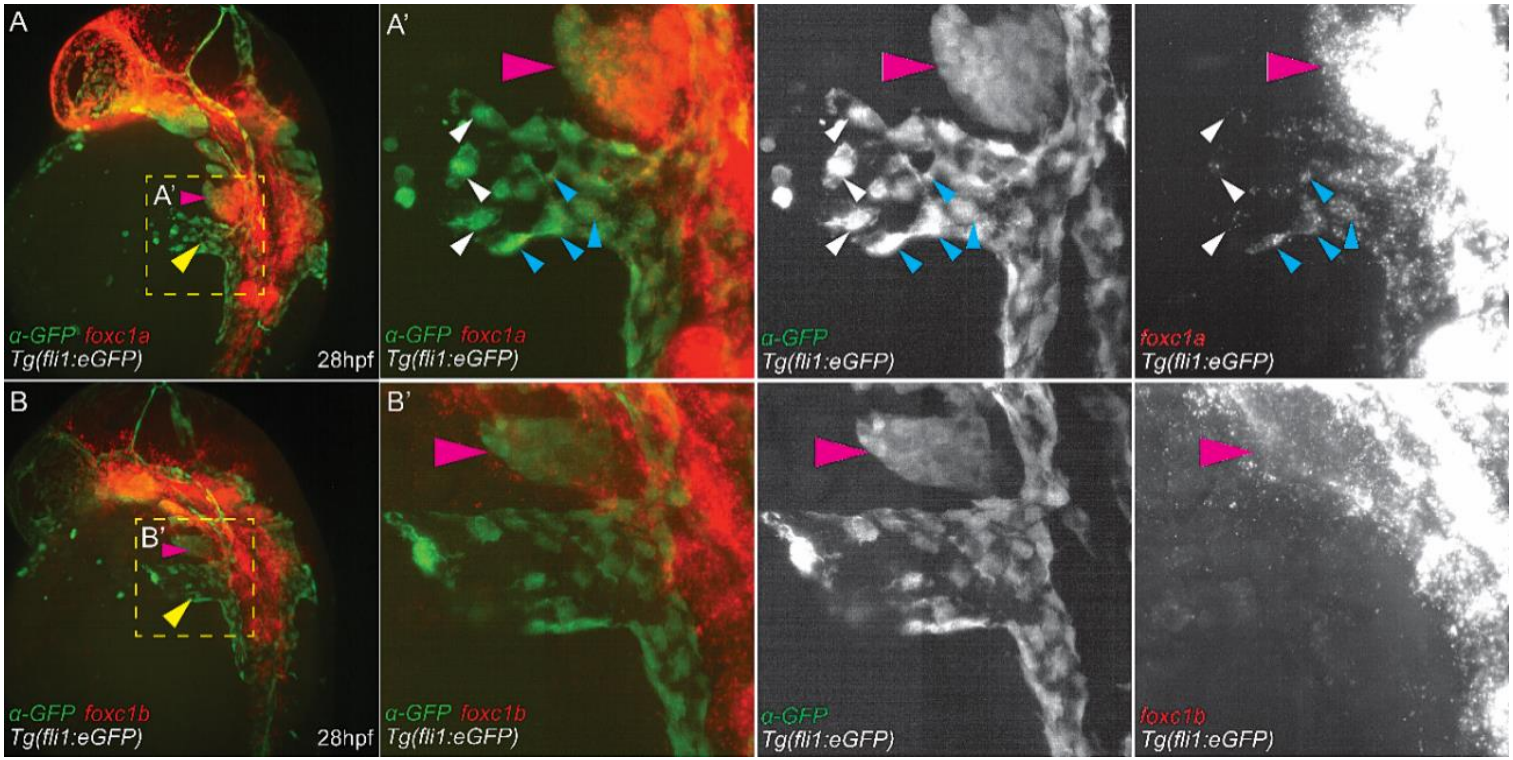

Figure 3.13 *foxc1a* is expressed in the developing common cardinal vein, while *foxc1b* is excluded from this vessel

(A, B) Dorsal lateral view of Cy3 fluorescent *in situ* of *foxc1a* and *foxc1b* (red channel) with α-GFP antibody staining (green channel) in *Tg(fli1a:EGFP)* in WT embryo head at 28hpf respectively. Yellow arrowheads highlight CCV; pink arrowheads indicate pharyngeal arch expression adjacent to CCV. (A') Higher magnification picture of yellow dotted boxed area in panel A. Small blue arrowheads indicate dorsal CCV with high level of *foxc1a* expression; small white arrowheads indicate ventral CCV with low level of *foxc1a* expression; pink arrowhead indicates mesenchyme adjacent to CCV. (B') Higher magnification picture of yellow dotted boxed areas in panel B. pink arrowhead indicates mesenchyme adjacent to CCV.CCV, common cardinal vein.

3.2.8 Vegf signalling is dispensable for common cardinal vein formation

Relatively little is understood about the mechanisms which control CCV formation. Vegfc and Vegfr3/ Flt4 signalling have been shown to regulate formation of angiogenic sprouts with venous origin (Karkkainen et al., 2004, Le Guen et al., 2014, Kuchler et al., 2006). To determine whether *foxc1a* controls CCV formation via interaction with Vegfc signalling, we treated the sibling embryos and *foxc1a* single mutants with AV951 (Fig. 3.14), which inhibits VEGF receptor 1, 2 and 3 (Eskens et al., 2011).

At 28hpf, control DMSO treated sibling embryos formed functional CCVs bilaterally above the yolk (Fig. 3.14 A, A' Red arrowheads). The AV951 treated sibling embryos showed abnormal formation of MCeV (Fig. 3.14 B Blue asterisk) and PHBC formation (Fig. 3.14 B White asterisk) indicating the AV951 treatment was effective. However, following Vegf inhibition, CCV formation was normal in sibling embryos (Fig. 3.14 B, B' Red arrowheads), indicating that Vegf signalling is dispensable for CCV formation. Interestingly, in the DMSO treated group, no sign of initiation of the EC collective migration to form CCV at 28hpf could be detected in *foxc1a* single mutants (Fig. 3.14 C, C' Red asterisks). This observation further confirmed the importance of *foxc1a* in CCV formation.

In addition, post AV951 treatment in *foxc1a* single mutants, abnormal CCV formation was observed (Fig. 3.14 D-D' Red asterisks), with almost complete loss of MCeV and PHBC formation (Fig. 3.14 D, D' Blue and white asterisks) when compared with the DMSO treated *foxc1a* mutant embryos (Fig. 3.14 C Blue and white arrowheads). These data indicate that major cranial vessel formation depends on the Vegf signalling pathway, whereas the Vegf signalling is not required during CCV formation. Here we have reported that *foxc1a* is required for CCV formation, which is independent of the Vegf signalling pathway.

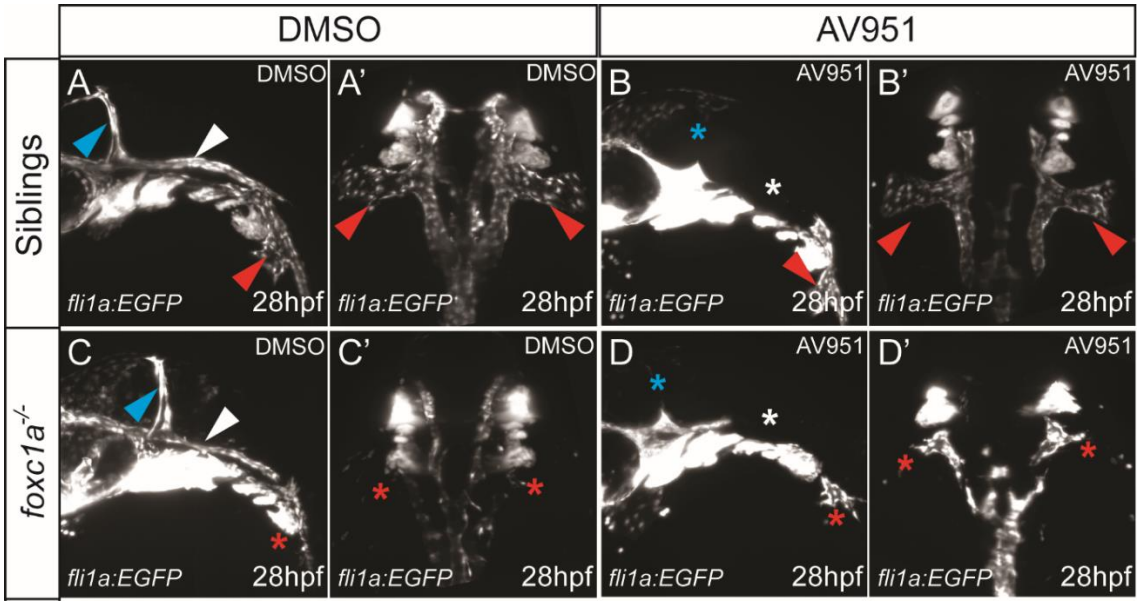

Figure 3.14 *foxc1a* is required for common cardinal vein formation while Vegf signalling is dispensable for common cardinal vein formation

(A, A', C, C') Lateral and dorsal view of DMSO treated WT embryos (A, A'), *foxc1a* single mutants (C, C') at 28hpf. Blue arrowheads indicate MCeV; white arrowheads point to PHBC; red arrowheads denote CCVs; red asterisks highlight absent CCVs. (B, B', D, D') Lateral and dorsal view of AV951 treated WT embryos (B, B'), *foxc1a* single mutants (D, D') at 28hpf. Blue asterisks indicate absent MCeV; white asterisks point to absent PHBC; red arrowheads denote CCVs; red asterisks highlight absent CCVs. CCV: common cardinal vein; MCeV: middle cerebral Vein; PHBC: primordial hindbrain channel.

3.2.9 *foxc1a* is required for cranial vessel formation

We further analysed cranial vessel formation in *foxc1a* mutants using *in vivo* timelapse imaging at 21-38hpf (Fig. 3.15 A-B', also see Supplementary movies 1 and 2) to investigate cranial angiogenesis in greater detail. In WT embryos (Supplementary movie 1), PHBC formation was completed by approximately 24hpf (Fig. 3.15 A, A' Blue colour coded), followed by medial migration of ECs from PHBCs to form the BA, which was completed by approximately 30hpf (Fig. 3.15 A, A' Red colour coded). During BA formation, the CtAs could be observed to sprout via angiogenesis from the anterior PHBC from 28hpf (Fig. 3.15 A, A' Purple colour coded), which were generated via angiogenesis. The CtA sprouts subsequently connected with the BA once it had formed (Fig. 3.15 A, A' Purple colour coded).

However, in *foxc1a* single mutants (Supplementary movie 2), PHBC and BA formation were delayed by approximately 2-3 hours (Fig. 3.15 B' Blue and red colour coded), such that in *foxc1a* single mutants, the formation of PHBC and BA finished at around 26hpf and 32hpf respectively. The formation of CtAs was not detectable in *foxc1a* single mutants (3.15 B, B'), which is in line with observations reported in section 3.2.3.

To understand how *foxc1a* regulates formation of CtAs, we quantified ECs in WT embryos and *foxc1a* mutants in *Tg(kdrl:HRAS-mCherry; flk1:nucEGFP)*, which labels the EC membrane in red and EC nuclei in green. At 60hpf, the total EC number of *foxc1a* single mutants remained unchanged when compared with the WT embryos within individual or combined cranial vessels (Fig. 3.16 A, C, N). However, there was a significant increase in the number of arterial-venous connections (AVC) in *foxc1a* mutants (Fig. 3.16 O), both in the AVCs between PHBC and BA and AVCs between PHBC and posterior communicating segment (PCS) (Fig. 3.16 O). These data indicate *foxc1a* limits the formation of AVCs potentially via regulating EC migration, but is unlikely to contribute to EC specification and/ or proliferation.

To test the role of *foxc1a* in CtA formation, we therefore examined whether the *foxc1a* single mutant phenotype could be rescued by overexpression of *foxc1a*. We injected full length *foxc1a* mRNA into WT siblings and *foxc1a* single mutants at one-cell stage (Fig. 3.16 E-H), GFP mRNA was also injected as a negative control (Fig. 3.16 A-D). Overexpression of *foxc1a* in WT did not cause any detectable morphological change (Fig. 3.16 E, F). Post *foxc1a* mRNA overexpression, no change in EC distribution could be detected within the major cranial basal vessels in either WT embryos or *foxc1a* single mutants (Fig. 3.16 N). This data suggests *foxc1a* is not sufficient to

induce EC specification and/ or proliferation. Overexpression of *foxc1a* in *foxc1a* single mutants partially restored CtA formation in *foxc1a* single mutants (Fig. 3.16 G, H White arrowheads, M).In addition, *foxc1a* overexpression also reduced the AVC number when compared with the control mRNA injected *foxc1a* single mutants (Fig. 3.16 O), and in particular, the AVCs between PHBC and BA in the head.

Previous zebrafish studies demonstrated conflicting results: Bussmann *et al*. showed that blood flow contributes to zebrafish cranial vessel remodelling (Bussmann et al., 2011), whereas Fujita *et al.* concluded blood circulation is dispensable for cranial vessel patterning (Fujita et al., 2011). To exclude the possibility that reduced blood circulation might be responsible for decreased CtA numbers in *foxc1a* single mutants, we injected *tnnt2* Mo (Sehnert et al., 2002) into both WT siblings and *foxc1a* mutants to prevent initiation of blood circulation. Injected embryos were analysed at 60hpf. In *tnnt2* Mo injected WT embryos, CtAs were thinner and unlumenised due to lack of blood flow in the head (Fig. 3.16 I, J White arrowheads). However, no significant alteration in CtA numbers was detected in the *tnnt2* Mo injected WT embryos when compared to the GFP mRNA injected WT embryos (Fig. 3.16 M), whereas the *tnnt2* Mo injected *foxc1a* single mutants still showed significantly reduced CtA numbers (Fig. 3.16 K, L White arrowheads, M). This data indicates that abnormal CtA formation displayed in *foxc1a* mutants is a result of loss of function of *foxc1a*. In addition, in *tnnt2* Mo-injected *foxc1a* single mutants, AVCs between PHBC and BA showed increased diameter (Fig. 3.16 K), indicating a potential role of head blood circulation in directing retraction of the AVCs, which is in line with previous report (Ulrich et al., 2016).

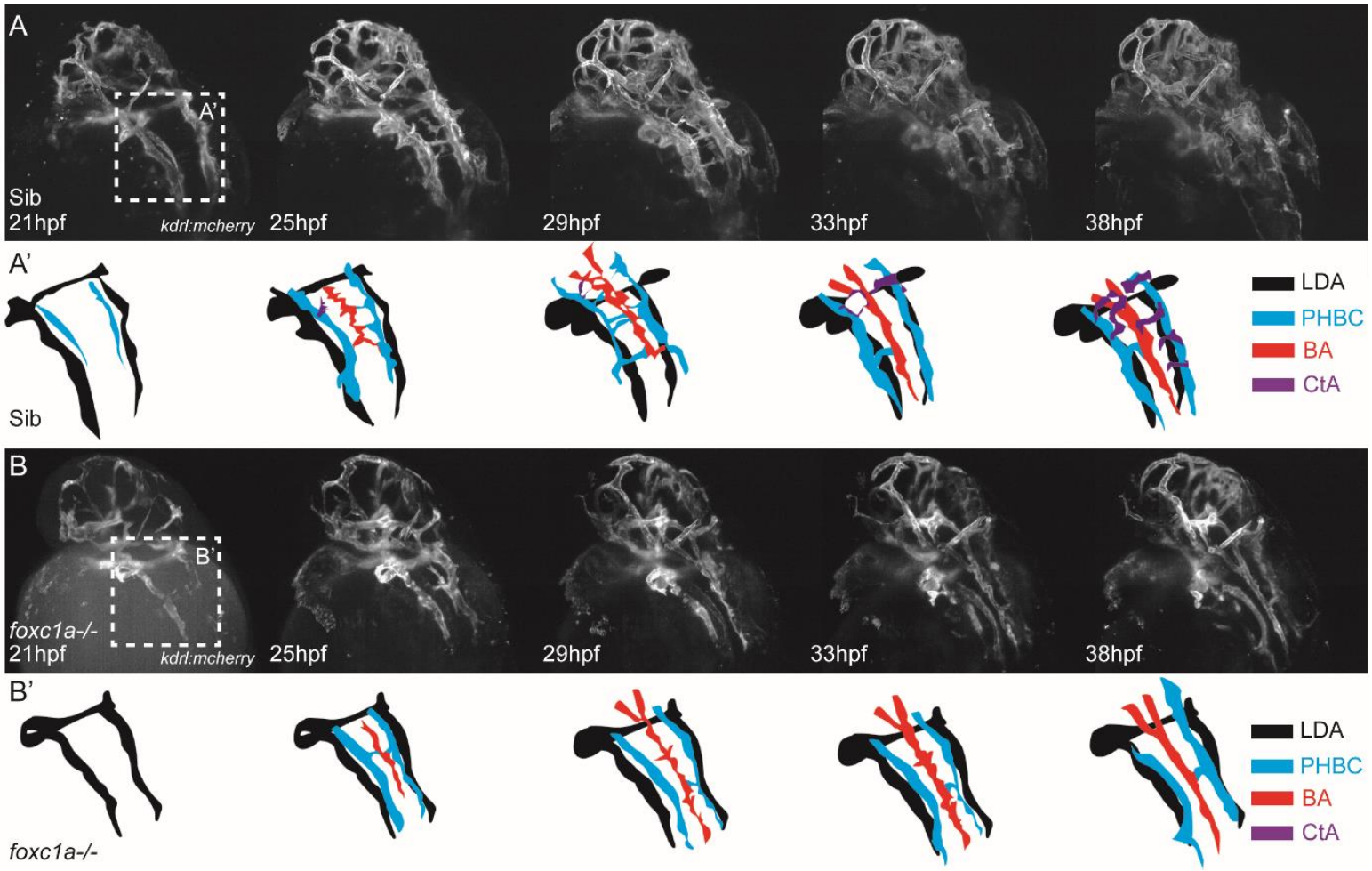

Figure 3.15 *foxc1a* is required for central artery formation

(A-B') Single frame images from confocal time lapses and corresponding illustrations of cranial vessel formation in *Tg(kdrl:mcherry)* WT embryos (A, A') and *foxc1a* single mutants (B, B') from 21hpf to 38hpf. LDA, lateral dorsal aorta; PHBC, primordial hindbrain channel; BA, basilar artery; CtA, central artery.

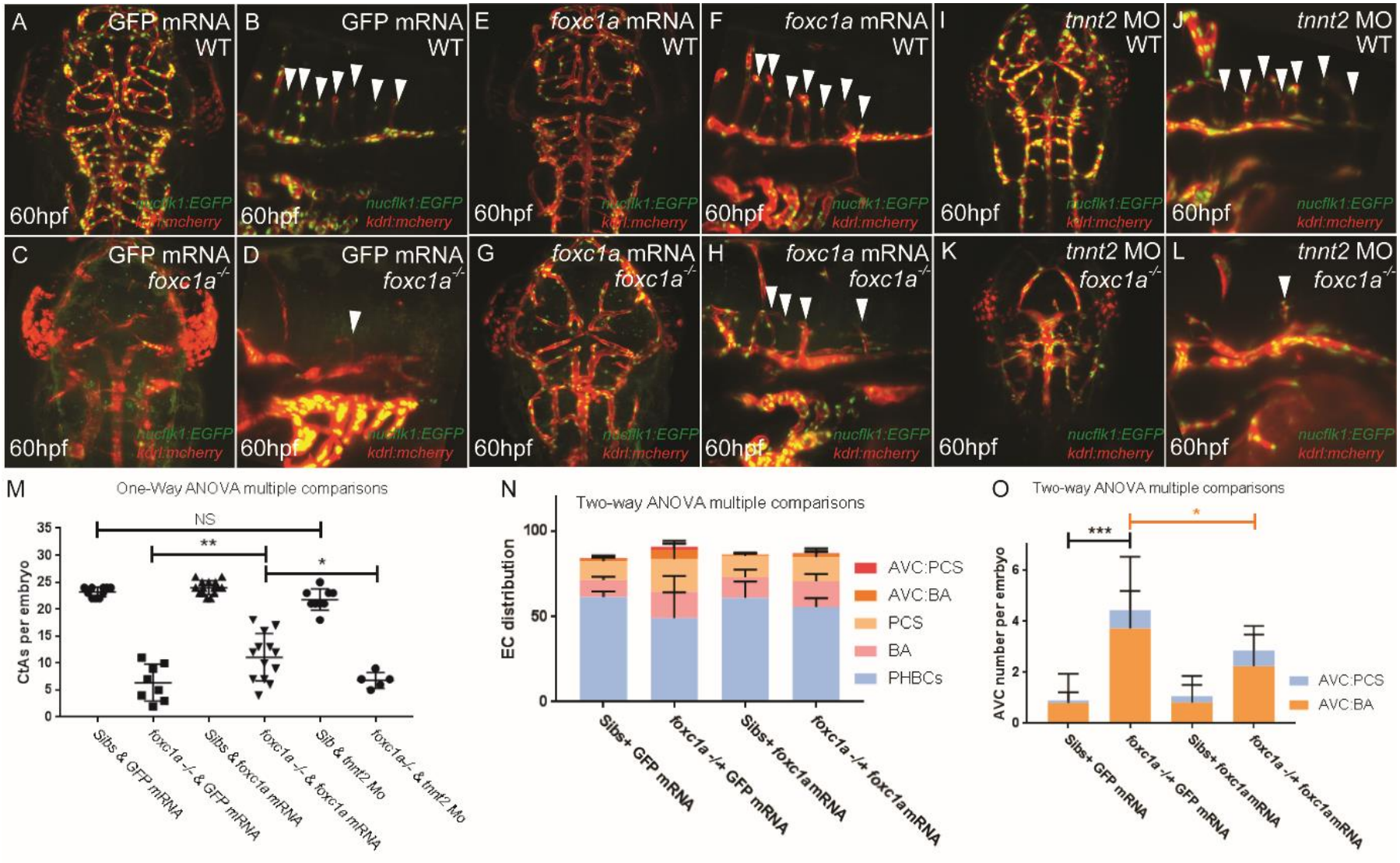
A GFP mRNA WT
B GFP mRNA WT
E foxc1a mRNA WT
F foxc1a mRNA WT
I tnnt2 MO WT
J tnnt2 MO WT
C GFP mRNA foxc1a-/-
D GFP mRNA foxc1a-/-
G foxc1a mRNA foxc1a-/-
H foxc1a mRNA foxc1a-/-
K tnnt2 MO foxc1a-/-
L tnnt2 MO foxc1a-/-
60hpf
nucflk1:EGFP kdrl:mcherry
M
One-Way ANOVA multiple comparisons
CtAs per embryo
NS
**
*
Sibs & GFP mRNA
foxc1a -/- & GFP mRNA
Sibs & foxc1a mRNA
foxc1a -/- & foxc1a mRNA
Sib & tnnt2 Mo
foxc1a-/- & tnnt2 Mo
N
Two-way ANOVA multiple comparisons
EC distribution
AVC:PCS
AVC:BA
PCS
BA
PHBCs
Sibs+ GFP mRNA
foxc1a -/+ GFP mRNA
Sibs+ foxc1a mRNA
foxc1a -/+ foxc1a mRNA
O
Two-way ANOVA multiple comparisons
AVC number per emrbyo
***
*
AVC:PCS
AVC:BA
Sibs+ GFP mRNA
foxc1a -/+ GFP mRNA
Sibs+ foxc1a mRNA
foxc1a -/+ foxc1a mRNA

Figure 3.16 *foxc1a* is required for central artery formation

(A-D) 700pg GFP mRNA injected *Tg(kdrl:mcherry; flk1:nlsEGFP)* WT and *foxc1a* single mutant embryos with dorsal (A, C) and lateral view (B, D) of head. (E-H) 700pg *foxc1a* full length mRNA injected *Tg(kdrl:mcherry; flk1:nlsEGFP)* WT and *foxc1a* single mutant embryos with dorsal (E, G) and lateral view (F, H) of the head. (I-K) 2ng *tnnt2* Mo injected *Tg(kdrl:mcherry; flk1:nlsEGFP)* WT and *foxc1a* single mutant embryos with dorsal (I, K) and lateral view (J, L) of the head. White arrowheads indicate CtA sprouts. (M) Quantification of CtA number per embryo at 60hpf. One-way ANOVA multiple comparisons, **<0.01; *< 0.05; NS, not significant. (N) Quantification of EC number in cranial basilar vessels at 60hpf. Two-way ANOVA multiple comparisons. AVC:PCS, EC numbers in AVC between PHBC and PCS; AVC:BA, EC numbers in AVC between PHBC and BA. Different vessels are colour coded. (O) Quantification of AVC number. Two-way ANOVA multiple comparisons. *<0.05, ***<0.001. AVC:PCS, AVC between PHBC and PCS; AVC:BA, AVC between PHBC and BA. AVC, arterial venous connection; BA, basilar artery; CtA, central artery; EC, endothelial cell; PHBC, primordial hindbrain channel; PCS, posterior communicating segment. .

3.2.10 *foxc1a* is expressed in endothelial cells of cranial vessels, whereas *foxc1b* expression is excluded from these

To further understand the mechanism of how *foxc1a, foxc1b* regulate cranial vessel formation, we analysed the expression of their transcripts in head at 28hpf by utilising florescent *in situ* hybridisation with endothelial cell α-GFP antibody staining in a *Tg(fli1a:EGFP)* transgenic background employed as a vessel reference as introduced in section 3.2.7.

In the head, the expression of *foxc1a* could be detected in mesenchymal derived tissues and the majority of cranial blood vessels, including the PHBC, LDA, CCV and MCeV, which exhibited co-localisation with α-GFP expression (Fig. 3.17 A-C''). Reconstructed transverse sections of single Z-planes of the hindbrain demonstrated co-localisation between *foxc1a* expression and α-GFP antibody staining in *Tg(fli1a:EGFP)* in PHBCs (Fig. 3.17 C-C'' Blue arrowheads). In addition, *foxc1a* was also strongly expressed in the eye and surrounding vessels (Fig. 3.17 A-A''), which supports the idea that the mutation of *Foxc1* is responsible for many eye abnormalities as described before in both mice and zebrafish (Smith et al., 2000, Seo et al., 2012, Skarie and Link, 2009).

The expression of *foxc1b* could be detected in the cranial mesenchyme, however, unlike the expression of *foxc1a*, *foxc1b* was excluded from the cranial vasculature (Fig. 3.17 D-F''). In reconstructed hindbrain transverse Z-plane, expression of *foxc1b* could be only detected perivascular to the PHBC but not within ECs of the PHBC (Fig. 3.17 F-F'' blue arrowheads). Taken together, expression of *foxc1a* and *foxc1b* overlap in non-endothelial tissues, but only *foxc1a* can be detected within the ECs of cranial vessels.

We also examined whether *foxc1a* was expressed in the CtAs at later stages. At 3dpf, the venous marker *flt4* was used as control, since CtAs are venous derived arteries and *flt4* expression is periodically retained in these (Bussmann et al., 2011). *flt4* expression could be detected within CtAs (Fig. 3.18 A'), overlapped with the EC α-GFP antibody staining (Fig. 3.18 B Yellow arrowheads). Similar to the early cerebral expression of *foxc1a*, which could be detected within the CtAs, at 3dpf *foxc1a* expression foci co-localised with EC α-GFP antibody staining (Fig. 3.18 C'-D Yellow arrowheads). On the contrary, no overlapping expression could be found between α-GFP antibody staining and expression of *foxc1b* (Fig. 3.18 F Red arrowheads). Interestingly, *foxc1b* expression could be found adjacent to CtAs (Fig. 3.18 E' Red arrowheads), suggesting potential expression of *foxc1b* in perivascular cells.

Taken together, we find that *foxc1a* is expressed in both cranial EC and surrounding mesenchyme whereas *foxc1b* is expressed perivascularly and excluded from cranial ECs.

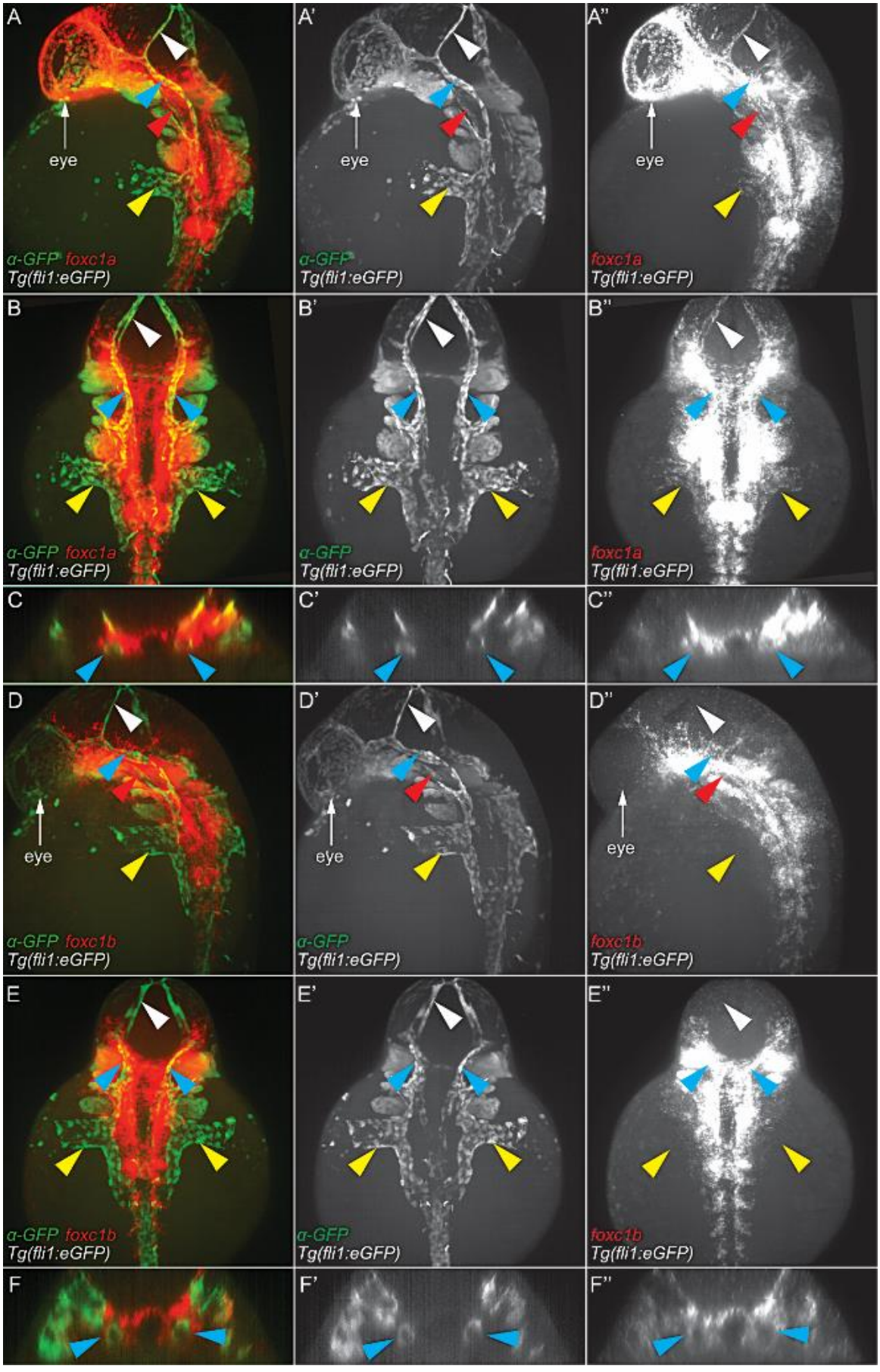
A
eye
α-GFP foxc1a
Tg(fli1:eGFP)
A'
eye
α-GFP
Tg(fli1:eGFP)
A''
eye
foxc1a
Tg(fli1:eGFP)
B
α-GFP foxc1a
Tg(fli1:eGFP)
B'
α-GFP
Tg(fli1:eGFP)
B''
foxc1a
Tg(fli1:eGFP)
C
C'
C''
D
eye
α-GFP foxc1b
Tg(fli1:eGFP)
D'
eye
α-GFP
Tg(fli1:eGFP)
D''
eye
foxc1b
Tg(fli1:eGFP)
E
α-GFP foxc1b
Tg(fli1:eGFP)
E'
α-GFP
Tg(fli1:eGFP)
E''
foxc1b
Tg(fli1:eGFP)
F
F'
F''

Figure 3.17 *foxc1a* is expressed in the major cranial vessels, while *foxc1b* is excluded from these

(A-A'') Lateral dorsal view of Cy3 fluorescent *in situ* of *foxc1a* (red channel) co-expresses with α-GFP (green channel) in *Tg(fli1a:EGFP)* in MCeV (white arrowheads), PHBC (blue arrowheads), LDA (red arrowheads) and CCV (yellow arrowheads) along with other mesenchymal derived tissue in WT embryo head at 28hpf. (B-B'') Dorsal view of Cy3 fluorescent *in situ* of *foxc1a* (red channel) co-expresses with α-GFP (green channel) in *Tg(fli1a:EGFP)* in MCeV (white arrowheads), PHBC (blue arrowheads), LDA (lateral dorsal aorta) and CCV (yellow arrowheads) and mesenchymal derived tissue in WT embryo head at 28hpf. (C-C'') Cross section of hindbrain shows the fluorescent *in situ* of *foxc1a* (red channel) expresses in the PHBC (blue arrowheads). (D-D'') Lateral dorsal view of Cy3 fluorescent *in situ* of *foxc1b* (red channel) expresses in the mesenchymal derived tissue but excluded from the cranial vasculature in WT embryo head at 28hpf. White arrowheads denote MCeV; Blue arrowheads indicate PHBC; Red arrowheads point to LDA and yellow arrowheads point to CCV. (E-E'') Dorsal view of Cy3 fluorescent *in situ* of *foxc1b* (red channel) expresses in the mesenchymal derived tissue but excluded from the cranial vasculature in WT embryo head at 28hpf. White arrowheads denote MCeV; Blue arrowheads indicate PHBC; Red arrowheads point to LDA and yellow arrowheads point to CCV. (F-F'') Cross section of hindbrain shows the expression of *foxc1b* (red channel) is excluded from the PHBC (blue arrowheads). PHBC: primordial hindbrain channel; CCV: common cardinal vein; LDA: lateral dorsal aorta; MCeV: middle cerebral vein; DA, dorsal aorta; PCV, posterior cardinal vein.

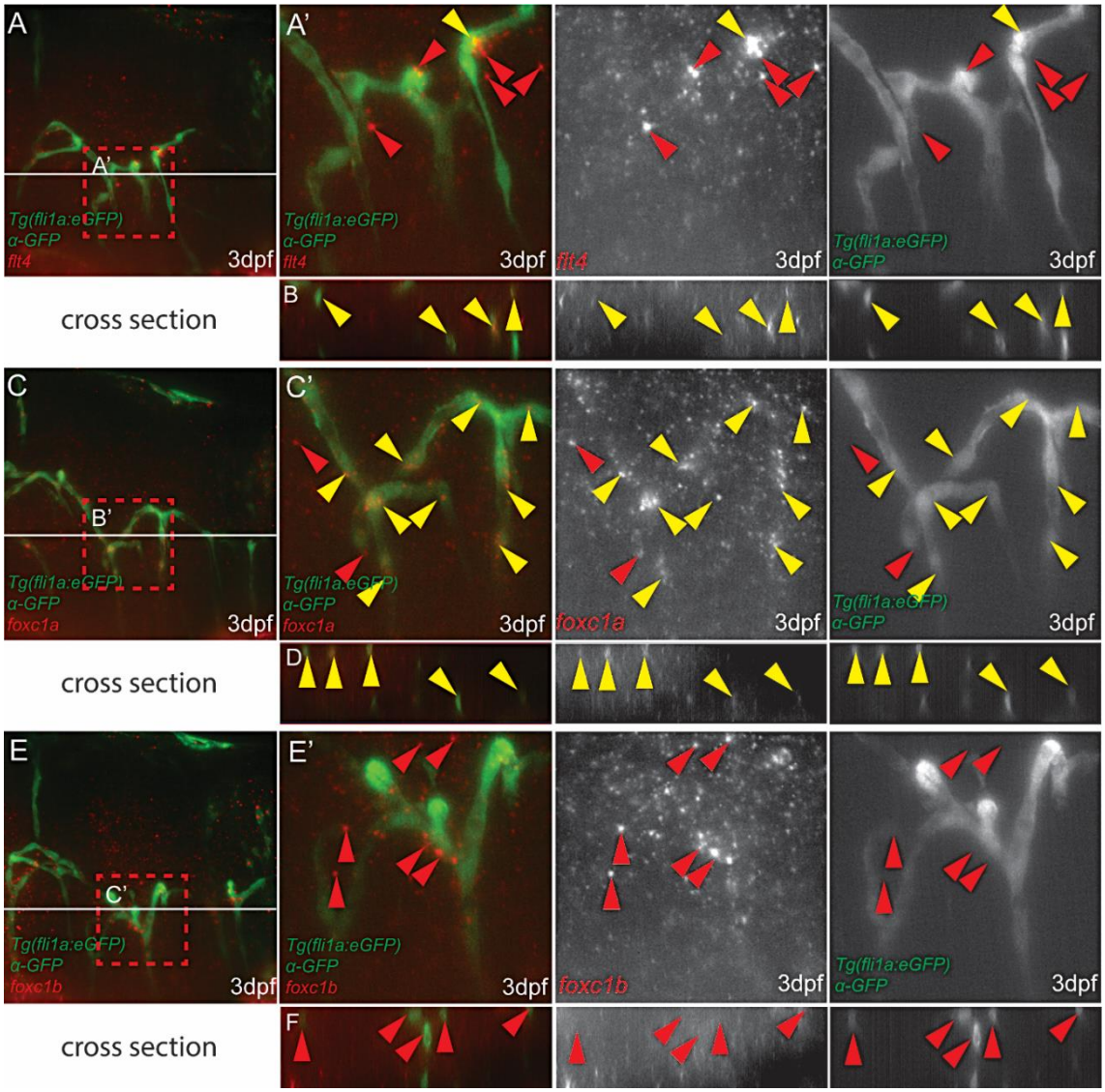

Figure 3.18 *foxc1a* is expressed in central arteries, while *foxc1b* is excluded from these vessels

(A) Lateral view of CtAs in the hindbrain of WT *Tg(fli1a:EGFP)* embryos with *flt4* Cy3 staining (Red) and α-GFP (Green). (A') Higher magnification of red dotted boxed area in panel A showing *flt4* expression can be detected within CtAs. Red arrowheads indicate *flt4* staining is not co-localised with α-GFP antibody staining in the CtAs; Yellow arrowheads point to *flt4* co-expressing with α-GFP antibody staining in the CtAs. (B) Horizontal cross section from the white line in panel A showing co-localisation of *flt4* and α-GFP antibody staining. Yellow arrowheads indicate co-localised expression. (C) Lateral view of CtAs in the hindbrain of WT *Tg(fli1a:EGFP)* embryos with *foxc1a* Cy3 staining (Red) and α-GFP (Green). (C') Higher magnification picture of red dotted boxed area in panel B showing *foxc1a* expression can be detected within CtAs. Red arrowheads indicate *foxc1a* staining is not co-localised with α-GFP antibody staining in the CtAs; Yellow arrowheads point to variable *foxc1a* co-expressing with α-GFP antibody staining in the CtAs. (D)

Horizontal cross section from the white line in panel C showing some co-localisation of *foxc1a* and α-GFP antibody staining. Yellow arrowheads indicate co-localised expression. (E) Lateral view of CtAs in the hindbrain of WT *Tg(fli1a:EGFP)* embryos with *foxc1b* Cy3 staining (Red) and α-GFP (Green). (E') Higher magnification picture of red dotted boxed area in panel C showing *foxc1b* expression is not co-localised with α-GFP staining in CtAs. Red arrowheads indicate *foxc1b* staining is not co-localised with α-GFP antibody staining in the CtAs at 3dpf. (F) Horizontal cross section from the white line in panel E showing *foxc1b* staining is not co-localised with α-GFP antibody staining in the CtAs. Red arrowheads indicate *foxc1b* staining is not co-localised with α-GFP antibody staining in the CtAs. CtA, central artery.

3.2.11 *foxc1a* is required for the expression of *vegf* receptors *flt4* and *kdrl* in developing cranial vessels

vegfr3/ flt4 promotes PHBC formation but not CtA sprouting (Villefranc et al., 2013, Shin et al., 2016a). Whereas, *vegfr4/ kdrl* is essential for both BA and CtA formation from the PHBC (Bussmann et al., 2011). Given that *foxc1a* single mutants displayed delayed PHBC formation and reduced CtA formation (Fig. 3.5, 3.11, 3.15, 3.16) we therefore examined the expression of *flt4* and *kdrl* in *foxc1a* mutants.

At 24hpf, in WT siblings, *flt4* expression could be found in PHBC (Fig. 3.19 A Black arrowhead), CCVs (Fig. 3.19 A' Red arrowheads) and other cranial vessels around the eye (Fig. 3.19 A). In *foxc1a* single mutants, the PHBC expression of *flt4* was significantly reduced (Fig. 3.19 B Black arrowhead). In addition, *flt4* expression was also significantly reduced within CCVs (Fig. 3.19 B' Red asterisks). At later stages, the expression of *flt4* was also reduced significantly in PHBC of the *foxc1a* mutants after its formation was complete (Fig. 3.19 C, D Black arrowheads and asterisk). In section 3.2.9, we reported that PHBC formation was accomplished at approximately 26hpf in the absence of *foxc1a*. Taken together, this reduced expression of *flt4* in *foxc1a* mutants at 34hpf further confirmed that this reduction is due to reduced *flt4* expression within ECs rather than abnormal PHBC formation.

Expression of *kdrl* can be detected in all cranial vessels, including PHBC in WT siblings (Fig. 3.19 E Black arrowhead) and CCVs (Fig. 3.19 E' Red arrowheads) at 24hpf. At 72hpf, in addition to PHBC and CCV, *kdrl* expression could also be observed in CtAs (Fig. 3.19 G Red arrowhead). Similar to the reduced expression of *flt4* that we observed in *foxc1a* mutants, *kdrl* expression was also significantly decreased in the PHBC (Fig. 3.19 F, black asterisk) and CCVs (Fig. 3.19 F' Red asterisks) at 24hpf. Furthermore, *kdrl* expression was reduced at 72hpf in the PHBC (Fig. 3.19 G, H White arrowheads) of *foxc1a* single mutants. Taken together, in the absence of *foxc1a*, expression of *flt4* and *kdrl* were significantly reduced in the cranial vessels, which suggests that *foxc1a* contributes to expression of these *vegf* receptors during formation of cranial blood vessels.

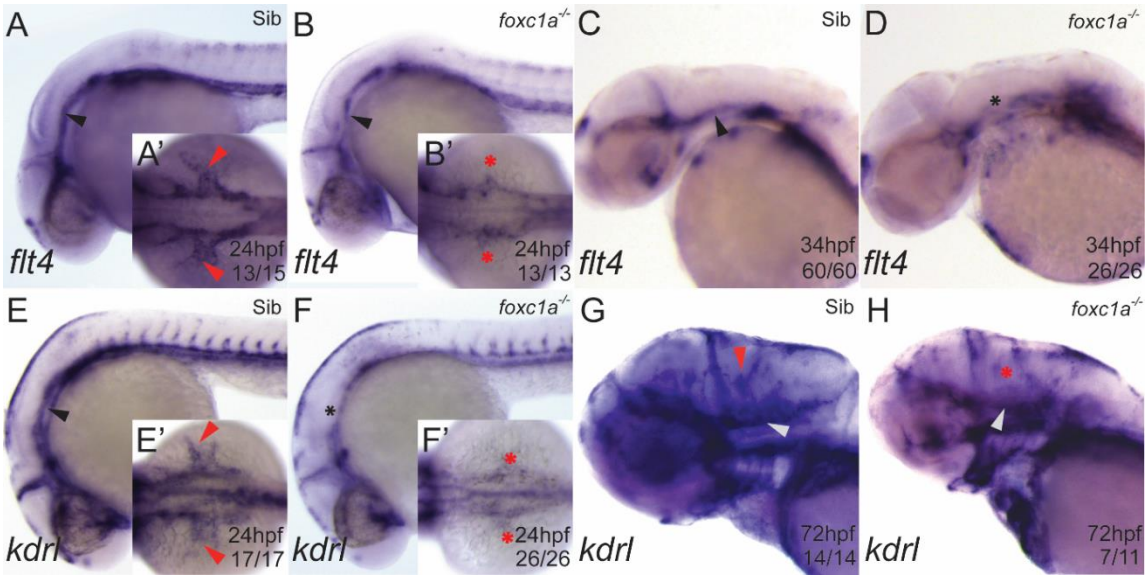

Figure 3.19 *foxc1a* is required for the expression of *vegfrs* in cranial vessels

(A-D) Lateral view of *in situ* hybridisation of *flt4* in WT (A, C), *foxc1a* single mutants (B, D) at 24hpf and 34hpf respectively. (A', B') Dorsal view of *in situ* hybridisation of *flt4* in WT (A'), *foxc1a* single mutants (B') at 24hpf. Black arrowheads indicate PHBC; red arrowheads denote CCVs; black asterisks indicate reduced PHCB expression; red asterisks highlight absent CCV formation. (E, F) Lateral view of *in situ* hybridisation of *kdrl* in the head of WT embryo (E) and *foxc1a* single mutants (F) at 24hpf. (E', F') Dorsal view of *in situ* hybridisation of *kdrl* in WT (E'), *foxc1a* single mutants (F') at 24hpf. Black arrowhead indicates PHBC; red arrowheads denote CCVs; black asterisk indicates reduced PHCB expression; red asterisks highlight absent CCV formation. (G-H) Lateral view of *in situ* hybridisation of *kdrl* in the head of WT embryo (G) and *foxc1a* single mutants (H) at 72hpf. White arrowheads indicate PHBC; red arrowhead points to CtAs; red asterisk highlight absent CtA formation. CCV, common cardinal vein; BA, basilar artery; PHBC, primordial hindbrain channel; CtA, central artery.

3.2.12 *kdrl* overexpression is not sufficient to rescue central artery formation in *foxc1a* mutants

Given that expression of *kdrl* was reduced significantly at both early and late stages in *foxc1a* single mutants (Fig. 3.19 F, H), we hypothesised that the reduced *kdrl* was responsible for reduced CtA formation in *foxc1a* mutants. We injected *kdrl* full length mRNA into the progeny of a *foxc1a* heterozygous incrosses at one-cell stage and quantified CtA frequency (Fig. 3.20).

An expression construct containing full length *kdrl* cDNA was generated by Dr Robert Wilkinson. *kdrl* overexpression did not cause any discernible vascular defects in WT embryos (Fig. 3.20 C) when compared with control mRNA-injected WT embryos (Fig. 3.20 A). Overexpression of *kdrl* mRNA could not rescue either the CtA defect or the ectopic AVCs displayed in *foxc1a* single mutants (Fig. 3.20 B, D, E-G), suggesting *kdrl* alone is not sufficient to rescue CtAs frequency in *foxc1a* single mutants.

3.2.13 *foxc1a* is required for expression of *sox7* and *sox18* in developing cranial vessels

In *sox7* zebrafish mutants, disturbed trunk blood circulation and reduced CtA formation were reported (Hermkens et al., 2015), which are similar to those observed in *foxc1a* mutants. In addition, *sox7* and *sox18* have been shown to function co-operatively to regulate blood vessel formation (Cermenati et al., 2008). *sox7* alone is essential for LDA formation and CtA sprouting (Hermkens et al., 2015). Given the phenotypic similarity between the *sox7* and *foxc1a* mutants, we hypothesised that *sox7* and/ or *sox18* may be regulated by *foxc1a*.

To test this, we first analysed expression of *sox7* and *sox18* in WT and *foxc1a* single mutant embryos. Expression of *sox7* and *sox18* could be detected in major cranial vessels of WT siblings (Fig. 3.21 A, A', C Black arrowheads indicate PHBC, red arrowheads point to CCVs), whereas both *sox7* and *sox18* expression were substantially reduced in cranial vessels of *foxc1a* single mutants (Fig. 3.21 B, B', D Black asterisks indicate PHBC, red asterisks high light CCVs). This data suggests that *foxc1a* is required for the expression of *sox7* and *sox18* in the developing cranial vasculature.

We therefore examined whether *sox7* and *sox18* could rescue abnormal vascular development displayed in *foxc1a* single mutants. We synthesised full length *sox7* and *sox18* mRNA and generated overexpression constructs (See sections 2.1.7 and 2.2.2.10). Overexpression of *sox7* and *sox18* did not cause any detectable gross vascular abnormalities in WT embryos (Fig. 3.21 G, G'' White arrowheads indicate CtAs). However, we detected mildly dilated LDA formation in *sox7* and *sox18* overexpressed WT embryos (Fig. 3.21 E', G'), indicating *sox7* and *sox18* are not only

required, but also sufficient to drive LDA formation. In addition, increased expression of *sox7* and *sox18* failed to rescue CtA formation in *foxc1a* single mutants, suggesting that *sox7* and *sox18* are insufficient to rescue reduced CtA formation in the absence of *foxc1a*.

3.2.14 Combined overexpression of *kdrl* and *sox7* are not sufficient to rescue reduced central artery formation in *foxc1a* single mutants

Both *sox7* and *kdrl* have been reported to directly interact with the Notch signalling pathway and regulate blood vessel formation (Hermkens et al., 2015, Sacilotto et al., 2013, Chiang et al., 2017, Herbert and Stainier, 2011, Clements et al., 2011). To examine whether *sox7* and *kdrl* could function co-operatively to promote CtA formation downstream of *foxc1a*, we overexpressed both *kdrl* and *sox7* in embryos.

Overexpression of both *kdrl* and *sox7* in WT embryos induced expansion of that developing LDA (Fig. 3.21 L) when compared with the control mRNA-injected WT embryos (Fig. 3.21 J'). This abnormal LDA formation was more severe than those observed in *sox7* and *sox18* overexpressed WT embryos (Fig. 3.21 G'), indicating *sox7* and *kdrl* may cooperate during LDA formation. However, combined overexpression of *kdrl* and *sox7* was not sufficient to rescue either reduced CtA frequency or ectopic AVCs in *foxc1a* single mutants (Fig. 3.21 K, M, N-P).

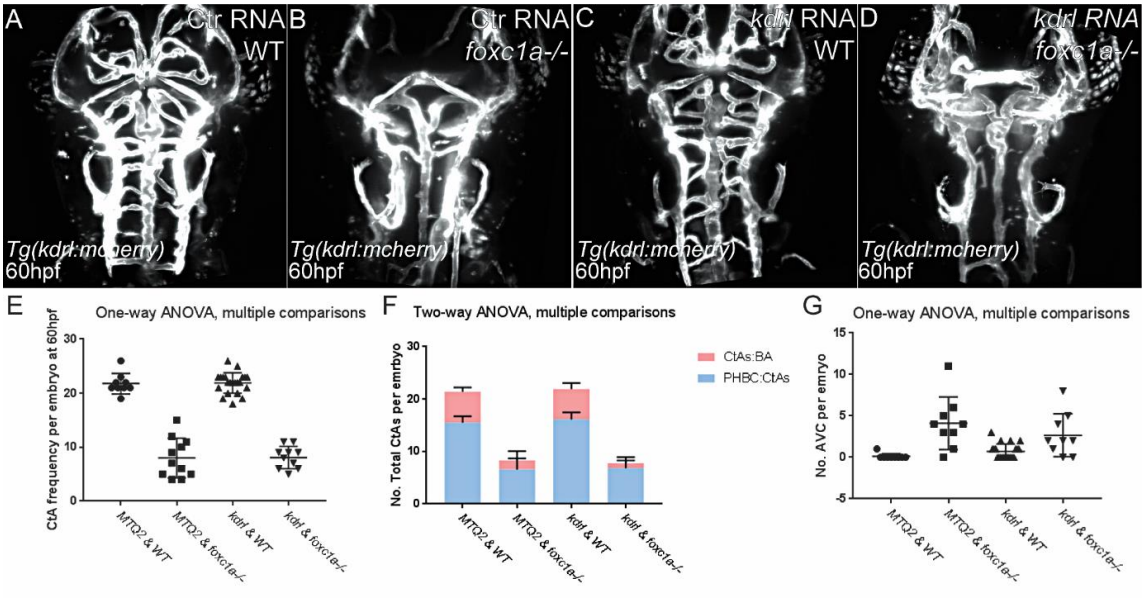

Figure 3.20 *kdrl* overexpression is not sufficient to rescue reduced central artery formation in *foxc1a* mutants

(A, B) Dorsal view of control RNA injected siblings (A) and *foxc1a* single mutants (B) in *Tg(kdrl:mcherry)* background at 60hpf. (C, D) 600pg *kdrl* mRNA injected siblings (C) and *foxc1a* single mutants (D) in *Tg(kdrl:mcherry)* background at 60hpf. (E) Quantification of the frequency of CtAs per embryo at 60hpf in Control RNA and *kdrl* mRNA injected WT and *foxc1a* single mutant embryos. One-way ANOVA multiple comparisons were used. (F) Quantification of CtA numbers. Two-way ANOVA multiple comparisons. CtA connection with different vessels are colour coded. (G) Number of AVC per embryo. One-way ANOVA multiple comparisons. CtA, central artery; AVC, arterial venous connection; PHBC, primordial hindbrain channel; BA, basilar artery.

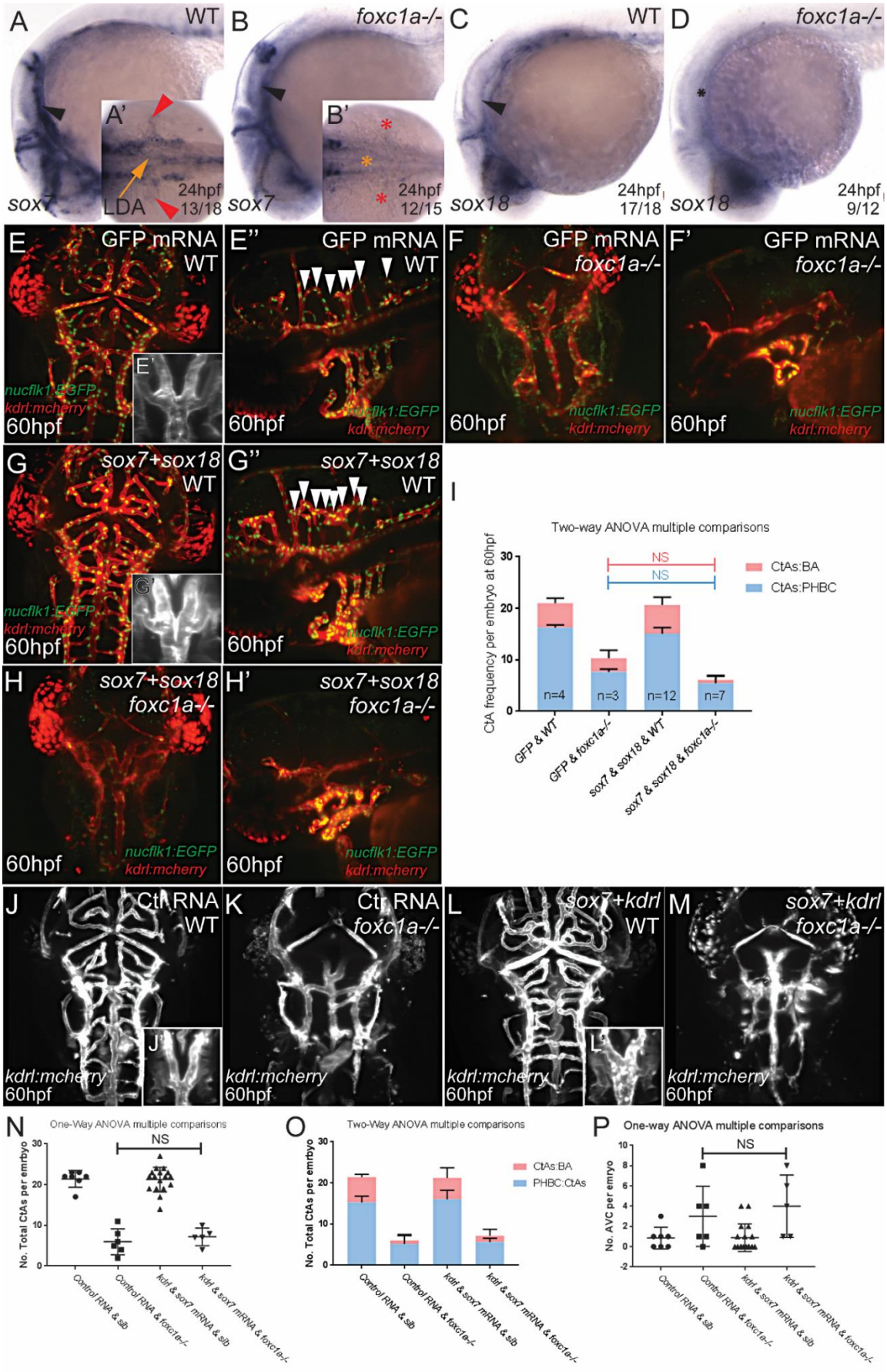
A
WT
A'
LDA
24hpf
13/18
sox7
B
foxc1a-/-
B'
24hpf
12/15
sox7
C
WT
24hpf
17/18
sox18
D
foxc1a-/-
24hpf
9/12
sox18
E
GFP mRNA
WT
E'
nucflk1:EGFP
kdrl:mcherry
60hpf
E''
GFP mRNA
WT
F
GFP mRNA
foxc1a-/-
F'
GFP mRNA
foxc1a-/-
G
sox7+sox18
WT
G'
G''
sox7+sox18
WT
H
sox7+sox18
foxc1a-/-
H'
sox7+sox18
foxc1a-/-
I
Two-way ANOVA multiple comparisons
CtA frequency per embryo at 60hpf
NS
NS
CtAs:BA
CtAs:PHBC
n=4
n=3
n=12
n=7
GFP & WT
GFP & foxc1a-/-
sox7 & sox18 & WT
sox7 & sox18 & foxc1a-/-
J
Ctr RNA
WT
J'
kdrl:mcherry
60hpf
K
Ctr RNA
foxc1a-/-
L
sox7+kdrl
WT
L'
M
sox7+kdrl
foxc1a-/-
N
One-Way ANOVA multiple comparisons
No. Total CtAs per embryo
NS
Control RNA & sib
Control RNA & foxc1a-/-
kdrl & sox7 mRNA & sib
kdrl & sox7 mRNA & foxc1a-/-
O
Two-Way ANOVA multiple comparisons
No. Total CtAs per embryo
CtAs:BA
PHBC:CtAs
P
One-way ANOVA multiple comparisons
No. AVC per embryo
NS

Figure 3.21 *foxc1a* is required for the expression of *sox7* and *sox18* and overexpression of *sox7/ sox18* and *sox7/ kdrl* are not sufficient to rescue central artery formation on *foxc1a* mutants

(A-B') Lateral and dorsal view *sox7* expression in WT embryos (A-A') and *foxc1a* ingle mutants (B, B') at 24hpf. Black arrowheads indicate PHBC; red arrowheads and asterisks denote CCV; orange arrow and asterisk indicate LDA. (C-D) Lateral view of *sox18* expression in WT embryos (C) and *foxc1a* single mutants (D) at 24hpf. Black arrowheads and asterisks indicate PHBC. (E-F') Dorsal and lateral view of control RNA injected siblings (E-E'') with magnified picture of LDA (E') and *foxc1a* single mutants (F-F') in *Tg(kdrl:mcherry; flk1:nlGFP)* at 60hpf. White arrowheads indicate CtAs. (G-H') 350pg *sox7* and 350pg *sox18* mRNA injected siblings (G-G'') with magnified picture of LDA (G') and *foxc1a* single mutants (H-H') at 60hpf. White arrowheads indicate CtAs. (I) Quantification of CtA numbers. Two-way ANOVA multiple comparisons. CtA connection with different vessels are colour coded. NS, not significant. (J. K) Dorsal view of control RNA injected siblings (J) with magnified picture of LDA (J') and *foxc1a* single mutants (J) in *Tg(kdrl:mcherry)* background at 60hpf. (L, M) 600pg *kdrl* and 700pg *sox7* mRNA injected siblings (L) with magnified picture of LDA (L') and *foxc1a* single mutants (M) in *Tg(kdrl:mcherry)* background at 60hpf. (N) Quantification of the frequency of CtAs per embryo at 60hpf in control RNA and *kdrl*+*sox7* mRNA injected WT and *foxc1a* single mutant embryos. One-way ANOVA multiple comparisons were used. NS, not significant. (O) Quantification of CtA numbers. Two-way ANOVA multiple comparisons. CtA connection with different vessels are colour coded. (P) Number of AVC per embryo. One-way ANOVA multiple comparisons. NS, not significant. CCV, common cardinal vein; CtA, central artery; AVC, arterial venous connection; PHBC, primordial hindbrain channel; BA, basilar artery.

3.2.15 *vegfa* overexpression is not sufficient to rescue reduced central artery formation in *foxc1a* mutants

While overexpression of *kdrl* was unable to rescue CtA sprouting in *foxc1a* mutants, we hypothesised that if reduced Vegf receptor expression was responsible for reduced CtA sprouting in *foxc1a* mutants, then overexpression of *vegfa*, the main ligand that binds to Vegfr2 and Vegfr4 (Herbert and Stainier, 2011), would not rescue CtA sprouting. The two dominantly expressed isoforms of *vegfa* in zebrafish are $vegfa_{165}$ and $vegfa_{121}$ (Liang et al., 1998).

$vegfa_{165}$ (200pg) and $vegfa_{121}$ (50pg) full length mRNA, had been previously reported to rescue a *vegfa* zebrafish mutant to viability (Rossi et al., 2016), and are thus biologically active at these doses. These two *vegfa* isoforms were injected individually and in combination into one-cell stage zebrafish embryos (Fig. 3.22) and CtA connections were quantified at 3dpf. Following injection, ectopic angiogenic sprouting was observed within the developing trunk, indicating that full length *vegfa* mRNA was functional at these doses (data not shown). Injection of $vegfa_{165}$ and $vegfa_{121}$ mRNA individually and in combination had no significant effect on CtA numbers in WT embryos (Fig. 3.22 C, C', E, E', G, G' Yellow arrowheads, I Blue colour coded, J). In addition, neither overexpression of $vegfa_{165}$ or $vegfa_{121}$ individually nor combined could rescue CtA formation in *foxc1a* single mutants (Fig. 3.22 D', F', H' Yellow arrowheads, I, J) when compared to control siblings (Fig. 3.22 A', C', E', G' Yellow arrowheads, I, J). Therefore, *vegfa* overexpression at minimum levels sufficient to induce ectopic trunk angiogenesis is not sufficient to rescue reduced CtA formation in *foxc1a* mutants, which is in line with observations of reduced *vegf* receptor expression in the PHBC (Section 3.2.11) since Vegfa ligand functions genetically upstream of Vegf receptors.

3.2.16 High level *vegfa* reduces central artery formation from primordial hindbrain channel

Distinct Vegf levels have been reported to selectively regulate trunk angiogenesis from arteries and veins (Casie Chetty et al., 2017). We therefore performed high-dose overexpression of $vegfa_{121}$ (700pg) and $vegfa_{165}$ (700pg) to determine whether higher levels of *vegfa* could rescue CtA sprouting in *foxc1a* mutants.

Interestingly, injection of a high dose of $vegfa_{165}$ or $vegfa_{121}$ mRNA resulted in reduction of CtA sprouts in WT embryos (Fig 3.23 A, A', C, C', E, E' Yellow arrowheads, G, H). In particular, the connections between CtA and PHBC were significantly reduced (Fig. 3.23 G Blue colour coded) when compared with the control mRNA-injected WT embryos (Fig. 3.23 A, A' Yellow arrowheads,

G). However, the BA to CtA connections were not significantly affected after *vegfa* high dose overexpression (Fig. 3.23 G). This data indicates that in WT embryos high Vegf signalling suppresses angiogenic sprouting from the PHBC/ vein but not from the BA/ artery. In addition, overexpression of a high dose of *vegfa* failed to rescue the reduced CtA formation displayed in *foxc1a* single mutants (Fig. 3.23 B, B', D, D', F, F' yellow arrowheads) suggesting that this dose-dependent Vegfa regulation of cranial angiogenesis lies upstream of *foxc1a* function.

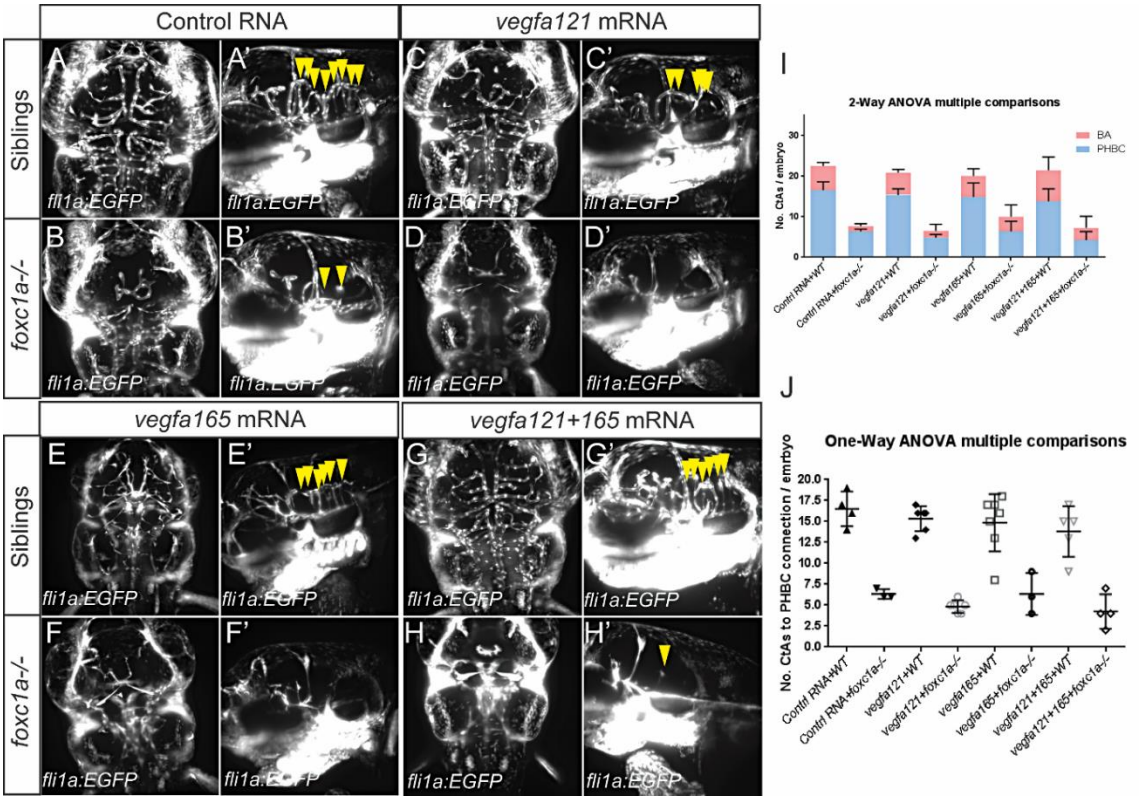

Figure 3.22 Low levels *vegfa* are not sufficient to rescue central artery formation in *foxc1a* single mutants

(A-H') Dorsal and lateral view of control RNA injected siblings (A, A') and *foxc1a* single mutants (B, B'); Low dose $vegfa_{121}$ overexpression in siblings (C, C') and *foxc1a* single mutants (D, D'); Low dose $vegfa_{165}$ overexpression in siblings (E, E') and *foxc1a* single mutants (F, F'); Low dose combined $vegfa_{121}$ and $vegfa_{165}$ overexpression in siblings (G, G') and *foxc1a* single mutants (H, H'). Yellow arrowheads indicate CtAs. (I) Quantification of CtA numbers. Two-way ANOVA multiple comparisons. CtA connection with different vessels are colour coded. (J) Number of CtAs to PHBC connections per embryo in WT and *foxc1a* single mutants. One-way ANOVA multiple comparisons. CtA: central artery; BA: basilar artery; PHBC: primordial hindbrain channel.

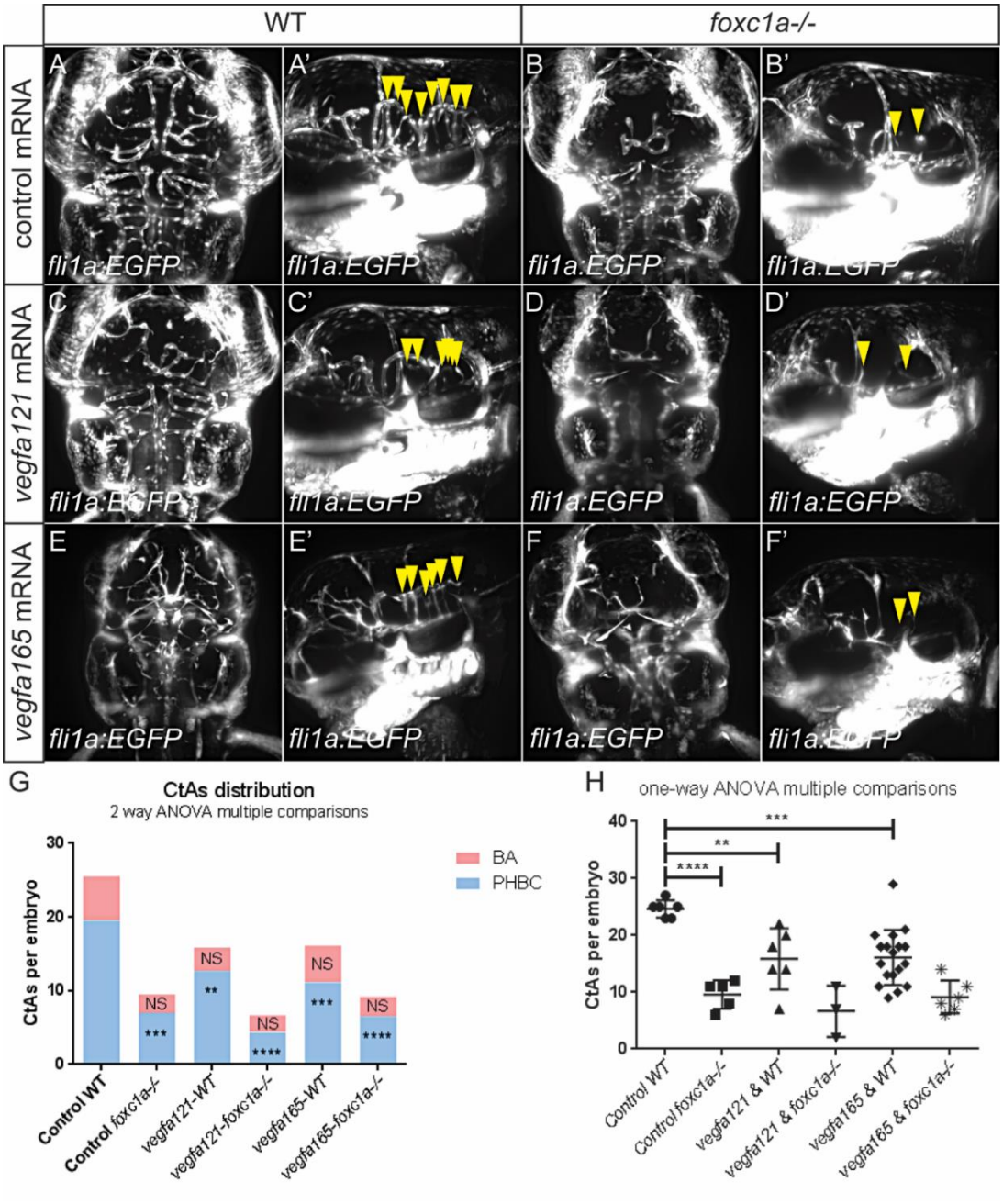

Figure 3.23 High dose overexpression of *vegfa* inhibits central artery sprouting

(A-F') Dorsal and lateral view of control RNA injected siblings (A, A') and *foxc1a* single mutants (B, B'); 700pg *vegfa*$_{121}$ mRNA injected siblings (C, C') and *foxc1a* single mutants (D, D'); 700pg *vegfa*$_{165}$ mRNA injected Wt embryos (E, E') and *foxc1a* single mutants (F, F'). Yellow arrowheads indicate CtAs. (G) Quantification of CtA numbers. Two-way ANOVA multiple comparisons. ****<0.0001; ***<0.001; **<0.01; NS, not significant. CtA connection with different vessels are colour coded. (H) Quantification of CtAs frequency per embryo. One-way ANOVA multiple comparisons. ****<0.0001; ***<0.001; **<0.01. CtA : central artery; BA: basilar artery; PHBC: primordial hindbrain channel.

3.3 Discussion

In this chapter, we describe the generation of novel *foxc1a* and *foxc1b* mutant alleles and have applied them to characterise the function of these genes during cranial blood vessel formation. Our data indicate that *foxc1a* is required for the formation of PHBC, LDA, CCV and CtAs, whereas *foxc1b* is dispensable for these processes. Here we highlight our findings below:

1. *foxc1a* promotes the formation of PHBC potentially by regulating the expression of *flt4*.
2. *foxc1b* alone is dispensable for cranial vascular development.
3. *foxc1a* is required for the expression of *kdrl*, *sox7* and *sox18*, which further contribute to cranial angiogenesis from the PHBC/ vein to LDA formation.

3.3.1 *foxc1a* and *foxc1b* are genetic orthologues of mammalian *Foxc1*

Early zebrafish studies had used amino acid sequence alignment to show that zebrafish *foxc1a* and *foxc1b* were genetic orthologues of mammalian *Foxc1* by sequence homology (Topczewska et al., 2001b). More recent studies have described zebrafish *foxc1a* as an orthologue of mammalian *Foxc1* and *foxc1b* as a orthologue of mammalian *Foxc2* (Veldman and Lin, 2012, Chen et al., 2017), or alternatively zebrafish *foxc1a* and *foxc1b* are orthologues of mammalian *Foxc2* (Jang et al., 2015). To overcome these discrepancies in interpretation we performed bioinformatics analysis to determine synteny using multiple species and demonstrated that, in keeping with previously published sequence homology (Topczewska et al., 2001b), *foxc1a* and *foxc1b* are orthologues of mammalian *Foxc1*, whereas *Foxc2* has been lost in teleosts during evolution (Fig. 3.1, 3.2).

3.3.2 *foxc1a* is required for common cardinal vein formation

Very little is known about the mechanisms that control formation of the CCV. In *foxc1a* single mutants and *foxc1a*; *foxc1b* double mutants at 22hpf, CCV formation was delayed (Fig. 3.11 B, C), but by 28hpf, disrupted CCV formation was evident in *foxc1a* single mutants (Fig. 3.12 C, E). This indicates an important requirement for *foxc1a* during CCV formation. Common cardinal veins have a unique open ended structure, they collect all venous blood and transfer it back to the heart to terminate the blood circulatory loop (Schuermann et al., 2014, Isogai et al., 2001, Helker et al., 2013). Therefore, abnormal CCV formation displayed in *foxc1a* single mutants and *foxc1a*; *foxc1b* double mutants could contribute to the absence of trunk blood circulation in these

embryos. Interestingly, CCV formation was normal following Vegf inhibition in WT embryos and was normal (Fig. 3.14 A', B' Red arrowheads) when compared with *foxc1a* single mutants (Fig. 3.14 D' Red asterisks) post AV951 treatment. This data indicates that *foxc1a* is required for CCV formation independently of the Vegf signalling.

Lumen ensheathment has been proposed as a novel mechanism for CCV formation in zebrafish (Helker et al., 2013). Signalling through Vegfc/ Flt4 was reported to be required for EC proliferation in the CCV, whereas *cdh5* and *sema3d* are required for extension and maintaining the integrity of the CCV EC sheets (Helker et al., 2013, Hamm et al., 2016). At 56hpf, CCVs in *foxc1a* single mutants were hypoplastic (Fig. 3.12 E), however, we did not detect lesions within the CCV sheets in *foxc1a* single mutants (Fig. 3.12 E) as described previously in *cdh5* mutants and *sema3d* mutants, which also display abnormal CCV formation (Hamm et al., 2016). Therefore, the CCV defect shown in *foxc1a* single mutants is unlikely to be caused by abnormal cell–cell contacts or reduced actin cables as shown in *sema3d* and *cdh5* mutants (Hamm et al., 2016). In addition, the expression of *sema3d* can be detected in the mesenchyme next to the CCV (Hamm et al., 2016). This mesenchymal *sema3d* has been reported to repulse ECs and guide the collective EC migration non-cell autonomously (Hamm et al., 2016). Overexpression of *sema3d* showed similar hypoplastic CCV formation to *foxc1a* single mutants (Hamm et al., 2016) (Fig. 3.12 E). Interestingly, we have observed expression of *foxc1a* at high levels in mesenchyme next to the developing CCV (Fig. 3.13 A, A' Pink arrowheads). Thus, *foxc1a* could potentially regulate CCV formation in a non-cell autonomous manner via *sema3d*. In addition, endothelial expression of *sema3d* has only been detected in the leading tip cells of the CCV (Hamm et al., 2016), whereas *foxc1a* expression can be detected in the EC of the posterior CCV (Fig. 3.13 A' Blue arrowheads) with higher intensity than the leading tip ECs (Fig. 3.13 A' White arrowheads) during CCV formation in WT embryos at 28hpf. This complementary expression within the CCV suggests a potential negative interaction between *foxc1a* and *sema3d*. It is formally possible that *foxc1a* may negatively regulate the expression of *sema3d* either in the mesenchyme or in ECs of the CCV to control CCV formation.

Taken together, we propose that *foxc1a* is essential for CCV formation and that this occurs independently of the Vegf signalling. *foxc1a* potentially contributes to CCV formation via cell-autonomous and/ or non-cell autonomous manners. However, further experiments are required to establish the cause of the CCV formation defect in *foxc1a* single mutants, for example the relative importance of EC specification, apoptosis or proliferation during this process.

3.3.3 *foxc1a* is required for cranial angiogenesis

In zebrafish, *foxc1a* and *foxc1b* displayed largely overlapping expression patterns during embryonic development (Fig. 3.17). However, our data indicate that only *foxc1a* can be detected in ECs of developing cranial vessels in the head (Fig. 3.17 A-C). Similar to murine *Foxc2*, the transcript of zebrafish *foxc1b* cannot be detected in ECs within the developing brain vasculature (Fig. 3.17, 3.18) (Siegenthaler et al., 2013). We observed almost total loss of CtAs in *foxc1a* single and *foxc1a*; *foxc1b* double mutants (Fig. 3.5 B-D). This reduction in brain angiogenesis has not been reported previously in murine *Foxc1*-depleted mutants. Very recently, reduced CtA formation was reported by Yue *et al.* in their *foxc1a* single mutants (Yue et al., 2017). In *foxc1a*; *foxc1b* double mutants, cranial angiogenic defects are similar to those observed in *foxc1a* single mutants (Fig. 3.5 D). In addition, *foxc1b* single mutants show normal blood vessel formation (Fig. 3.6). Taken together, *foxc1a* is likely to be responsible for the absence of CtAs displayed in both single and double mutants, whereas *foxc1b* is dispensable for this process. By utilising *tnnt2* Mo (Sehnert et al., 2002) to stop the blood circulation in both WT and *foxc1a* single mutants (Fig 3.16 I-L), we conclude that cranial angiogenesis is independent of blood circulation. This finding is in line with previously published data (Fujita et al., 2011). Therefore the defective cranial angiogenesis displayed in the mutants resulted from loss of function of *foxc1a* rather than disrupted blood circulation.

In mouse brains, *Foxc1* is expressed in both perivascular cells and ECs (Siegenthaler et al., 2013, Kume et al., 2001). Conditional KO of *Foxc1* in pericytes and vSMCs leads to proliferation of these two cell types, which contributes to failure of establishing blood brain barrier (BBB) integrity and leads to mild focal cerebral haemorrhage (Siegenthaler et al., 2013). Global *Foxc1* KO mice show similar but more severe defects than pericyte-specific *Foxc1* KO mice (Siegenthaler et al., 2013, Kume et al., 1998). Interestingly, EC specific KO of *Foxc1* did not result in abnormal vascular development as displayed in either the pericyte KO mice or the global KO mice (Siegenthaler et al., 2013, Kume et al., 1998, Hayashi and Kume, 2008a). Taken together, *Foxc1* from pericytes is mainly required for maintaining BBB integrity in mice. However, the possibility that *Foxc1* and *Foxc2* can compensate for each other during cerebral vasculature and BBB development still remains unclear. To be noted, *Foxc2* expression cannot be detected in brain EC in E14.5 mice (Siegenthaler et al., 2013). Therefore, this yet identified interaction between murine *Foxc1* and *Foxc2* in the brain is more likely to be in the pericytes than in ECs.

Unlike mouse mutants, we did not observe haemorrhage in either *foxc1a* single or *foxc1a*; *foxc1b* double mutant zebrafish (Siegenthaler et al., 2013) and also in zebrafish following knockdown of *foxc1a/ b* by Mos (French et al., 2014, Skarie and Link, 2009). Brain haemorrhage has been reported in the *notch3* zebrafish mutant with significant reduction of pericytes and vSMCs (Wang et al., 2014). This phenotype is similar to that reported in the dominant-negative *pdgfrb* (pericyte and vSMC marker) transgenic line (Stratman et al., 2017) and *pdgfrb* mutant zebrafish (Ando et al., 2016). Interestingly, normal vasculature patterns were reported in these zebrafish lines (Stratman et al., 2017, Ando et al., 2016, Wang et al., 2014). Thus the reduced CtA formation displayed in *foxc1a* single mutants and *foxc1a*; *foxc1b* double mutants is unlikely to be due to abnormal pericyte and/ or vSMC recruitment.

While neuronal *Foxc1* negatively regulates lymphangiogenesis in mice cornea (Seo et al., 2012) and zebrafish *foxc1a* is required for neural circuit development (Banerjee et al., 2015), abrogation of neural crest formation by Mo KD in zebrafish did not perturb CtA formation (Ando et al., 2016). Therefore, neuronal *foxc1a* is unlikely to contribute to cranial angiogenesis.

Taken together, the reduced angiogenesis observed within the developing brain of zebrafish *foxc1a* mutants is more likely due to loss of Foxc1a function in ECs rather than perivascular tissues or neural crest. Our data reveals an important difference in *foxc1a*-mediated control of cranial angiogenesis between teleosts and mammals.

3.3.4 *foxc1a* positively regulates expression of *flt4* and *kdrl* in developing cranial blood vessels

Among the many Vegf receptors, Vegfr3/ Flt4 and Vegfr4/ Kdrl have been reported to be essential for PHBC and CtA formation respectively (Shin et al., 2016a, Bussmann et al., 2011, Villefranc et al., 2013). Significant down-regulation of *flt4* and *kdrl* expression were detected in *foxc1a* mutants (Fig. 3.19), suggesting *foxc1a* promotes cranial blood vessel formation by positively regulating the expression of *flt4* and *kdrl.* Delayed formation of cranial blood vessels was more pronounced in *foxc1a; foxc1b* double mutants than *foxc1a* single mutants (Fig. 3.11 B, C). These data indicate a genetic interaction between *foxc1a* and *foxc1b* during cranial vasculogenesis.

Zebrafish *foxc1b* has previously been proposed as a functional orthologue of mammalian *Foxc2* (Skarie and Link, 2009). Murine *Foxc2* single mutants were reported with pre- and perinatal lethality, which display defective patterned arterial arches and reduced ISV formation in the trunk (Iida et al., 1997, Winnier et al., 1997). Here we report that zebrafish *foxc1b* single mutants are homozygous viable and fertile. During embryogenesis, no morphological or vascular defects could

be detected, which suggests that zebrafish *foxc1b* is not a functional orthologue of mammalian *Foxc2*. However, we cannot exclude the possibility that zebrafish *foxc1a* could have retained some functions of *Foxc2* in addition to *Foxc1*. Further functional conservations between mammalian *Foxc* genes and zebrafish *foxc1* genes will be discussed in Chapter 4.

3.3.5 *foxc1a* promotes expression of *sox7* in developing cranial blood vessels

sox7 and *sox18* are members of the SRY-related high mobility group box superfamily F-subgroup (SoxF) (Pendeville et al., 2008). Physical interaction with RBPJ/ Notch intracellular domain (NICD) and SoxF transcription factors with *Dll4* gene are required for normal arterial *dll4* expression (Sacilotto et al., 2013). Further evidence suggests that partially redundant but collectively essential roles of SoxF transcription factors located directly upstream of Notch signalling during early arterial differentiation (Sacilotto et al., 2013, Chiang et al., 2017, Hermkens et al., 2015). SoxF transcription factors have also been reported to be important for venous specification via Notch-mediated regulation of *nr2f2/ coup-tf2* expression (Swift et al., 2014). *sox7* has been shown to be required for cranial CtA formation and LDA patterning in zebrafish (Hermkens et al., 2015). We report that *foxc1a* single mutants display deformed LDA with abnormal connections to PHBC and/ or the DA (Fig. 3.7 B-D), which is similar to *sox7* zebrafish mutants (Hermkens et al., 2015). The variable defects in LDA formation are also likely to account for the variable blood circulation defects in addition to the defectively formed CCV displayed in *foxc1a* single mutants. Expression of *sox7* was significantly reduced in the absence of *foxc1a* (Fig. 3.21 A, B) suggesting *foxc1a* is required for endogenous *sox7* expression, and this may contribute to the CtA and LDA formation. In addition, dilated LDA formation after overexpression of *sox7* and *sox18* in WT embryos (Fig. 3.21 G') more likely resulted from gain of function of *sox7* alone, since *sox7* is required for LDA formation in zebrafish (Hermkens et al., 2015). Furthermore, gain of function of *kdrl* and *sox7* in the WT embryos showed more pronounced LDA abnormality (Fig. 3.21 J', L') suggesting genetic interaction between *kdrl* and *sox7* during LDA formation.

We were unable to rescue cranial angiogenesis in *foxc1a* single mutants by constitutive overexpression of *kdrl* and/ or *sox7* (Fig. 3.20-3.21). These data indicate: (1) Foxc1a may control expression of additional unidentified regulatory genes critical for this process; (2) Timing, expression level and tissue specificity of *kdrl* and *sox7* could also be critical in regulating angiogenesis from the PHBC.

3.3.6 *foxc1a* positively regulates cranial lymphatic formation potentially by promoting expression of *flt4* and *sox18*

flt4 is not only required for vasculogenesis, but also has been well-established to be required for lymphangiogenesis in both mice and zebrafish (Hogan et al., 2009a, Karkkainen et al., 2004, Kuchler et al., 2006, Villefranc et al., 2013, Yaniv et al., 2006). Severe facial lymphatic defects have been reported with truncated lateral facial lymphatic (LFL) vessel, absent medial facial lymphatic (MFL) vessel, otolithic lymphatic vessel (OLV) and lymphatic branchial arches (LAA) in the absence of zebrafish *flt4* (Shin et al., 2016a). Similar facial lymphatic defects were also observed in *foxc1a* single mutants at 5dpf with absent MFL and LAA (Fig. 3.8 B, B'). This is likely due to the reduced activity of Flt4/ Vegfc signalling in *foxc1a* single mutants. The initiation of facial lymphatic formation begins from the facial lymphatic sprout, which originates from the CCV at 26hpf (Astin et al., 2014). In section 3.2.7, we report abnormal CCV formation in *foxc1a* single mutants, which could also contribute to the abnormal facial lymphatic patterning. In addition, *vegfd* also compensates with *vegfc*, and together they control facial lymphatic development, trunk lymphangiogenesis and angiogenesis (Astin et al., 2014, Bower et al., 2017). More strikingly, Vegfd functions via binding to Kdr (Vegfr2) rather than Vegfr3 or Vegfr4 which are bound by Vegfc (Bower et al., 2017). Thus, *vegfd/ vegfr2* may provide a potential compensatory pathway for lymphatic defects mediated by interaction between *foxc1a* and *vegfc/ flt4*. This requires further investigation but could potentially explain why facial lymphatic defects displayed in *foxc1a* single mutants were less severe than *vegfc/ flt4* mutants (Shin et al., 2016a).

A novel LEC in the brain has been discovered and described recently as the brain lymphatic endothelial cell (BLEC) in zebrafish (van Lessen et al., 2017). The formation of this unique venous-derived cell type is positively regulated by the Ccbe1-mediated Flt4/ Vegfc pathway (van Lessen et al., 2017). In *foxc1a* single mutants, the initial BLEC sprout from the PMBC was undetectable at 56hpf in comparison to WT siblings (Fig. 3.9 B-B''). At 5dpf, BLECs can be detected in *foxc1a* single mutants with severely disrupted organisation (Fig. 3.10 B-B''). Collectively, *foxc1a* might have a role for BLEC specification potentially via regulating the Flt4/ Vegfc signalling pathway. It has been shown that SeAs are essential for providing guidance for LEC migration along the SeAs in zebrafish trunk (Bussmann et al., 2010). Since BLECs migrate alongside with the mesencephalic vein (MsV) (van Lessen et al., 2017), it is possible that the MsV potentially guides the migration of BLECs. Therefore, *foxc1a* might also indirectly contribute to BLEC migration via regulation of cranial vessel patterning. However, further experiments are needed to examine this hypothesis.

The spatiotemporal relationship between the facial lymphatic development and the BLEC sprouting suggests a potential contribution from the facial lymphatics to the BLEC specification (Okuda et al., 2012, van Lessen et al., 2017, Venero Galanternik et al., 2017). However, this potential interaction between the facial lymphatics and BLECs remains to be examined. Ccbe1 contributes to lymphangiogenesis via regulation of maturation of Vegfc (Le Guen et al., 2014). Interestingly, unlike the completely abolished BLEC specification displayed in the *ccbe1* zebrafish mutant (van Lessen et al., 2017), *foxc1a* single mutants displayed a milder BLEC defect. This could also be explained by *vegfd/ kdr-vegfc/ flt4* compensation.

In addition, *sox18* is essential for venous angiogenesis and lymphangiogenesis (Cermenati et al., 2013). In mice, Sox18 acts as a direct upstream activator of Prox1 to specify lymphatic ECs (Francois et al., 2008). In zebrafish, *sox18* genetically interacts with *vegfc* to promote venous and lymphatic sprouting (Cermenati et al., 2013). Therefore, the lymphatic defect displayed in *foxc1a* single mutants could also be explained by *foxc1a*-mediated down regulation of *sox18* expression level (Fig. 3.21 C, D).

3.3.7 Different *vegfa* levels selectively regulate angiogenesis in the head

Vegfa as the major Vegf ligand has been reported many times to drive angiogenesis positively (Herbert and Stainier, 2011). However, we reported that overexpression of *vegfa* led to dose-dependent regulation of angiogenesis in WT embryos (Fig. 3.22, 3.23).

Given that the expression of *vegf* receptors was reduced significantly in the cranial vessels (Fig. 3.19), it was not a surprise to see that low dose overexpression of *vegfa* failed to rescue the reduced CtA formation in *foxc1a* single mutants (Fig. 3.22). Because Vegf ligands act upstream of Vegf receptors (Herbert and Stainier, 2011).

High dose $vegfa_{121}$ and $vegfa_{165}$ mRNA individual injections led to reduction of CtA numbers from the PHBC/ vein, whereas BA angiogenesis remained unchanged (Fig. 3.23 G). This data indicates the possibility that high level Vegf negatively regulates cranial angiogenesis from the PHBC/ vein. Interestingly, that high Vegf signalling induces arterial marker expression and inhibits venous specification has been reported recently in zebrafish trunk vessels (Casie Chetty et al., 2017). This specific Vegf level requirement during cranial angiogenesis explains why constitutive overexpression of *kdrl* and/ or *sox7* failed to rescue the reduced CtA formation in *foxc1a* single mutants.

A potential explanation for this unusual reduction of venous CtA numbers following the high-dose *vegfa* overexpression in WT embryos (Fig. 3.23 G) would be that high level Vegf signalling promotes arterial gene expression while inhibiting venous marker expression in the PHBC. Thus high-dose *vegfa* injection potentially arterialises the PHBC/ vein, which subsequently reduces the venous angiogenesis from the PHBC. More experiments are needed to address how the Vegf level selectively regulates angiogenesis and to find the key signalling pathways involved in this complex regulation process.

CHAPTER 4

Investigating the Role of *foxc1a* and *foxc1b* Transcription Factors during Trunk Blood Vessel Formation and Haematopoiesis

4.1 Introduction

In the previous chapter we introduced the mechanism by which *foxc1a* and *foxc1b* promote cranial blood vessel formation and the key signalling pathways involved in this process. Given that *foxc1a; foxc1b* double mutants exhibited hypersprouting of intersegmental vessels (ISV) within the trunk, this indicates that in contrast to cranial angiogenesis, these genes antagonise angiogenesis within the developing trunk. In this chapter we will focus on the functions of *foxc1a* and *foxc1b* during trunk blood vessel formation and also haematopoietic stem cell (HSC) formation from the aortic endothelium, both of which are controlled by similar cellular signalling pathways. This chapter will also briefly describe the roles of *foxc1a* and *foxc1b* in zebrafish somitogenesis.

4.1.1 *Foxc* genes in somitogenesis

Foxc1 and *Foxc2* are co-expressed within the pre-somitic mesoderm and somites during early somitogenesis (Miura et al., 1993, Kaestner et al., 1996, Winnier et al., 1997, Kume et al., 2001, Kume et al., 1998). Both murine *Foxc1* and *Foxc2* have been reported to be required for axial skeleton formation (Kume et al., 2001, Winnier et al., 1997), which develops from sclerotome progenitor cells formed during somitogenesis (reviewed in (Mead and Yutzey, 2012)). Murine *Foxc1* and *Foxc2* single mutant mice displayed normal patterning of initial somites from the very beginning of somitogenesis but display a malformed cervical vertebral column with fused or absent ribs in new-born embryos (Kume et al., 1998, Winnier et al., 1997). Murine *Foxc2* has an important role in regulating the proliferation and differentiation of sclerotome cells (Winnier et al., 1997), which potentially function through sclerotome-specific *Pax* genes (Smith et al., 2000). In addition, both *Foxc1* mutant mice and *Foxc2* mutant mice have been reported with more severely malformed anterior skeleton than posterior skeleton (Kume et al., 1998, Winnier et al., 1997). This suggests that *Foxc1* and *Foxc2* might specifically regulate anterior somite formation.

In *Foxc1*; *Foxc2* compound homozygous mutant mice, somite boundaries in presomitic mesoderm were completely absent with a significantly reduced frequency of sclerotomal cells. This was further validated via the observation of substantially reduced expression of genes related to somite patterning and differentiation, including *Pax1* and *MyoD* (Kume et al., 2001). This severe defect was detected from the initiation of somitogenesis (Kume et al., 2001). The somite defect observed in *Foxc1*; *Foxc2* double mutants is more severe than *Foxc1* single mutants

(Kume et al., 1998) and *Foxc2* single mutants (Winnier et al., 1997), which indicates redundant function between *Foxc1* and *Foxc2* during somitogenesis in mice. Kume *et al.* further reported reduced expression of Notch signalling components, in *Foxc1; Foxc2* double mutant mice (Kume et al., 2001), which are known to be involved in the segmentation clock mechanism during somite formation (reviewed in (Liao and Oates, 2017)). Taken together, murine *Foxc1/ Foxc2* compensate for each other and interact with the Notch signalling pathway to regulate somitogenesis.

Gene knockdown (KD) studies using morpholinos (Mo) in zebrafish have described that *foxc1a*, but not *foxc1b*, is required for somite patterning in zebrafish via regulating Notch/ Delta signalling and *mespb* expression (Topczewska et al., 2001a), which are key components of the segmentation clock (Takahashi et al., 2000). Interestingly, *foxc1a* loss of function induces abnormal anterior somitogenesis up to 12 hours post fertilisation (hpf) (*i.e.* the 6 somite stage), followed by gradual recovery within these anterior somites (Topczewska et al., 2001a). Furthermore, *foxc1a*-mediated promotion of somitogenesis has recently been reported in distinct *foxc1a* mutant backgrounds (Li et al., 2015, Hsu et al., 2015). Hsu *et al.* reported completely abolished somite segmentation up to the 10 somite stage (s) followed by less defined boundaries in established somites post 14hpf in mib^{nn2002} mutants, whose deletion covers both *foxc1a* and *mib* loci (Hsu et al., 2015), whereas other *mib* mutants, including mib^{ta52b} mutants, show normal anterior 10-12 somite formation (Zhang et al., 2007, Hsu et al., 2015). Furthermore, only the absent segmentation within anterior somites displayed in mib^{nn2002} mutants could be partially rescued by *foxc1a* overexpression, indicating *foxc1a* is required for anterior somite formation rather than posterior somite formation (Hsu et al., 2015). Inconsistent with the *foxc1a* morphant phenotype, Li *et al.* reported normal somitogenesis up to 5s (10hpf) in their *foxc1a* mutants (Li et al., 2015). However, at 9s, significantly reduced somite size with vague somite boundaries were observed in *foxc1a* mutants, followed by moderate recovery in somitogenesis (Li et al., 2015). *aldh1a2* expression was supressed by *foxc1a*, chromatin immunoprecipitation indicated Foxc1a directly binds the promotor of *aldh1a2* (Li et al., 2015), which further interacts with the Notch signalling pathway in paraxial mesoderm to regulate somitogenesis (Li et al., 2015).

4.1.2 *Foxc* genes and Notch signalling pathway

The compensatory roles of *Foxc1* and *Foxc2* during murine blood vessel formation were described in chapter 3 (Section 3.2.3). Here we focus on the interaction between the *Foxc* genes and the Notch signalling pathway during angiogenesis and HSC formation.

Reduced expression of Notch pathway components including *Notch1* and its ligand *Dll4* are observed in arterial ECs following loss of *Foxc1* and *Foxc2* (Seo et al., 2006), indicating *Foxc1* and *Foxc2* regulate arterial development via the Notch signalling pathway. Consistent with this observation, overexpression of *Foxc* genes *in vitro* significantly induced the expression of *Notch1* and *Dll4* (Seo et al., 2006). Furthermore, in cultured murine ECs, Foxc1 and Foxc2 physically activate the *Dll4* and *Hey2* promoters to activate downstream Notch signalling (Seo et al., 2006, Hayashi and Kume, 2008b). *In vitro* data has also suggested physical interaction between FOXC2 and suppressor of hairless protein (Su(H)), which further functions along with Notch intracellular domain (NICD) to induce Notch function (Hayashi and Kume, 2008b). Taken together, *Foxc1* and *Foxc2* function upstream of the Notch signalling pathway *in vitro*. Interestingly, *Foxc2* has also been suggested to positively regulate haematopoiesis as a target downstream of the *Notch1* receptor (Jang et al., 2015). A significant decrease in expression of the HSC marker, *runx1*, was reported in *Foxc2* mutant mice, with a reduction in definitive blood cell specification (Jang et al., 2015). Jang *et al.* further showed *Notch1* is capable of inducing *Foxc2* expression in haemogenic endothelial cells (Jang et al., 2015), from which haematopoietic stem cells (HSC) are derived (Lancrin et al., 2009). Taken together, *Foxc2* is a key regulator of definitive blood formation in mice downstream of Notch signalling (Jang et al., 2015).

Similar to mammalian studies, the interaction between *foxc1a* and the Notch signalling pathway has also been described in zebrafish. *In situ* hybridisation of HSC related genes including *runx1*, *cmyb* and *rag1* in *foxc1a; foxc1b* double morphants revealed a continuous decreased expression of HSC markers from 24hpf up to 4 days (Jang et al., 2015), consistent with reduced HSC formation in murine *Foxc2* mutants (Jang et al., 2015). Following Notch induction, Jang *et al.* further showed expanded *cmyb* (haematopoietic stem/ progenitor cell marker) expression in zebrafish, while the expression remained completely lost in Notch induced *foxc1a*/ *b* morphants. In addition, during podocyte development, Foxc1a binds Wt1a and CLS (also known as Rbpj) to form a protein complex, which subsequently facilitates the interaction of CLS and the NICD to activate Notch signalling (O'Brien et al., 2011). Taken together, these data indicate *foxc1a* and *foxc1b* are essential to induce Notch function to promote definitive blood development.

4.1.3 Objectives

In the previous chapter we have introduced the mechanism by which *foxc1a* and *foxc1b* promote cranial angiogenesis via positively regulating VEGF signalling and pro-angiogenic gene expression. Given the hypersprouting phenotype displayed in *foxc1a*; *foxc1b* double mutants, we concluded that *foxc1a* and *foxc1b* genetically interact while regulating ISV formation in the trunk. In this chapter we show *foxc1a* and *foxc1b* negatively regulate segmental artery (SeA) formation in the developing trunk by positively regulating the Dll4/ Notch signalling, which in turn supresses Vegfc/ Flt4 signalling. In addition, we report that *foxc1a* is required for HSC formation likely via promotion of non-cell autonomous somitic Wnt16-Dlc/ Dld signalling and promotion of endothelial Notch signalling. Conversely, *foxc1b* only contributes to HSC formation non-cell autonomously.

4.2 Results

4.2.1 *foxc1a* and *foxc1b* show dynamic transcript expression in trunk

Using *in situ* hybridisation, *foxc1a* expression could be detected in the anterior somitic mesoderm and the presomitic mesoderm at 10s (Fig. 4.1 A Red and orange arrowheads respectively) during early somite formation. At 16s, the expression of *foxc1a* could be detected strongly in the anterior somitic mesoderm (Fig. 4.1 B Red arrowhead) and was expressed less strongly in the posterior somitic mesoderm (Fig. 4.1 B Orange arrowhead). At 24-30 hpf, expression of *foxc1a* could be found in the axial mesoderm and sclerotome (Fig. 4.1 C-E Red and black arrowheads respectively) as previously described (Topczewska et al., 2001b, Skarie and Link, 2009). Interestingly, *foxc1a* was also expressed in the posterior blood island (PBI) (Fig. 4.1 C, D Green arrowheads) at 24hpf and caudal haematopoietic tissue (CHT) at 30hpf (Fig. 4.1 E Green arrowhead). The CHT has been described as a niche for HSC colonisation and proliferation post initiation of blood circulation (Tamplin et al., 2015). At 50hpf, the expression of *foxc1a* was reduced substantially but retained weak expression in the CHT (Fig. 4.1 F Green arrowhead).

The expression pattern of *foxc1b* at 10s was similar to the expression of *foxc1a*, but less enriched in the posterior developing somites (Fig. 4.1 G Orange arrowhead) and more strongly expressed in the anterior somitic mesoderm (Fig. 4.1 G Red arrowhead) when compared with *foxc1a* expression at 10s (Fig. 4.1 A). At 16s, *foxc1b* was expressed more strongly in the posterior somitic mesoderm (Fig. 4.1 H Orange arrowhead) than anterior somitic mesoderm (Fig. 4.1 H Red arrowhead). From 24hpf to 30hpf, expression of *foxc1b* could be detected in axial-mesoderm (Fig. 4.1 I-K Red arrowheads), sclerotome (Fig. 4.1 I-K Black arrowheads) and posterior somites around the tail bud (Fig. 4.1 I-K Orange arrowheads). Unlike *foxc1a* expression, *foxc1b* expression was excluded from the PBI (Fig. 4.1 I, J Green arrowheads) and the CHT (Fig. 4.1 K, L Green arrowheads). At 50hpf, the expression of *foxc1b* was also reduced substantially in the trunk (Fig. 4.1 L).

4.2.2 *foxc1a* single mutants display abnormal somite formation

Abnormal somite formation has been reported in both mice and zebrafish *Foxc* mutants (Kume et al., 2001, Li et al., 2015) suggesting *Foxc* genes play essential roles during somitogenesis. Subtle phenotypic differences were reported among zebrafish *foxc1a* morphants and *foxc1a* mutants as

introduced in section 4.1.1. We therefore examined somite formation in our *foxc1a* mutants and *foxc1a; foxc1b* double mutants.

At 12s, WT and *foxc1b* single mutant embryos displayed normal somites and a clear definition of the somite boundaries (Fig. 4.2 A, B Black arrowheads). We observed abnormal formation of somites in *foxc1a* single mutants with less defined somite boundaries (Fig. 4.2 C Red and black arrowheads), which could be observed from the very beginning of somite formation (data not shown). In addition, similar abnormally formed somites were also observed in *foxc1a; foxc1b* double mutants (Fig. 4.2 D Red and black arrowheads). Interestingly, the abnormality of the anterior somites were more pronounced than the posterior somites in both *foxc1a* single mutants and *foxc1a*; *foxc1b* double mutants (Fig. 4.2 C, D Red and black arrowheads respectively). To further determine the functions of *foxc1a* and *foxc1b* in somitogenesis, we performed blind genetic testing of somitic phenotype severity. *foxc1a; foxc1b* double heterozygous incrossed embryos were collected and grouped based on the severity of abnormal somite formation at 9s followed by PCR based genotyping for *foxc1a* and *foxc1b*. Around 25% of *foxc1a; foxc1b* double heterozygous incrossed embryos showed variable somite abnormalities. No significant difference in severity of the abnormal somite formation could be detected between *foxc1a* single mutants and *foxc1a*; *foxc1b* double mutants at 9s (data not shown). This data indicates that between *foxc1a* and *foxc1b*, *foxc1a* is more likely to be required for somite formation, whereas *foxc1b* is unlikely to contribute to the early development of somites since *foxc1b* single mutants displayed normal somite patterning (Fig. 4.2 B).

xirp2a is expressed within somite boundaries from 22hpf onwards (Otten et al., 2012). To further examine the potential requirement of *foxc1a* in somite formation, we performed whole mount *in situ* hybridisation in both siblings and *foxc1a* mutants of *xirp2a* at 24hpf. *xirp2a* expression in *foxc1a* single mutants revealed abnormal boundaries between the 4 most anterior somites (Fig. 4.2 E, F Red arrowheads). Quantification of the average length of these 4 most anterior somite boundaries showed a significant reduction in somite boundary length of *foxc1a* single mutants when compared with WT embryos (Fig. 4.2 G). Further quantification of the somite boundary angle at 24hpf embryos showed a significant increased somite boundary angle in *foxc1a* single mutants (Fig. 4.2 E, F black arrowheads, H). Taken together these data suggest *foxc1a* is required for early somitogenesis as reported previously (Kume et al., 2001, Li et al., 2015, Hsu et al., 2015).

Therefore, the abnormality observed during somite formation in both *foxc1a* single mutants and *foxc1a; foxc1b* double mutants was more likely due to lost function of *foxc1a* alone and this suggests *foxc1b* is dispensable for somite formation.

4.2.3 *foxc1a* is required for sclerotome patterning

foxc1a is required for somite formation (Section 4.2.2), and is expressed in somitic mesoderm and sclerotome (Fig. 4.1 A-E Red and black arrowheads respectively). In addition, *foxc1a* was previously described as a sclerotome marker (Clements et al., 2011). Therefore, we hypothesised that *foxc1a* might play an essential role in sclerotome formation. To test this, we analysed the sclerotome patterning in WT embryos and *foxc1a* single mutants at 24hpf.

Expression of sclerotome markers was reduced in *foxc1a* mutants by 24hpf (Fig. 4.3 D, F, H Black arrowheads). The specification of hypochord was normal in *foxc1a* single mutants (Fig. 4.3 B Green arrowhead) with unimpaired *twist2* expression (Fig. 4.3 B black arrowhead) when compared with the WT *twist2* expression (Fig. 4.3 A). The expression of *twist1b* was significantly reduced in the axial mesoderm (Fig. 4.3 D Red arrowhead), but enriched within the somite boundaries in *foxc1a* single mutants (Fig. 4.3 D Black arrowhead) when compared with WT embryos (Fig. 4.3 C Black arrowheads) at 24hpf. *pax1a* and *pax9* displayed reduced 'tip' sclerotome expression in the absence of *foxc1a* (Fig. 4.3 F, H Black arrowheads) indicating disrupted sclerotome patterning in *foxc1a* single mutants. Taken together these data indicate that *foxc1a* is required for sclerotome patterning.

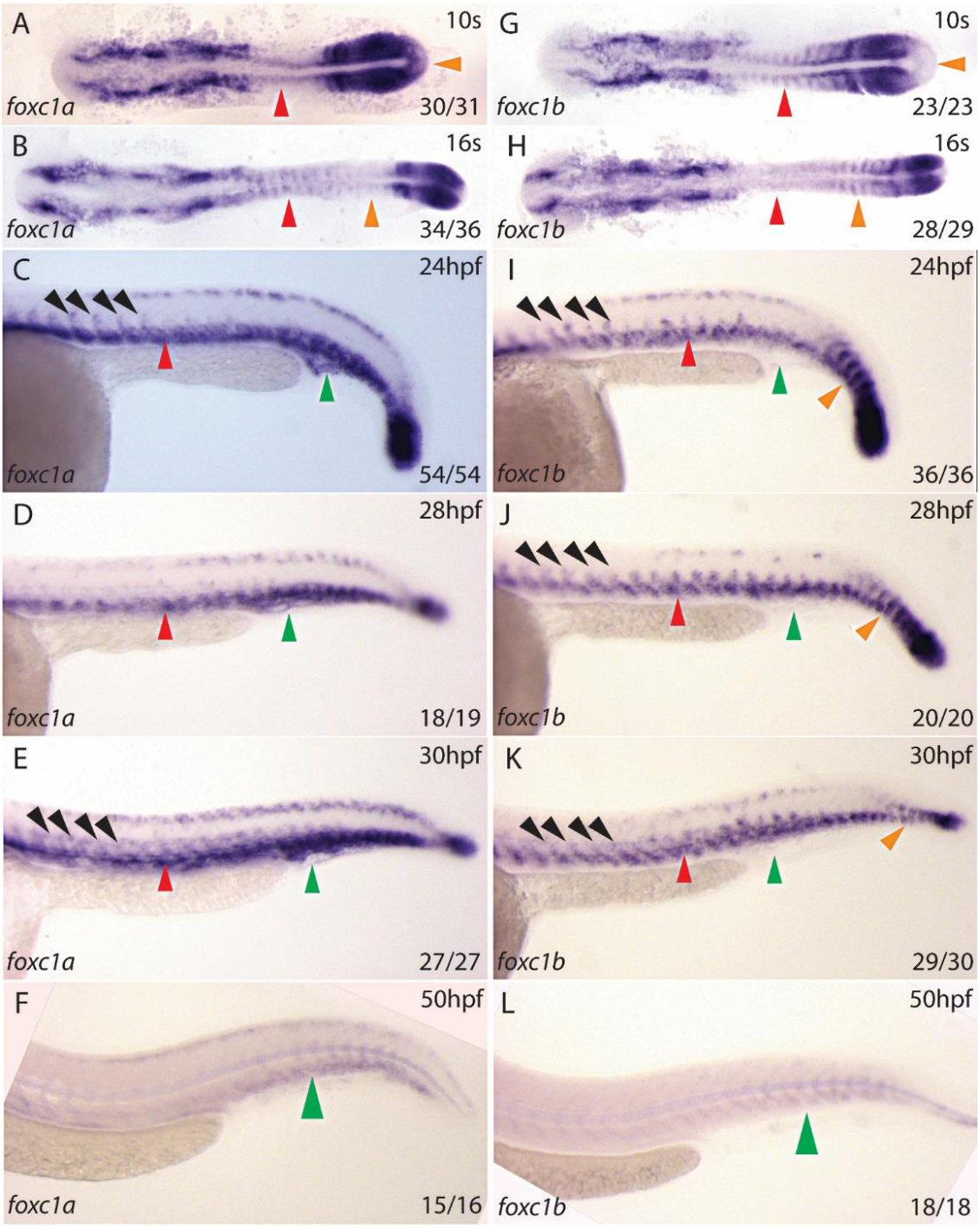

Figure 4.1 *foxc1a* and *foxc1b* are expressed within the developing trunk

(A) Expression of *foxc1a* in WT embryos at 10s (A). Red arrowhead points to anterior somitic mesoderm, orange arrowhead indicates pre-somitic mesoderm. (B) Expression of *foxc1a* in WT embryos at 16s. Red arrowhead points to anterior somitic mesoderm, orange arrowhead indicates posterior somitic mesoderm. (C-E) Lateral view of *foxc1a* expression in the trunk at 24hpf (C), 28hpf (D) and 30hpf (E) of WT embryos respectively. Black arrowheads highlight sclerotome expression, red arrowheads point to axial-mesoderm, green arrowheads point to PBI.

(F) Lateral view of expression of *foxc1a* in the CHT at 50hpf (green arrowhead). (G) Expression of *foxc1b* in WT embryos at 10s (G). Red arrowhead points to anterior somitic mesoderm, orange arrowhead indicates pre-somitic mesoderm. (H) Expression of *foxc1b* in WT embryos at 16s. Red arrowhead points to anterior somitic mesoderm, orange arrowhead indicates posterior somitic mesoderm. (I-K) Lateral view of *foxc1b* expression in the trunk at 24hpf (I), 28hpf (J) and 30hpf (K) of WT embryos respectively. Black arrowheads highlight sclerotome expression, red arrowheads point to axial-mesoderm, green arrowheads point to PBI, orange arrowheads point to posterior somites. (L) Lateral view of expression of *foxc1b* is absent from the CHT at 50hpf (green arrowhead). PBI, posterior blood island; CHT, caudal haematopoietic tissue

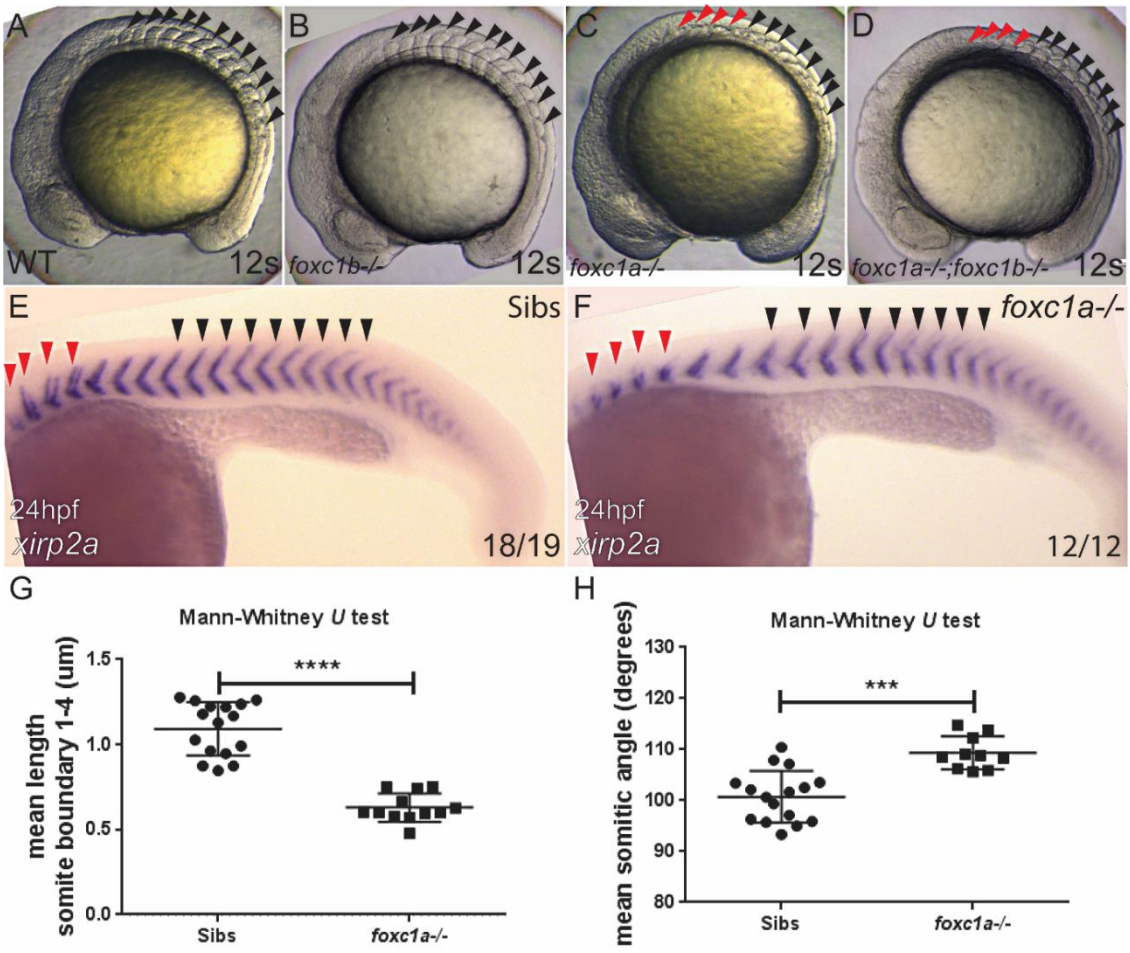

Figure 4.2 *foxc1a* is required for normal somitogenesis

(A-D) Lateral view of somite patterning in WT (A), *foxc1b* single mutant (B), *foxc1a* single mutants (C) and *foxc1a; foxc1b* double mutants (D) at 12s. Black arrowheads indicate formed somites; red arrowheads point to abnormal somites. (E-F) Lateral view of *xirp2a* expression within the somite boundaries at 24hpf of WT embryos (E) and *foxc1a* single mutants (F). (G, H) Quantification of boundaries length of the first 4 somite (red arrowheads in panel E and F) and average somite angle of the selected 9 somites (black arrowheads in panel E and F). Mann-Whitney *U* test. ****<0.0001, ***<0.001.

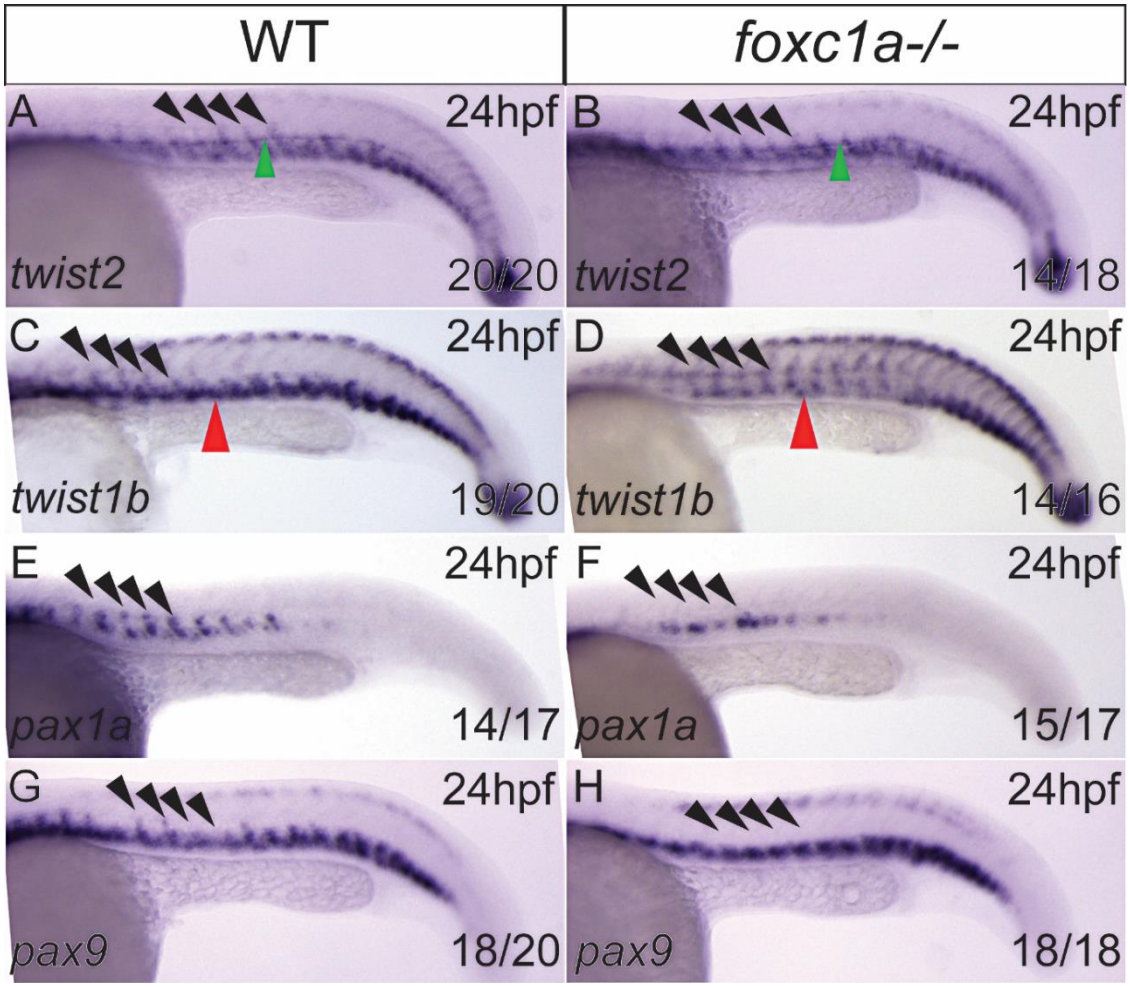

Figure 4.3 *foxc1a* is required for normal expression of sclerotome markers

(A, C, E, G) Lateral view of *in situ* hybridisation of sclerotome markers expression in WT embryos at 24hpf. (B, D, F, H) Lateral view of *in situ* hybridisation of sclerotome markers expression in *foxc1a* single mutants at 24hpf. Black arrowheads point to sclerotome; red arrowheads point to axial-mesoderm; green arrowheads highlight hypochord.

4.2.4 *foxc1a* single mutants display delayed trunk lymphangiogenesis

In the previous chapter we describe abnormal facial lymphatic formation, which could contribute to the oedema displayed in *foxc1a* single mutants (Section 3.2.5). To further examine whether *foxc1a* contributes to trunk lymphatic development, we analysed major trunk lymphatic formation in *foxc1a* mutants.

We utilised *Tg(kdrl:mcherry; fli1a:EGFP)* to analyse lymphatic vessel formation. ECs negative for *kdrl:mcherry* but positive for *fli1a:EGFP* expression were identified as lymphatic endothelial cells (LEC). The thoracic duct (TD), the first major trunk lymphatic vessel, forms via venous sprouting from the PCV (Karpanen and Schulte-Merker, 2011). In wild-type (WT) embryos, TD formation was first detected in the mesenchyme between the dorsal aorta (DA) and PCV around 3 days post fertilisation (dpf) (Fig. 4.4 A, A' Yellow arrowhead) while LECs were migrating horizontally beneath the DA. At 4dpf, LEC migration was completed and TD coverage was complete (Fig. 4.4 B, B' Yellow arrowhead). At 5dpf, TD formation was completed (Fig. 4.4 C, C' Yellow arrowhead). In *foxc1a* single mutants, at 3dpf, LECs were not detectable (Fig. 4.4 E, E' Yellow arrowhead). At 4dpf and 5dpf, LECs were detected between the DA and PCV in *foxc1a* single mutants (Fig. 4.4 F', G' Yellow arrowheads), however, the TD was discontinuous (Fig. 4.4 F, G White asterisks) when compared with the WT embryos at these stages (Fig. 4.4 B, C).

To further examine whether the abnormal TD formation is due to reduced LEC specification and/ or delayed LEC migration, we analysed the expression of *wnt5b* in WT and *foxc1a* single mutants. *wnt5b* has been recently reported as a novel lymphatic regulator, which can induce the Wnt-β-catenin pathway to promote LEC specification (Nicenboim et al., 2015). The expression of *wnt5b* in *foxc1a* single mutants was normal in the endoderm beneath the PCV (Fig. 4.4 H Red arrowhead) when compared with WT embryos (Fig. 4.4 D Red arrowhead). This data indicates that the *wnt5b*-mediated specification of LECs was unlikely to have been affected in *foxc1a* single mutants.

To summarise, *foxc1a* is required for normal TD formation in the trunk. The abnormality of TD formation displayed in *foxc1a* mutants is unlikely to have been caused by reduced *wnt5b*-mediated LEC specification. Rather, the likelihood is that delayed LEC migration and/ or reduced secondary PCV angiogenesis results in delayed TD formation. This will be further discussed in section 4.2.9.

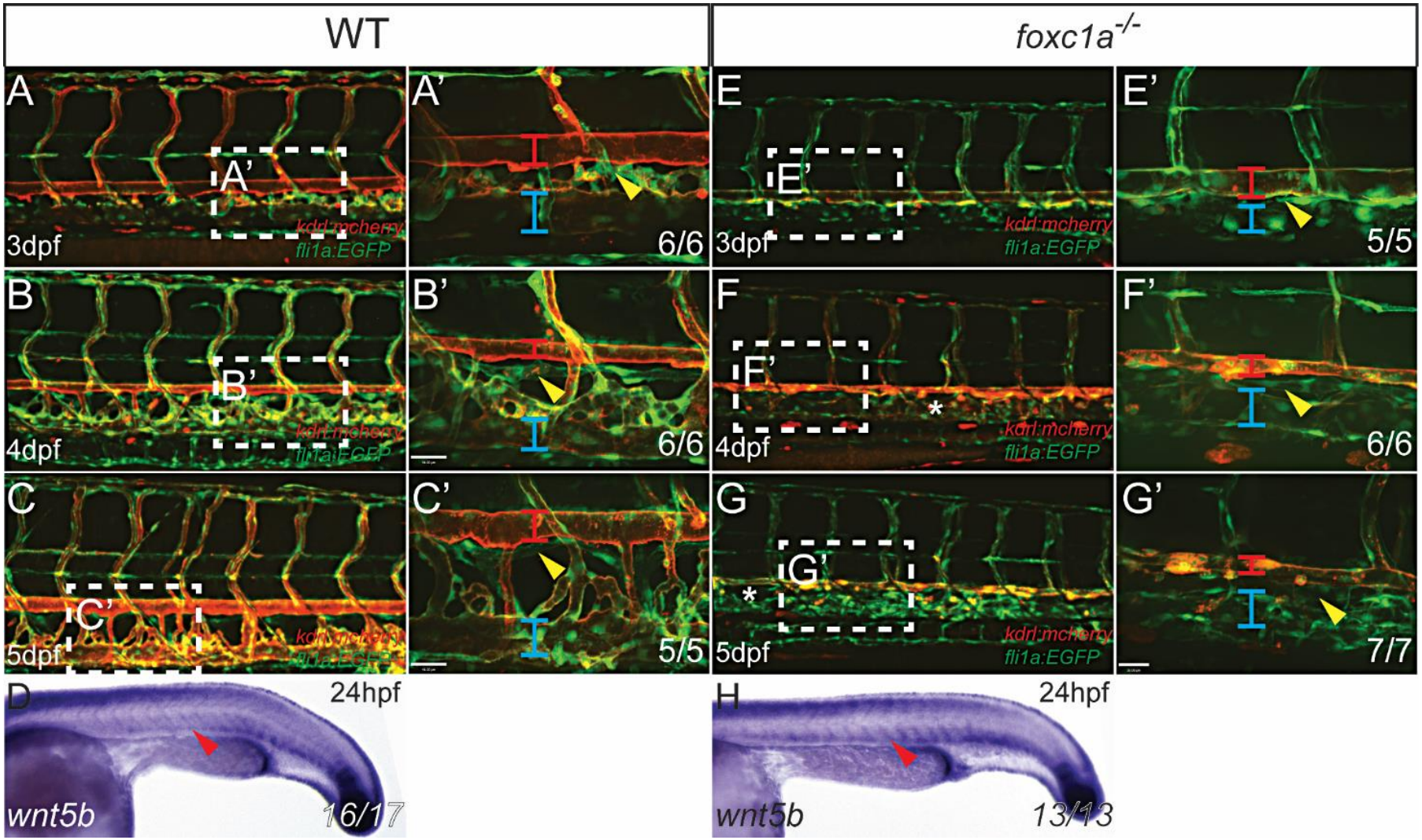
WT
foxc1a-/-
A
A'
3dpf
kdrl:mcherry
fli1a:EGFP
6/6
E
E'
5/5
B
B'
4dpf
F
F'
*
6/6
C
C'
5dpf
5/5
G
G'
7/7
D
24hpf
wnt5b
16/17
H
13/13

Figure 4.4 *foxc1a* single mutants display delayed trunk lymphangiogenesis

(A-C) Lateral view of the trunk vasculature at 3dpf (A), 4dpf (B) and 5dpf (C) in WT embryos with *Tg(kdrl:mcherry; fli1a:EGFP)* background. (A'-C') Higher magnification pictures of white dotted boxed area in panel A-C. Red bar highlight DA, blue bar point to PCV, yellow arrowheads denote TD. (D) *In situ* hybridisation of *wnt5b* in WT embryos at 24hpf. (E-G) Lateral view of the trunk vasculature at 3dpf (E), 4dpf (F) and 5dpf (G) in *foxc1a* single mutant embryos with *Tg(kdrl:mcherry; fli1a:EGFP)* background. (E'-G') Higher magnification pictures of white dotted boxed area in panel E, F. Red bar highlight DA, blue bar point to PCV, yellow arrowheads denote TD. (H) *In situ* hybridisation of *wnt5b* in *foxc1a* single mutant embryos at 24hpf. DA, dorsal aorta; PCV, posterior cardinal vein; TD, thoracic duct.

4.2.5 *foxc1a* single mutants display reduced transgelin positive cells

Knockdown of *foxc1a* using Mo has been reported to induce haemorrhage and pericardial oedema in zebrafish, whereas *foxc1b* morphants have no vascular phenotype (Skarie and Link, 2009). This observation suggests *foxc1a* may be required to promote blood vessel stability (Skarie and Link, 2009). Interestingly, our *foxc1a* mutants and *foxc1a*; *foxc1b* double mutants displayed similar morphological phenotypes with pericardial oedema but no haemorrhage (Fig 3.4 C, D Red arrowheads). To examine whether *foxc1a* induces MC recruitment to contribute to blood vessel stability, we analysed the pericyte gene expression and vSMC recruitment.

We analysed expression of *pdgfrb* (Wang et al., 2014), which has been described as a pericyte marker (Wang et al., 2014). At 24hpf, *pdgfrb* expression in WT embryos could be observed within the ventral somites (Fig. 4.5 A Black arrowheads), paraxial mesoderm (Fig. 4.5 A Red arrowhead) and hypochord (Fig. 4.5 A Green arrowhead). In *foxc1a* single mutants, while *pdgfrb* expression in the paraxial mesoderm (Fig. 4.5 B Red arrowhead) and hypochord (Fig. 4.5 B Green arrowhead) remained unchanged, expression within the ventral somite was reduced (Fig. 4.5 B Black arrowheads). At 48hpf, *pdgfrb* expression in WT embryos was associated with the DA, particularly enriched along the endothelium where ISVs were formed (Fig. 4.5 C Black arrowheads). A substantial reduction of *pdgfrb* expression was observed in the region of axial vessels (Fig. 4.5 D Black arrowheads) in *foxc1a* mutants. Taken together, this suggests *foxc1a* is required for normal *pdgfrb* expression, which may positively regulate pericyte recruitment.

To examine vSMC recruitment in *foxc1a* mutants, we utilised a *sm22a-b* enhancer (transgelin1) (Seiler et al., 2010) to label vSMCs and generated a transgenic line *Tg(sm22ab:mcherry)*^{sh441} (generated by Dr Robert Wilkinson) which we crossed with *Tg(fli1a:EGFP)* to label ECs in green and vSMCs in red. At 5dpf, WT embryos showed clear recruitment of vSMCs with *sm22ab:mcherry* expression, which localised to trunk arteries (Fig. 4.6 A-A'' Yellow arrowheads). However, in the absence of *foxc1a*, the intensity of *sm22ab:mcherry* expression was reduced substantially (Fig. 4.6 B''). This data indicates transgelin positive cell coverage is abnormal in the absence of *foxc1a*.

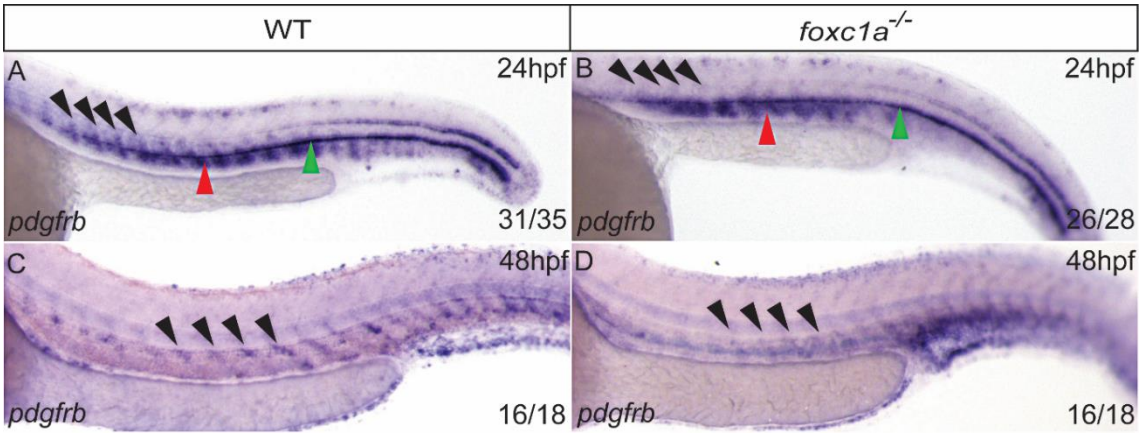

Figure 4.5 *foxc1a* regulates the expression of *pdgfrb* in trunk

(A, B) Lateral view of *in situ* hybridisation of *pdgfrb* in WT embryos (A) and *foxc1a* single mutants (B) at 24hpf. Black arrowheads point to sclerotome; red arrowheads point to DA; green arrowheads highlight hypochord. (C-D) Lateral view of *in situ* hybridisation of *pdgfrb* in WT embryos (C) and *foxc1a* single mutants (D) at 48hpf. DA, dorsal aorta.

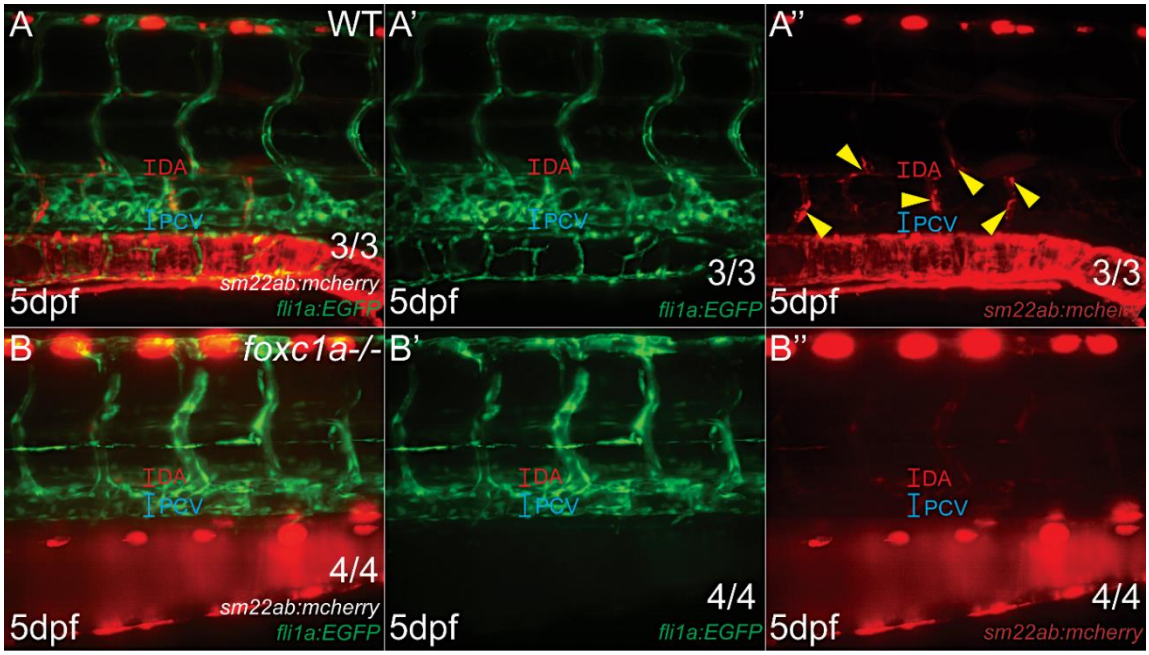

Figure 4.6 *foxc1a* is required for recruitment of vascular smooth muscle cells

(A-A'') Lateral view of WT embryos' trunk with merged (A) or single channel of *Tg(flia:EGFP)* (A') and *Tg(sm22ab:mcherry)* (A'') at 5dpf. Red bar highlight DA, blue bars highlight PCV, yellow arrowheads point to vSMC. (B-B'') Lateral view of *foxc1a* single mutant embryos' trunk with merged (B) or single channel of *Tg(flia:EGFP)* (B') and *Tg(sm22ab:mcherry)* (B'') at 5dpf. Red bars highlight DA, blue bars highlight PCV. DA, dorsal aorta; PCV, posterior cardinal vein.

4.2.6 *foxc1a* and *foxc1b* co-operatively antagonise angiogenesis in the trunk

Unlike cranial angiogenesis, where a significant reduction in frequency of cranial vessels was observed in both *foxc1a* single mutants and *foxc1a*; *foxc1b* double mutants (Fig. 3.5 B, C), *foxc1a; foxc1b* double mutants displayed ectopic ISV branching in the trunk (Fig. 4.7 C, F Yellow arrowheads, G). Interestingly, the hypersprouting phenotype could not be observed in *foxc1a* single mutants (Fig. 4.7 B, E, G). These data indicate *foxc1a* and *foxc1b* genetically interact during ISV formation. The initiation of ISV formation was normal in both *foxc1a* single mutants and in *foxc1a*; *foxc1b* double mutants (data not shown), however, ectopic ISV sprouting was observed as early as 28hpf in *foxc1a; foxc1b* double mutants (Fig. 4.7 C Yellow arrowheads). At later stages, the hypersprouting phenotype displayed in *foxc1a*; *foxc1b* double mutants was more pronounced (Fig. 4.7 F Yellow arrowheads).

Formation of the DA and PCV was normal in both *foxc1a* single mutants and *foxc1a*; *foxc1b* double mutants (Fig. 4.7 B, C). However, in both *foxc1a* single mutants and *foxc1a*; *foxc1b* double mutants, the PCV was dilated (Fig. 4.7 B, C Blue bars), whereas the DA showed reduced diameter (Fig. 4.7 B, C Red bars) when compared with WT siblings (Fig. 4.7 A Blue and red bars). This phenotype likely resulted from the disrupted trunk blood circulation in mutants as discussed previously (Section 3.2.3).

Taken together, these data suggest redundant function between *foxc1a* and *foxc1b* during ISV formation and that these genes work co-operatively to antagonise angiogenesis in the trunk.

4.2.7 *foxc1a* single and *foxc1a; foxc1b* double mutants show significantly reduced endothelial cell number

To determine whether hypersprouting observed in *foxc1a; foxc1b* double mutants was caused by elevated EC proliferation, we quantified the average EC number within 9 pairs of ISVs above the yolk extension of the WT embryos, *foxc1a* single mutants and *foxc1a*; *foxc1b* double mutants (Fig. 4.8). Interestingly, *foxc1a* single mutants (Fig. 4.8 B, B', D) and *foxc1a*; *foxc1b* double mutants (Fig. 4.8 C, C', D) displayed significantly reduced EC numbers in ISVs when compared with WT siblings at 4dpf (Fig. 4.8 A, A', D). Furthermore, no significant difference could be detected in EC number between *foxc1a* single mutants and *foxc1a*; *foxc1b* double mutants (Fig. 4.8 D). Thus, the ectopic angiogenesis displayed in the *foxc1a*; *foxc1b* double mutants is unlikely caused by abnormal EC proliferation. In addition, this reduced EC number displayed in *foxc1a* single mutants and *foxc1a*; *foxc1b* double mutants is potentially caused by loss of function of *foxc1a* alone.

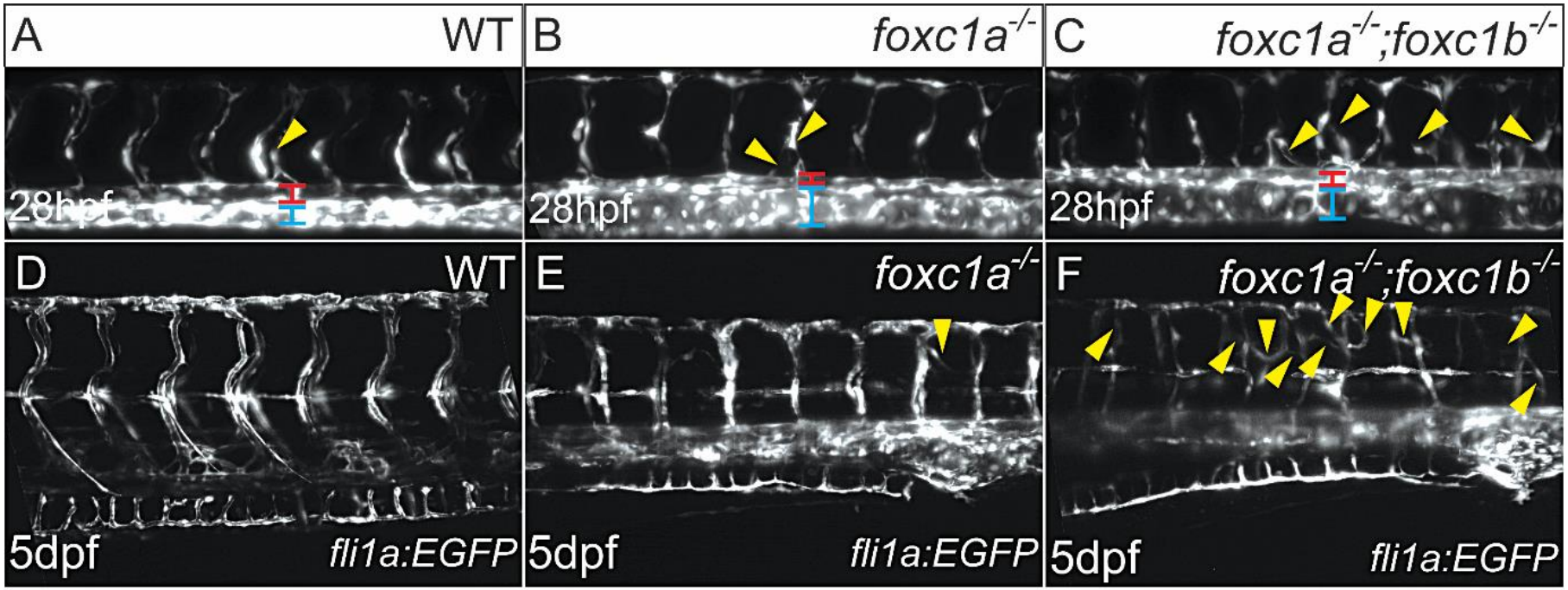
A
WT
28hpf
B
foxc1a-/-
28hpf
C
foxc1a-/-;foxc1b-/-
28hpf
D
WT
5dpf
fli1a:EGFP
E
foxc1a-/-
5dpf
fli1a:EGFP
F
foxc1a-/-;foxc1b-/-
5dpf
fli1a:EGFP

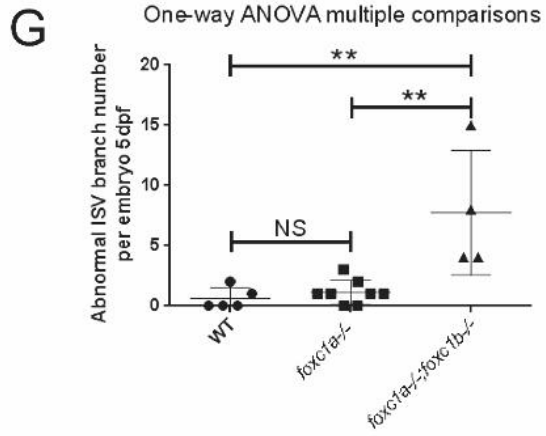
G
One-way ANOVA multiple comparisons
Abnormal ISV branch number per embryo 5dpf
20
15
10
5
0
**
**
NS
WT
foxc1a-/-
foxc1a-/-;foxc1b-/-

Figure 4.7 *foxc1a* and *foxc1b* negatively regulate trunk angiogenesis

(A-C) Lateral view of trunk ISV formation at 28hpf in WT (A) *foxc1a* single mutants (B) and *foxc1a*; *foxc1b* double mutants (C) in *Tg(fli1a:EGFP)* background. Yellow arrowheads indicate ectopic angiogenesis; red bars indicate DA; blue bars highlight PCV. (D-F) Lateral view of trunk ISV formation at 5dpf in WT (D) *foxc1a* single mutants (E) and *foxc1a*; *foxc1b* double mutants (F) in *Tg(fli1a:EGFP)* background. Yellow arrowheads indicate ectopic angiogenesis. (G) Quantification of ectopic sprouts numbers within 8 pairs of ISV above yolk extension. One-way ANOVA multiple comparisons. **<0.01, NS: not significant. ISV, intersomitic vessel; DA, dorsal aorta; PCV, posterior cardinal vein.

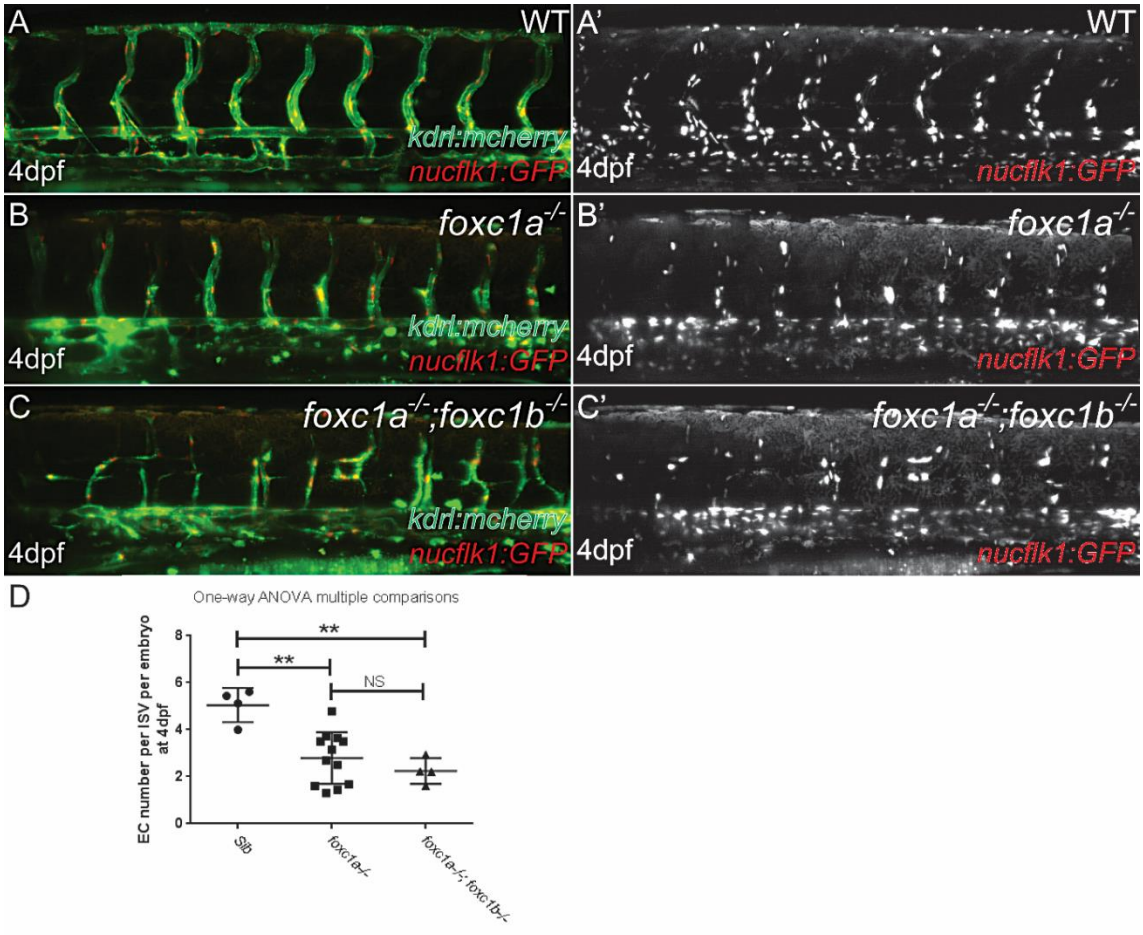

Figure 4.8 *foxc1a* single mutants and *foxc1a*; *foxc1b* double mutants display reduced EC number in intersomitic vessels

(A-C) Lateral view of ISV formation in the trunk of WT (A) *foxc1a* single mutants (B) and *foxc1a*; *foxc1b* double mutants (C) at 4dpf in *Tg(kdrl:mcherry; nucflk1:GFP)* background. (A'-C') Lateral view of EC within the ISVs in the trunk of WT (A') *foxc1a* single mutants (B') and *foxc1a*; *foxc1b* double mutants (C') at 4dpf in *Tg(nucflk1:GFP)* background. (D) Quantification of EC frequency per ISV within 9 pairs of ISV above yolk extension per embryo. One-way ANOVA multiple comparisons, **<0.01. ISV: Intersegmental vessel.

4.2.8 Lost function of *foxc1a* indirectly leads to reduced EC numbers within developing intersegmental vessels

foxc1a mutants display absent or reduced blood circulation throughout the trunk, and this is known to contribute to abnormal EC proliferation (Johnson et al., 2011, Levesque et al., 1990). We therefore analysed EC number and ISV formation before and after blood circulation had commenced at 24hpf and 60hpf respectively. At 24hpf, blood circulation was not detectable in either WT or *foxc1a* single mutants. The average EC number in ISVs in the absence of *foxc1a* (Fig. 4.9 B, C) was similar to that observed in WT embryos (Fig. 4.9 A, C) indicating EC specification was not adversely affected by loss of function of *foxc1a* before blood circulation initiated. Interestingly, at 60hpf, the average EC number was dramatically reduced within the ISV of *foxc1a* single mutants (Fig. 4.9 E, J) when compared with the WT embryos (Fig. 4.9 D, J).

To determine whether the reduction of EC in ISVs at later stages directly resulted from loss of function of *foxc1a*, we performed a *foxc1a* gain of function experiment by injecting the *foxc1a* full length mRNA into the one-cell stage of WT embryos and *foxc1a* single mutant embryos. Overexpression of *foxc1a* did not cause gross morphological change or abnormal vascular formation (Fig. 4.9 F). Interestingly, the mean EC number per ISV still remained significantly reduced in *foxc1a* single mutants post *foxc1a* overexpression (Fig. 4.9 G, J) when compared with WT embryos injected with *foxc1a* full length mRNA (Fig. 4.9 F, J) at 60hpf. Therefore, *foxc1a* is not sufficient to rescue EC number in *foxc1a* single mutants. Since *foxc1a* mRNA was able to partially restore abnormal cranial angiogenesis, but unable to restore blood circulation (data not shown) or ISV EC number (Fig. 4.9 J), this suggests that reduced EC number in *foxc1a* single mutants may be an effect of disruption of trunk circulation.

To test this, we injected the *tnnt2* Mo to stop blood circulation in WT siblings and *foxc1a* single mutants (Fig. 4.9 H, I). Interestingly, WT *tnnt2* morphants showed significant reduction in EC numbers (Fig. 4.9 H, J), when compared with control siblings (Fig. 4.9 D, J). Furthermore, the difference of average EC number within ISVs between WT embryos and *foxc1a* single mutants was no longer significant after *tnnt2* Mo injection (Fig. 4.9 H-J). Taken together, reduced EC numbers in *foxc1a* single mutants at 60hpf was likely a secondary defect caused by loss of trunk blood circulation in the absence of *foxc1a* function.

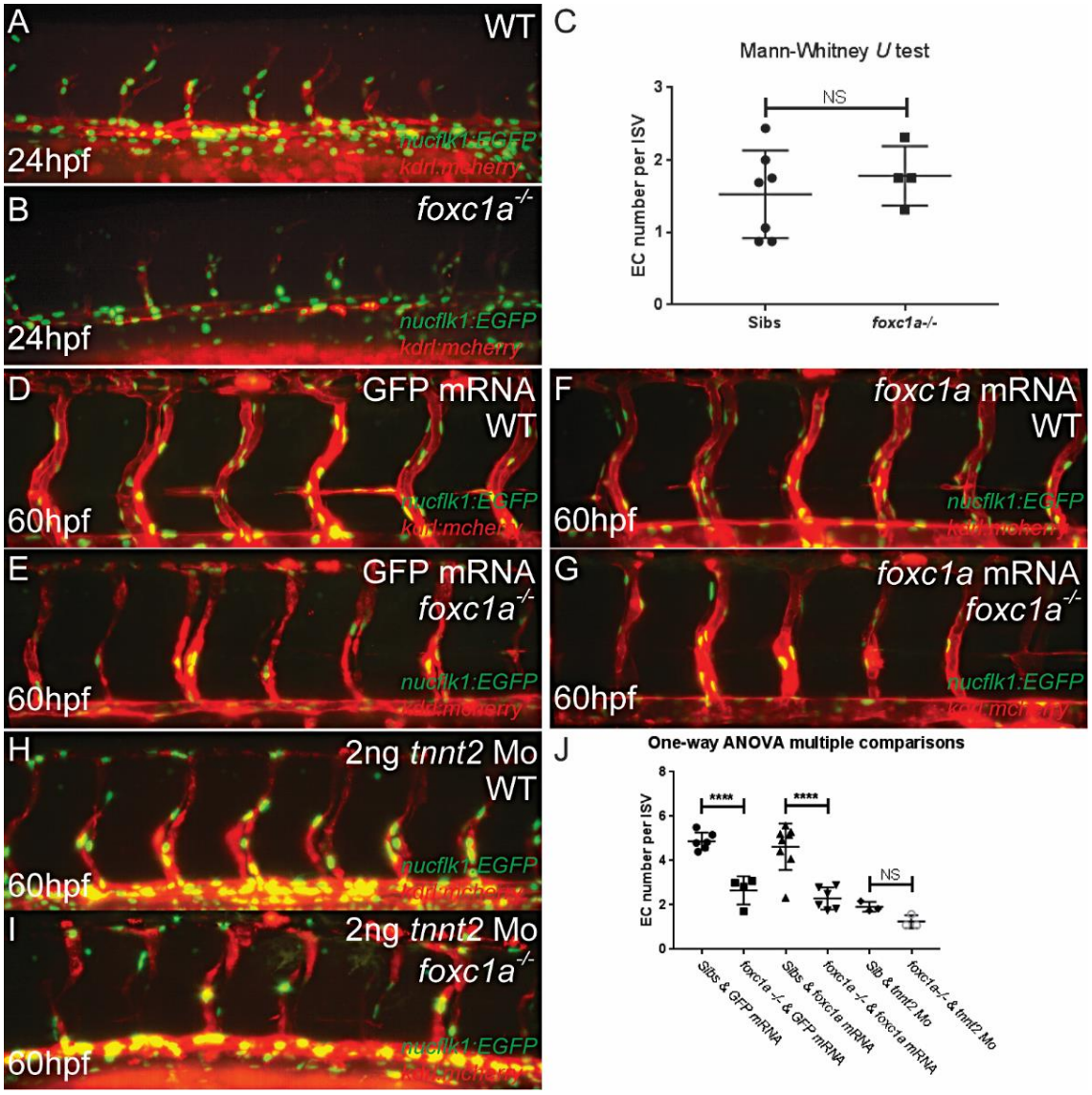

Figure 4.9 Reduced trunk blood circulation limits endothelial cell number in *foxc1a* mutants

(A, B) Lateral view of trunk ISV sprouting at 24hpf in WT (A) and *foxc1a* single mutant embryos (B) with *Tg(kdrl:mcherry; flk1:nlsEGFP)* background. (C) Quantification of average EC number per ISV within 8 pairs of ISV above yolk extension. Mann-Whitney *U* test was used. NS, not significant. (D, E) 700pg control GFP full-length mRNA injected *Tg(kdrl:mcherry; flk1:nlsEGFP)* WT (D) and *foxc1a* single mutant embryos (E) with lateral view of the trunk. (F, G) 700pg *foxc1a* full length mRNA injected *Tg(kdrl:mcherry; flk1:nlsEGFP)* WT (F) and *foxc1a* single mutant embryos (G) with lateral view of the trunk. (H, I) 2ng *tnnt2* Mo injected *Tg(kdrl:mcherry; flk1:nlsEGFP)* WT (H) and *foxc1a* single mutant embryos (I) with lateral view of the trunk. (J) Quantification of average EC number per ISV within 6 pairs of ISV above yolk extension at 3dpf. One-way ANOVA multiple comparisons, ****<0.0001, NS, not significant. ISV: Intersegmental vessel.

4.2.9 *foxc1a; foxc1b* double mutants display ectopic arterial angiogenesis and reduced venous angiogenesis within the trunk

To better understand the mechanism of how *foxc1a*, *foxc1b* regulate angiogenesis in the trunk, we further analysed the origin of the ectopic ISVs displayed in *foxc1a*; *foxc1b* double mutants (Fig. 4.10) using *Tg(fli1a:EGFP; flt1:RFP)*. *Tg(fli1a:EGFP)* labels ECs with GFP, whereas *Tg(flt1:RFP)* labels only arterial ECs with RFP (Bussmann et al., 2010). At 4dpf, ectopic angiogenesis was observed in *foxc1a; foxc1b* double mutants (Fig. 4.10 C, C'). Interestingly, the majority of ectopic vessels in *foxc1a*; *foxc1b* double mutants expressed the arterial marker *flt1:RFP* (Fig. 4.12 C, C' Yellow arrowheads) indicating these were ectopic segmental arteries (SeA).

Since arterial angiogenesis was increased in *foxc1a; foxc1b* double mutants, we examined whether this occurred at the expense of venous sprouting from the PCV. While the relative distribution of SeAs and segmental veins (SeVs) in WT embryos, occurred at a 1:1 ratio at 3dpf (Fig. 4.11 A). In *foxc1a* single and *foxc1a; foxc1b* double mutants, this ratio increased to around 3:1, indicating a 50% reduction in SeV frequency in both single and double mutants (Fig. 4.11 A). Consistent with this, expression of venous marker *flt4* was reduced substantially within the SeVs and expanded in the PCV of both *foxc1a* single mutants (Fig. 4.11 C Green asterisk, blue arrowhead respectively) and *foxc1a; foxc1b* double mutants (Fig. 4.11 D Green asterisk, blue arrowhead respectively), when compared with WT embryos (Fig. 4.11 A Green arrowhead and blue arrowhead respectively) at 48hpf. These data indicate that *foxc1a* is required for secondary angiogenesis from the PCV.

Taken together, the ectopic angiogenesis in *foxc1a; foxc1b* double mutants occurs at the expense of venous sprouting in the trunk. This data is in line with our observation that ectopic sprouting is first observed from 28hpf (Fig. 4.7 C), which occurs slightly earlier than venous angiogenesis (32hpf) as previously reported (Yaniv et al., 2006).

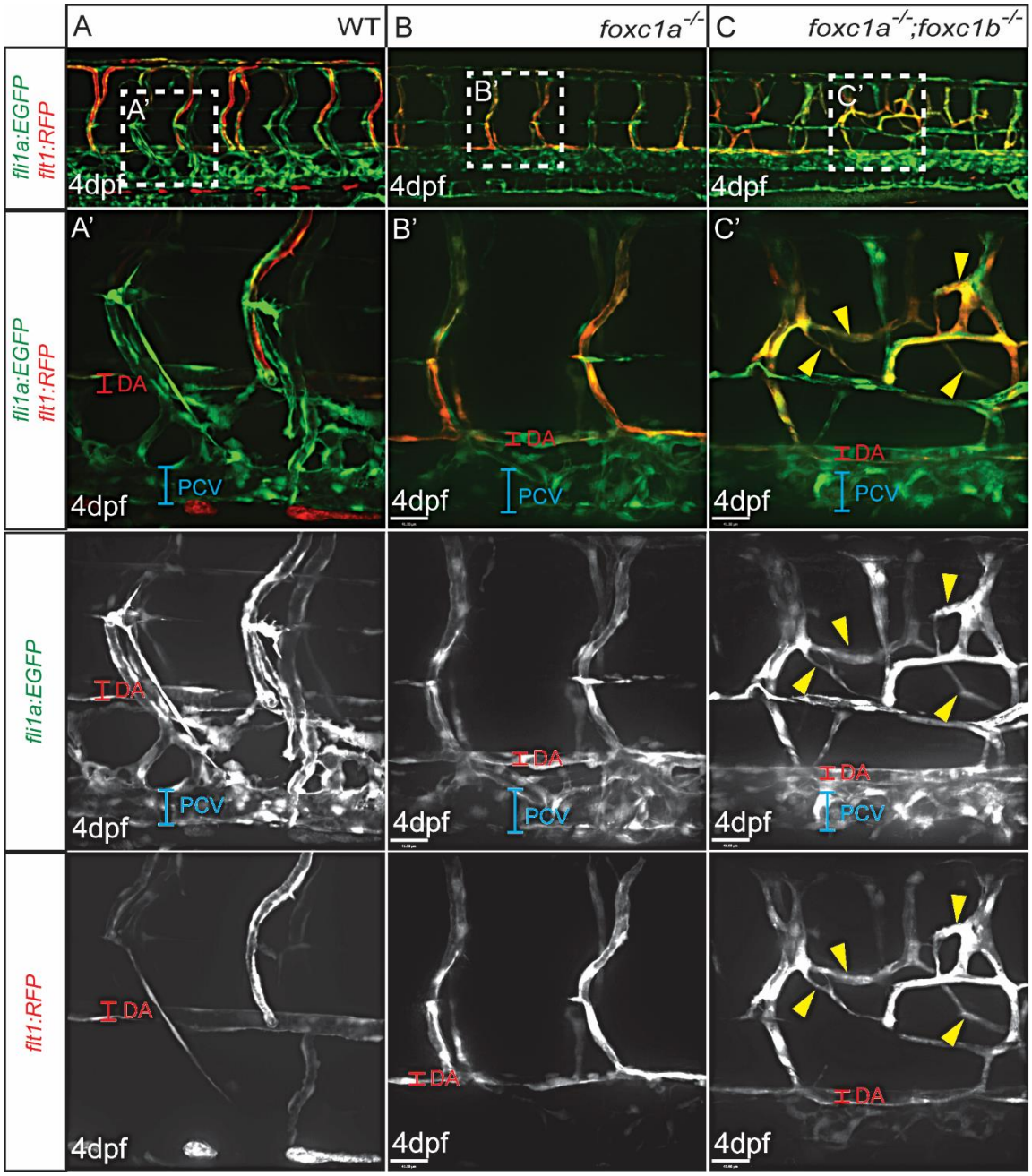

Figure 4.10 *foxc1a*; *foxc1b* double mutants display ectopic arterial angiogenesis

(A, B, C) Lateral view of trunk vasculature in WT (A), *foxc1a* single mutant (B) and *foxc1a*; *foxc1b* double mutant embryos (C) in *Tg(fli1:EGFP; flt1:RFP)* at 4dpf. (A', B', C') Merged pictures of higher magnifications of the white boxed area in panel A-C showed ectopic ISV sprouts in *foxc1a*; *foxc1b* double mutants express *flt1:RFP*. Yellow arrowheads indicate ectopic sprouts, red bars indicate DA, blue bars highlight PCV. ISV, intersegmental vessel; DA, dorsal aorta; PCV, posterior cardinal vein.

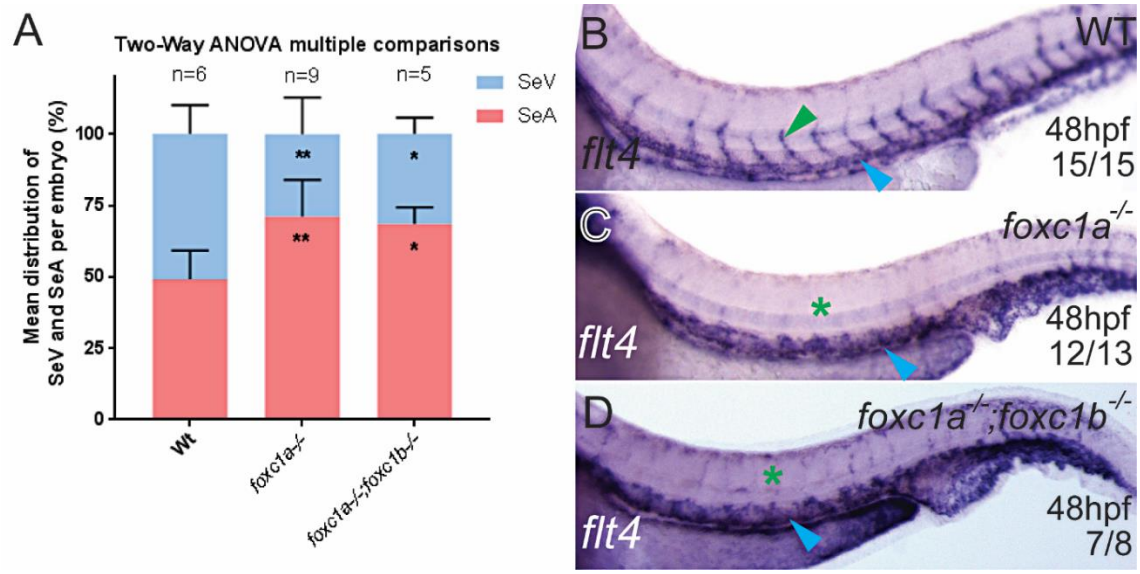

Figure 4.11 *foxc1a* single mutants and *foxc1a; foxc1b* double mutants display reduced secondary angiogenesis and abnormal *flt4* expression

(A) Quantification of mean distribution of SeA and SeV in WT embryos (n=6), *foxc1a* single mutants (n=9) and *foxc1a; foxc1b* double mutants (n=5) with *Tg(fli1a:EGFP; flt1:RFP)* back ground at 3dpf. 9 ISVs above the yolk extension were analysed. SeA and SeV were colour coded. Two-Way ANOVA multiple comparisons. **<0.01; *<0.05. (B) Lateral view of trunk *flt4* expression in WT embryos at 48hpf. Green arrowhead indicates SeV expression, blue arrowheads highlights PCV expression. (C-D) Lateral view of trunk *flt4* expression in *foxc1a* single mutants (C) and *foxc1a*; *foxc1b* double mutants (D) at 48hpf. Green asterisks highlight reduced SeV expression, blue arrowheads denote PCV expression. SeA, segmental artery; SeV, segmental vein; PCV, posterior cardinal vein.

4.2.10 *foxc1a* single mutants and *foxc1a*; *foxc1b* double mutants display reduced expression of *vegf* receptors

Vegf signalling is essential for SeA and SeV formation in zebrafish (Kuchler et al., 2006, Isogai et al., 2003, Yaniv et al., 2006, Hogan et al., 2009a, Bahary et al., 2007, Covassin et al., 2006, Habeck et al., 2002, Lawson et al., 2003a, Nasevicius et al., 2000, Rossi et al., 2016, Shin et al., 2016a, Shin et al., 2016b). In Chapter 3, we reported reduced expression of *vegfrs* in cranial vessels of *foxc1a* mutants (Fig. 3.19). To examine whether *foxc1a* and *foxc1b* potentially contribute to SeA formation via modulation of *vegfr* expression, we analysed the expression of Vegf signalling components in the mutants (Fig. 4.12).

The expression of the major Vegf ligand *vegfaa*, which is essential for angiogenesis (Nasevicius et al., 2000, Rissanen et al., 2005), remained unchanged in both *foxc1a* and *foxc1a; foxc1b* double mutants (Fig. 4.12 B, C). *kdrl* expression was moderately reduced in the DA (Fig. 4.12 E, F Red arrowheads) and SeAs (Fig. 4.12 E, F Black arrowheads) of *foxc1a* and *foxc1a; foxc1b* double mutants, in line with our observations of reduced *kdrl* expression within cranial vessels (Chapter 3, Fig. 3.19). Given that Kdrl promotes SeA formation (Habeck et al., 2002) and its expression was not significantly altered between *foxc1a* and *foxc1a*; *foxc1b* double mutants (Fig. 4.12 E, F), we concluded that the moderate reduction in *kdrl* expression was unlikely to account for the ectopic SeA sprouting observed in *foxc1a; foxc1b* double mutants.

Unlike the rostral *flt4* expression, which was significantly reduced in cranial veins of *foxc1a* mutants (Chapter 3, Fig. 3.19), the expression of *flt4* in the trunk of *foxc1a* single mutants was normal within the PCV (Fig. 4.12 H Blue arrowhead) and SeA tip cells (Fig. 4.12 H Black arrowhead) when compared with the WT embryos (Fig. 4.12 G Blue and black arrowheads). Interestingly, in *foxc1a*; *foxc1b* double mutants, *flt4* has not only expressed in the tip cells but also in the stalk cells of the SeAs at 24hpf (Fig. 4.12 I Black arrowhead). In the PCV, the expression of *flt4* remained unchanged in the absence of *foxc1a* and *foxc1b* (Fig. 4.12 I Blue arrowhead). We will further discuss this ectopic *flt4* expression in section 4.2.13.

We also analysed expression of the Vegf decoy receptor, *flt1*. Two major isoforms of *flt1* are expressed in zebrafish embryos, soluble *flt1* (*sflt1*) and membrane-bound *flt1* (*mflt1*) (Krueger et al., 2011). In WT embryos, *sflt1* expression could be detected within the SeAs (Fig. 4.12 J Black arrowhead) and DA (Fig. 4.12 J Red arrowhead), whereas in *foxc1a* single mutants, *sflt1* expression was reduced in both the SeAs (Fig. 4.12 K Black arrowhead) and the DA (Fig. 4.12 K Red arrowhead). More importantly, this reduction was more pronounced in the vasculature of

foxc1a; *foxc1b* double mutants (Fig. 4.12 L Red and black arrowhead). Expression of *mflt1* in WT siblings was detected in the SeA (Fig. 4.12 M Black arrowhead), DA (Fig. 4.12 M Red arrowhead) and also in the PBI (Fig. 4.12 M Green arrowhead). Expression of *mflt1* was reduced in *foxc1a* single mutants (Fig. 4.12 N), in a similar manner to *sflt1* expression (Fig. 4.12 K), and also in *foxc1a*; *foxc1b* double mutants with a greater down-regulation (Fig. 4.12 O). This data indicates that both *foxc1a* and *foxc1b* are required for arterial *flt1* expression.

To further examine the regulation between Vegf signalling and *foxc1a/ b*, we treated embryos with the VEGFR inhibitor AV951 (Eskens et al., 2011). *Tg(fli1a:EGFP)* embryos were treated as a positive control (Fig. 4.13 A, B) followed by whole mount *in situ* hybridisation for *foxc1a* and *foxc1b*. AV951 treatment completely abolished ISV formation and displayed a single 'vein-like' vessel within the trunk (Fig. 4.13 B Blue bar) as previously described (Buchanan et al., 2012), which indicates the AV951 treatment was functional. Expression of *foxc1a* and *foxc1b* remained unchanged post AV951 treatment in the trunk (Fig. 4.13 A-D Red arrowheads). These data provided the evidence of *foxc1a/ foxc1b* function either upstream or in parallel to Vegfrs.

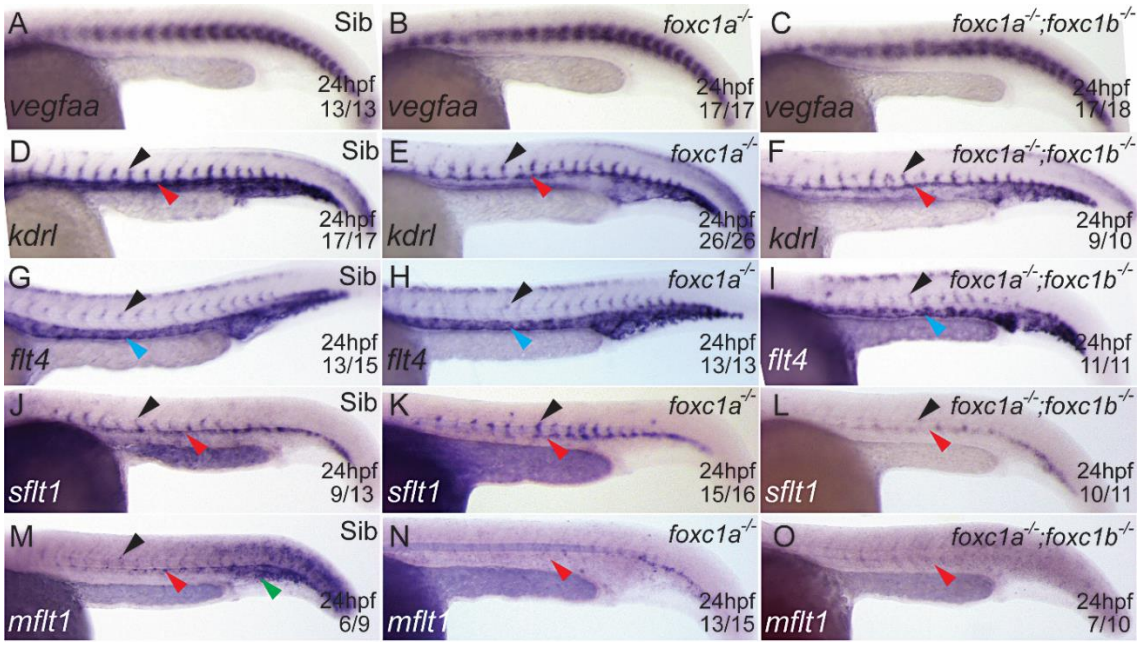

Figure 4.12 *foxc1a* and *foxc1b* are required for normal expression of *vegfrs*

(A-C) *In situ* hybridisation of *vegfaa* in sibling embryos (A), *foxc1a* single mutants (B) and *foxc1a*; *foxc1b* double mutants (C) at 24hpf. (D-O) *In situ* hybridisation of *kdrl* in sibling embryos (D), *foxc1a* single mutants (E) and *foxc1a*; *foxc1b* double mutants (F) at 24hpf. Black arrowheads point at SeA, red arrowheads indicate DA. *In situ* hybridisation of *flt4* in sibling embryos (G), *foxc1a* single mutants (H) and *foxc1a*; *foxc1b* double mutants (I) at 24hpf. Black arrowheads point at SeA, blue arrowheads indicate PCV. *In situ* hybridisation of *sflt1* in sibling embryos (J), *foxc1a* single mutants (K) and *foxc1a*; *foxc1b* double mutants (L) at 24hpf. *In situ* hybridisation of *mflt1* in sibling embryos (M), *foxc1a* single mutants (N) and *foxc1a*; *foxc1b* double mutants (O) at 24hpf. Red arrowheads indicate DA; black arrowheads denote SeA expression; green arrowhead points to PBI. DA, dorsal aorta; PCV, posterior cardinal vein; SeA, segmental artery; PBI, posterior blood island.

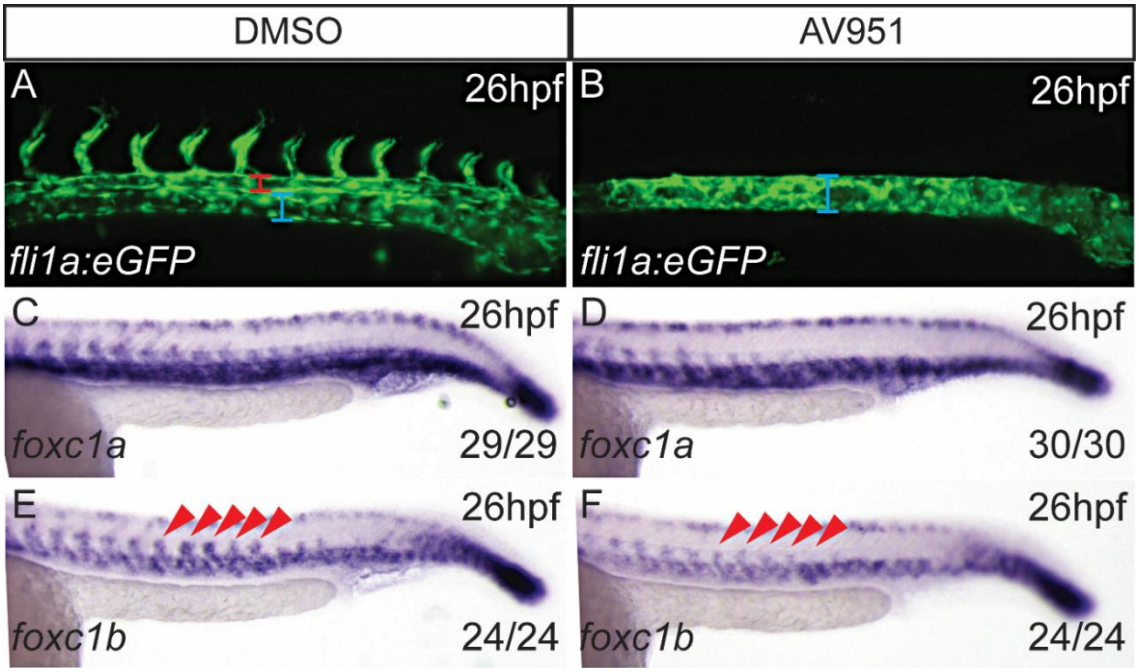

Figure 4.13 Expression of *foxc1a* and *foxc1b* are not dependent on Vegf signalling

(A-B) Lateral view of trunk vessels in WT embryos following DMSO treatment (A) and AV951 treatment (B) with *Tg(fli1a:EGFP)* background at 26hpf. Red bars highlight DA, blue bars indicate PCV. (C-D) Lateral view of *foxc1a in situ* at 26hpf in DMSO treated (C) and AV951 treated (D) WT embryos. (E-F) Lateral view of the expression of *foxc1b* after DMSO (E) and AV951 treatment (F) at 26hpf. Red arrowheads indicate sclerotome expression. DA, dorsal aorta; PCV, posterior cardinal vein.

4.2.11 *sflt1* is not sufficient to rescue ectopic segmental artery formation in *foxc1a*; *foxc1b* double mutants

Since the expression of both *sflt1* and *mflt1* were substantially reduced in *foxc1a*; *foxc1b* double mutants, when compared with *foxc1a* single mutants and WT embryos (Fig. 4.12), and previous studies have demonstrated that *sflt1* negatively regulates trunk angiogenesis, whereas *mflt1* is dispensable for this process (Krueger et al., 2011), we therefore hypothesised that reduction of *sflt1* expression might be responsible for the hypersprouting phenotype displayed in *foxc1a*; *foxc1b* double mutants. To test this, we overexpressed full length *sflt1* mRNA (Krueger et al., 2011) in WT and *foxc1a*; *foxc1b* double mutants and quantified the frequency of ectopic angiogenic sprouts.

sflt1 overexpression in WT embryos did not cause any detectable phenotypic changes at 28hpf or 3dpf (Fig. 4.14 B, F). In *foxc1a*; *foxc1b* double mutants, the ectopic sprouts were still visible at 28hpf following *sflt1* overexpression (Fig. 4.14 D Yellow arrowheads), which was similar to those shown in control RNA injected *foxc1a*; *foxc1b* double mutants (Fig. 4.14 C Yellow arrowheads). At 3dpf, ectopic sprout numbers were comparable between *foxc1a*; *foxc1b* double mutants with and without *sflt1* overexpression (Fig. 4.14 G, H Yellow arrowheads, I) indicating *sflt1* is not sufficient to rescue the hypersprouting phenotype and thus reduced *sflt1* expression does not account for ectopic sprout formation in *foxc1a*; *foxc1b* double mutants.

4.2.12 *foxc1a and foxc1b* negatively regulate arterial angiogenesis by promoting Dll4/ Notch signalling

Murine *Foxc1* and *Foxc2* have been shown to function upstream of the Notch signalling pathway to regulate blood vessel formation (Hayashi and Kume, 2008b), however, a conflicting study has reported that zebrafish *foxc1a/ b* function downstream of Notch signalling (Jang et al., 2015). To determine epistasis between *foxc1a/ b* and Notch signalling, we performed DAPT treatment to antagonise Notch signalling followed by *in situ* hybridisation for *foxc1a* and *foxc1b* at 30hpf (Fig. 4.15). *her12,* was employed as a positive control since it is a Notch downstream target, whose expression is induced by Notch signalling (Zhen Jiang MSc thesis, University of Sheffield). *her12* expression was reduced globally by DAPT treatment (Fig. 4.15 A, B) indicating the DAPT treatment was effective. Interestingly, neither *foxc1a* nor *foxc1b* expression was altered by DAPT treatment (Fig.4.15 D, F) when compared with the DMSO treated control group (Fig. 4.15 C, E). These data indicate *foxc1a* and *foxc1b* expression is independent of Notch signalling.

Dll4/ Notch signalling limits angiogenic sprouting from arteries (Siekmann and Lawson, 2007, Lawson et al., 2001), we therefore hypothesised that ectopic arterial angiogenesis in *foxc1a; foxc1b* double mutants could be due to reduced Dll4/ Notch signalling. To test this, we analysed the expression level of Notch signalling components in *foxc1a* and *foxc1a; foxc1b* double mutants.

We employed the *Tg(dll4in3:GFP)*, in which GFP expression is driven by an arterial specific Dll4 enhancer (Sacilotto et al., 2013), and we observed a substantial reduction of GFP fluorescence within SeAs (Fig. 4.16 B Black arrowhead) and the DA (Fig. 4.16 B Red arrowhead) of *foxc1a* single mutants when compared with WT embryos (Fig. 4.16 A). This reduction was more substantial in *foxc1a*; *foxc1b* double mutants (Fig. 4.16 Black and red arrowheads respectively). Consistent with this, expression of *dll4* (Fig. 4.16 D-F), displayed a more pronounced reduction in SeAs and the DA of *foxc1a*; *foxc1b* double mutants (Fig. 4.16 F Black and red arrowheads respectively) when compared with WT embryos and *foxc1a* single mutants (Fig. 4.16 D, E Black and red arrowheads respectively). In addition, expression of the Notch target *gridlock* (*grl*)/ *hey2* was more substantially reduced in *foxc1a*; *foxc1b* double mutants (Fig. 4.16 I) when compared with WT and *foxc1a* single mutants (Fig. 4.16 G, H). These results indicate that Dll4/ Notch signalling was reduced in both single and double mutants, but the greater down-regulation of Notch signalling components in *foxc1a*; *foxc1b* double mutants might account for the ectopic SeA formation following loss of both *foxc1a* and *foxc1b*.

To determine whether the ectopic sprouting in *foxc1a*; *foxc1b* double mutants was Notch-dependent, we crossed the *Tg(hs-gal4; 5xUAS-E1b:6xMYC-notch1a)* (Scheer and Campos-Ortega, 1999) into the *foxc1a; foxc1b* double heterozygotes using a *Tg(kdrl:mcherry)* background to label blood vessels and subjected progeny to heat shock at 18s to induce expression of NICD. Heat shock induction of Notch signalling substantially reduced the ectopic sprouting phenotype in *foxc1a*; *foxc1b* double mutants (Fig. 4.16 L, O Yellow arrowheads) demonstrating that the ectopic SeA sprouting in *foxc1a*; *foxc1b* mutants was due to reduced Notch signalling. Taken together, these data indicate that *foxc1a* and *foxc1b* function upstream of Notch signalling and positively regulate the expression of Notch.

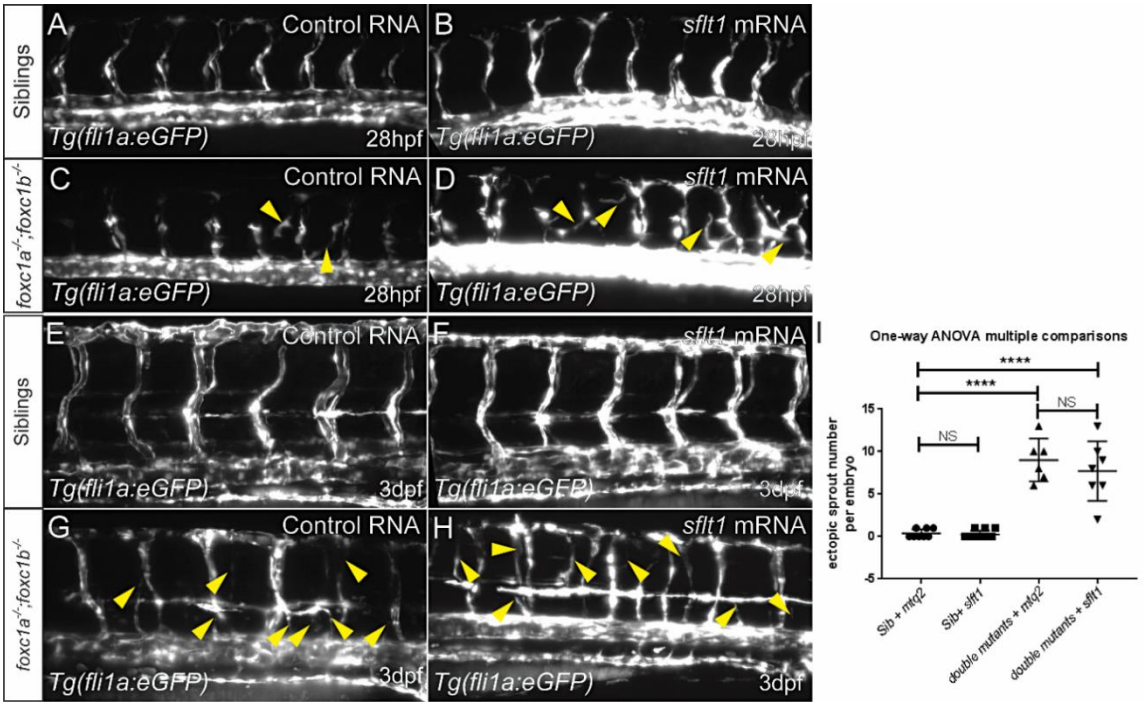

Figure 4.14 Gain of function of *sflt1* is not sufficient to rescue ectopic angiogenesis displayed in *foxc1a*; *foxc1b* double mutants

(A, B) Lateral view of trunk of control mRNA injected (A) and *sflt1* mRNA injected (B) WT embryos at 28hpf with *Tg(fli1a:EGFP)* background. (C, D) Lateral view of trunk of control mRNA injected (C) and *sflt1* mRNA injected (D) *foxc1a*; *foxc1b* double mutant embryos at 28hpf with *Tg(fli1a:eGFP)* background. Yellow arrowheads indicate ectopic angiogenesis. (E, F) Lateral view of trunk of control mRNA injected (E) and *sflt1* mRNA injected (F) WT embryos at 3dpf with *Tg(fli1a:EGFP)* background. (G, H) Lateral view of trunk of control mRNA injected (G) and *sflt1* mRNA injected (H) *foxc1a*; *foxc1b* double mutant embryos at 3dpf with *Tg(fli1a:EGFP)* background. Yellow arrowheads indicate ectopic angiogenesis. (I) Quantification of ectopic SeA number within 6 pairs of ISV above yolk extension per embryo at 3dpf. One-Way ANOVA multiple comparisons. ****<0.0001; NS, not significant.

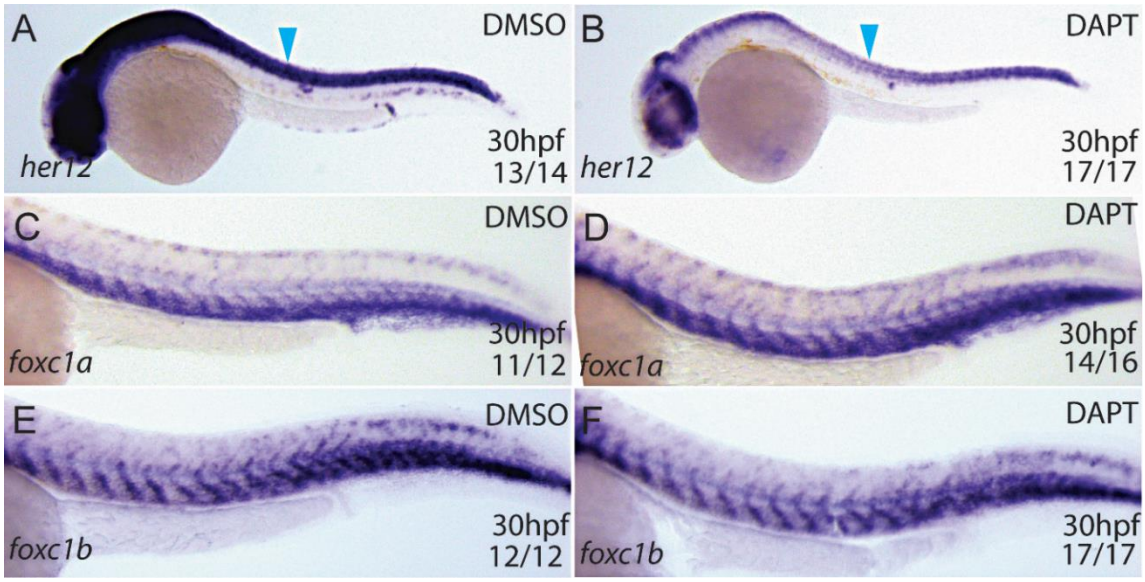

Figure 4.15 Expression of *foxc1a* and *foxc1b* are not dependent on Notch signalling

(A, B) Expression of *her12* in WT embryos following 20 hours of DMSO treatment (A) and DAPT treatment (B) at 30hpf. Blue arrowheads indicate neural tube. (C-D) Expression of *foxc1a* in WT embryos following 20 hours of DMSO treatment (C) and DAPT treatment (D) at 30hpf. (E) Expression of *foxc1b* in WT embryos following DMSO treatment (E) and DAPT treatment (F) at 30hpf.

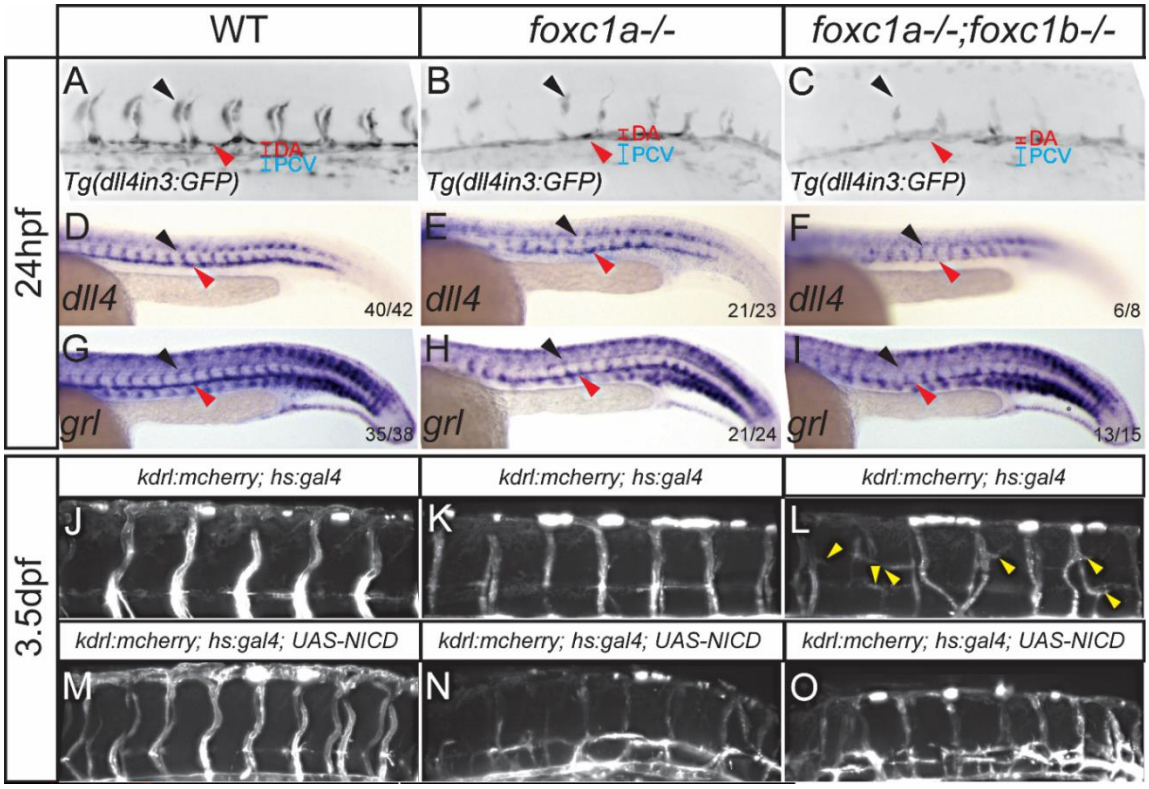

Figure 4.16 *foxc1a*; *foxc1b* double mutants display reduced Dll4/ Notch signalling and ectopic arterial angiogenesis can be suppressed by induction of Notch

(A-C) Expression level of GFP of *Tg(dll4in3:GFP)* in WT embryos (A), *foxc1a* single mutants (B) and *foxc1a*; *foxc1b* double mutants (C) at 24hpf with lateral view. Black arrowheads indicate SeA, red bars highlight DA, blue bars denote PCV. (D-F) *In situ* hybridisation of *dll4* in WT (D), *foxc1a* single mutants (E) and *foxc1a*; *foxc1b* double mutants (F) at 24hpf. (G-I) *In situ* hybridisation of *grl* in WT embryos (G), *foxc1a* single mutants (H) and *foxc1a*; *foxc1b* double mutants (I) at 24hpf. Black arrowheads indicate SeAs; red arrowheads denote DA. (J-O) Lateral view of light-sheet microscopy images at 3.5dpf of heat shocked *Tg(kdrl:mcherry)* in WT (J), *foxc1a* single mutants (K) and *foxc1a*; *foxc1b* double mutants (L) and *Tg(kdrl:mcherry; hs-gal4; UAS-NICD)* in WT (M), *foxc1a* single mutants (N) and *foxc1a*; *foxc1b* double mutants (O). Yellow arrowheads point to ectopic SeAs. SeA, segmental artery; DA, Dorsal aorta; PCV, posterior cardinal vein.

4.2.13 *foxc1a and foxc1b* negatively regulate arterial angiogenesis by promoting Notch-mediated suppression of Vegfc/ Flt4 signalling

Dll4/ Notch signalling limits angiogenic sprouting from arteries (Siekmann and Lawson, 2007, Lawson et al., 2001) via suppression of Vegfc/ Flt4 signalling in SeAs (Hogan et al., 2009b). As shown in section 4.2.10, in *foxc1a*; *foxc1b* double mutants, *flt4* expression was observed within both tip cells and stalk cells of the SeAs (Fig. 4.12 I Black arrowhead) in contrast to WT siblings and *foxc1a* single mutants, which displayed enrichment of *flt4* expression in tip cells (Fig. 4.12 G, H Black arrowheads). Notch signalling supresses *flt4* in SeAs (Lawson et al., 2001), and Dll4/ Notch signalling is reduced in *foxc1a* single and *foxc1a; foxc1b* double mutants (Fig. 4.16 A-I) and hypersprouting in *foxc1a; foxc1b* mutants can be suppressed by induction of Notch (Fig. 4.16 J-O). We therefore hypothesised that ectopic SeA formation in *foxc1a; foxc1b* double mutants was induced by failure of Notch-mediated repression of Vegfc/ Flt4 signalling. To test this, we KD *vegfc* in *foxc1a; foxc1b* mutant embryos using Mo and quantified frequency of ectopic SeAs (Fig. 4.17). Delayed formation of PHBC at 26hpf (Data not shown) and absent parachordal lymphangioblast at 3dpf (Fig. 4.17 C Blue asterisks) were observed in the WT morphants as previously described (Hogan et al., 2009b), indicating *vegfc* function was inhibited. The frequency of ectopic SeAs was significantly reduced by *vegfc* KD in *foxc1a; foxc1b* double mutants in comparison to uninjected double mutants (Fig. 4.17 B, D Yellow arrowheads, E).

Collectively, these data indicate that *foxc1a* and *foxc1b* co-operatively limit arterial sprouting by positively regulating Dll4/ Notch signalling and negatively regulating Flt4/ Vegfc signalling. Reduced Notch signalling in *foxc1a*; *foxc1b* double mutants leads to activation of *flt4*/ *vegfc* signalling, which results in ectopic angiogenesis from arteries.

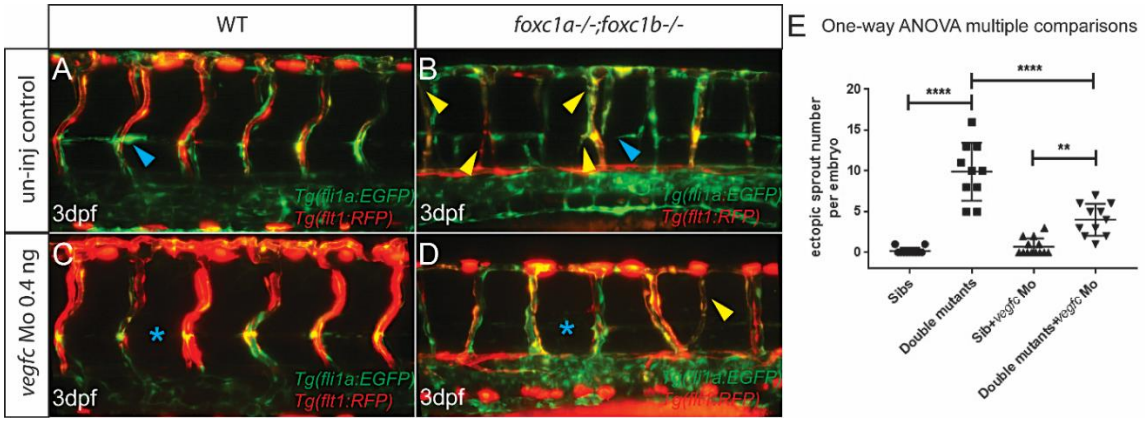

Figure 4.17 Knockdown of *vegfc* supresses ectopic segmental artery formation in *foxc1a*; *fox1b* double mutants

(A-D) Lateral view of uninjected WT (A) and *foxc1a*; *foxc1b* double mutants (B) in *Tg(fli1a:EGFP; flt1RFP)* background at 3dpf. *vegfc* Mo injected WT (C) and *foxc1a*; *foxc1b* double mutants (D) in *Tg(fli1a:EGFP; flt1RFP)* background at 3dpf. Blue arrowheads highlight parachordal lymphangioblasts, blue asterisks indicate absent parachordal lymphangioblasts, yellow arrowheads indicate ectopic SeA. (E) Quantification of ectopic SeA number within 6 pairs of ISV above yolk extension in control group and vegfc Mo injected group at 3dpf. One-way ANOVA multiple comparisons. **<0.01; ****<0.0001. SeA, segmental artery; ISV, intersegmental vessel.

4.2.14 *foxc1a* is expressed in endothelial cells of trunk vessels, whereas *foxc1b* expression is excluded from these

Since *foxc1a* and *foxc1b* promote arterial Notch signalling, we wished to determine whether these genes were expressed in arteries. We utilised a combination of fluorescent *in situ* hybridisation and immuno-fluorescence to increase the resolution of detection as previously described in chapter 3 (Section 3.2.7).

Similar to its expression in the head, *foxc1a* expression could be detected in the trunk, both in the mesenchymal tissue and in axial vessels (Fig. 4.18 A-A'') at 28hpf. Reconstructed transverse section of a single z-plane through the trunk revealed *foxc1a* expression in SeAs (Fig. 4.18 B-B'' Yellow arrowheads), DA and PCV (Fig. 4.18 C-C''). By contrast, expression of *foxc1b* was only present in mesenchymal tissue, including sclerotome and was excluded from ECs (Fig.4.18 D-F). Absence of *foxc1b* expression from ECs was confirmed in the reconstructed transverse section of a single z-plane through trunk (Fig. 4.18 E-F). Co-localisation of *foxc1b* expression and EC α-GFP staining was not detected in the SeAs (Fig. 4.18 E-E'' Yellow arrowheads), DA and PCV (Fig. 4.18 F-F''). Taken together, our data indicates *foxc1a* is expressed in both ECs and surrounding mesenchyme whereas *foxc1b* expression is restricted to trunk mesenchyme and excluded from ECs.

4.2.15 Lost function of *foxc1a* does not alter expression of *foxc1a* and *foxc1b*

We described in section 4.2.6 that *foxc1a* and *foxc1b* genetically interact during ISV formation, yet *foxc1a* is expressed in ECs, while *foxc1b* is excluded from these. This may explain the lack of vascular phenotype in *foxc1b* single mutants, but also suggests either non-cell autonomous function of *foxc1b* or the possibility that under normal circumstances *foxc1a* may suppress *foxc1b* in ECs. We therefore examined whether *foxc1b* expression was induced in ECs of *foxc1a* mutants.

In *foxc1a* single mutants, the expression of *foxc1a* remained unchanged (Fig. 4.19 A-C) when compared with *foxc1a* expression in WT siblings (Fig. 4.18 A-C). *foxc1a* expression could be detected in ECs of the trunk vasculature (Fig. 4.19 A, B, C) in addition to the expression within the sclerotome in *foxc1a* mutants. *foxc1b* expression was excluded from the vasculature in *foxc1a* mutants (Fig. 4.19 D, E, F) as shown in WT embryos (Fig. 4.18 D-F). Viewed dorsally, *foxc1a* expression could be detected within the midline between somites (Fig. 4.19 B-B'') indicating its expression within axial trunk vasculature. By contrast, the expression of *foxc1b* was not visible at the midline between somites, where the α-GFP antibody staining was detected (Fig. 4.19 E-E''). Reconstructed transverse sections of single z-plane of trunk further confirmed the co-localisation

of *foxc1a* expression with α-GFP antibody staining in both the DA and PCV (Fig. 4.19 C-C'' Red and blue bars), whereas the expression of *foxc1b* could only be observed in the sclerotome and was excluded from ECs (Fig.4.19 F-F'' Red and blue bars). These data indicate that expression of *foxc1b* is not altered by loss of *foxc1a*. Taken together, this data indicates that *foxc1b* is not expressed in ECs normally, or in the absence of *foxc1a* function, and *foxc1b* must therefore function non-cell autonomously to promote Notch signalling.

4.2.16 *foxc1a* single mutants and *foxc1a*; *foxc1b* double mutants display reduced haematopoietic stem cell formation

Notch signalling is required for many essential aspects of embryogenesis. In addition to regulating arterial angiogenesis, it is also required for haematopoietic stem cell (HSC) formation from the ventral wall of the DA (Kumano et al., 2003, Rowlinson and Gering, 2010, Guiu et al., 2013, Kim et al., 2014). We therefore examined whether HSC formation was perturbed by loss of function of *foxc1a* and/ or *foxc1b*.

As reported in section 4.2.12, Notch signalling was significantly reduced in *foxc1a* single mutants and *foxc1a*; *foxc1b* double mutants. We therefore hypothesised that HSC formation may be reduced in the absence of *foxc1a* and/ or *foxc1b*. We first analysed the expression of the HSC marker, *runx1*, at 24hpf and found its expression was reduced in *foxc1a* single mutants (Fig. 4.20 C). In the absence of both *foxc1a* and *foxc1b*, the *runx1* expression reduction was more pronounced in the trunk (Fig. 4.20 D). This observation is in line with the increased reduction in Notch signalling in *foxc1a*; *foxc1b* double mutants than that observed in *foxc1a* single mutants (Fig. 4.16 A-I). Taken together, *foxc1a* and *foxc1b* function co-operatively to induce expression of HSC markers.

We further validated this result by analysing the emergence of HSCs budding from ventral arterial endothelium in WT and *foxc1a* single mutant embryos at 2dpf (Fig. 4.21). By utilising the *Tg(flt1:RFP; gfi1aa:GFP)* line, which label arterial endothelium in red (Bussmann et al., 2010) and haemogenic endothelium in green (Thambyrajah et al., 2016) respectively, ECs positive for both *flt1:RFP* and *gfi1aa:EGFP* expression could be identified as HSCs. Consistent with reduced *runx1* expression in *foxc1a* single mutants, HSC frequency was significantly reduced at 2dpf in the absence of *foxc1a* (Fig. 4.21 B Yellow arrowheads, C) when compared with WT siblings (Fig. 4.21 A Yellow arrowheads, C).

Taken together, these results indicate *foxc1a* and *foxc1b* are required for HSC formation potentially via regulation of Notch signalling. In addition, *foxc1a*; *foxc1b* double mutants show

greater reduction in *runx1* expression than *foxc1a* single mutants and indicate *foxc1a* and *foxc1b* promote HSC emergence co-operatively.

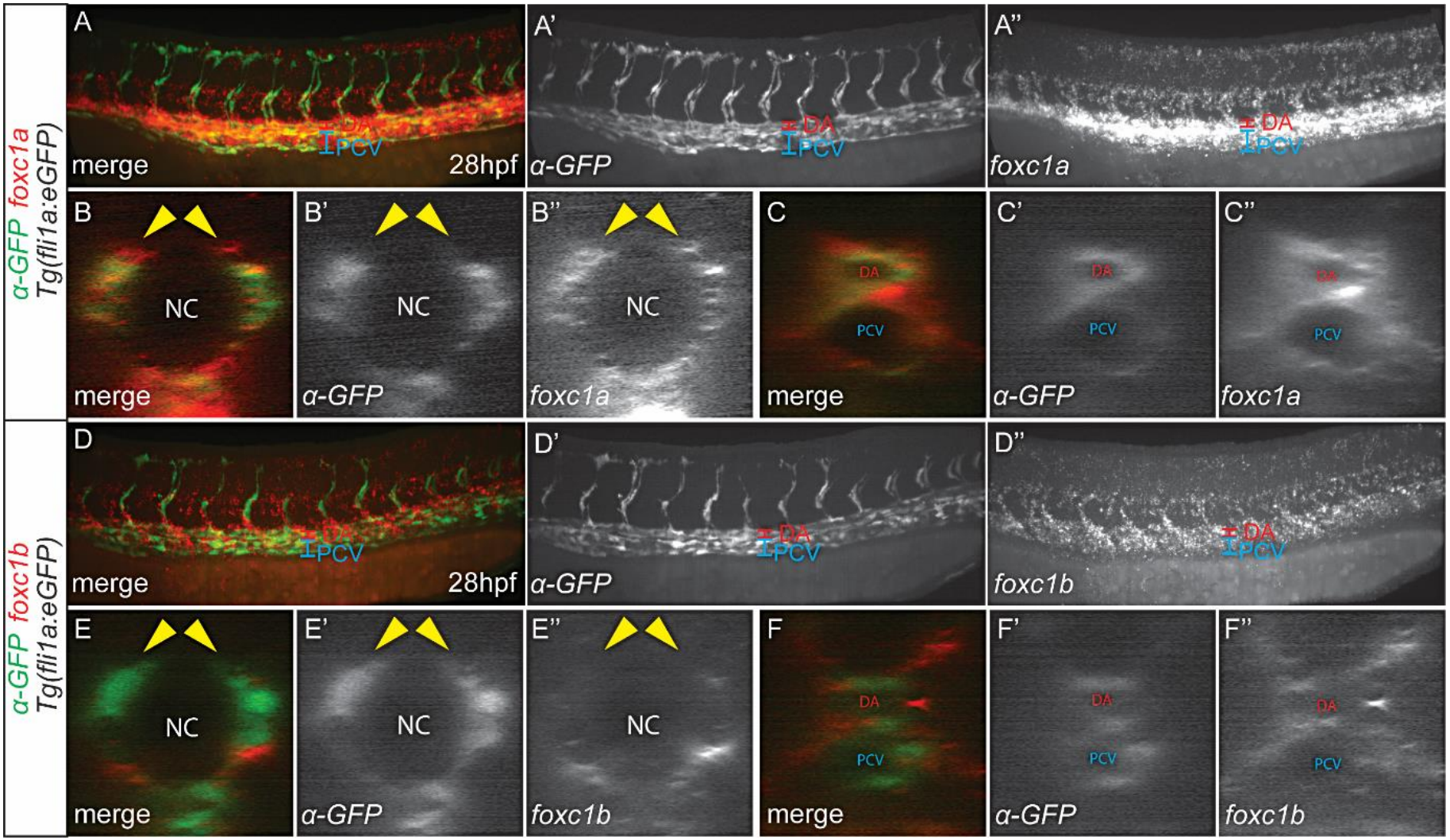
α-GFP foxc1a
Tg(fli1a:eGFP)
A
merge
28hpf
DA
PCV
A'
α-GFP
A"
foxc1a
B
NC
merge
B'
α-GFP
B"
foxc1a
C
DA
PCV
merge
C'
α-GFP
C"
foxc1a
α-GFP foxc1b
Tg(fli1a:eGFP)
D
merge
28hpf
D'
α-GFP
D"
foxc1b
E
NC
merge
E'
α-GFP
E"
foxc1b
F
DA
PCV
merge
F'
α-GFP
F"
foxc1b

Figure 4.18 *foxc1a* is expressed in trunk vessels, whereas expression of *foxc1b* is excluded from these

(A-C'') Antibody staining of α-GFP (green channel) and *foxc1a* fluorescent *in situ* (red channel) in *Tg(fli1a:EGFP)* in WT embryos at 28hpf with lateral view (A-A''), cross section of the SeA (B-B'') and cross section view of axial vessel (C-C'') showing *foxc1a* expression can be detected within trunk vessels. Red bar indicate DA, blue bar demote PCV, yellow arrowheads highlight SeA. (D-F'') Antibody staining of α-GFP (green channel) and *foxc1b* fluorescent *in situ* (red channel) in *Tg(fli1a:EGFP)* in WT embryos at 28hpf with lateral view (D-D''), cross section of SeA (E-E'') and cross section of axial vessels (F-F'') showing *foxc1b* expression is excluded from trunk vessels. Red bar indicate DA, blue bar demote PCV, yellow arrowheads highlight SeA. DA, dorsal aorta; PCV, posterior cardinal vein; SeA, segmental artery.

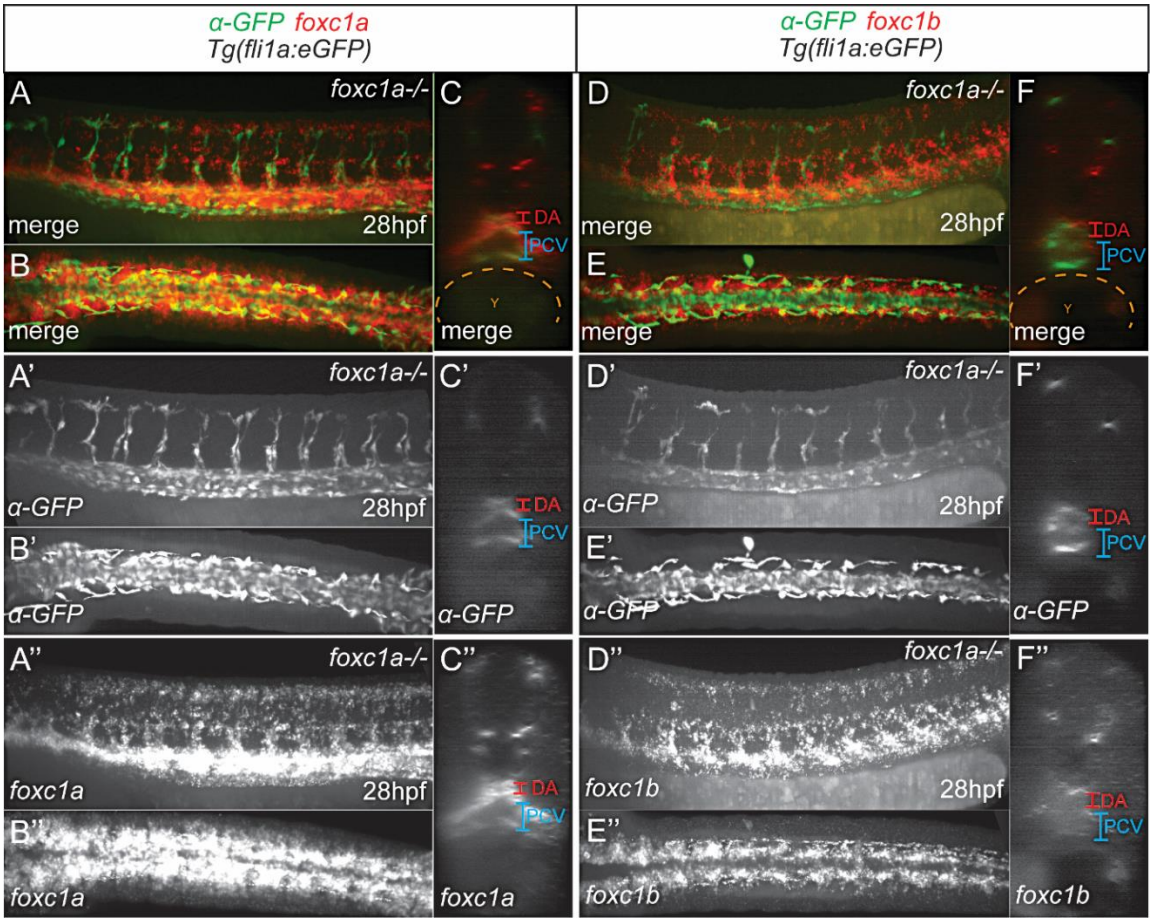

Figure 4.19 *foxc1b* expression is not induced in endothelial cells in the absence of *foxc1a*

(A, A', A'') Lateral view of the fluorescent Cy3 staining of *foxc1a* (red channel) in trunk vessels and the scolerotome at 28hpf in *foxc1a* single mutants with α-GFP antibody staining (green channel) in *Tg(fli1a:EGFP)*. (B, B', B'') Dorsal view of the fluorescent Cy3 staining of *foxc1a* (red channel) in the trunk vessels and the scolerotome at 28hpf in *foxc1a* single mutants with α-GFP antibody staining (green channel) in *Tg(fli1a:EGFP)*. (C, C', C'') Cross section shows fluorescent Cy3 staining of *foxc1a* (red channel) co-expresses with α-GFP antibody staining (green channel) in the trunk vessels. Red bar indicates DA, blue bar points to PCV, yellow darsh circles the yolk. (D, D', D'') Lateral view of the fluorescent Cy3 staining of *foxc1b* (red channel) in the scolerotome at 28hpf in *foxc1a* single mutants with α-GFP antibody staining (green channel) in *Tg(fli1a:EGFP)*. (E, E', E'') Dorsal view of the fluorescent Cy3 staining of *foxc1b* (red channel) in the scolerotome at 28hpf in *foxc1a* single mutants with α-GFP antibody staining (green channel) in *Tg(fli1a:EGFP)*. (F, F', F'') Cross section shows fluorescent Cy3 staining of *foxc1b* (red channel) not co-expresses with α-GFP antibody staining (green channel) in the trunk vessels. Red bar indicates DA, blue bar points to PCV, yellow darsh circles the yolk. DA, dorsal aorta; PCV, posterior cardinal vein; Y, yolk.

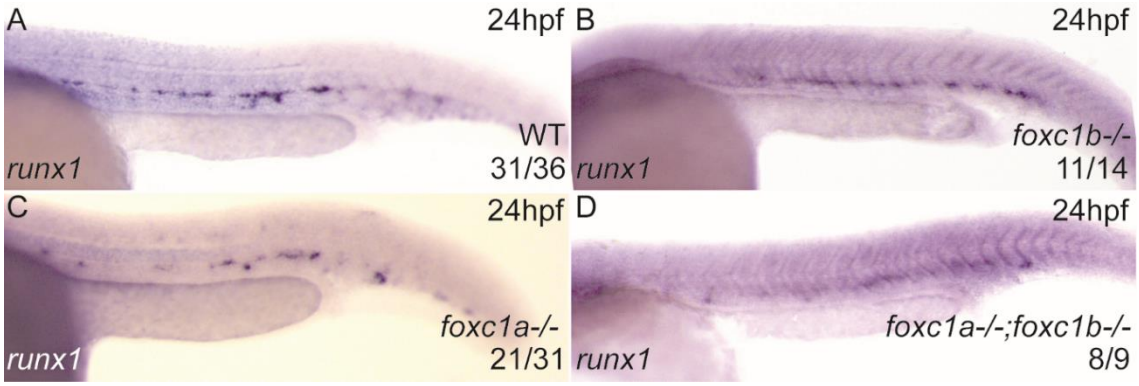

Figure 4.20 *foxc1a* and *foxc1b* function co-operatively to promote *runx1* expression

(A-D) Lateral view of *in situ* hybridisation of *runx1* expression in the trunk of WT embryos (A), *foxc1b* single mutants (B), *foxc1a* single mutants (C) and *foxc1a*; *foxc1b* double mutants (D) at 24hpf.

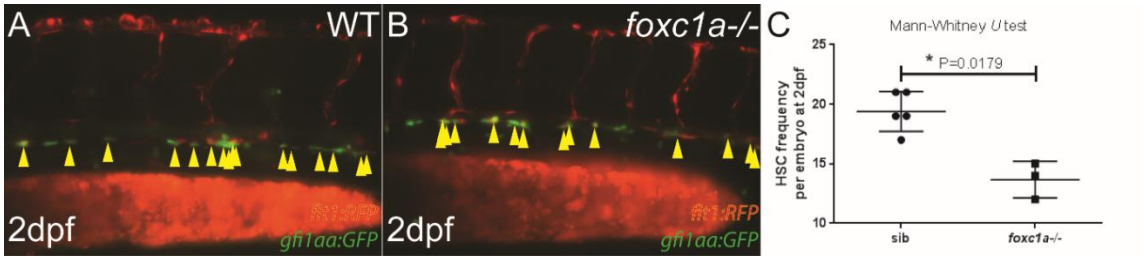

Figure 4.21 *fox1a* is required for HSC emergence

(A, B) Lateral view of trunk of WT embryos (A) and *foxc1a* single mutants (B) with *Tg(flt1:RFP; gfi1aa:GFP)* background at 2dpf. Yellow arrowheads indicate budding HSC from the DA. (C) Quantification of HSC number per embryo at 2dpf. Mann-Whitney *U* test. P=0.0179. DA, dorsal aorta.

4.2.17 The dorsal aorta and posterior cardinal vein were specified in *foxc1a* mutants

HSC are generated from the ventral wall of the DA, therefore the intact and functional DA is necessary for the HSC formation (Burns et al., 2005, Gering and Patient, 2005, Bertrand et al., 2010). To further understand the mechanism of how *foxc1a* regulates HSC formation we examined arterial-venous specification in *foxc1a* mutants.

The arterial marker and Notch target, *ephrinb2a*, remained unchanged in *foxc1a* single mutants (Fig. 4.22 B Red arrowhead) indicating that DA formation was not affected by the absence of *foxc1a*. We further analysed expression of the major Notch receptor involved in arterial-venous specification, *notch1b* (Fig. 4.22 C Red arrowhead) (Lawson et al., 2001). Consistent with the unchanged *ephrinb2a* expression in *foxc1a* single mutants, arterial *notch1b* also remained unchanged (Fig. 4.22 D Red arrowheads) at 24hpf. In addition, arterial-specific *notch3* showed similar expression in *foxc1a* single mutants compare to WT embryos (Fig. 4.22 E, F Red arrowheads), which further indicates normal DA formation in the absence of *foxc1a*. In summary, the expression of major Notch receptors remained unchanged in *foxc1a* mutants indicating DA formation was normal in the absence of *foxc1a*, consistent with previous data (Fig. 3.5). The venous marker *aplnr2a/ msr* showed expanded expression in the absence of *foxc1a* (Fig. 4.22 H Red bar), which could be explained by the dilated PCV (Fig. 4.7 B) caused by reduced trunk blood circulation in *foxc1a* single mutants.

Taken together, these data indicate that the DA is formed normally in *foxc1a* mutants. Therefore, the reduced HSC formation displayed in *foxc1a* single mutants is not likely to be caused by abnormal arterial specification. In addition, the expression of major Notch receptors remained unchanged in the absence of *foxc1a*, indicating *foxc1a* might potentially regulate the Notch ligands to control Notch function.

4.2.18 *foxc1a* is required for haematopoietic stem cell formation potentially via regulating the expression of the Notch ligands

Given that Notch receptor expression was normal in *foxc1a* mutants (Fig. 4.22) and activity of Dll4 enhancer was moderately reduced in *foxc1a* mutants (Fig. 4.16 B), we checked multiple Notch ligands and targets, which have been reported to be essential for HSC formation (Kim et al., 2014, Shankaran et al., 2007, Butko et al., 2015).

Expression of Notch ligand *dlc* was abolished in the DA (Fig. 4.23 B Red arrowhead) and reduced in SeAs (Fig. 4.23 B Black arrowheads) in *foxc1a* single mutants, indicating *foxc1a* promotes expression of multiple Notch ligands including *dll4* and *dlc*.

Unpublished data from the Wilkinson lab has demonstrated that *her12* is a downstream target of the Notch signalling pathway required for HSC emergence (Zhen Jiang MSc thesis, University of Sheffield) (Jack Adams MSc Thesis, University of Sheffield) (Shankaran et al., 2007). We therefore analysed the expression of *her12* in WT and *foxc1a* single mutants. The expression of *her12* was reduced within the DA (Fig. 4.23 D Red arrowhead) but not the neural tube (Fig. 4.23 D Blue arrowhead) in the absence of *foxc1a*, consistent with reduced Dll4 activity reported in section 4.2.12. This data also indicates *foxc1a* induces *her12* expression selectively in the DA, but not the neural tube in keeping with lack of expression of *foxc1a* in the neural tube (Fig. 4.18 A-A''). This suggests *foxc1a* might regulate HSC formation via a cell-autonomous mechanism. Interestingly, the expression of the Notch target *gata2a* remained unchanged in *foxc1a* single mutants (Fig. 4.23 F) at 26hpf. Furthermore, expression of *gata2b*, which was shown to promote HSC formation from haemogenic endothelium (Butko et al., 2015), was unchanged in *foxc1a* mutants at 26hpf (Fig. 4.23 H Red arrowhead).

tbx20 is an arterial marker restricted to the roof of the DA during HSC emergence (Szeto et al., 2002; Wilkinson et al., 2009). Interestingly, we observed a dramatic reduction of *tbx20* expression at 24hpf in most *foxc1a* mutant embryos (Fig. 4.23 J Red arrowhead). We previously reported that DA formation was normal in the absence of *foxc1a* (Fig. 4.22), therefore this reduction of *tbx20* expression was not due to loss of ECs, but reduced expression within ECs of the DA roof.

Taken together, *foxc1a* is required for HSC emergence from the DA potentially by promoting the expression of Notch ligands and Notch downstream target *her12*, but independently of Notch receptor expression and *gata2a*/ *gata2b* signalling. In addition, our data also suggests *foxc1a* is potentially required for establishing dorsal-ventral differentiation of DA.

4.2.19 *foxc1a* is required for somitic Notch contributions to HSC formation

In addition to cell-autonomous requirements for Notch signalling, a non-cell autonomous Wnt16/ Notch regulatory pathway was identified within the developing somites for HSC specification (Clements et al., 2011). In section 4.2.1, we demonstrated that *foxc1a* and *foxc1b* are expressed in developing somites and *foxc1a* is required for normal somite formation and patterning (Fig. 4.1, 4.2). We therefore hypothesised that *foxc1a* and *foxc1b* might also contribute to HSC specification via Wnt16/ Dlc/ Dld signalling during early embryogenesis.

To test this, we examined the expression of components of this pathway in WT embryos, *foxc1a* single mutants and *foxc1a; foxc1b* double mutants at 12s. Interestingly, the expression of *wnt16* was significantly reduced in the somitic mesoderm of *foxc1a* single mutants (Fig. 4.24 B Red bar) when compared with the WT embryos (Fig. 4.24 A Red bar). Reduced expression of *dlc* was also observed in the somitic mesoderm, particularly within the 4 most anterior somites of *foxc1a* single mutants (Fig. 4.24 E, E' Red arrowheads and red bars), which is in line with previous studies (Julich et al., 2005, Topczewska et al., 2001a, Kume et al., 2001). Expression of *dld* remained unchanged in *foxc1a* single mutants (Fig. 4.24 H, H' Red arrowheads) when compared with WT siblings (Fig. 4.24 G, G' Red arrowheads). Interestingly, the reduction of *wnt16* expression and *dlc* expression were more significant in *foxc1a; foxc1b* double mutants (Fig. 4.24 C, F, F'), which could account for the greater reduced *runx1* expression show in section 4.2.16.

Expression of *wnt16*, *dlc* and *dld* were normal in *foxc1b* single mutants (data not shown). Collectively, these data support our hypothesis that *foxc1a* and *foxc1b* co-operatively contribute to HSC specification via a non-cell-autonomous Wnt-Dlc pathway in the developing somites. Consistent with this, *foxc1b* expression is excluded from ECs yet a greater reduction of *runx1* expression was observed in *foxc1a; foxc1b* double mutants than in *foxc1a* single mutants (Fig. 4.20). These data also suggest that *foxc1a* and *foxc1b* promote Notch signalling by inducing expression of Notch ligands and that *foxc1a* and *foxc1b* influence EC physiology via cell-autonomous and non-cell-autonomous mechanisms.

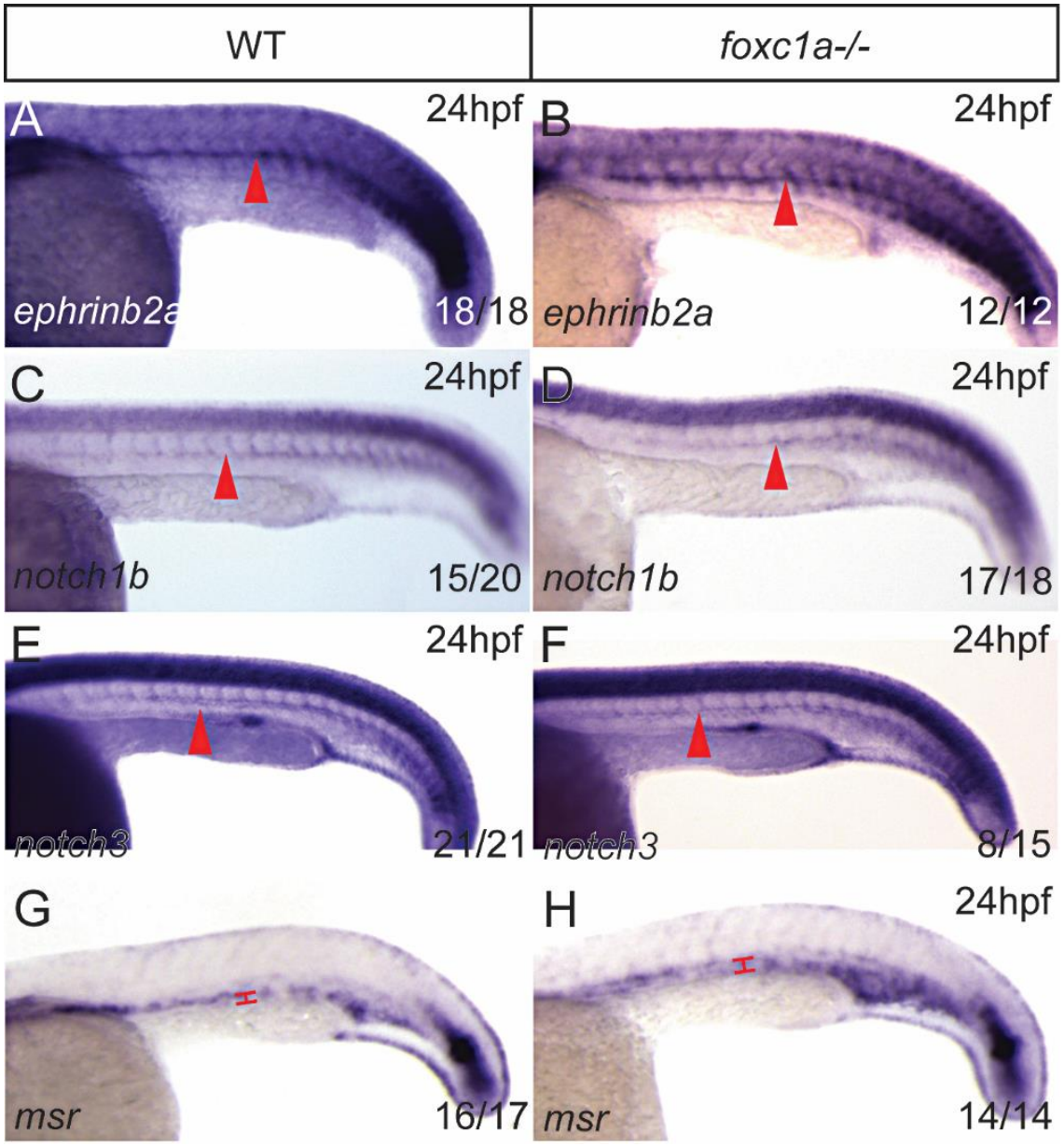

Figure 4.22 *foxc1a* is dispensable for arterial-venous specification

(A-F) Lateral view of *in situ* hybridisation of arterial specific markers expression in WT (A, C, E) and *foxc1a* single mutants (B, D, F) at 24hpf. Red arrowheads indicate DA. (G, H) Lateral view of *in situ* hybridisation of venous marker *msr* expression in WT embryos (G) and *foxc1a* single mutants (H) at 24hpf. Red bars indicate PCV. DA, dorsal aorta; PCV, posterior cardinal vein.

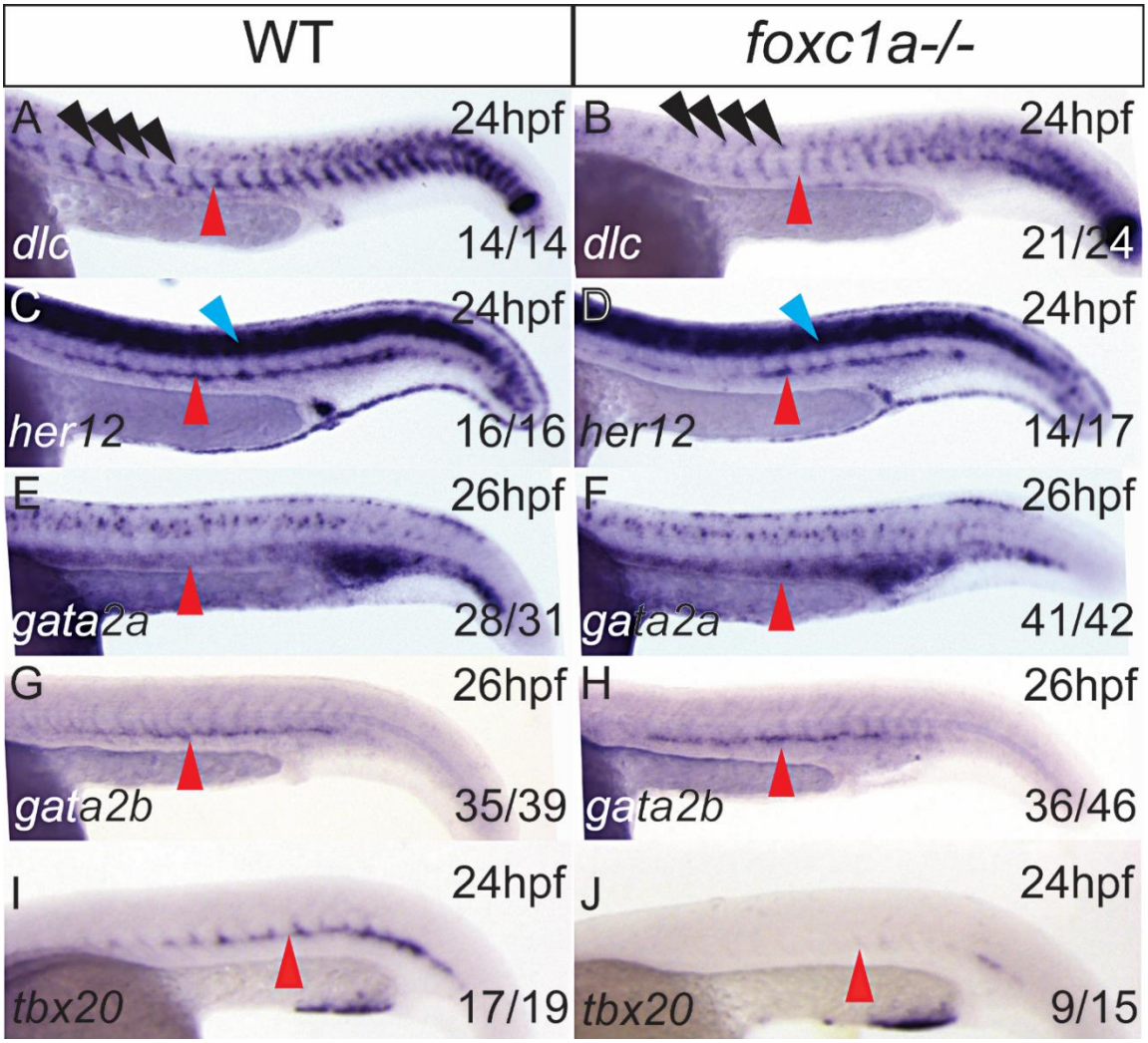

Figure 4.23 *foxc1a* is required for arterial Notch contributions to HSC formation

(A, B) *In situ* hybridisation of *dlc* expression in WT embryos (A) and *foxc1a* single mutants (B) at 24hpf. Red arrowheads indicate DA, black arrowheads point to ISVs. (C, D) *in situ* hybridisation of *her12* expression in WT embryos (C) and *foxc1a* single mutants (D) at 24hpf. Red arrowheads indicate DA, blue arrowheads highlight neural tube. (E-H) *In situ* hybridisation of *gata2a* and *gata2b* expression in WT embryos (E, G) and *foxc1a* single mutants (F, H) at 26hpf. (I, J) Lateral view of *in situ* hybridisation of *tbx20* expression in WT embryos (I) and *foxc1a* single mutants (J) at 24hpf. Red arrowheads indicate DA. DA, dorsal aorta; PCV, posterior cardinal vein; ISV, intersegmental vessel.

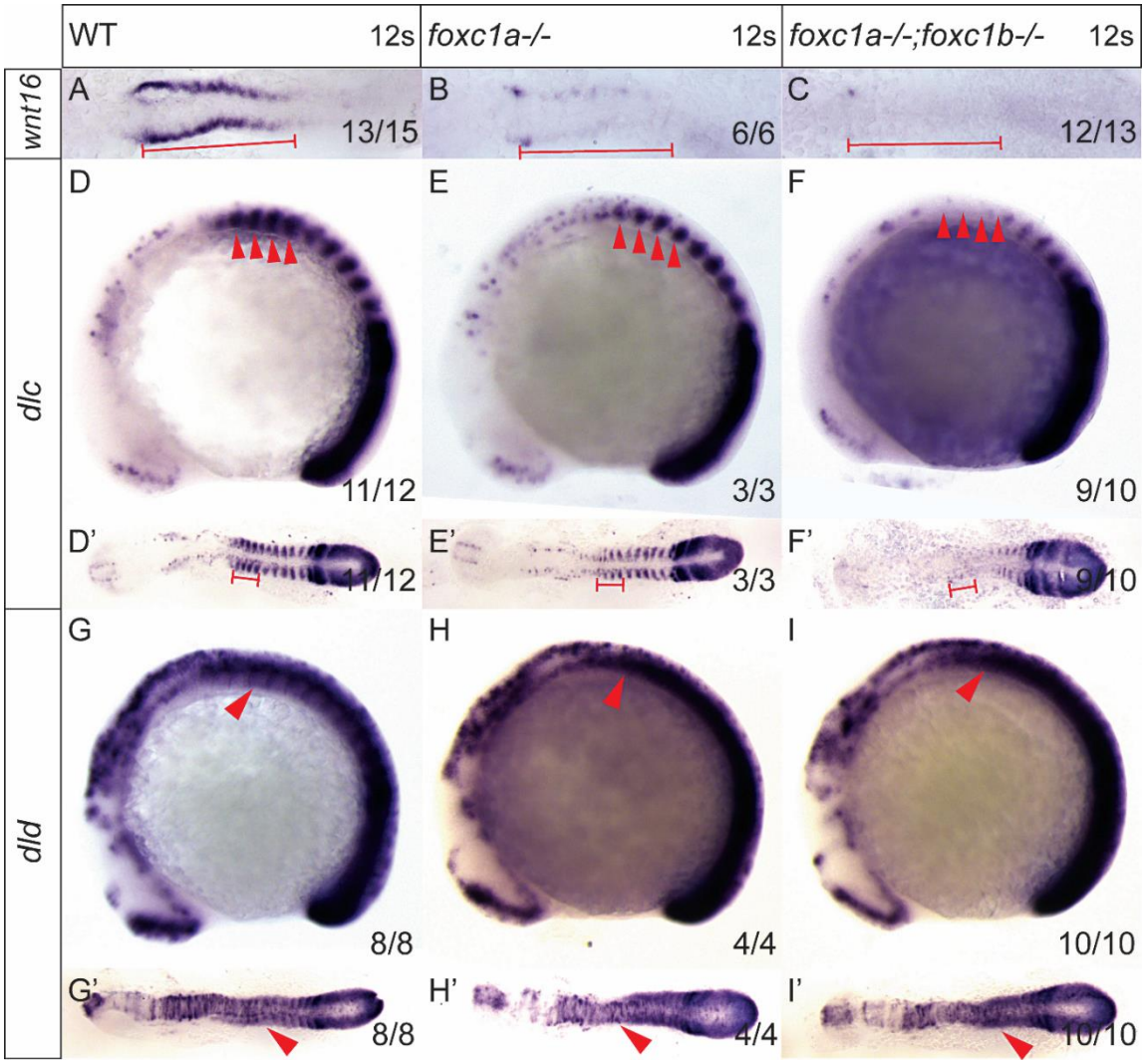

Figure 4.24 *foxc1a* is required for somitic Notch contributions to HSC formation

(A-C) Dorsal view of flat mount of *in situ* hybridisation of *wnt16* in WT (A) *foxc1a* single mutants (B) and *foxc1a*; *foxc1b* double mutants (C) at 12s. Red bars highlight the somitic expression. (D-F) Lateral view of *in situ* hybridisation of *dlc* in WT (D) *foxc1a* single mutants (E) and *foxc1a*; *foxc1b* double mutants (F) at 12s. (D'-F') Dorsal view of flat mount of *in situ* hybridisation of dlc in WT (D') *foxc1a* single mutants (E') and *foxc1a*; *foxc1b* double mutants (F') at 12s. Red arrowheads and red bars indicate the first 4 anterior somites. (G-I) Lateral view of *in situ* hybridisation of *dld* in WT (G) *foxc1a* single mutants (H) and *foxc1a*; *foxc1b* double mutants (I) at 12s. (G'-I') Dorsal view of flat mount of *in situ* hybridisation of dld in WT (G') *foxc1a* single mutants (H') and *foxc1a*; *foxc1b* double mutants (I') at 12s. Red arrowheads indicate somitic expression.

4.3 Discussion

In this chapter, we have demonstrated that *foxc1a* is required for somitogenesis and sclerotome patterning, whereas *foxc1b* is dispensable from this process. Here we highlight our findings below:

1. *foxc1a* and *foxc1b* cooperate to antagonise arterial angiogenesis in trunk.
2. *foxc1a* and *foxc1b* limits trunk angiogenesis via induction of Notch signalling to suppress pro-angiogenic signalling via the Flt4/ Vegfc pathway.
3. *foxc1a* and *foxc1b* are required for HSC formation potentially via non-cell-autonomous and/ or cell-autonomous regulation of Notch signalling.

4.3.1 *foxc1a* and *foxc1b* suppress arterial angiogenesis via induction of Notch-mediated suppression of Flt4/ Vegfc signalling

Elegant experiments have demonstrated that murine Foxc1 and Foxc2 directly activate the *Dll4* and *Hey2* promoters during vascular development (Seo et al., 2006, Hayashi and Kume, 2008b). FOXC2 was shown to interact with the Notch transcriptional activation complex physically and functionally (Hayashi and Kume, 2008b). *In vitro* evidence also supports that *Foxc* genes can induce Notch signalling (Seo et al., 2006). In zebrafish, Foxc1a has been reported to physically interact with Rbpjk, which binds to NICD to form the Notch transcriptional activation complex and activate the Notch signalling pathway during podocyte development (O'Brien et al., 2011). However, it remains unclear whether zebrafish *foxc1* genes interact with the Notch signalling pathway during vascular development.

Here we have reported that *foxc1a* and *foxc1b* function collectively upstream of Notch signalling and positively regulate *dll4* expression during SeA formation. In the absence of both *foxc1a* and *foxc1b*, we observed increased angiogenesis in trunk vessels, which has never been reported in either murine or zebrafish studies previously. In *foxc1a*; *foxc1b* double mutants, more substantial down regulation of *dll4* and *grl* was detected when compared to the *foxc1a* single mutants and WT siblings (Fig. 4.16). More importantly, this abnormal angiogenesis could be rescued by either induction of Notch signalling or inhibition of Vegfc function in the trunk. Taken together, the negative regulation of trunk angiogenesis by *foxc1a* and *foxc1b* occurred via Notch-mediated suppression of *vegfc/ flt4* expression. As shown in section 4.2.14, expression of *foxc1b* is excluded from ECs in trunk vessels, instead being expressed in perivascular tissue and sclerotome (Fig. 4.18

D-F''). Furthermore, *foxc1b* expression is also excluded from ECs in *foxc1a* mutants (Fig. 4.19 D-F). This suggests that *foxc1b* can induce *dll4*-mediated suppression of *vegfc/ flt4* in a non-cell-autonomous manner. Taken together, the *foxc1a* and *foxc1b* induce expression of *dll4* and positively regulate Notch signalling pathway.

Foxc proteins and ETS transcription factors have been demonstrated to work co-operatively and these FOXC:EST motifs function as enhancers of endothelial-specific genes including the VEGFRs FLT4, and NRP1 (De Val et al., 2008). As introduced in section 4.2.14 *foxc1a* is expressed in ECs of trunk vasculature (Fig. 4.18 A-C). Therefore, it is more likely that *foxc1a* positively regulates the Dll4/ Notch-mediated suppression of *vegfc/ flt4* cell-autonomously.

In addition, the ectopic SeAs in *foxc1a*; *foxc1b* double mutants could not be rescued by overexpression of *sflt1* mRNA. Consistent with our observation, recent studies have reported that *sflt1* selectively limits sprouting from veins, but not arteries (Wild et al., 2017, Matsuoka et al., 2016), which could explain why *sflt1* gain of function failed to rescue the ectopic SeA formation in *foxc1a*; *foxc1b* double mutants (Fig. 4.14).

The VEGF decoy receptor, FLT1, has been described to function as a VEGFA sink, in which excess VEGFA is unable to bind to pro-angiogenic VEGFRs such as KDR. FLT1 and KDR function antagonistically to balance angiogenesis through interaction with VEGFA (Gerhardt et al., 2003, Ambati et al., 2006, Roberts et al., 2004). In *foxc1a* single mutants and *foxc1a; foxc1b* double mutants comparable expression levels of *kdrl* were observed, along with unchanged *vegfaa* expression (Fig 4.12). However, while *foxc1a* single mutants displayed reduced anti-angiogenic *sflt1*, *foxc1a; foxc1b* double mutants displayed a greater reduction (Fig 4.12). Furthermore, *foxc1a; foxc1b* double mutants displayed ectopic trunk angiogenesis, while *foxc1a* single mutants do not. Therefore, it is possible that the reduction in s*flt1* and *kdrl* observed in *foxc1a* single mutants can balance their pro- and anti-angiogenic effects, whereas in *foxc1a; foxc1b* double mutants *sflt1* expression was lower than single mutants, leading to an imbalance between Kdrl and sFlt1. Therefore, in *foxc1a; foxc1b* double mutants, increased free Vegfa could potentially contribute to ectopic angiogenesis, binding more freely to the relatively less reduced Kdrl in the double mutants. Further experiments will be needed to test this hypothesis.

4.3.2 *foxc1a* is required for trunk lymphatic development

In the previous chapter we introduced *foxc1a* being essential for facial lymphatic development and brain lymphatic cell specification. In this chapter we have reported that thoracic duct (TD)

formation in the trunk was delayed in the absence of *foxc1a* at 3dpf and the TD coverage was reduced in the *foxc1a* single mutants by 4-5dpf.

The TD originates from ECs which sprout from the PCV (Karpanen and Schulte-Merker, 2011). In general, every second SeV from the PCV will migrate dorsally and stop at the horizontal myoseptum to form the parachordal lymphangioblast, which will eventually migrate ventrally to form the TD (Koltowska et al., 2013, Bussmann et al., 2010). In *foxc1a* single mutants, secondary angiogenesis was reduced by approximately 50% when compared with the WT embryos (Section 4.2.9). Also *flt4* expression within SeV was also reduced in *foxc1a* single mutants and *foxc1a*; *foxc1b* double mutants (Fig. 4.11 C, D) when compared with WT embryos (Fig. 4.11 B). Therefore, the reduced SeV formation displayed in *foxc1a* single mutants is likely to account for the delayed TD formation and reduced TD coverage. In chapter3 (Section 3.2.11) we have demonstrated that *foxc1a* promotes venous CtA formation potentially via positive regulation of *flt4* expression (Fig. 3.19 A-D). Flt4/ Vegfc is a master regulatory pathway for venous angiogenesis and lymphatic development (Gordon et al., 2013, Le Guen et al., 2014, Villefranc et al., 2013). Taken together, *foxc1a* and *foxc1b* differentially regulate the Flt4/ Vegfc pathway in arteries and veins. In arteries, *foxc1a/ foxc1b* positively regulate the Dll4/ Notch-mediated suppression of Flt4/ Vegfc signalling, whereas, in veins, *foxc1a/ foxc1b* directly promote the Flt4/ Vegfc pathway.

In addition, *foxc1a* single mutants displayed reduced mesenchyme distance between the DA and the PCV (Fig. 4.4 E-G), which could potentially become physical obstacles for the LEC horizontal migration. This also likely contributes to the abnormal TD formation displayed in *foxc1a* single mutants.

4.3.3 *foxc1a* is dispensable for arterial-venous specification

We reported that in the absence of *foxc1a* or both *foxc1a* and *foxc1b*, the DA and PCV could be observed in the trunk, however the DA displayed reduced diameter and the PCV displayed increased diameter, which likely resulted from disrupted blood circulation as introduced in the previous chapter. The relatively normal DA formation displayed in both *foxc1a* single mutants and *foxc1a*; *foxc1b* double mutants conflicts with previous zebrafish morphants and mouse studies, which reported severe arterial-venous malformations in the absence of both *Foxc* genes (De Val et al., 2008, Skarie and Link, 2009, Kume et al., 2001, Seo et al., 2006). We further validated our data using *in situ* hybridisation for arterial markers including *ephrinb2a, notch1b* and *notch3* and showed that their expression was not obviously affected in *foxc1a* mutants. Interestingly, the expression of *tbx20* was significantly reduced in the DA roof of *foxc1a* single mutants. Wilkinson

et al. previously showed that Hedgehog (Hh)-mediated *tbx20* expression in the dorsal DA alongside Bmp signalling from the ventral DA are important for defining the dorsal-ventral patterning of the DA (Wilkinson et al., 2009). Taken together, the reduction of *tbx20* expression displayed in *foxc1a* single mutants could potentially result in disrupted dorsal-ventral patterning of the DA. In summary, *foxc1a* is dispensable for arterial-venous specification, however, we cannot exclude the possibility that *foxc1a* might be essential for establishing dorsal-ventral patterning of the DA.

Hh from the notochord regulates the expression of *tbx20* in the DA roof, which is located upstream of Notch signalling (Gering and Patient, 2005, Murayama et al., 2006, Zhang and Rodaway, 2007, Wilkinson et al., 2009, Lawson et al., 2001). Further study showed that the expression of *tbx20* is also VEGF signalling dependent (Carroll et al., 2014). Interestingly, Sonic hedgehog (*Shh)* was reported to be required for expression of murine *Foxc1* and *Foxc2* (Yamagishi et al., 2003). In addition, Foxc1 physically and functionally interacts with the Hh effector, Gli2, during endochondral ossification (Yoshida et al., 2015), which further confirmed the interaction between mammalian *Foxc* genes and Hh signalling. These data are in line with the unpublished data from the Wilkinson lab, which showed reduced *foxc1a* expression following down-regulation of Hh signalling (Wilkinson lab unpublished data). Taken together, similar to mammalian *Foxc1/ 2*, *foxc1a* potentially acts as a downstream target of the Hh signalling pathway in zebrafish. In addition, we have also reported that *foxc1a* acts upstream of the Vegfrs. This data supports the idea that Vegf signalling increases the induction of *Foxc1* downstream signalling as previously reported in mice (Hayashi and Kume, 2008b). Taken together the reduced expression of *tbx20* from the DA roof in *foxc1a* single mutants could either be regulated by Hh-*foxc1a* directly or by *foxc1a*-mediated reduction of *vegfr* expression indirectly in the trunk. Further experiments would be needed to address this hypothesis.

4.3.4 *foxc1a* is required for haematopoietic stem cell formation via cell-autonomous Notch pathways

Notch1 is essential for regulating HSC specification from the ventral wall of the DA (Kumano et al., 2003, Hadland et al., 2004). Notch signal strength has been demonstrated to be important for establishing cell fate within murine haemogenic endothelium (Gama-Norton et al., 2015). In the absence of *Jag1*-induced low Notch signalling, HSC formation was reduced with unimpaired endothelial programming. Conversely, in the absence of Dll4-induced high level Notch signalling, the endothelial programme was blocked. Taken together this competitive regulation of Notch signalling between Jag1-Notch1 (low Notch signal strength) and Dll4-Notch1 (high Notch signal

strength) is essential for arterial programming and HSC formation specifically (Gama-Norton et al., 2015).

In the previous section, we discussed that *foxc1a* is dispensable for arterial-venous specification. We described the unchanged expression of Notch receptors including *notch1b* and *notch3* (Fig. 4.22), but moderately reduced expression of Notch ligands including *dll4* and *dlc* within the DA of *foxc1a* single mutants (Fig. 4.16, 4.23). In *foxc1a* single mutants, reduced HSC formation but relatively normal vascular patterning was observed (Fig. 4.7, 4.20). Taken together, this reduced HSC formation is likely due to the *foxc1a*-mediated moderate down-regulation of Notch signalling post DA formation.

foxc1a is expressed in the DA, therefore this *foxc1a*-mediated Notch regulation is likely functioning cell-autonomously. Unpublished data from the Wilkinson lab has demonstrated that *her12* is a downstream target of Notch signalling, essential for HSC formation via a cell-autonomous mechanism (Zhen Jiang MSc Thesis, University of Sheffield) (Jack Adams MSc Thesis, University of Sheffield). In *foxc1a* single mutants, we have shown that *foxc1a* is required for *her12* expression in the DA but not the neural tube (Fig. 4.23). Therefore, *foxc1a* contributes to HSC emergence potentially via regulating this Notch-*her12* cell-autonomous pathway.

Furthermore, murine studies proved that *Gata2* is essential for haemogenic endothelium to adapt its progeny during early development (Kumano et al., 2003, Hadland et al., 2004, Robert-Moreno et al., 2005, de Pater et al., 2013), whose expression is regulated by *Notch1* (Robert-Moreno et al., 2005). In zebrafish, two murine orthologues exist, namely *gata2a* and *gata2b* (Gillis et al., 2009). Having showed that the expression of both *gata2a* and *gata2b* remained unchanged in the absence of *foxc1a* (Fig. 4.23), we concluded that this *Notch1-gata2a/ b* pathway is dispensable for *foxc1a*-regulated HSC formation. Our data further provides evidence that the *foxc1a*-Notch-*her12* pathway might be in parallel with the *Notch1-gata2a/ b* cascade during HSC formation.

Having shown *foxc1a* is dispensable for DA specification, however, substantially reduced *tbx20* expression was observed within the DA roof of *foxc1a* single mutants (Fig. 4.23). We could not rule out the possibility that *foxc1a* contributes to establishing DA dorsal-ventral patterning, abnormalities which might also contribute to reduced HSC specification.

Given expression of *foxc1b* is excluded from the ECs of the trunk vasculature, it is unlikely that *foxc1b* can regulate HSC specification cell-autonomously. Interestingly, we observed more pronounced down-regulation of *runx1* expression within the DA of *foxc1a; foxc1b* double mutants

(Fig. 4.20), when compared with *foxc1a* single mutants (Fig. 4.20), which proved *foxc1a* and *foxc1b* co-operatively promote HSC formation. In section 4.3.1 we discussed that *foxc1a* and *foxc1b* function co-operatively to antagonise angiogenesis via promoting the Notch-mediated suppression of the Flt4/ Vegfc pathway. We also demonstrated that *foxc1b* functions non-cell-autonomously to antagonise angiogenesis in the absence of *foxc1a* (Section 4.2.15). Therefore, *foxc1b* likely contributes to HSC specification non-cell-autonomously in the absence of *foxc1a*.

4.3.5 *foxc1a* is required for somite formation, *foxc1a* and *foxc1b* are required for the somitic Notch pathway to promote haematopoietic stem cell specification.

Our *foxc1a* single mutants showed similar morphology to recently published *foxc1a* mutants and morphants with abnormal anterior somite formation (Hsu et al., 2015, Li et al., 2015, Topczewska et al., 2001a). This is also similar to somite abnormalities observed in murine *Foxc1* mutants (Kume et al., 2001, Topczewska et al., 2001a, Schuermann et al., 2014). We further reported, similar abnormal somite formation in *foxc1a*; *foxc1b* double mutants, whereas *foxc1b* single mutants showed no obvious defect in somitogenesis (Fig. 4.2). Interestingly, no severity difference of the somite deficit between *foxc1a* single and *foxc1a*; *foxc1b* double mutants was observed, indicating *foxc1b* is dispensable for somite formation.

Further analysis of expression of sclerotome markers (Fig. 4.3) revealed *foxc1a* is also required for sclerotome patterning. The expression of *pax1a* and *pax9* were both reduced in the absence of *foxc1a* indicating an interaction between the *pax* genes and *foxc1a* while regulating sclerotome formation. Interestingly, mammalian *Foxc2* was previously reported to potentially interact with *Pax* genes to regulate sclerotome formation (Smith et al., 2000). Taken together, zebrafish *foxc1a* and murine *Foxc2* may share similar functions during sclerotome specification.

Dld/ Dlc-Notch3 has been reported to promote sclerotome formation (Kim et al., 2014). Kim *et al.* further proposed that, in zebrafish, Notch induction between 6-15h is required for sclerotome specification, whereas Notch induction at 15-26h is required for arterial-venous specification (Kim et al., 2014). Interestingly, we have shown reduced expression of *dlc* at both stages (Fig. 4.23, Fig. 4.24) in *foxc1a* single mutants but with normal arterial-venous specification (Fig. 4.22). Given the reduction of *dlc* expression in *foxc1a* single mutants (Fig. 4.24), these data indicate that *foxc1a* promotes somitogenesis and sclerotome formation potentially via regulating this Dlc-Notch3 pathway at 6-15hpf prior to completion of DA formation. Furthermore, the reduced expression of *dlc* in *foxc1a* single mutants at 24hpf (Fig. 4.23) did not result in arterial-venous malformation as previously demonstrated (Kim et al., 2014, Quillien et al., 2014). This observation could be

explained by either insufficient reduction of *dlc* expression in *foxc1a* single mutants to adversely affect normal arterial-venous patterning or that the *dlc*-Notch3-mediated abnormal arterial-venous specification could potentially be compensated by Notch1, the expression of which is normal in *foxc1a* single mutants (Fig. 4.22).

In addition, the Wnt16-Dlc/ Dld-Notch3 signalling cascade in developing somites promotes HSC specification (Kim et al., 2014, Clements et al., 2011). The expression of *wnt16* and *dlc* were substantially reduced in *foxc1a* single mutants (Fig. 4.24). Furthermore, greater reduction of this signalling pathway component expression was observed in *foxc1a; foxc1b* double mutants at 12s (Fig. 4.24). Therefore, we conclude that *foxc1a* and *foxc1b* both promote induction of this somitic Notch pathway to promote HSC emergence at early stages. Conversely, in the absence of *foxc1b*, expression of *wnt16*, *dlc* and *dld* remained unchanged (data not shown). This data indicates that *foxc1a* and *foxc1b* have redundant functions during regulation of this somitic Notch signalling.

Furthermore, the Jam1a-Jam2a interaction was reported by the Traver lab to maintain the interaction between the posterior lateral mesoderm and the somite, which is essential for Dld/ Dlc-mediated Notch signalling transduction to specify HSCs (Kobayashi et al., 2014). Overexpression of *dld* but not *dlc* could almost fully recover the HSC deficiency observed in *jam1a*-depleted embryos (Kobayashi et al., 2014). This data indicates that *dld* is more important to facilitate the Notch signal transmission. In section 4.2.19 we reported reduced *dlc* expression but not *dld* expression in the somitic mesoderm (Fig. 4.24) with moderately reduced *runx1* expression (Fig. 4.20) in *foxc1a* single mutants, whereas significant reduction of *wnt16*, *dlc* and *runx1* expression was observed in *foxc1a*; *foxc1b* double mutants (Fig. 4.20, 4.24). The moderate reduction of *runx1* expression in *foxc1a* mutants could be explained by retention of *wnt16* and *dlc* expression at 12s and the remaining Notch signalling at 24hpf in *foxc1a* single mutants facilitating HSC formation. Whereas in the absence of both *foxc1a* and *foxc1b*, a more substantial reduction of *wnt16/ dlc* expression and more pronounced reduced expression of Notch pathway components was observed, which may contribute to the more substantial reductions in *runx1* expression in *foxc1a; foxc1b* double mutants.

Furthermore, retinoic acid (RA) secreted from the somite was also reported to regulate HSC emergence prior to 19hpf and is dispensable for DA formation (Pillay et al., 2016), this early somitic pathway has been demonstrated this function independently of the Wnt16-Dlc/ Dld-Notch3 pathway (Pillay et al., 2016). Abnormal expression of *jam1a* and *jam2a* was observed in RA-depleted embryos, which further provides evidence for the potential interaction between the

somitic RA and the Jam1a-Jam2a pathway in regulating HSC formation (Pillay et al., 2016). Murine studies have shown RA secretion from the meninges is positively regulated by *Foxc1*, which is critical for cerebrovascular development (Mishra et al., 2016, Siegenthaler et al., 2009). Taken together, it is also possible that *foxc1a* and *foxc1b* could be involved in this somitic RA pathway to specify HSC via the Jam1a/ Jam2a pathway non-cell-autonomously. This could be an interesting direction for further studies.

4.3.6 *foxc1a* may be important for pericyte recruitment

In addition to its role in non-cell autonomous promotion of HSC formation, Notch3 has also been reported as a key regulator of mural cell (MC) recruitment (Wang et al., 2014).

In section 2.5, we reported that *foxc1a* is required for the expression of the pericyte marker *pdgfrb* at 24hpf and 48hpf and also for vSMC recruitment at 5dpf in the trunk. The reduction of *pdgfrb* expression in *foxc1a* single mutants could be detected at 24hpf (Fig. 4.5) as reported previously in an Mo study (French et al., 2014), which was prior to the initiation of blood circulation. Therefore, we can exclude the possibility that the reduced *pdgfrb* expression is a secondary defect caused by *foxc1a*-mediated failure of blood circulation. However, we could not exclude the contribution of disrupted blood circulation to later pericyte recruitment. Taken together, *foxc1a* is required for *pdgfrb* expression. In addition, Vegf signalling is required for the expression of *pdgfrb* (Kuhnert et al., 2008). Therefore, this disrupted *pdgfrb* expression could also potentially be due to impaired Vegf signalling in ECs following mutation of *foxc1a*.

Unlike zebrafish, conditional KO of murine *Foxc1* in pericytes leads to proliferation of pericytes (Siegenthaler et al., 2013). In addition, KO of *Foxc2* results in up-regulation of *Pdgfrb* (Petrova et al., 2004), on the contrary, *Foxc2* positively regulates mural cell recruitment in B16 tumour cells (Sano et al., 2010). The similar functions between zebrafish *foxc1a* and *Foxc2* in tumorigenesis suggest zebrafish might be a better model organism to study *Foxc* gene functions in tumorigenesis. Taken together, our data suggest a surprising divergence of how *Foxc* genes control pericyte recruitment between mammals and teleosts.

As discussed in section 4.3.5, *foxc1a* but not *foxc1b* is required for sclerotome patterning, which conflicts with previous zebrafish data (Chen et al., 2017). Chen *et al.* used the CRISPR/ Cas9 system to conditionally KO *foxc1a* and *foxc1b* in ECs and proposed that *foxc1b* but not *foxc1a* function in ECs is required for vSMC formation (Chen et al., 2017). We have reported that *foxc1b* expression was excluded from the ECs in both WT and *foxc1a* single mutant embryos (Section 4.2.14, 4.2.15). Therefore, it is unlikely that *foxc1b* functions in ECs to promote vSMC recruitment. The vSMC

recruitment in the DA is associate a with a specified cell population of the sclerotome (Stratman et al., 2017). Thus, the reduced vSMC coverage in *foxc1a* single mutants could also be potentially explained by the disrupted sclerotome patterning. In addition, blood circulation was reported to contribute to vSMC recruitment in zebrafish (Chen et al., 2017). Given the reduced blood circulation in *foxc1a* mutants, it is therefore more likely the vSMC reduction could be a secondary defect caused by reduced blood circulation in the absence of *foxc1a*.

Collectively, our data indicate *foxc1a* and *foxc1b* play compensatory and context-dependent roles during co-ordination of head and trunk angiogenesis via differential regulation of Vegf and Notch signalling (Fig. 4.25). In the head, *foxc1a* positively regulates expression of *kdrl* and *sox7* in ECs to induce angiogenesis, whereas in the trunk, *foxc1a* and *foxc1b* co-operatively promote Notch-mediated suppression of Flt4/ Vegfc to antagonise arterial angiogenesis. This novel regulation by *foxc1a* and *foxc1b* helps establish a competitive balance between anti- and pro-angiogenic factors throughout the body.

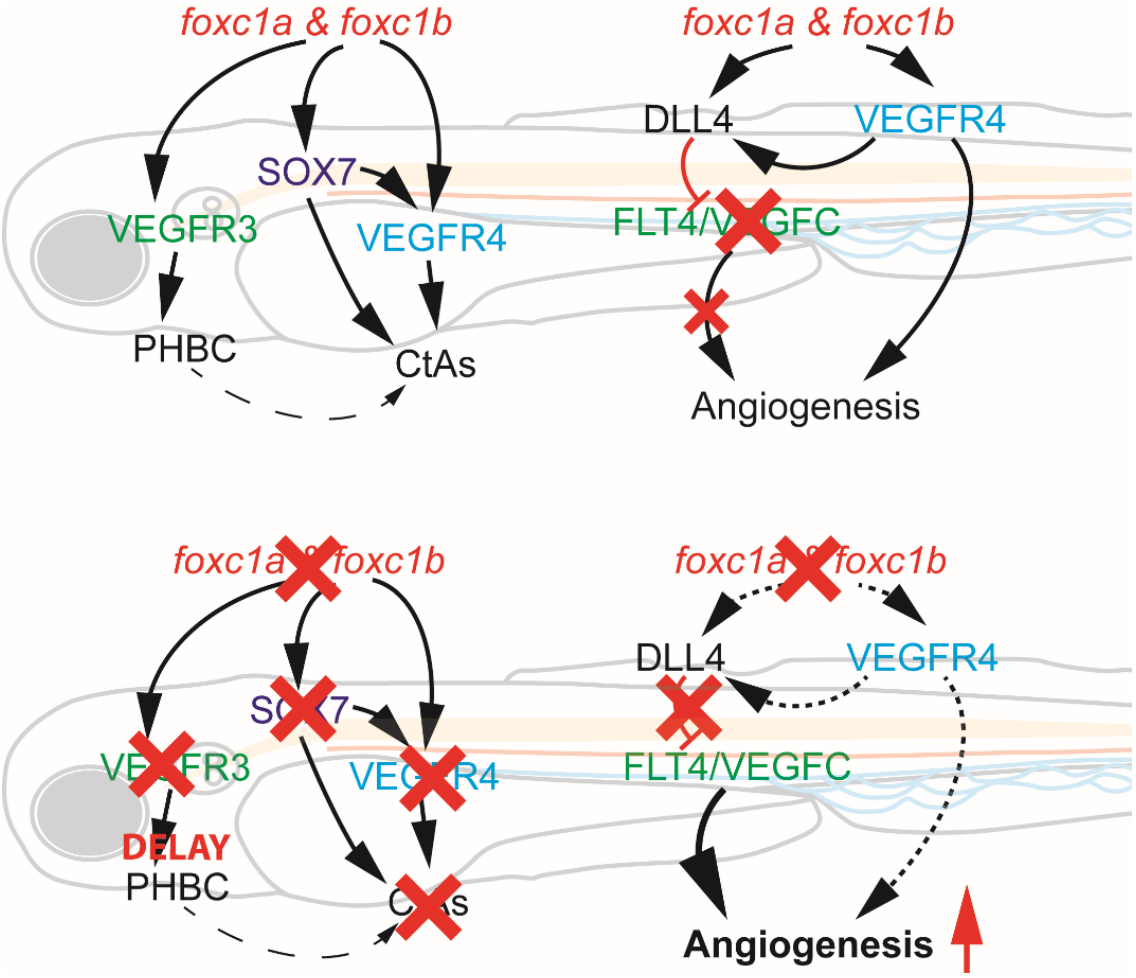

Figure 4.25 *foxc1a* and *foxc1b* balance angiogenesis by induction of competing pro- and anti-angiogenic signalling

CHAPTER 5

The Role of the G-Protein Coupled Receptors *calcrla* and *calcrlb* during Vascular Development in Zebrafish

5.1 Introduction

As briefly introduced in Chapter 1, the Calcitonin receptor-like receptor (CALCRL, formerly known as CLR and CRLR) can bind to numerous receptor activity-modifying proteins (RAMPs), which are single pass transmembrane proteins, to regulate receptor trafficking and activation of downstream signalling (Sexton et al., 2006, McLatchie et al., 1998). RAMP1 and CALCRL comprise the receptor for the calcitonin gene-related peptide (CGRP), whereas RAMP2-CALCRL and RAMP3-CALCRL are the receptor complexes for Adrenomedullin (AM) (McLatchie et al., 1998). Taken together, the functions of the receptor complexes formed by interaction between RAMPs and CALCRL are largely dependent on RAMPs since RAMPs confer ligand specificity to the GPCR (McLatchie et al., 1998, Dunworth and Caron, 2009). Intermedin (IMD), also known as Adrenomedullin 2 (AM2), is a more recently discovered ligand, which also binds RAMP-CALCRL complexes (Bell and McDermott, 2008). However, unlike CGRP or AM, IMD showed no specific binding preference among these RAMP-CALCRL receptor complexes (Roh et al., 2004). The regulations among CALCRL, RAMPs and their ligands have been show to play essential roles under numerous disease conditions, particularly in cardiovascular diseases including chronic heart failure and hypertension (Jacob et al., 2012). Due to the ligand selectivity of RAMPs-CALCRL interactions, RAMP-CALCRL complexes have become attractive candidates for therapeutic targets (reviewed in (Sexton et al., 2012)).

Despite extensive mammalian studies of the CALCRL-RAMP pathway, the mechanisms by which this pathway functions in these pathological conditions still remain largely unclear. Unlike mammals, in teleostan zebrafish, 4 andrenomedullin genes (namely *adma*: ENSDARG00000015263, *admb*: ENSDARG00000069027, *adm2a*: ENSDARG00000045708 and *adm2b*: ENSDARG00000078875), one *crcp* (ENSDARG00000069373) encoding a calcitonin gene-related peptide-receptor component protein, 2 *calcrl* genes (termed *calcrla*: ENSDARG00000011473, *calcrlb*: ENSDARG00000011571) and 4 *ramp* genes (*ramp1*: ENSDARG00000056704, *ramp2a*: ENSDARG00000037895, *ramp2b*: ENSDARG00000087020 and *ramp3*: IMAGE:8151627 (5')) have been identified (Zerbino et al., 2018) (Wilkinson Lab unpublished data). Given the duplication of *calcrl* and *ramp* genes in zebrafish, the number of possible combinations is increased compared to mammals, which increases the possibility for tissue-specific combinations and therefore tissue-specific functions of Calcrl-Ramp pathways. Among all Ams in teleosts, Ama shares the largest conserved amino acid sequence with the

mammalian AM (Nag et al., 2006). Previous studies in pufferfish *T. obscurus* have shown combinations of Calcrla/ Calcrlb with certain Ramps comprise the receptors for Am, which has the widest expression in various tissues (Nag et al., 2006). As introduced in previous chapters, the zebrafish is an ideal model organism for studying blood vessel formation *in vivo*. In this chapter, we employed the zebrafish to investigate the functions of *calcrla* and *calcrlb* during establishment of blood vessel integrity and lymphatic development.

5.1.1 Calcitonin receptor-like receptor and receptor activity-modifying proteins

Hydrops fetalis occurs in *Am*, *Calcrl* or *Ramp2*-knockout (KO) mice (Fritz-Six et al., 2008, Dackor et al., 2007, Dackor et al., 2006, Caron and Smithies, 2001), and these mutants die mid-gestation with severe oedema (Fritz-Six et al., 2008, Dackor et al., 2007, Dackor et al., 2006, Caron and Smithies, 2001). Conversely, neither *Ramp1*-/- mice nor *Ramp3*-/- mice display apparent abnormalities during development and both *Ramp1* and *Ramp3*-KO mice survive until adulthood (Tsujikawa et al., 2007, Dackor et al., 2007). These data indicate the importance of Am-Ramp2-Calcrl signalling for embryonic survival, and that *Ramp1* and *Ramp3* are not sufficient to compensate for loss of *Ramp2* function.

Interestingly, phenotypic onset differs among *Am*-, *Calcrl*- or *Ramp2*-KO mice. *Calcrl*-/- mice showed the earliest onset of oedema at E12.5 while at E13.5 the *Am*-/- mutant mice became distinguishable from WT littermates (Dackor et al., 2006). *Ramp2* mutant mice exhibit the latest phenotypic onset and oedema is visible at E14.5 (Fritz-Six et al., 2008). This late oedema onset provides evidence for the potential compensatory relations among the 3 AM components-mediated pathways.

Similar *Am*-/- and *Ramp2*-/- mice generated independently by the Shindo group in a C57BL/6 background exhibit a similar hydrops fetalis phenotype to the *Am*-/- and *Ramp2*-/- mutants generated by the Caron lab in a 129/S6-SvEv-TC1 background (Fritz-Six et al., 2008, Dackor et al., 2007, Dackor et al., 2006, Caron and Smithies, 2001, Shindo et al., 2014, Ichikawa-Shindo et al., 2008). Interestingly, the typical oedema phenotype was not fully penetrant in the *Am*-/- mice published by Shindo *et al.* (Shindo et al., 2001). In addition, severe haemorrhage under the skin and inside organs were reported in both *Am*-/- and *Ramp2*-/- in these studies (Ichikawa-Shindo et al., 2008, Shindo et al., 2001), whereas no haemorrhage was observed in *Am*-/- and *Ramp2*-/- mice generated by Fritz-Six *et al.* (Fritz-Six et al., 2008). This phenotypic difference between the two independent mutant strains could potentially arise from the different genetic backgrounds

used to generate the mutants (Kadmiel et al., 2012), and this will be discussed further in the following sections.

5.1.2 Calcitonin receptor-like receptor in lymphatic development

As introduced in previous chapters, the lymphatic system is essential to regulate tissue fluid homeostasis. Abnormalities in lymphatics could lead to lymphoedema, tissue fibrosis and inflammation, which result from failure of tissue fluid drainage (Lagerstrom and Schioth, 2008, Dunworth and Caron, 2009). Abnormal lymphatic formation has been reported in *Ramp2*, *Calcrl* and *Am* mutant mice and has been proposed to underline the stereotypical oedema which present without haemorrhage in these mice (Fritz-Six et al., 2008, Dackor et al., 2007, Dackor et al., 2006, Caron and Smithies, 2001). The murine tail lymphoedema model has been proposed as a powerful real-time experimental system to examine lymphangiogenesis *in vivo* (Boardman and Swartz, 2003). In this model, a ring of dermal tissue is surgically removed from the mouse tail resulting in complete interruption of interstitial fluid drainage but normal blood circulation, which will induce secondary lymphoedema as a result of reduced lymphatic function (Boardman and Swartz, 2003). Consistent with the previously published murine studies, AM treated BALB/c mice exhibited a significantly increased recovery rate post-operation when compared with the untreated control group (Jin et al., 2008). This data indicates AM signalling is required for lymphangiogenesis (Jin et al., 2008). Fritz-Six *et al*. further reported AM-Ramp2-Calcrl signalling specifically contributes to lymphatic endothelial cell (LEC) proliferation, but not venous endothelial cell (EC) proliferation (Fritz-Six et al., 2008). This reduced LEC proliferation-mediated by Am-Ramp2-Calcrl signalling resulted in smaller lymphatic sac formation in *Ramp2*, *Calcrl* and *Am* mutant mice (Fritz-Six et al., 2008). The specific effect of *Calcrl* in LEC was further confirmed in human dermal lymphatic microvascular endothelial cells, in which *Calcrl* expression was controlled by the master regulator of lymphatic fate, Prox1 (Fritz-Six et al., 2008). In addition, the AM associated protein, complement factor H, is characteristically enriched in LEC rather than in EC (Wick et al., 2007, Pio et al., 2001), which further indicates that AM-RAMP2-CALCRL signalling functions in LEC. Furthermore, LEC-conditional KO of *Calcrl* revealed a cell-autonomous function of *Calcrl* in regulating intestinal lymphatic vessel function and restoration following disease exposure. More interestingly, substantial down-regulation of the expression of DLL4 was observed in the LEC-conditional KO of *Calcrl* mutant mice, similar downregulation of DLL4 expression was also observed following the KD of *CALCRL* in human LEC culture (Davis et al., 2017).Taken together, these data suggeste that *Calcrl* functions upstream of the *Dll4*, and it

governs the LEC function and restoration following disease exposure through this *AM-Calcrl-Ramp-Dll4* cascade (Davis et al., 2017).

Previous studies have shown *AM-Ramp3-Calcrl* is dispensable for vasculogenesis and angiogenesis (Yamauchi et al., 2014). Interestingly, abnormal lipid absorption was reported in *Ramp3*-KO mice fed with a high-fat diet, however, this phenotype was described as subclinical, since it could be rescued by free-feeding (Yamauchi et al., 2014). In addition, delayed lymphatic drainage has also been reported in *Ramp3*-/- mice (Yamauchi et al., 2014), which indicates abnormal lymphatic function. Indeed, further *in vitro* experiments showed reduced migration and proliferation of LECs from *Ramp3*-/- mice (Yamauchi et al., 2014). Taken together, the *AM-Ramp3-Calcrl* signalling is also required for lymphatic function when the system is overloaded.

Yamauchi *et al.* also performed the mouse tail lymphoedema assay in WT, *Ramp3*-/-, LEC-conditional KO of *Ramp2* mutants and EC-conditional KO of *Ramp2* mutants (Yamauchi et al., 2014). Strikingly, only *Ramp3*-/- showed significantly increased lymphoedema after this procedure (Yamauchi et al., 2014). Taken together, Yamauchi *et al.* proposed that *Ramp3* but not *Ramp2* is involved in regulating lymphatic function, which conflicts with the murine study performed by Fritz-six *et al.* (Fritz-Six et al., 2008). This will be further discussed in section 5.1.5.

5.1.3 Calcitonin receptor-like receptor in blood vessel formation

In the mouse hind-limb ischemia model, AM treatment can restore blood circulation in the ischemic limb via up-regulation of local *Vegf* expression (Iimuro et al., 2004). Iimuro *et al.* further showed reduced density of capillary development and reduced levels of VEGF in *Am* heterozygous mutant mice (Iimuro et al., 2004). These data indicate that *Am* functions upstream of *Vegf* in regulating vascular development. Given that the *Am-Ramp2-Calcrl* signalling cascade has been shown to be essential for angiogenesis *in vitro* (Zhao et al., 1998, Kim et al., 2003, Nikitenko et al., 2000), surprisingly, no obvious defects in blood vessel formation were detected in *Calcrl*, *Ramp2* and *Am* mutant mice (Shindo et al., 2001, Dackor et al., 2006, Fritz-Six et al., 2008). In zebrafish, morpholino (Mo) KD of *calcrla* (orthologue of mammalian *Calcrl*) revealed a novel function of *calcrla* in arterial specification (Nicoli et al., 2008). In zebrafish, *calcrla* is expressed throughout embryonic development where it is enriched within the developing endothelium and somites, whereas the paralogous gene *calcrlb* was described to exhibit maternal expression only at 1 hour post fertilisation (hpf) (Nicoli et al., 2008). Knockdown of *calcrla* disrupted blood circulation as a result of arterial-venous malformation and delayed intersegmental vessel (ISV) sprouting (Nicoli et al., 2008). Furthermore, reduced arterial gene expression induced by *calcrla*

KD could be rescued by overexpression of the major secreted isoform of *vegfa* in zebrafish, *vegfaa*$_{121}$ (Liang et al., 1998, Nicoli et al., 2008). Taken together, these studies proposed that in zebrafish, *calcrla* is essential for arterial-venous specification via induction of downstream Vegf signalling. This is in line with studies in mouse which indicate *Am* functions upstream of *Vegf* signalling (Iimuro et al., 2004).

However, *in vitro* studies have indicated a more complicated interaction between AM and VEGF signalling (Fernandez-Sauze et al., 2004). Using capillary tube formation assays on Matrigel® both AM and VEGF treatment were demonstrated to induce capillary tube formation independently, however, inhibition of VEGF signalling using a neutralising antibody, only VEGF-induced and not AM-induced capillaries were significantly reduced, indicating these pathways may function in parallel. Furthermore, the AM-induced capillary formation could be inhibited effectively by applying neutralising RAMP2 and CALCRL antibodies. These data indicated AM and VEGF may not function as a linear hierarchical pathway (Fernandez-Sauze et al., 2004). Further *in vitro* studies proposed that the AM signalling pathway cooperates with VEGF signalling to induce arterial cell specification from vascular progenitors (Yurugi-Kobayashi et al., 2006). This conclusion was further supported by an *in vivo* zebrafish study utilising the same Mo targeting *calcrla* as previously described (Nicoli et al., 2008, Wilkinson et al., 2012). In zebrafish, Hedgehog (Hh) signalling normally induces *vegfaa* to promote arterial development via induction of Notch signalling (Lawson et al., 2002). However, Hh is also able to signal in parallel to Vegfaa and induce Notch signalling independently via a mechanism mediated by *calcrla* (Wilkinson et al., 2012). Collectively, these data suggest both human *CALCRL* and zebrafish *calcrla* promote blood vessel formation independently of VEGF signalling.

5.1.4 Calcitonin receptor-like receptor in angiogenesis

Adrenomedullin (AM) has been established as a pro-angiogenic factor, whose expression is enriched in vascular ECs and induced by hypoxic activation of HIF-1α (Garayoa et al., 2002, Cormier-Regard et al., 1998, Nakayama et al., 1998, Nguyen and Claycomb, 1999). The pro-angiogenic functions of AM have been shown both *in vivo* and *in vitro* (Zhao et al., 1998, Kim et al., 2003, Nikitenko et al., 2000). Similar to AM, the expression of CALCRL, but not RAMPs, also can be induced by a hypoxic microenvironment in ECs (Nikitenko et al., 2003). The role of *Calcrl* in angiogenesis is also conserved in zebrafish, as zebrafish *calcrla* morphants showed delayed ISV formation (Nicoli et al., 2008). In adult *Ramp2* heterozygous mice, the protein expression level of AM was significantly elevated indicating a compensatory relationship may exist between these genes (Ichikawa-Shindo et al., 2008). Reduced neovasculosation in Matrigel® plug assays in adult

Ramp2+/- mice, indicates that *Ramp2* is not only required for embryonic vascular function but also required for vessel function during adulthood (Ichikawa-Shindo et al., 2008). Consistent with this finding, elegant *ex vivo* studies showed that VEGF-mediated angiogenesis was greatly reduced in *Ramp2*+/- explants (Ichikawa-Shindo et al., 2008). In addition, substantially reduced vascular density was observed in *Ramp2*-/- aorta-gonad-mesonephros (AGM) cultures, when compared with the WT AGM cultures (Ichikawa-Shindo et al., 2008). Taken together, these data suggest an important role of *Am-Ramp2-Calcrl* in promoting angiogenesis.

5.1.5 Calcitonin receptor-like receptor in vessel integrity

As discussed earlier, distinct phenotypes have been reported between independently generated *Ramp2*-/- and *AM*-/- mutant mice (Shindo et al., 2001, Dackor et al., 2006, Fritz-Six et al., 2008, Ichikawa-Shindo et al., 2008). The Shindo group have reported widespread haemorrhage and diminished expression of endothelial adhesion genes but not abnormalities in lymphatic development, suggestive of reduced endothelial integrity in these mutants (Ichikawa-Shindo et al., 2008). Electron microscopy images of these mutants revealed numerous lesions in blood vessels in *Am*-/- mutant mice (Shindo et al., 2001). Furthermore, AM expression could be detected in mural cells (MCs) and ECs (Yurugi-Kobayashi et al., 2006). Signalling cross-talk between perivascular cells and ECs coordinated via VEGF-NOTCH signalling was proposed to contribute to vascular development and maintain vessel function (Yurugi-Kobayashi et al., 2006). The small GTPases, Rac1 and RhoA, were reported to interact with the AM-RAMP2-CALCRL pathway to regulate permeability of ECs (Koyama et al., 2013, Aslam et al., 2011). Drug-induced EC-conditional KO of *Ramp2* mutant mice displayed reduced Rac1 activation and disorganised actin polymerisation in ECs (Koyama et al., 2013).This abnormally formed EC barrier was proposed to underline intracellular leakage. Interestingly, when activity of the AM-RAMP2 pathway was elevated, the cortical actin formation was induced, which could be rescued by Rac1 inhibitor treatment. Taken together, the AM-RAMP2-CALCRL pathway may also be important to contribute to the EC integrity (Yokoyama et al., 2016).

5.1.6 Objectives

While many studies have shed light on functions of the AM-RAMPs-CALCRL pathway, has remained unclear what is the cause of the stereotypical hydrops fetalis phenotype displayed in AM signalling deficient mutants and whether this was caused by abnormal lymphatic formation, reduced vascular integrity or both. To further understand the function of *Calcrl* during vascular development, we generated novel zebrafish mutants of *calcrla* and *calcrlb*. In this chapter, we

will focus on characterisation of *calcrla* and *calcrlb* mutants, the interactions between *calcrla*/ *calcrlb* and with other key signalling pathways. Here we show, unlike previously published *calcrla* morphants (Nicoli et al., 2008, Wilkinson et al., 2012), that *calcrla* mutants exhibit no obvious vascular abnormalities during embryonic development, but displayed reduced body length. By contrast, *calcrlb* mutants displayed severe oedema and abnormal trunk lymphatic formation but with normal vascular patterning. Furthermore, our data further suggests that *calcrla* genetically interacts with *calcrlb* and *calcrlb* can fully compensate for loss of *calcrla* function, whereas *calcrla* can only partially compensate for loss of *calcrlb* during embryonic development. Collectively this suggests that AM signalling is required for both vascular integrity and formation of lymphatics in zebrafish.

5.2 Results

5.2.1 Generation of *calcrla*^{sh404} and *calcrla*^{sh405} mutant alleles

Zebrafish *calcrla* contains 13 exons, which encodes 475 amino acids (Zerbino et al., 2018). The *calcrla*^{sh404} and *calcrla*^{sh405} alleles were generated by Dr Robert Wilkinson via genome editing using Transcription Activator-Like Effector Nucleases (TALENs) (Cermak et al., 2011) before I joined the lab. Both of these mutations contain distinct 1bp deletions. The *calcrla*^{sh404} mutant allele was predicted to retain the first 46 amino acids of wild-type (WT) Calcrla before shifting frame, inducing 7 incorrect amino acids after the genetic lesion before prematurely truncating the protein before the conserved hormone receptor domain (HRM) (Fig. 5.1 A, C). The *calcrla*^{sh405} mutant allele was predicted to shift frame after the first 45 amino acids and truncate the protein following 8 incorrect amino acids before the conserved hormone receptor domain (Fig. 5.1 A, D).The conserved HRM and the 7 transmembrane receptor (7TM-2) were predicted to be lost in both *calcrla*^{sh404} and *calcrla*^{sh405} alleles (Fig. 5.1 C, D), therefore *calcrla*^{sh404} and *calcrla*^{sh405} alleles are likely to represent severe loss of function or null mutations. All *calcrla* single mutant data generated in this chapter employed *calcrla*$^{sh404/sh405}$ compound homozygous embryos, hereafter referred to as *calcrla*, unless otherwise stated.

5.2.2 *calcrla* mutants exhibit reduced body length

Zebrafish *calcrla* mutants were morphologically normal during embryonic stages (Fig. 5.2 A-D) and homozygous viable and fertile in adulthood. However, *calcrla* mutants displayed reduced body length (Fig. 5.2 E). Body length of 7 embryos from the same parental intercross were measured every 4 weeks from week 14 to week 35 post fertilisation by Dr Robert Wilkinson. WT, *calcrla* heterozygote siblings and *calcrla* homozygous mutants were genotyped using embryonic fin clips at 3dpf and identified, and raised in tanks at equal density and with the same feeding regime. *calcrla* mutants displayed significantly reduced mean body length throughout the 20 weeks, in comparison to *calcrla* heterozygotes or WT siblings (Fig. 5.2 E).

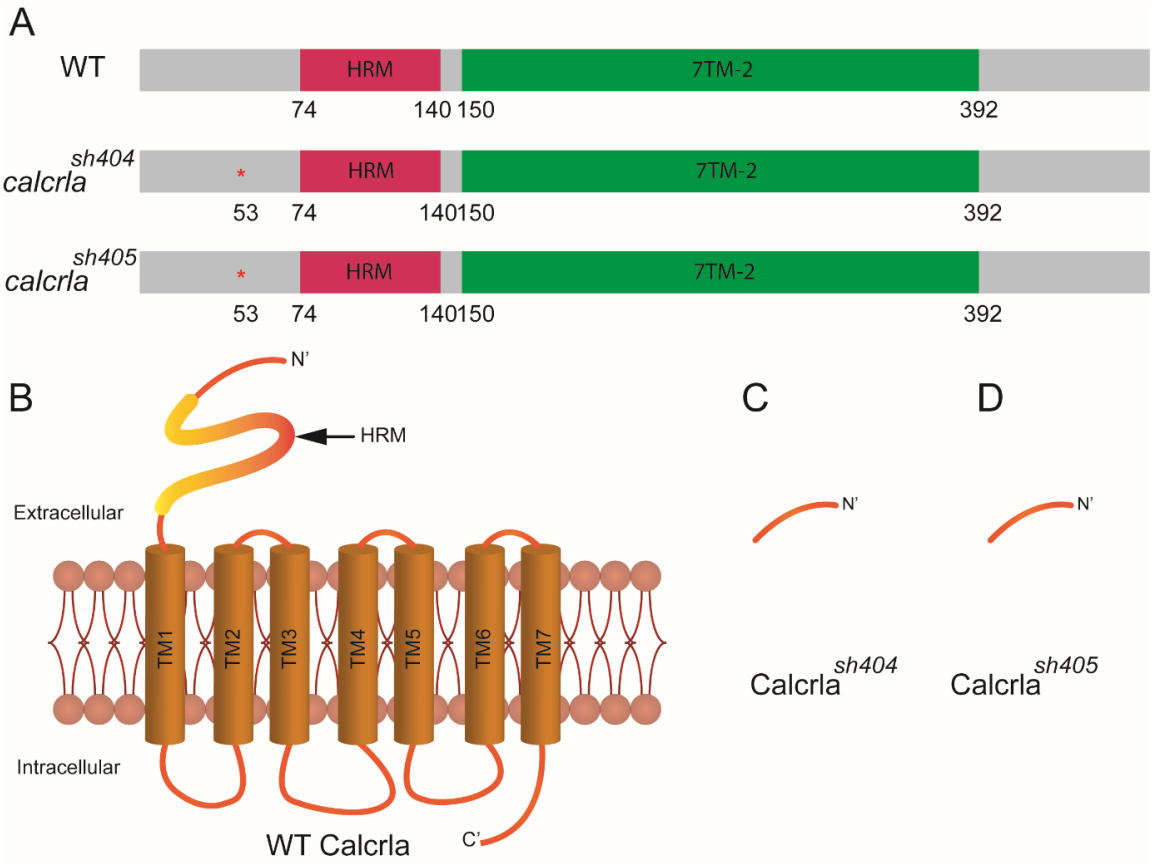

Figure 5.1 Schematic representation of *calcrla*^{sh404} and *calcrla*^{sh405} alleles and their predicted proteins

(A) Schematic representation of the *calcrla*^{sh404} and *calcrla*^{sh405} alleles with premature stop codon after amino acid position 53 (asterisk) before the conserved hormone receptor domain (HRM, red box) and the 7 transmembrane receptor (7TM-2, green box). (B) Schematic representation of the WT Calcrla composed of extracellular hormone receptor domain (HRM) and 7 transmembrane receptors (TM1-7). (C, D) Predicted protein structures of Calcrla^{sh404} and Calcrla^{sh405}.

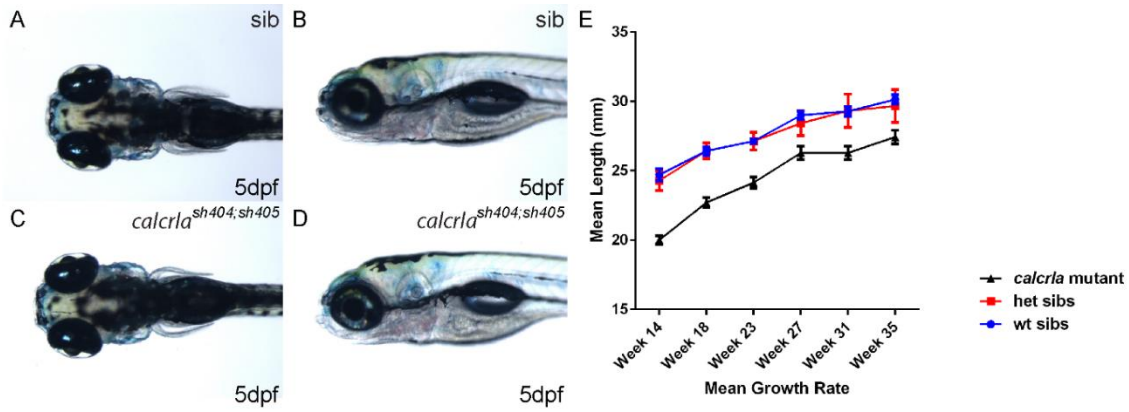

Figure 5.2 *calcrla* mutants are morphologically normal but display reduced body length

(A, B) Dorsal and lateral view of WT embryos at 5dpf. (C, D) Dorsal and lateral view of *calcrla* compound mutant embryos at 5dpf. (E) Quantification of mean body length through 21 weeks among WT, *calcrla* heterozygous and *calcrla* homozygous mutant embryos. N=7 of each group. (Panel E, courtesy of Robert Wilkinson).

5.2.3 Generation of *calcrlb*^{sh468}, *calcrlb*^{sh469} and *calcrlb*^{sh487} mutant alleles

Zebrafish *calcrlb* contains 13 exons, which encodes 466 amino acids (Nicoli et al., 2008). We generated three *calcrlb* mutant alleles, namely *calcrlb*^{sh468}, *calcrlb*^{sh469} and *calcrlb*^{sh487} using genome editing via CRISPR/Cas9 (See sections 2.1.8 and 2.2.4) (Hwang et al., 2013).

Calcrlb^{sh468} was predicted to retain the first 132 amino acids of WT Calcrlb, then shift frame due to a 7bp deletion (ΔGTCGGTG) followed by an 8bp insertion (TAATTACA), truncating after this point and before the conserved 7TM-2 domain (Fig. 5.3 A, B, Fig. 5.4 B). Therefore this *calcrlb*^{sh468} allele is likely to represent severe loss of function or null mutation.

Calcrlb^{sh469} retained the first 130 amino acids of WT Calcrlb, followed by a 4bp deletion (ΔAGTC) and a 10bp insertion (GGTGTAATTC) prior to the conserved 7TM-2 domain (Fig. 5.3 C Red star, D, Fig. 5.4 C). Since the *calcrlb*^{sh469} mutation is an in-frame mutation, to further examine the protein function of Calcrlb^{sh469}, we performed amino acid sequence alignment among the human, mouse, zebrafish WT Calcrlb and Calcrlb^{sh469} (Fig. 5.5). The amino acid alignment suggested the amino acid mutation caused by *calcrlb*^{sh469} was located at amino acid position 131-134 (Fig. 5.5 A, B Red boxed area) between the conserved HRM domain (Fig. 5.5 A Yellow shade) and the 7TM-2 domain (Fig. 5.5 A Green shade). Furthermore, using PROVEAN analysis (Choi et al., 2012, Choi and Chan, 2015), the cysteine (C) to leucine (L) substitution at position 132 scored -8.767 and the two arginine (R) insertions between position 133 and 134 scored -6.680 (Fig. 5.5 C) were both classified as deleterious by the PROVEAN system.

In addition, Calcrlb^{sh487} contained the first 129 amino acids of WT Calcrlb, then shifted frame due to a 7bp deletion (ΔCAGTCGG) and a 3bp insertion (GGC), truncating after 18 amino acids, before the conserved 7TM-2 domain (Fig. 5.3 E, F, Fig. 5.4 D).

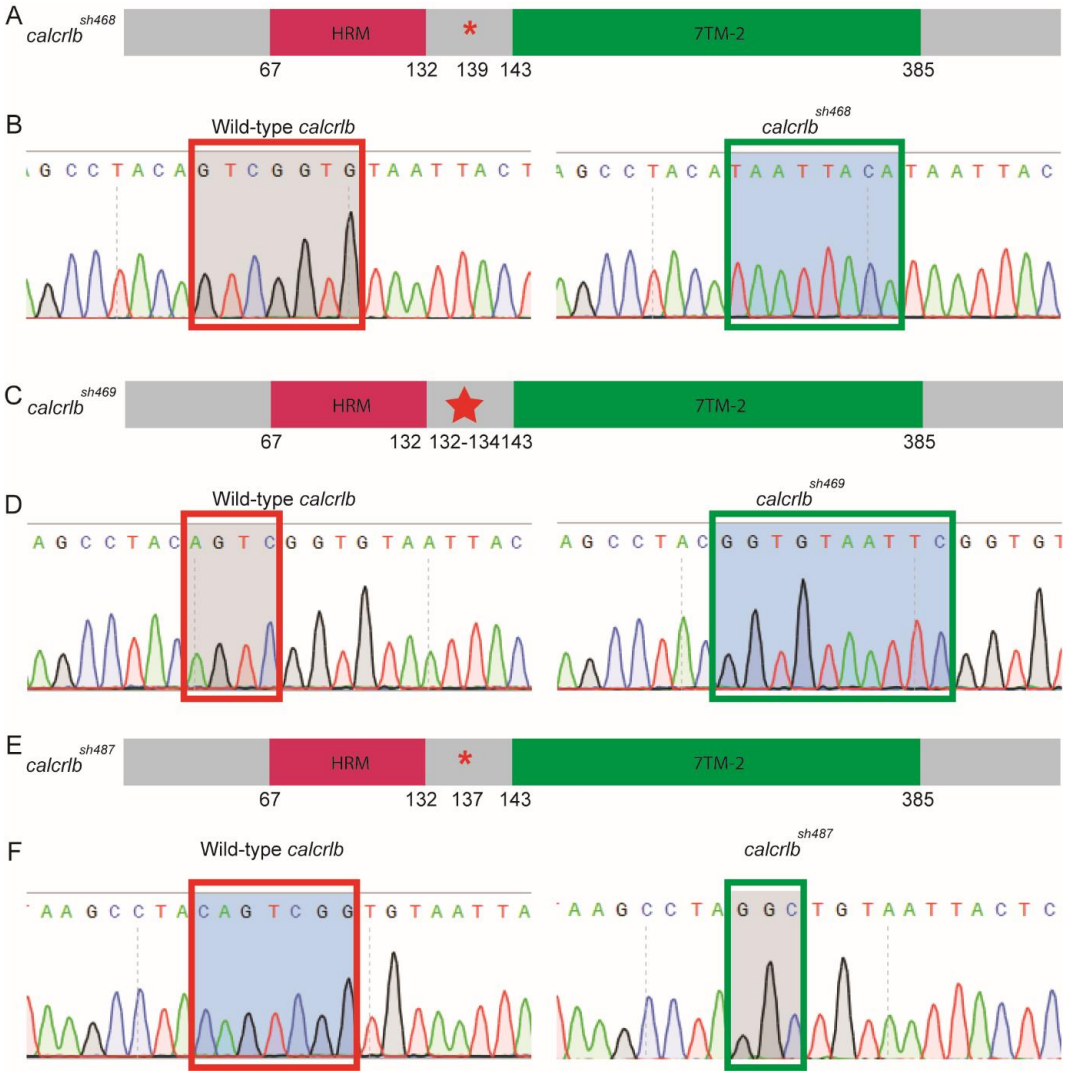

Figure 5.3 Schematic representation and sequences of the *calcrlb*^{sh468}, *calcrlb*^{sh469} and *calcrlb*^{sh487} alleles

(A) Schematic representation of the *calcrlb*^{sh468} allele with premature stop codon after amino acid position 139 (asterisk), between the conserved hormone receptor domain (HRM, red) and the 7 transmembrane receptor (7TM-2, green). (B) Sequence traces of WT *calcrlb* and *calcrlb*^{sh468} allele with 7bp deletion (Red box in WT *calcrlb*) and 8bp insertion (Green box in *calcrlb*^{sh468} allele). (C) Schematic representation of the *calcrlb*^{sh469} allele with mutations at amino acid position 132-134 (star), between the conserved hormone receptor domain (HRM, red) and the 7 transmembrane receptor (7TM-2, green). (D) Sequence traces of WT *calcrlb* and *calcrlb*^{sh469} allele with 4bp deletion (Red box in WT *calcrlb*) and 10bp insertion (Green box in *calcrlb*^{sh469} allele). (E) Schematic representation of the *calcrlb*^{sh487} allele with premature stop codon after amino acid 137 (asterisk), between the conserved hormone receptor domain (HRM, red) and the 7 transmembrane receptor (7TM-2, green). (F). Sequence traces of WT *calcrlb* and *calcrlb*^{sh487} allele with 7bp deletion (red box in WT *calcrlb*) and 3bp insertion (green box in *calcrlb*^{sh487} allele).

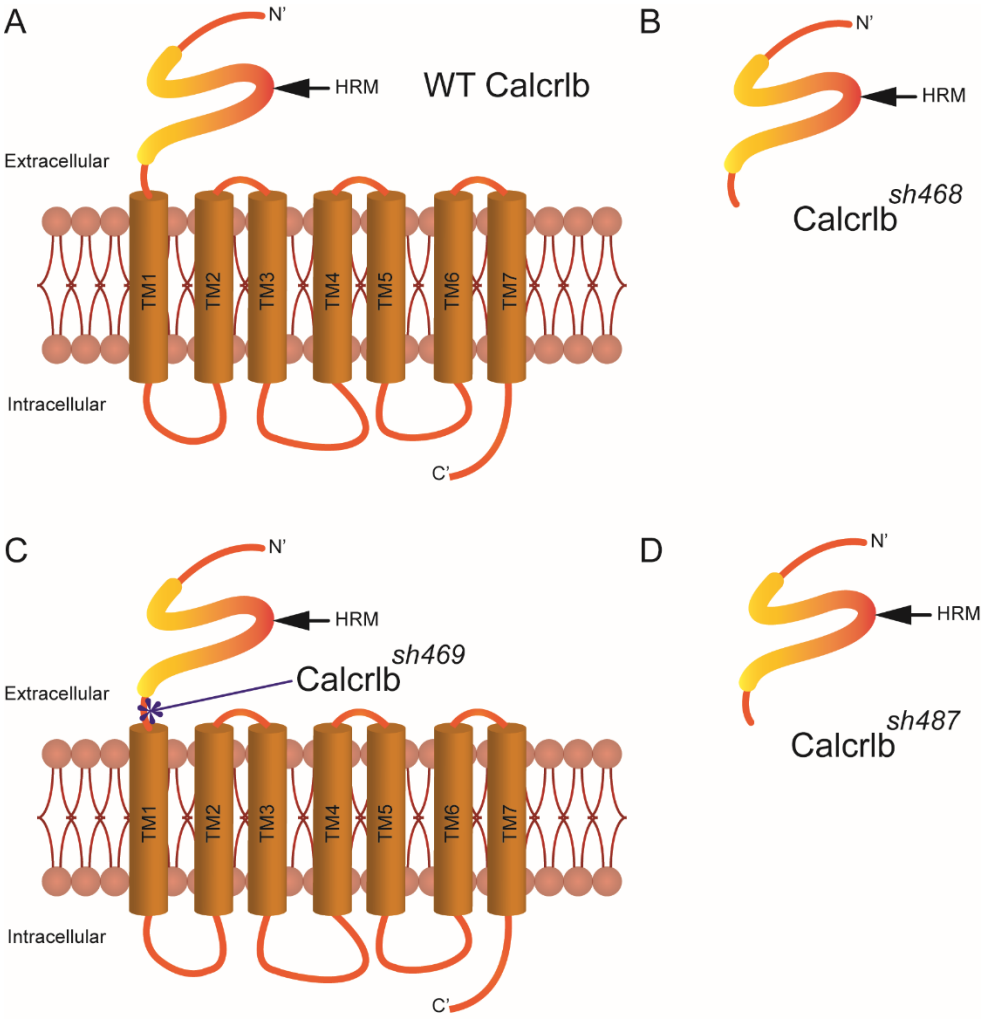

Figure 5.4 Schematic representation of predicted protein structures of the Calcrlb^{sh468}, Calcrlb^{sh469} and Calcrlb^{sh487}

(A) Schematic representation of the WT Calcrlb composed of extracellular hormone receptor domain (HRM) and 7 transmembrane receptors (TM1-7). (B, D) Calcrlb^{sh468} and Calcrlb^{sh487} are predicted to retain the hormone receptor domain. (C) Calcrlb^{sh469} is predicted to mutate the region between the hormone receptor domain (HRM) and 7 transmembrane receptors (TM1-7).

Variant	PROVEAN score	Prediction (cutoff= -2.5)
D131E	0.796	Neutral
C132L	-8.767	Deleterious
R133H	0.311	Neutral
R133_L134insRR	-6.680	Deleterious

Figure 5.5 PROVEAN analysis of *calcrlb*^{sh469} allele

(A) Amino acid sequence alignment of human, mouse, WT zebrafish Calcrlb with Calcrlb^{sh469}. Yellow highlighted area indicates the conserved hormone receptor domain (HRM) and green highlighted area indicates the 7 transmembrane receptor domain (7TM-2). (B) Magnified area highlighting the mutated region of red boxed area in panel A. (C) PROVEAN output indicating prediction of mutations induced by the *calcrlb*^{sh469} allele as deleterious.

5.2.4 *calcrlb*$^{sh468/sh468}$, *calcrlb*$^{sh469/sh469}$ and *calcrlb*$^{sh487/sh486}$ mutants display similar oedema phenotype

To establish whether these *calcrlb* alleles represented loss of function mutations, we analysed the phenotypes of all three *calcrlb* homozygous mutants (Fig. 5.6). *calcrlb* homozygous mutants were obtained by independent *calcrlb* heterozygous incrosses. *calcrlb*$^{sh468/sh468}$, *calcrlb*$^{sh469/sh469}$ and *calcrlb*$^{sh487/sh487}$ mutants were morphologically normal prior to day 3. Interestingly, mild oedema was first detected around the eyes and heart as early as late day 3 (data not shown). Between 4-5 days post fertilisation (dpf), oedema was clear and equally severe in homozygous embryos of all three *calcrlb* alleles. Approximately 25% of *calcrlb* heterozygous incrossed offspring displayed oedema, indicating recessive Mendelian transmission (data not shown). Distinct classes of the oedema severity were defined according to level of oedema and involvement of different tissues. Class I mutant embryos displayed oedema around the eyes and mild cardiac oedema (Fig. 5.6 B, B', E, E', G, G' Red and purple arrowheads); and class II mutants displayed severe ocular oedema and severe pericardiac oedema and involvement of the yolk (Fig. 5.6 C, C', F, F', H, H' Red and purple arrowheads). Interestingly, the class I embryos of *calcrlb*$^{sh468/sh468}$, *calcrlb*$^{sh469/sh469}$ and *calcrlb*$^{sh487/sh486}$ mutants retained functional blood circulation (data not shown), whereas the majority of class II embryos did not have blood circulation (data not shown). No haemorrhage was observed in any *calcrlb* mutants. Notably, some mutants displayed abnormal pectoral fin position which could result from severe oedema beneath the yolk. Furthermore, no obvious morphological abnormalities could be detected among *calcrlb*$^{sh468/sh468}$, *calcrlb*$^{sh469/sh469}$ and *calcrlb*$^{sh487/sh486}$ mutants and the phenotypic similarity between these suggests all three mutated *calcrlb* alleles, including the in-frame *calcrlb*^{sh469} mutation represent similar loss of function. *calcrlb*$^{sh468/sh468}$, *calcrlb*$^{sh469/sh469}$ and *calcrlb*$^{sh487/sh486}$ are hereafter referred as *calcrlb*.

Class I *calcrlb* mutants were viable to juvenile stage and at 4 weeks *calcrlb* mutants showed reduced body length (Fig. 5.7 B), smaller fins (Fig. 5.7 B4) and displayed severe periocular oedema (Fig. 5.7 B1 Red arrowhead) and oedema in the ventral trunk (Fig. 5.7 B2 Blue arrowhead) when compared with the WT embryos of the same age (Fig. 5.7 A-A4). No haemorrhage could be detected under the skin. Subsequently, we analysed sagittal tissue sections of WT and *calcrlb* mutant 4 week-old juveniles to investigate internal development. *calcrlb-/-* juveniles displayed smaller eyes with an enlarged space with few cells present underneath the retina (Fig. 5.8 A1, B1 Red arrowheads), likely a consequence of oedema around the eyes as previously described (Fig. 5.7 B, B1 Red arrowheads). Abnormally developed gill filaments were observed in *calcrlb* mutants

with shorter filaments and fewer secondary lamellae (Fig. 5.8 A4, B4). In the gut, *calcrlb* single mutants displayed disorganised swim bladder and enlarged tissue spaces (Fig. 5.8 A3, B3 Red arrows), which could also result from severe oedema. No haemorrhages were observed in the gut (Fig. 5.8 A3, B3). In the trunk, the muscle fibres were normally developed in the absence of *calcrlb* (Fig. 5.8 A5, B5). These histological analyses are consistent with our previous observation in *calcrlb-/-* juveniles at 4 weeks, which displayed severe oedema but no haemorrhage (Fig. 5.7).

5.2.5 *calcrla* and *calcrlb* genetically interact during embryogenesis

To understand the genetic relationship between *calcrla* and *calcrlb*, we generated *calcrla*; *calcrlb* double mutants. Double mutant embryos were generated via *calcrla; calcrlb* double heterozygous incrosses. Similar to *calcrlb* single mutants*, calcrla; calcrlb* double mutants developed mild oedema at late day 3 (data not shown). At 5dpf, progeny were grouped in classes based on severity of oedema. Interestingly, among the progeny of *calcrla*; *calcrlb* double heterozygous incrosses, a more severe group class III was defined. Class III embryos were similar to class II and exhibited severe oedema behind the eyes, around the heart and beneath the yolk (Fig. 5.9 C), but also displayed oedema involving the head and displayed curvature of body axis with more increased oedema in the ventral trunk (Fig. 5.9 D, D' Orange, black and purple arrowheads respectively). Following blind phenotyping, we performed genotyping of *calcrla* and *calcrlb*. We observed a correlation between increasing phenotypic severity and mutation of both *calcrla* and *calcrlb* (Fig. 5.9 E). No *calcrlb* mutants were present within the morphologically normal class (WT) (Fig. 5.9 E), but *calcrlb* mutants were present in all other oedematous classes (Fig. 5.9 E class I-class III). The most prevalent genotype in class I embryos was *calcrla*+/+; *calcrlb*-/-. The most frequent genotype of class II embryos was *calcrla*+/-; *calcrlb*-/-, whereas *calcrla*-/-; *calcrlb*-/- double mutants were only present in the class III group. Taken together, this genotype-phenotype correlation indicates *calcrla* and *calcrlb* genetically interact and that *calcrlb* can compensate for loss of *calcrla* with respect to presence of oedema, whereas *calcrla* can only partially compensate for loss of *calcrlb*.

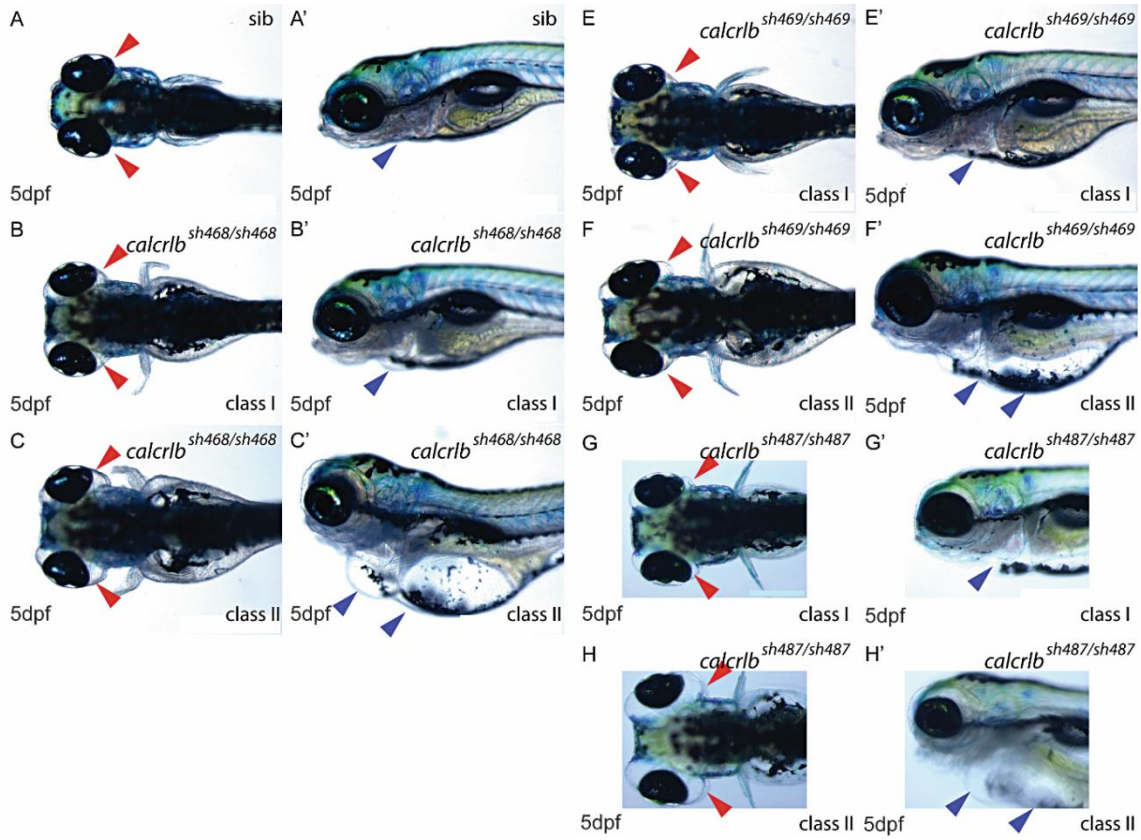

Figure 5.6 *calcrlb* mutants display two classes of oedema phenotypes

(A, A') Dorsal and lateral view of WT embryos at 5dpf. (B, B') Dorsal and lateral view of the class I oedema in *calcrlb*$^{sh468/sh468}$ mutants. (C, C') Dorsal and lateral view of the class II oedema in *calcrlb*$^{sh468/sh468}$ mutants. (E, E') Dorsal and lateral view of the class I oedema in *calcrlb*$^{sh469/sh469}$ mutants. (F, F') Dorsal and lateral view of the class II oedema in *calcrlb*$^{sh469/sh469}$ mutants. (G, G') Dorsal and lateral view of the class I oedema in *calcrlb*$^{sh487/sh487}$ mutants. (F, F') Dorsal and lateral view of the class II oedema in *calcrlb*$^{sh487/sh487}$ mutants. Red arrowheads indicate oedema around eyes, purple arrowheads indicate oedema around heart and involving the yolk.

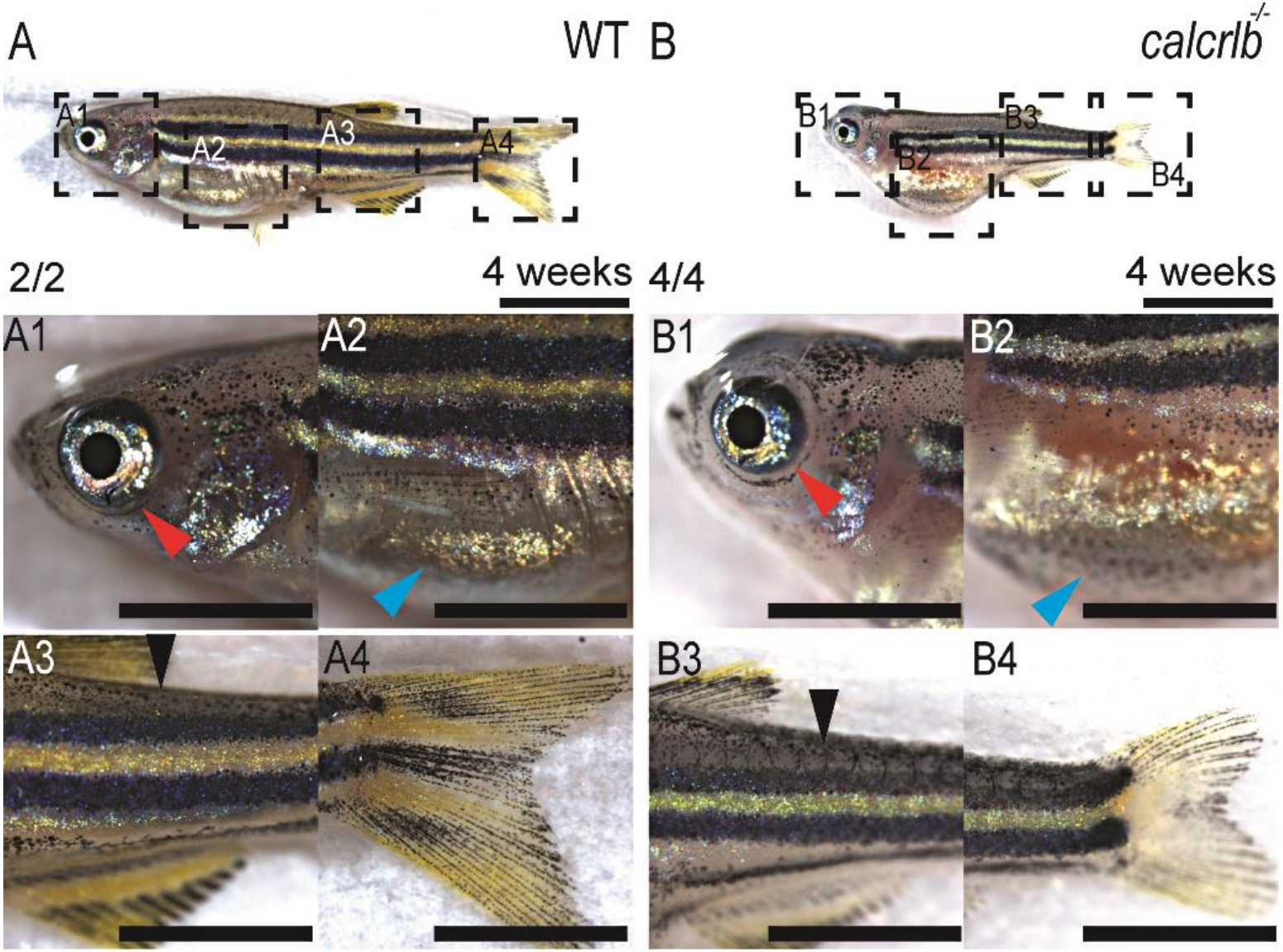
A
WT
B
calcrlb-/-
A1
A2
A3
A4
B1
B2
B3
B4
2/2
4 weeks
4/4
4 weeks
A1
A2
B1
B2
A3
A4
B3
B4

Figure 5.7 Class I *calcrlb* mutants survive to juvenile stage and display severe oedema

(A) Lateral view of 4 weeks old WT juvenile. Scale bar equals 1mm. (A1-A4) Magnified pictures of black dotted boxed areas in panel A. Scale bar equals 500µm. (B) Lateral view of 4 weeks old Class I *calcrlb* single mutants. Scale bar equals 1mm. (B1-B4) Magnified pictured of black dotted boxed areas in panel B. Scale bar equals 500µm. Red arrowheads indicate eyes; blue arrowheads indicate guts and black arrowheads highlight scales.

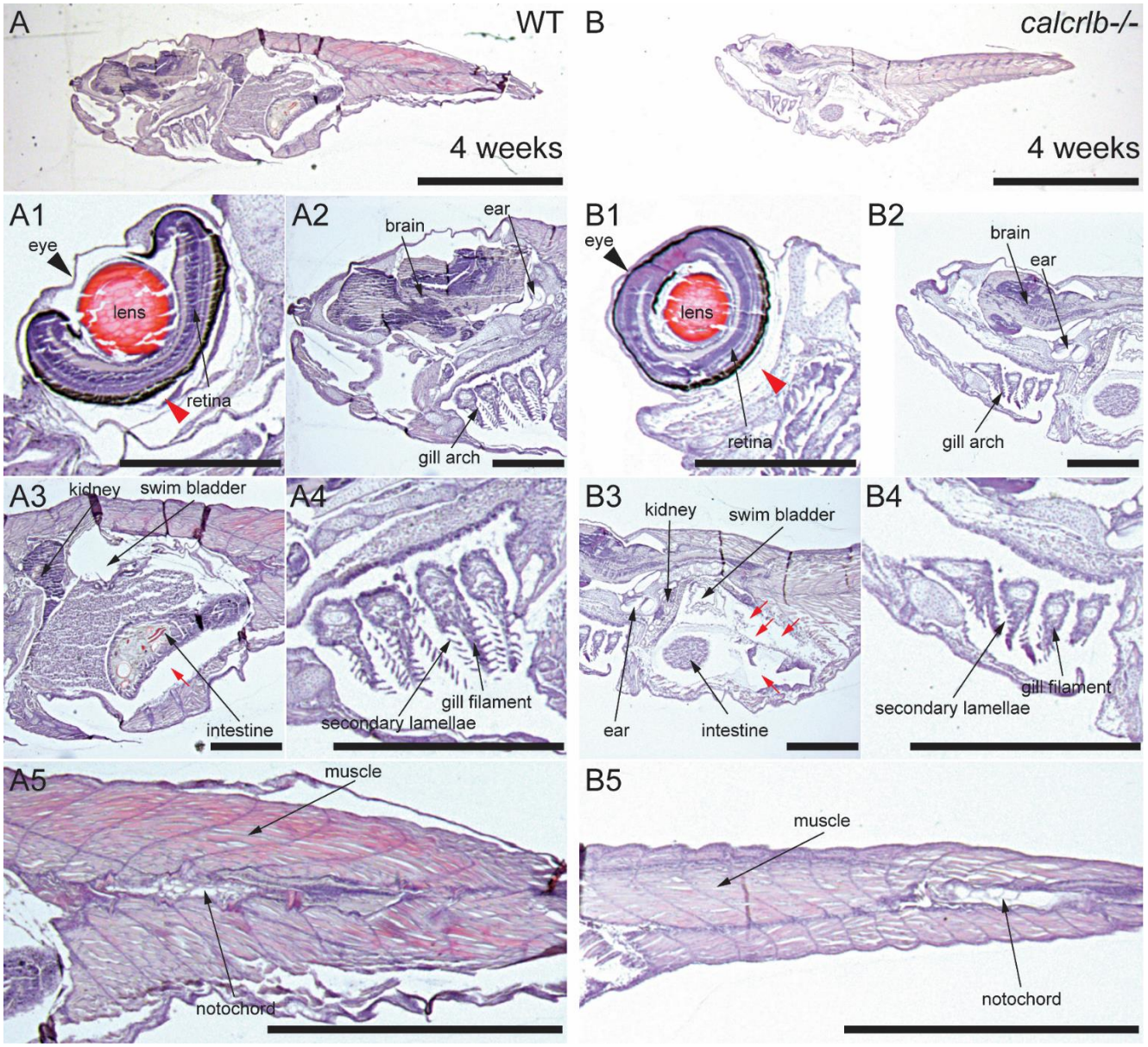
A
WT
4 weeks
B
calcrlb-/-
4 weeks
A1
eye
lens
retina
A2
brain
ear
gill arch
B1
eye
lens
retina
B2
brain
ear
gill arch
A3
kidney
swim bladder
intestine
A4
gill filament
secondary lamellae
B3
kidney
swim bladder
ear
intestine
B4
gill filament
secondary lamellae
A5
muscle
notochord
B5
muscle
notochord

Figure 5.8 4 week old class I *calcrlb* mutants display severe oedema

(A, B) Overview of sagittal tissue slides of 4 weeks old WT zebrafish juvenile (A) and class I *calcrlb* mutant (B). Scale bar equals 1mm. (A1-A5) Magnified picture of eye (A1), brain (A2), gut (A3), gill (A4) and trunk (A5). Pictures were taken from tissue slide series of one single WT zebrafish juvenile. (B1-B5) Magnified picture of eye (B1), brain (B2), gut (B3), gill (B4) and trunk (B5). Pictures were taken from tissue slide series of one single *calcrlb* mutant juvenile. Scale bar equals 500µm. Red arrows and arrowheads indicate enlarged spaces with few cells.

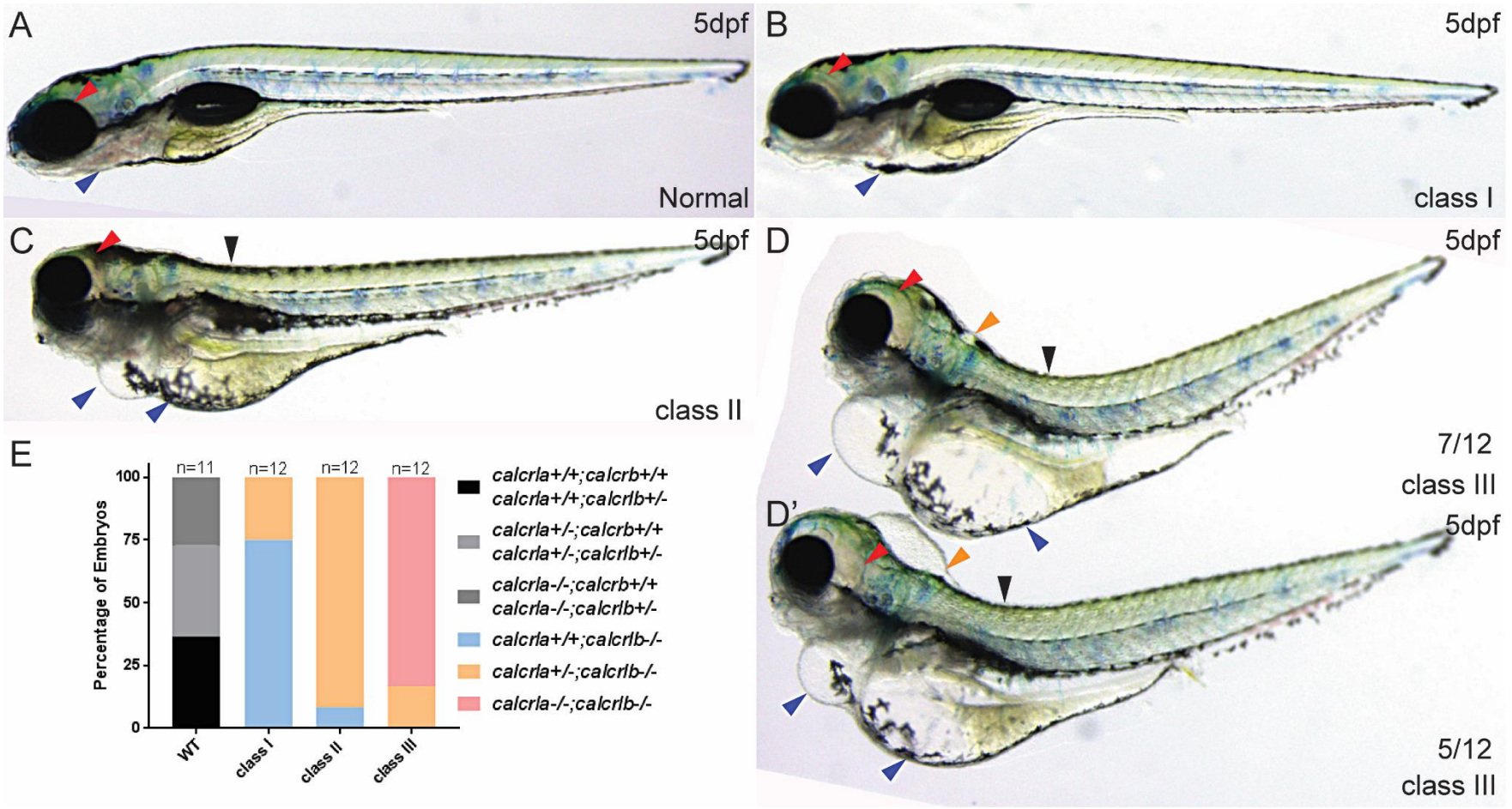
A
5dpf
Normal
B
5dpf
class I
C
5dpf
class II
D
5dpf
7/12
class III
D'
5dpf
5/12
class III
E
n=11
n=12
n=12
n=12
100
75
50
25
0
Percentage of Embryos
WT
class I
class II
class III
calcrla+/+;calcrb+/+
calcrla+/+;calcrlb+/-
calcrla+/-;calcrb+/+
calcrla+/-;calcrlb+/-
calcrla-/-;calcrb+/+
calcrla-/-;calcrlb+/-
calcrla+/+;calcrlb-/-
calcrla+/-;calcrlb-/-
calcrla-/-;calcrlb-/-

Figure 5.9 *calcrla* and *calcrlb* genetically interact

(A-D') Lateral view of 5dpf WT (A), class I embryos (B), class II embryos (C) and class III embryos (D, D'). Red arrowheads indicate eyes; purple arrowheads point to heart and beneath the yolk; orange arrowheads highlight the oedema above the head; black arrowheads denote the bending notochord. (E) Quantification of genotype-phenotype correlation. Different genotypes were colour coded.

5.2.6 *calcrla* is expressed within the developing vasculature and skeletal system and is dispensable for blood vessel formation

To investigate the potential cause of the different phenotypes in *calcrla* and *calcrlb* mutants we examined in which tissues each genes were expressed. At 9 somite stage (s), the expression of *calcrla* could be found in the somitic mesoderm (Fig. 5.10 A). Consistent with this observation, at 26-28hpf, *calcrla* was expressed at high levels within the posterior somites (Fig. 5.10 B-E Black arrowheads). At 26hpf, *calcrla* was expressed throughout the vasculature, but was more strongly expressed within the DA and PCV (Fig. 5.10 B, C Red bar). Between 26-28hpf, *calcrla* was also expressed in the first aortic arch (AA1) (Fig. 5.10 B', D' Red arrowheads), lateral dorsal aorta (LDA) (Fig. 5.10 B, B', D, D' White arrowheads), major trunk vessels (Fig. 5.10 C, E) and posterior blood island (PBI) (Fig. 5.10 B-E Green arrowheads). After 48hpf, *calcrla* expression was reduced in the vasculature (Fig. 5.10 F, G). At 4dpf and 5dpf, *calcrla* expression could be detected in the aortic arches (AA') (Fig. 5.10 H Red arrowheads), whereas trunk vascular expression was barely detectable (Fig. 5.10 I, K). Interestingly, we also detected *calcrla* expression within the notochord from 28hpf up to 4dpf (Fig. 5.10 D-E Orange arrowheads), which could potentially be responsible for the reduced body length that displayed in *calcrla* mutant juvenile as demonstrated in section 5.2.2.

Given expression of *calcrla* in developing vasculature during embryonic development and previous gene KD studies demonstrating a requirement for *calcrla* in this tissue (Wilkinson et al., 2012, Nicoli et al., 2008), we employed *Tg(kdrl:mcherry; flk1:nucEGFP)* to examine blood vessel formation. Cranial and trunk blood vessels were unremarkable in *calcrla* single mutants (Fig. 5.11 D-F) when compared with WT siblings (Fig. 5.11 A-C). Since *calcrla* single mutants are homozygous viable and fertile and displayed no morphological abnormalities, yet these mutants enhance the morphological phenotype of *calcrlb* and therefore represent a loss of function allele, we conclude that *calcrla* is dispensable for vascular development, potentially due to compensation from *calcrlb*.

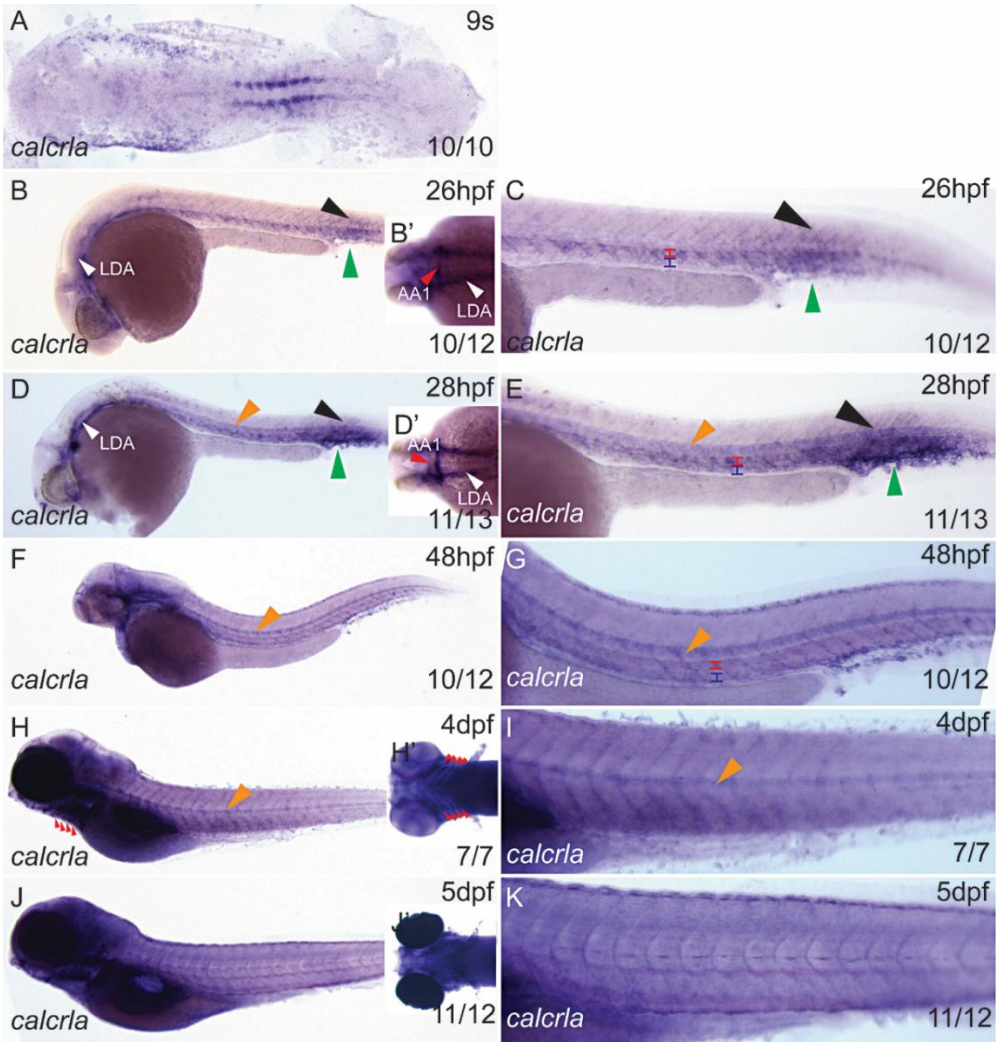

Figure 5.10 *calcrla* is expressed in the developing vasculature, skeletal muscle and notochord

(A) *In situ* hybridisation of *calcrla* in WT embryos at 9s stage showing *calcrla* is expressed within the developing somites. (B-C) *calcrla* expression at 26hpf with lateral view (B), dorsal view of head (B') and magnified lateral view of trunk (C) in the posterior somites and vasculature. (D-E) *calcrla* expression at 28hpf with lateral view (D), dorsal view of head (D') and magnified lateral view of trunk (E) in the posterior somites, vasculature and notochord. Red arrowheads indicate expression in AA1; white arrowheads point to LDA; green arrowheads indicate PBI; red bar highlights DA, blue bar denotes the PCV and orange arrowheads point to notochord. (F-G) *calcrla* expression at 48hpf with lateral view (F) and magnified lateral view of trunk (G). Red bar highlights DA, blue bar denotes the PCV and orange arrowheads point to notochord. (H-K) *calcrla* expression at 4dpf (H-I) and 5dpf (J-K) with lateral view (H, J), ventral view of head (H', J') and magnified lateral view of trunk (I, K). Red arrowhead indicate AA', orange arrowheads point to notochord. AA1, first aortic arch; AA', aortic arches; LDA, lateral dorsal aorta; DA, dorsal aorta; PCV, posterior cardinal vein; PBI, posterior blood island.

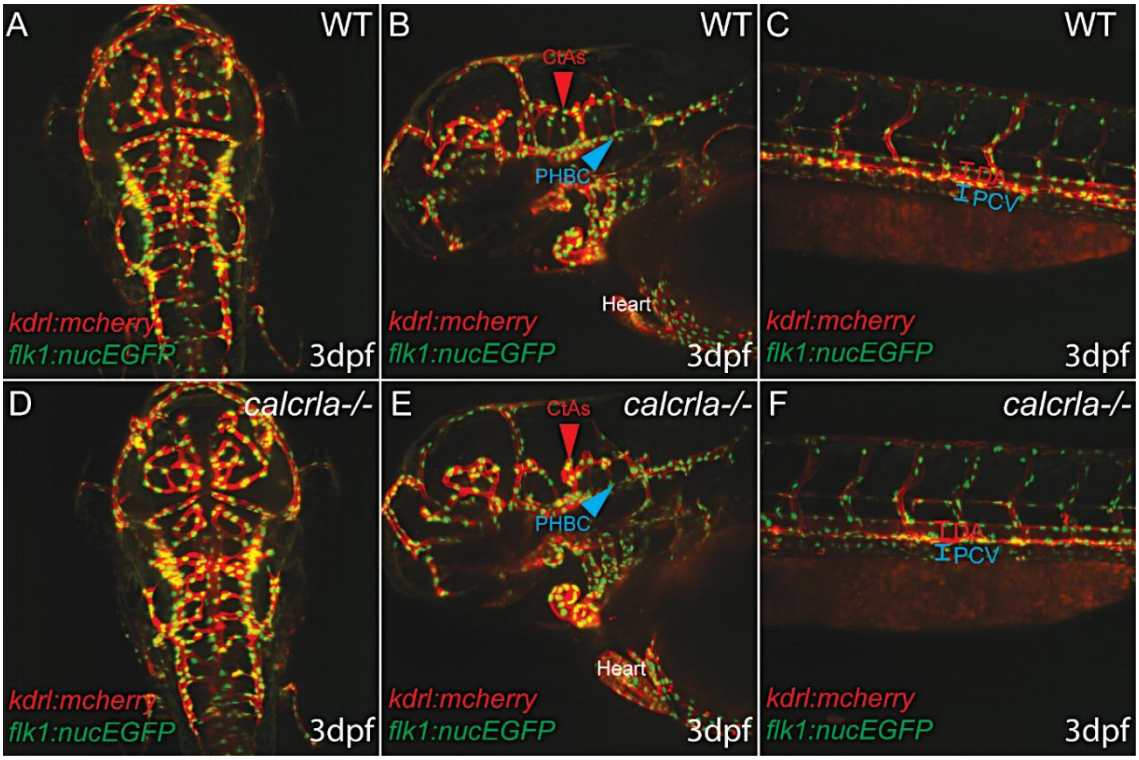

Figure 5.11 *calcrla* single mutants display normal vascular development

(A-C) Lightsheet image of 3dpf WT embryos with *Tg(kdrl:mcherry; flk1:nucEGFP)* background with dorsal view of head (A), lateral view of head (B) and lateral view of trunk (C). Red arrowhead points to CtAs; blue arrowhead indicates PHBC; red bar highlights the DA and blue bar denotes the PCV. (D-F) Lightsheet image of 3dpf *calcrla* single mutants with *Tg(kdrl:mcherry; flk1:nucEGFP)* background with dorsal view of head (D), lateral view of head (E) and lateral view of trunk (F). Red arrowhead points to CtAs; blue arrowhead indicates PHBC; red bar highlights the DA and blue bar denotes the PCV. CtAs, central arteries; PHBC, primordial hindbrain channel; DA, dorsal aorta; PCV, posterior cardinal vein.

5.2.7 *calcrlb* is expressed in the developing vasculature and notochord and is dispensable for blood vessel patterning

calcrlb was previously reported to be expressed maternally and not zygotically (Nicoli et al., 2008). Given the relatively late onset and nature of the *calcrlb* mutant phenotype we sought to verify this. Two *calcrlb* (ENSDARG00000011571) transcripts have been identified in zebrafish, containing 8 and 13 exons respectively (Fig. 5.2 A) (Zerbino et al., 2018). Therefore, we designed and generated two probes which would detect both isoforms (*calcrlb*-both) covering the first 8 exons and a second probe (*calcrlb*-long) covering the final 5 exons which would only detect the longer isoform (Fig. 5.12 A). *In situ* hybridisation using both probes showed similar expression patterns, however, the probe which detected the longer isoform showed much reduced staining in comparison to the probe which detected both isoforms, suggesting that the long isoform is expressed at lower level than the short isoform. Expression of *calcrlb* could be detected in major veins, including the primordial hindbrain channel (PHBC) in the head (Fig. 5.12 B, C White arrowheads), posterior cardinal vein (PCV) (Fig. 5.12 B, D Red arrowheads) and PBI in trunk (Fig. 5.12 D Green arrowheads). The expression of the longer *calcrlb* isoform was also present albeit at lower levels in the PCV and PBI (Fig. 5.12 E, G Red and green arrowheads respectively). We also observed high expression of the long isoform within the hindbrain region (Fig. 5.12 E, F Black arrowheads), which was likely due to the extended staining time used to detect low levels of expression of this isoform and likely represents non-specific probe trapping in the brain ventricles.

We therefore analysed the expression profile of *calcrlb* during embryonic development using the probe which detected both isoforms (Fig. 5.13). Unlike *calcrla* expression, at 9s the expression of *calcrlb* could not be observed in developing somites (Fig. 5.13 A), whereas expression of *calcrlb* in the developing rhombomeres was detected at this stage (Fig. 5.13 A). From 26hpf to 48hpf, *calcrlb* was expressed in major veins, including PHBC (black arrowhead), PCV (blue arrowheads) and PBI (green arrowheads) in both the head and trunk (Fig. 5.13 B-G). The strongest expression of *calcrlb* was observed at 28hpf. At 4dpf, weak expression of *calcrlb* could be observed in the PCV (Fig. 5.13 H, I Blue arrowheads), whereas at 5dpf, *calcrlb* expression was barely detectable by *in situ* hybridisation (Fig. 5.13 J, K). Interestingly, unlike *calcrla* expression, which was expressed more strongly in arteries, *calcrlb* was expressed more strongly in veins. Consistent with this, in contrast to *calcrla*, *calcrlb* expression was excluded from AA' (Fig. 5.13 H, J) during embryonic development. We also detected *calcrlb* expression within the notochord from 26hpf up to 4dpf

(Fig. 5.13 B-I Orange arrowheads), which could potentially be responsible for the reduced body length that was displayed in *calcrlb* mutant juveniles as demonstrated in section 5.2.4.

We next employed the *Tg(fli1a:EGFP; kdrl:mcherry)* transgenic line to examine vascular patterning in *calcrla; calcrlb* double mutants (Fig. 5.14). Despite strong expression of *calcrlb* within developing vasculature (Fig. 5.13), no obvious difference in vascular development could be observed between the WT and *calcrla*; *calcrlb* double mutant embryos prior to onset of oedema (data not shown). Interestingly, at 4dpf while *calcrla; calcrlb* double mutants displayed severe oedema as shown in section 5.2.5, these embryos displayed unremarkable vascular patterning (Fig. 5.14 D-F'') when compared with the WT embryos (Fig. 5.14 A-C''). Collectively, this indicates that both *calcrla* and *calcrlb* are dispensable for vascular patterning and that oedema in *calcrlb* single or *calcrla*; *calcrlb* double mutants is not a consequence of aberrant blood vessel formation.

5.2.8 *calcrlb* is dispensable for facial and brain lymphatic formation

Both *calcrlb* single mutants and *calcrla*; *calcrlb* double mutants displayed severe oedema and no haemorrhage, which is similar to those observed in mouse *AM*, *Calcrl*, *Ramp2* knockouts (Fritz-Six et al., 2008, Dackor et al., 2007, Dackor et al., 2006, Caron and Smithies, 2001). We therefore hypothesised oedema in *calcrlb* mutants may be caused by an abnormally formed lymphatic system. To test this hypothesis, and since periocular oedema was prevalent in these mutants, we first analysed formation of facial lymphatics at 5dpf by utilising *Tg(fli1a:LifeACT-mClover; kdrl:mcherry)* transgenes as introduced in previous chapters. The facial lymphatics showed normal formation in *calcrlb* single mutants at 5dpf (Fig. 5.15 B-B''') when compared with WT embryos (Fig. 5.15 A-A'''). Furthermore, as previously described in chapter 3, brain lymphatic endothelial cells (BLECs) formed stereotypical loop structures located bilaterally in the forehead behind the eyes of WT zebrafish embryos (Fig. 5.15 C-C'' Blue arrowheads). Similarly, these loop structures were normally patterned in the *calcrlb* mutants (Fig. 5.15 D-D'').Taken together, these results indicate that *calcrlb* is dispensable for facial and brain lymphatic formation and abnormal cranial lymphatic formation does not account for oedema observed in *calcrlb* mutants. However, we did not perform the same experiment in *calcrla; calcrlb* double mutants. Therefore, we cannot exclude the possibility that *calcrla* and *calcrlb* potentially compensate for each other during facial and brain lymphatic development and if so, may contribute to development of cranial oedema in *calcrla; calcrlb* double mutants as shown in section 5.2.5.

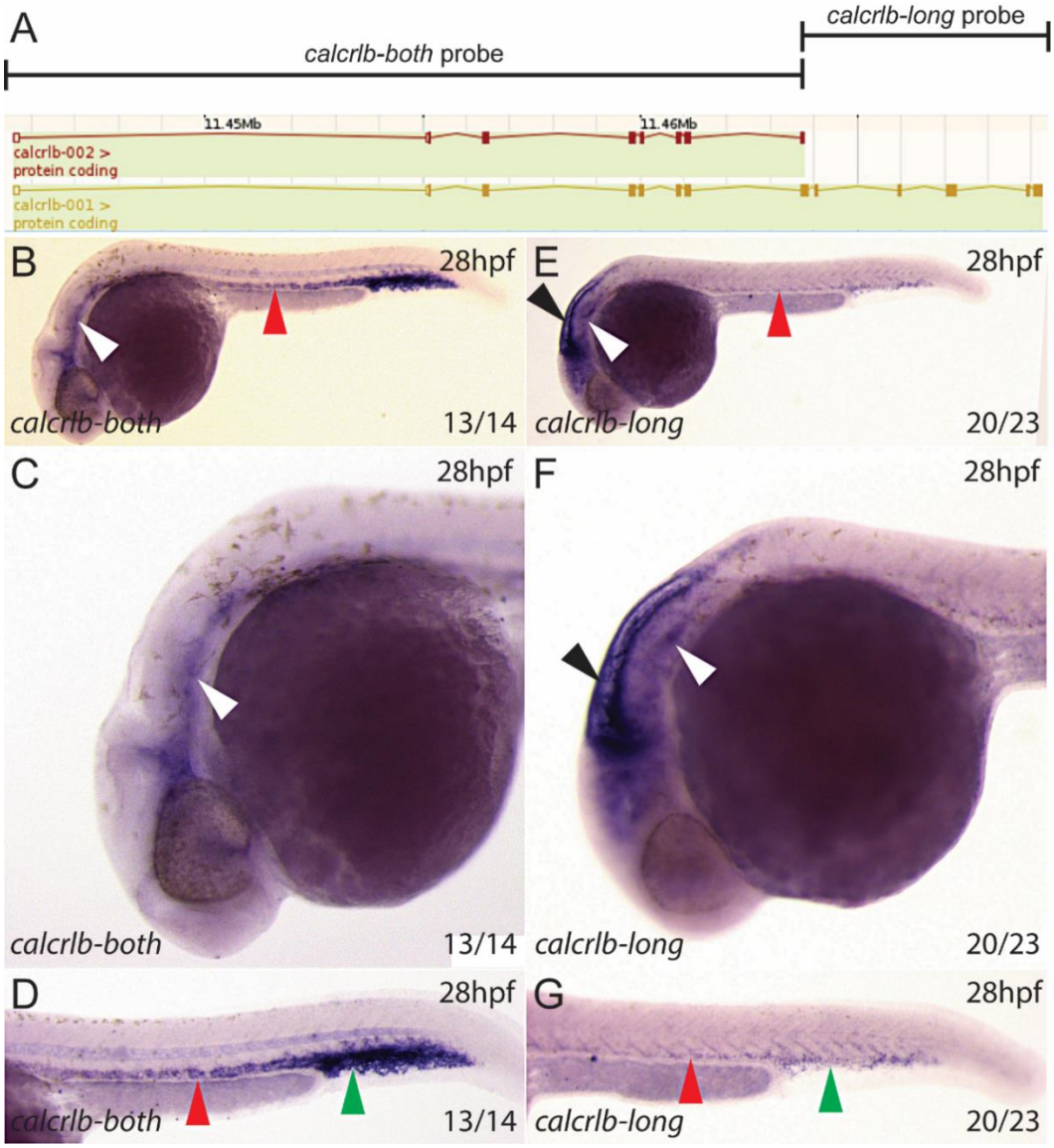

Figure 5.12 *calcrlb* is preferentially expressed in veins

(A) Schematic representation of the two *calcrlb* transcripts (ENSDARG00000011571) (Zerbino et al., 2018), *calcrlb*-both probe covers the first 8 exons, whereas *calcrlb*-long probe covers the last 5 exons of the longer transcript to detect the longer isoform specifically. (B-D) *In situ* of *calcrlb*-both probe at 28hpf WT embryos with lateral view (B), magnified lateral view of head (C) and magnified lateral view of trunk (D) showing both *calcrlb* isoforms are expressed in veins. (E-G) *In situ* of *calcrlb*-long probe at 28hpf WT embryos with lateral view (E), magnified lateral view of head (F) and magnified lateral view of trunk (G) showing the expression of the longer *calcrlb* isoform can be detected in the veins and hindbrain. White arrowheads point to the PHBC; red arrowheads donate the PCV, green arrowheads highlight the PBI, black arrowheads indicate the brain. PHBC, primordial hindbrain channel; PCV, posterior cardinal vein; PBI, posterior blood island.

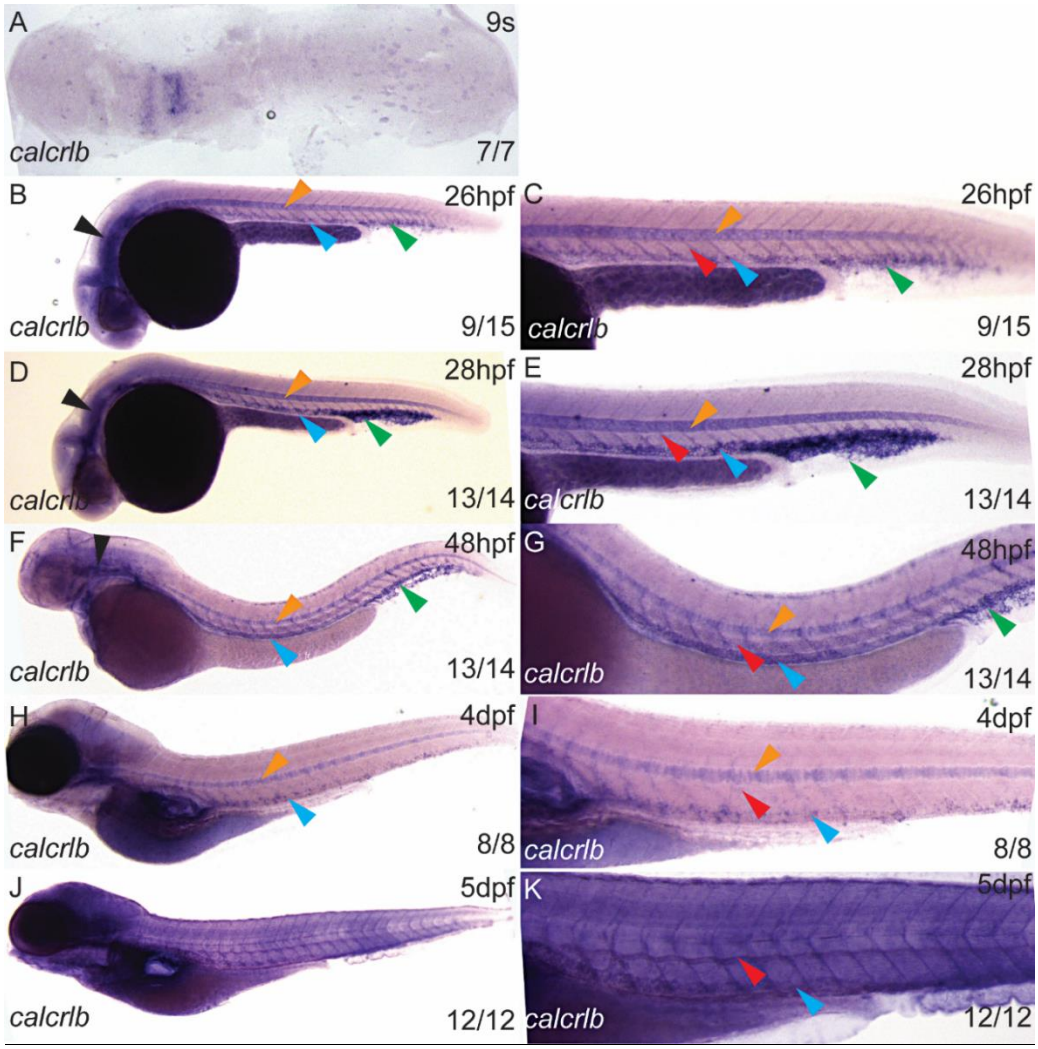

Figure 5.13 *calcrlb* is expressed in the developing notochord and vasculature

(A) *In situ* hybridisation of *calcrlb* in WT embryos at 9s stage showing *calcrlb* is expressed in the developing rhombomeres. (B-E) *In situ* hybridisation of *calcrlb* at 26hpf with lateral view (B) and magnified lateral view of trunk (C). *In situ* hybridisation of *calcrlb* at 28hpf with lateral view (D) and magnified lateral view of trunk (E). The expression of *calcrlb* can be detected in veins and notochord at 26hpf and 28hpf. Black arrowhead points to the PHBC; green arrowheads indicate PBI; red arrowheads highlight DA and blue arrowheads denote the PCV. (F-K) *calcrlb* expression at 48hpf with lateral view (F) and magnified lateral view of trunk (G) in major vessels and notochord. *calcrlb* expression at 4dpf (H-I) and 5dpf (J-K) with lateral view (H, J) and magnified lateral view of trunk (I, K). The expression of *calcrlb* can be detected in major vessels and notochord. Black arrowhead points to the PHBC; green arrowheads indicate CHT; red arrowheads highlight DA and blue arrowheads denote the PCV. PHBC, primordial hindbrain channel; DA, dorsal aorta; PCV, posterior cardinal vein; PBI, posterior blood island; CHT, caudal haematopoietic tissue.

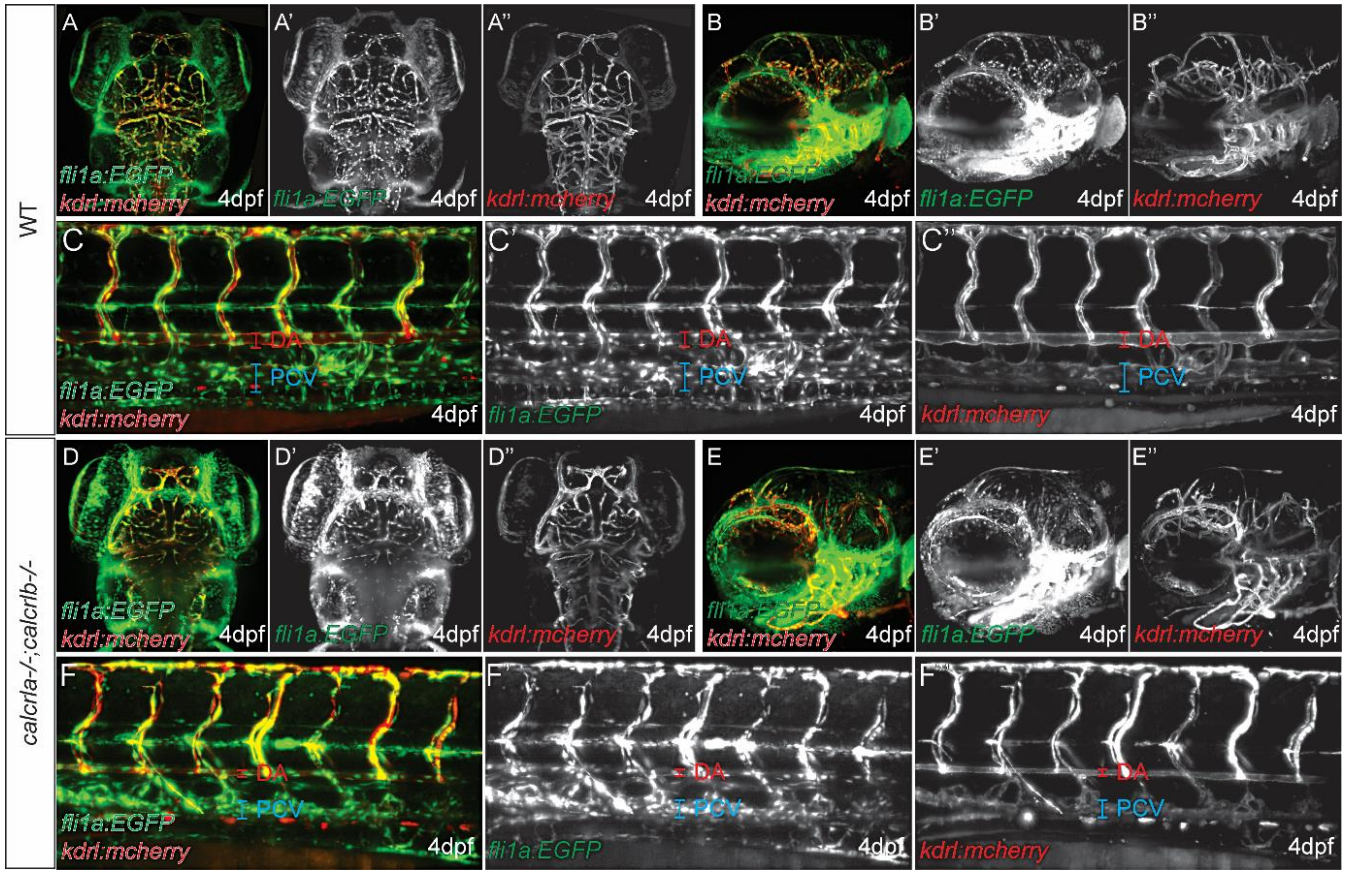

Figure 5.14 *calcrla* and *calcrlb* are dispensable for blood vessel patterning

(A-C'') Lightsheet images of WT embryos with *Tg(fli1a:EGFP; kdrl:mcherry)* background with dorsal view of head (A-A''), lateral view of head (B-B'') and lateral view of trunk (C-C'') at 4dpf. (D-F'') Lightsheet images of *calcrla*; *calcrlb* double mutants with *Tg(fli1a:EGFP; kdrl:mcherry)* background with dorsal view of head (D-D''), lateral view of head (E-E'') and lateral view of trunk (F-F'') at 4dpf showing unremarkable vascular patterning when compared with the WT embryos. Red bars highlight the DA; blue bars indicate the PCV. DA, dorsal aorta; PCV, posterior cardinal vein.

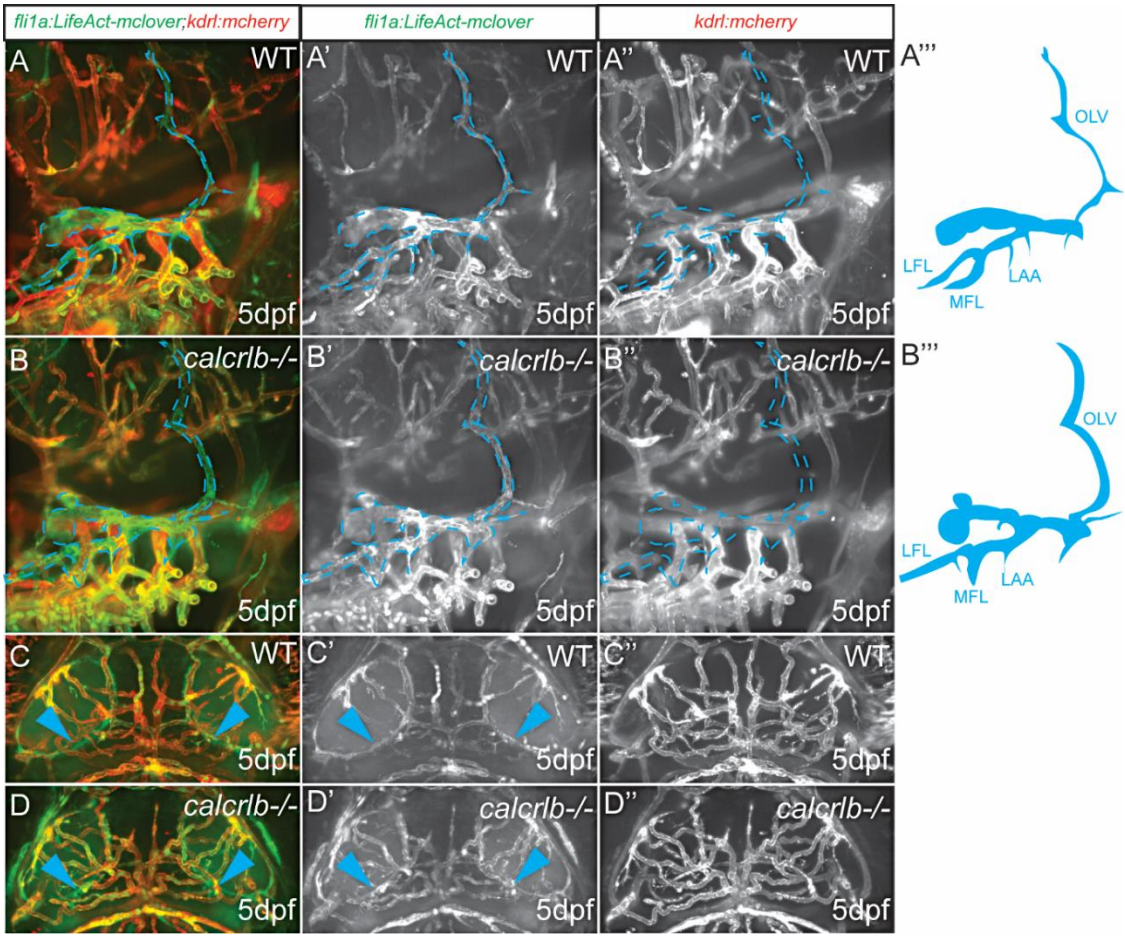

Figure 5.15 *calcrb* is dispensable for cranial lymphatic formation

(A-A''') Lateral view of facial lymphatics with schematic representation in WT embryos with *Tg(fli1a:LifeACT-mClover; kdrl:mcherry)* at 5dpf. (B-B''') Lateral view of facial lymphatics with Schematic representation in *calcrlb* mutant embryos with *Tg(fli1a:LifeACT-mClover; kdrl:mcherry)* at 5dpf showing unremarkable facial lymphatic development, when compared with the WT embryos. (C-C'') Dorsal view of head in WT embryos with *Tg(fli1a:LifeACT-mClover; kdrl:mcherry)* background showing normally formed BLEC loops located bilaterally in the forebrain (blue arrowheads) at 5dpf. (D-D'') Dorsal view of head in *calcrlb* single mutants with head circulation showing normal BLEC patterning (Blue arrowheads). BLEC, brain lymphatic cell; LFL, lateral facial lymphatic; MFL, medial facial lymphatic; OLV, otolithic lymphatic vessel; LAA, lymphatic branchial arch.

5.2.9 *calcrlb* is required for thoracic duct formation

Since cranial lymphatic formation was unremarkable in *calcrlb* single mutants, we also investigated formation of the first trunk lymphatic vessel, the thoracic duct (TD), to further investigate the underlying cause of oedema in *calcrlb* single mutants and *calcrla; calcrlb* double mutants. In WT embryos, at 4dpf, the mean TD coverage across 9 ISVs above the yolk extension was 100% (Fig. 5.16 A Yellow arrowhead). Conversely, a discontinuous TD was observed in both *calcrlb* single mutants and *calcrla*; *calcrlb* double mutants (Fig. 5.16 B, C Yellow asterisks). These data indicate that *calcrlb* positively regulates trunk lymphatic formation. Interestingly, disruption of TD formation occurred in 36% of *calcrlb* single mutants (n=11) whereas 60% of *calcrla; calcrlb* double mutants (n=5) showed a discontinuous TD (Fig. 5.16 D). These preliminary data suggest zebrafish *calcrla* and *calcrlb* genetically interact to promote trunk lymphangiogenesis. Furthermore, abnormal trunk lymphatics may contribute to the oedema observed in *calcrlb* and *calcrla*; *calcrlb* double mutants.

5.2.10 *calcrlb* single mutants display increased vascular permeability

Zebrafish *ccbe1*, *flt4* and *vegfc* mutants exhibit a failure of LEC specification and are devoid of functional lymphatics, but interestingly, only display mild oedema with onset at early day 5, considering with the onset of functional lymphatic drainage (van Impel et al., 2014, Hogan et al., 2009a). This phenotypic onset is much later than observed in *calcrlb* single mutants and *calcrla*; *calcrlb* double mutants and thus failure of lymphatic drainage arising from abnormal TD development is unlikely to be responsible for the early onset of oedema displayed in *calcrlb* single mutants and *calcrla*; *calcrlb* double mutants.

Mouse *Calcrl* knockouts have been reported to display reduced vascular integrity, albeit with associated haemorrhage (Ichikawa-Shindo et al., 2008, Shindo et al., 2001). Therefore to investigate whether reduced vascular permeability may be responsible for the early onset of oedema in *calcrlb* mutants, we performed dextran microangiography at 4dpf and injected high molecular weight tetramethylrhodamine (TAMRA) dye (2,000,000 Da) into the PCV in WT and *calcrlb* single mutants with blood flow lacking any transgenic marker, followed by Lightsheet time-lapse imaging for 15 hours (Fig. 5.17). Post TAMRA injection, *calcrlb* single mutants displayed extravasation of fluorescent dye (Fig. 5.17 D-F'' Yellow arrowheads) when compared with WT siblings post injection (Fig. 5.17 A-C''). Interestingly, fluorescent dye was observed to extravasate via microvesicles less than 1µm in diameter (Fig. 5.17 D-F'' Yellow arrowheads). This preliminary

data suggests *calcrlb* mutants display increased vascular permeability, which may contribute to the early onset of oedema in these mutants.

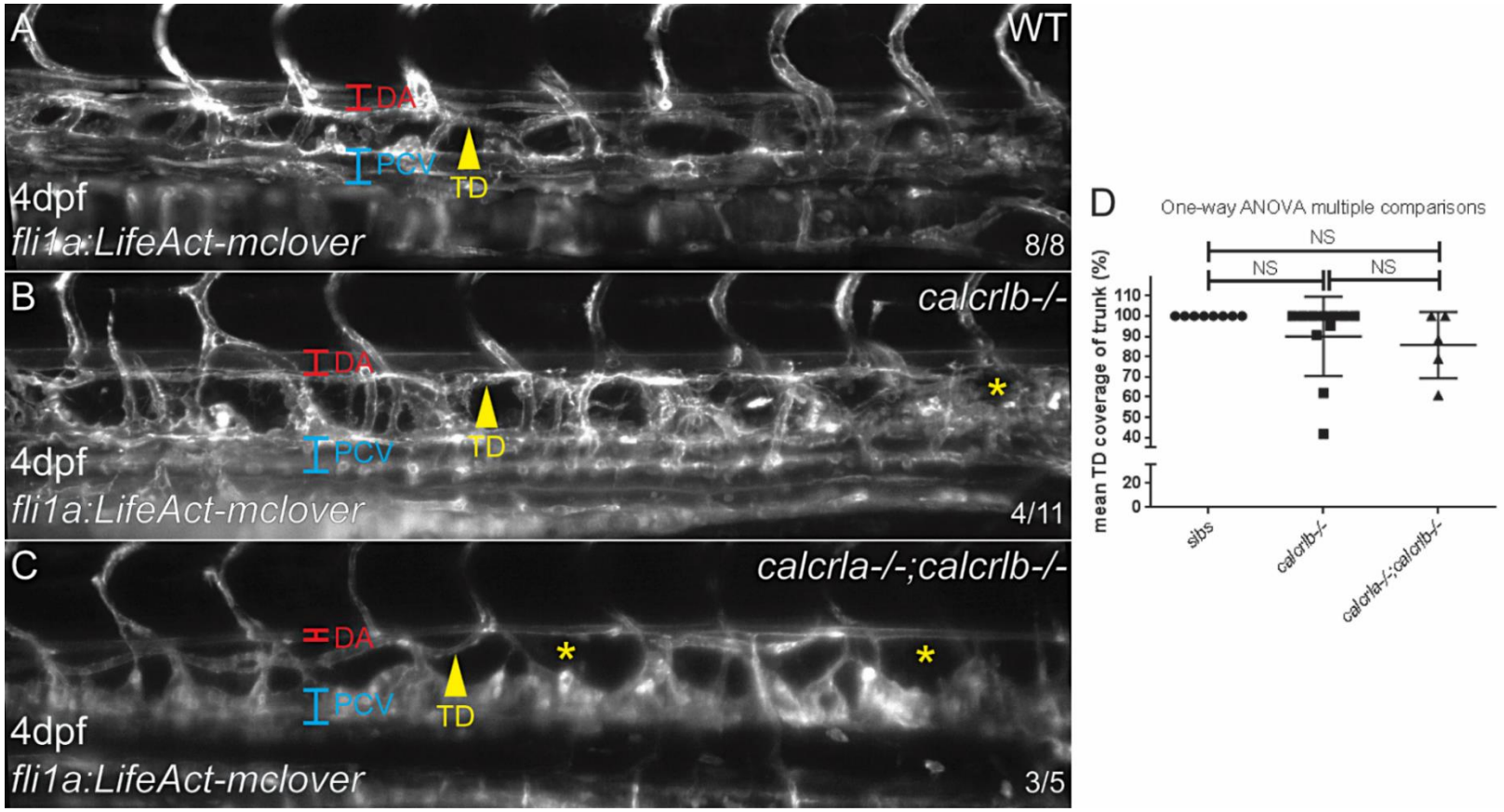

Figure 5.16 *calcrlb* is required for thoracic duct formation

(A-C) Lateral view of trunk of WT embryos, n=8 (A), *calcrlb* single mutants, n=11 (B) and *calcrla; calcrlb* double mutants, n=5 (C) with *Tg(fli1a:LifeACT-mClover)* background at 4dpf. Red bars denote DA; blue bars highlight PCV; yellow arrowheads point to TD and yellow asterisks highlight the discontinued TD. (D) Quantification of mean percentages of TD coverage of trunk. One-way ANOVA multiple comparisons. NS: not significant. DA, dorsal aorta; PCV, posterior cardinal vein, TD thoracic duct.

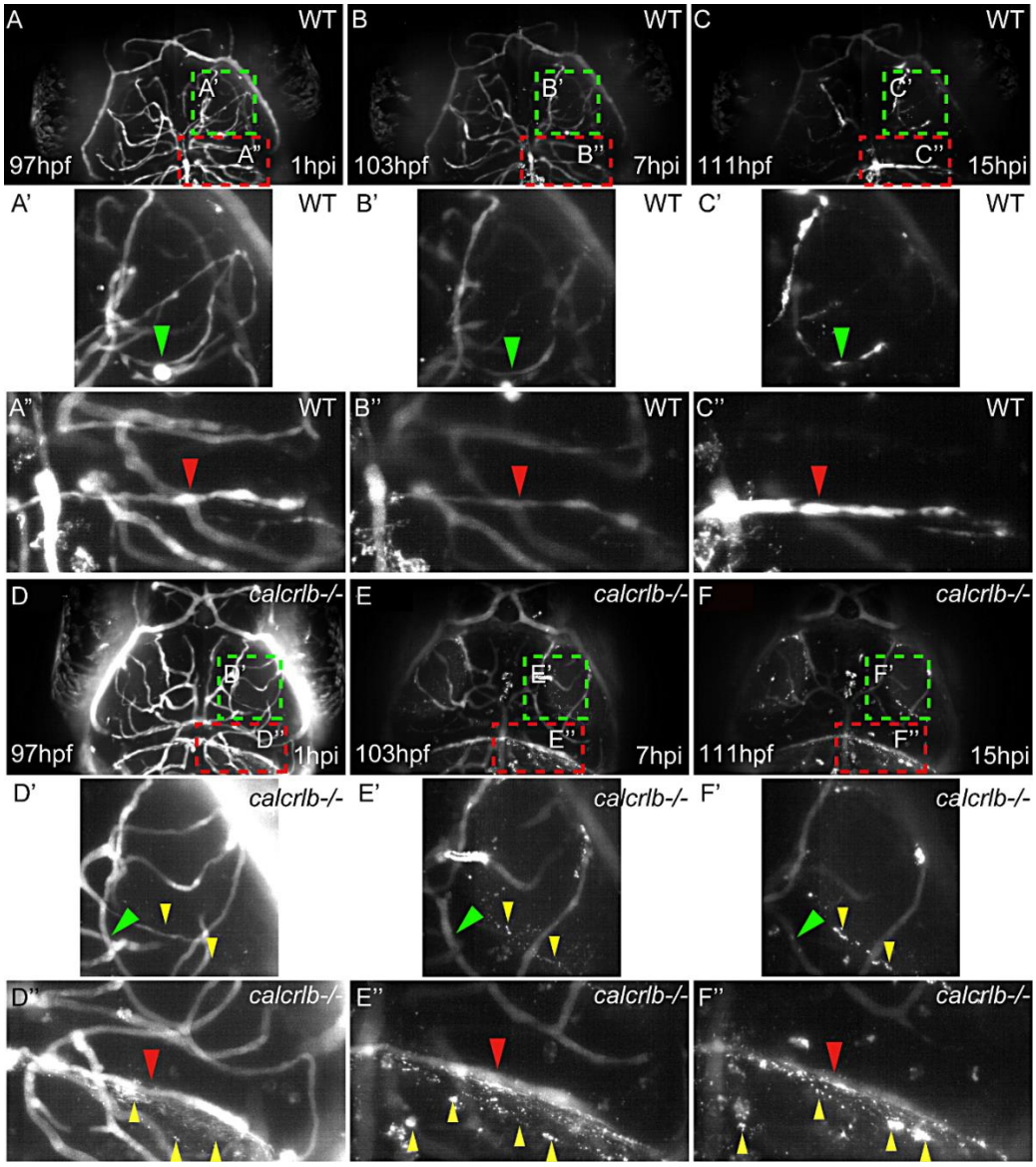

Figure 5.17 *calcrlb* mutants displays reduced vascular permeability

(A-C) Single frame images from 15h confocal time-lapses post injection of 20µg dextran tetramethylrhodamine dye (2,000,000 Da) into the PCV of WT embryos at 4dpf. (A'-C') Higher magnification picture of green dotted boxed areas in panel A-C. Green arrowheads indicate anterior mesencephalic central artery. (A''-C'') Higher magnification pictures of red dotted boxed areas in panel A-C. Red arrowheads indicate middle cerebral vein. (D-F) Single frame images from 15h confocal time lapses post injection of 20µg dextran tetramethylrhodamine (2,000,000 Da) into *calcrlb* single mutant embryos at 4dpf. (D'-F') Higher magnification picture of green dotted boxed area in panel A-C. Green arrowheads indicate anterior mesencephalic central artery. Yellow arrows heads point to dextran leakage. (D''-F'') Higher magnification picture of red dotted boxed area in panel A-C. Red arrowheads indicate middle cerebral vein. Yellow arrows heads point to dextran leakage.

5.3 Discussion

In this chapter we describe the generation of novel *calcrla* and *calcrlb* mutant zebrafish and present detailed characterisation of *calcrla* single mutants, *calcrlb* single mutants and *calcrla*; *calcrlb* double mutants. Here we highlight our findings below:

1. Zebrafish *calcrla* and *calcrlb* act co-operatively to promote vascular integrity and trunk lymphangiogenesis.
2. Both *calcrla* and *calcrlb* are dispensable for blood vessel patterning and cranial lymphatic formation in zebrafish.

5.3.1 *calcrla* and *calcrlb* are expressed within the vasculature

As reported by Nicoli *et al.*, expression of zebrafish *calcrla* can be detected as early as 4s (11hpf) (Nicoli et al., 2008). Its expression could be detected in major vessels and somites during embryonic development (Nicoli et al., 2008). Nicoli *et al.* reported at 26hpf *calcrla* expression has unique arterial preference, whereas at 48hpf *calcrla* expression could also be detected within veins (Nicoli et al., 2008). Interestingly, we also observed *calcrla* was preferentially expressed in arteries, which peaks at 26hpf, in line with previous data (Nicoli et al., 2008). At 28hpf, *calcrla* still shows arterial expression in cranial vessels, however, *calcrla* expression could also be detected in both the DA and PCV in the trunk (Fig. 5.10). In addition, we also showed *calcrla* expression within AA' during embryonic development (Fig. 5.10). Interestingly, Calcrla and Ramp5 expression have been shown in the interlamellar vessels in the gill filaments in pufferfish *T. obscurus*, which facilitate the blood circulation between lamellae and filaments (Nag et al., 2006, Wilson and Laurent, 2002). Taken together, these observations indicate the pufferfish Calcrla and Ramp5 may represent an Am receptor on the gill structures. Given the functional similarity between the fish gill and mammalian lungs, this is not surprising since mammalian AM is a well-known pulmonary vasodilator (Dschietzig et al., 2002, Heaton et al., 1995).

Unlike *calcrla* expression, we showed that expression of *calcrlb* displays a venous preference in both cranial and trunk vessels (Fig. 5.12, 5.13). This observation conflicts with previous studies in zebrafish, which indicates that *calcrlb* expression is maternally but not zygotically expressed (Nicoli et al., 2008). Consistent with our data, zebrafish *calcrlb* expression during embryogenesis has been previously confirmed using RT-PCR (Lafont et al., 2011). Interestingly, no *calcrlb* expression could be detected in AA' by *in situ* hybridisation during embryonic development (Fig.

5.13), this data indicates that *calcrlb* is unlikely to be required for AA' formation cell-autonomously during embryogenesis. In adult pufferfish, Calcrlb and Ramp2a expression can be detected in gill lamellae, particularly in the pillar cells of lamellae (Nag et al., 2006). The pillar cell is a fish-specific EC type, which is essential for establishing the blood spaces and controlling the microcirculation within secondary lamellae (Wilson and Laurent, 2002). Histological analysis of 4 weeks zebrafish *calcrlb* mutant juveniles, revealed abnormal gill formation, including shortened gill filament formation and significantly reduced secondary lamella development (Fig. 5.8 A4, B4). Our observation reinforced a requirement for *calcrlb* in zebrafish lamella formation post embryogenesis, in line with previous study in pufferfish (Nag et al., 2006).

5.3.2 Mutants in *calcrla* and *calcrlb* display strikingly different phenotypes

calcrla single mutants do not have morphological abnormalities during embryonic development (Fig. 5.2), which conflicts with the published phenotype of zebrafish *calcrla* morphants (Nicoli et al., 2008, Wilkinson et al., 2012). Therefore, our data suggest *calcrla* is not essential for vascular development. The expression of *calcrla* was detected in the notochord during embryogenesis (Fig. 5.10). In addition, we showed *calcrla* single mutants display reduced body length during the embryo to larval transition (Fig. 5.2). Taken together, these data suggest *calcrla* may be involved in skeletal development.

In mammals, CGRP is essential for bone growth and healing post injury (Naot et al., 2008). Interestingly, among the identified Calcrl proteins in pufferfish, Calcrla is the only one that binds to Ramp1 to construct receptors for the CGRP ligand (Nag et al., 2006). Therefore, this growth delay shown in our *calcrla* single mutants during early embryo-larval transition could potentially be due to Calcrla-CGRP-mediated abnormalities in bone development, rather than Am-Calcrla-Ramp2 Signalling.

In this thesis we generated 3 independent *calcrlb* mutant alleles, which possessed distinct mutations (Fig. 5.3, 5.4, 5.5). Interestingly, analyses of gross morphology of individual *calcrlb* mutants revealed all 3 independent *calcrlb* homozygous mutants, including the in-frame mutation *calcrlb*^{sh469}, showed similar oedematous phenotypes with two defined classes of severity (Fig. 5.6). Therefore, all 3 *calcrlb* alleles are likely to represent similar severe loss of function mutations. In addition, as described in section 5.2.4 class I *calcrlb* mutants displayed normal blood circulation, whereas class II *calcrlb* mutants exhibited reduced blood circulation post phenotypic onset. Therefore, reduced blood circulation displayed in class II *calcrlb* single

mutants is likely to be a secondary effect resulting from oedema, which may in turn contribute to the severity of oedema observed.

5.3.3 *calcrla* and *calcrlb* display overlapping functions during embryonic development

As shown in section 5.2.5, *calcrla; calcrlb* double mutants display more severe oedema than *calcrla* and *calcrlb* single mutants. The strong genotype-phenotype correlation suggests *calcrla* and *calcrlb* genetically interact and exhibit overlapping functions, disruption of which induces oedema. Since *calcrla* single mutants were morphologically unremarkable, whereas *calcrlb* single mutants showed a milder but similar phenotype to *calcrla*; *calcrlb* double mutants during embryonic development, we conclude *calcrla* can partially compensate for the lost function of *calcrlb*, however, *calcrlb* can fully compensate for loss of function of *calcrla* during embryonic development. In the pufferfish *T. obscurus*, Calcrla and Calcrlb have been demonstrated to bind to either Ramp2a or Ramp2b to form an Am receptor (Nag et al., 2006). Therefore, in the absence of Calcrlb, Calcrla could theoretically still interact with Ramp2 proteins to respond to Am ligand. Taken together, to our knowledge our results show the first *in vivo* evidence to support this compensatory relationship between *calcrla* and *calcrlb* in teleosts.

Conflicting results have been reported in murine studies using independent AM signalling-depleted mutants (Shindo et al., 2001, Dackor et al., 2006, Fritz-Six et al., 2008, Ichikawa-Shindo et al., 2008). Data reported by the Shindo group showed that severe haemorrhage in mutant mice results from reduced endothelial adhesion and increased EC permeability (Ichikawa-Shindo et al., 2008, Shindo et al., 2001), whereas the Caron group have provided evidence indicating that an abnormally developed lymphatic system is more likely to be responsible for the hydrops fetalis phenotype in their mutants (Fritz-Six et al., 2008). We observed no haemorrhage in either *calcrlb* single mutants (Fig. 5.6) or *calcrla*; *calcrlb* double mutants (Fig. 5.9) during embryogenesis. In addition, no haemorrhage was observed in *calcrlb* mutant juveniles (Fig. 5.7, 5.8). These morphological phenotypes are in line with those reported by the Caron group (Fritz-Six et al., 2008).

Interestingly, subcutaneous dextran injection into zebrafish larvae demonstrated that the trunk lymphatic system becomes functional at 5dpf (Karpanen and Schulte-Merker, 2011). The typical zebrafish mutants with completely abolished lymphatic formation including *ccbe1*, *flt4* and *vegfc* mutants have been demonstrated previously (van Impel et al., 2014, Hogan et al., 2009a), which

display mild oedema onset from early day 5 (van Impel et al., 2014). Despite having shown abnormal lymphatic formation in *calcrlb* single mutants and *calcrla*; *calcrlb* double mutants (Fig. 5.16). The phenotypic onset in both *calcrlb* single mutants and *calcrla*; *calcrlb* double mutants is late day 3 to day 4, which is earlier than the oedema onset displayed in the zebrafish mutants with failure in tissue fluid drainage (van Impel et al., 2014, Hogan et al., 2009a). Therefore, this early onset oedema displayed in *calcrlb* single mutants and *calcrla*; *calcrlb* double mutants is unlikely due to failed lymphatic drainage. However, we cannot discount the possibility that abnormal trunk lymphatic formation mediated by loss of function of *calcrla* and *calcrlb* might contribute to the oedema post embryogenesis. Furthermore, our preliminary dextran TAMRA injection into WT and *calcrlb*-depleted embryos followed by time lapse imaging indicates that the permeability of cranial vasculature was increased in the absence of *calcrlb* (Fig. 5.17). Therefore, we hypothesised that the increased vascular permeability is likely to cause the early onset oedema directly.

Furthermore, despite our results indicating increased vascular permeability in the absence of *calcrlb*, we observed no haemorrhage in the absence of *calcrla* and/ or *calcrlb*, which could potentially be explained by the lesions caused by these defects not being big enough for erythrocytes to go through. As introduced in chapter 1 section 1.4.1, transcellular gaps including the vesiculo-vascuolar organelle (VVO) are the major pathways that facilitate transcytosis in the developing brain (Claesson-Welsh, 2015, Kohn et al., 1992). Interestingly, the fluorescent dye extravasates potentially via microvesicles in *calcrlb* single mutants (Fig. 5.17 D-F'' Yellow arrowheads). Therefore, it is possible that *calcrlb* promotes vascular permeability via negatively regulating transcellular VVO formation.

Murine mutants of Ramp2 or *AM*/ *CALCRL* displayed thin vSMC (Fritz-Six et al., 2008, Dackor et al., 2006, Kamitani et al., 1999, Caron and Smithies, 2001), indicating that the AM signalling pathway is required for normal vSMC recruitment to stabilise the formed vascular network. Given that vascular permeability was increased in the absence of *calcrlb* (Fig. 5.17) and since *calcrla* and *calcrlb* compensate for each other during the onset of oedema (Fig. 5.9), *calcrla* and/ or *calcrlb* may also contribute to maintaining the stability of the formed vasculature via recruitment of supportive non-endothelial cells in zebrafish.

5.3.4 *calcrlb* is required for trunk lymphatic development

We have shown abnormal trunk lymphatic development in *calcrlb* single mutants and *calcrla*; *calcrlb* double mutants at 4dpf (Fig. 5.16). Interestingly, cranial lymphatic formation including

facial lymphatics and BLECs were formed normally in the absence of *calcrlb* (Fig. 5.15). These data suggest *calcrlb* alone is unlikely to be required for cranial lymphangiogenesis. As reported, *calcrla* and *calcrlb* compensate for each other during embryogenesis. Therefore, we cannot discount the possibility that *calcrla* and *calcrlb* potentially have redundant functions during facial lymphatic development. Future experiments to examine the formation of cranial lymphatic development in *calcrla; calcrlb* double mutants would address this hypothesis.

Reduced TD coverage was also observed in the trunk of *calcrlb* single mutants and *calcrla*; *calcrlb* double mutants at 4dpf (Fig. 5.16). There was no significant difference in reduced TD coverage between *calcrlb* single mutants and *calcrla*; *calcrlb* double mutants. This preliminary data indicates that *calcrlb* is indispensable for trunk lymphatic development. In addition, we observed a higher proportion of *calcrla; calcrlb* double mutant embryos (60%, n=5) displayed TD abnormalities, when compared with *calcrlb* single mutants (36%, n=11) (Fig. 5.16). *calcrla* single mutants showed normal TD formation (data not shown) suggesting *calcrla* alone is dispensable for lymphangiogenesis. The expression of *calcrla* was detected within the PCV from 26hpf to 48hpf (Fig. 5.10 B-G). Therefore, these data indicate the involvement of *calcrla* during trunk lymphatic formation when *calcrlb* function is absent. As mentioned earlier, pufferfish Calcrla expression could be detected within interlamellar vessels (Nag et al., 2006), which have been suggested to be similar to the lymphatic duct in mammals (Evans et al., 2005). This data supports our conclusion that *calcrla* also contributes to lymphangiogenesis.

5.3.5 *calcrla* and *calcrlb* are dispensable for vascular patterning

While many murine studies have described abnormalities in lymphatic formation and blood vessel stability and integrity, which resulted in extreme hydrops fetalis in AM signalling-depleted mutant mice (Shindo et al., 2001, Dackor et al., 2006, Fritz-Six et al., 2008, Ichikawa-Shindo et al., 2008), strikingly, no abnormality was detected in the formation of major blood vessels in these animals (Shindo et al., 2001, Dackor et al., 2006, Fritz-Six et al., 2008). As introduced in section 5.1.3, zebrafish *calcrla* morphants have been reported to have severe arterial-venous malformations and disrupted trunk angiogenesis (Nicoli et al., 2008). Furthermore, reduced diameter of the lateral dorsal aorta (LDA) and failure in lumenisation were also reported in *calcrla* morphants (Nicoli et al., 2008). Conflicting with these data, our *calcrla* mutants showed no obvious phenotype, the homozygous mutant adult fish were viable and fertile (Fig. 5.2), whereas *calcrlb* single mutants showed severe oedema during embryonic stages (Fig. 5.6). By employing endothelial transgenic reporter lines, we have reported relatively normal vasculature patterning in the absence of *calcrla* and/ or *calcrlb* during embryogenesis (Fig. 5.11, 5.14). This observation

is in line with previous published murine data (Shindo et al., 2001, Dackor et al., 2006, Fritz-Six et al., 2008). Therefore, our data indicate both *calcrla* and *calcrlb* are likely to be dispensable for vascular patterning.

Previous studies from the Wilkinson lab using *calcrla* Mo have revealed that injection of 0.67pmol *calcrla* Mo (Wilkinson et al., 2012) into one-cell stage embryos, which is lower than initial published dosage (0.8pmol) (Nicoli et al., 2008) induced a 22 fold increase in *p53* expression when compared with the uninjected control group (A. Savage, unpublished observations). This data indicates the severe vascular abnormalities displayed in *calcrla* morphants as previously reported (Nicoli et al., 2008, Wilkinson et al., 2012) may be caused by the off-target effects of the *calcrla* Mo, since normal vascular patterning was observed in *calcrla* single mutants (Fig. 5.11). However, we cannot exclude the possibility that genetic compensation may also cause this phenotypic difference between morphants and knockouts (Rossi et al., 2015) (Reviewed in (El-Brolosy and Stainier, 2017)). Future experiments of KD *calcrla* using Mo in the *calcrla* single mutants will address this issue.

CHAPTER 6

Discussion

How blood vessel formation is regulated is an interesting and challenging developmental biology subject, which has great potential in therapeutic development. Haematopoietic stem cells (HSCs) are derived from the embryonic artery during early development and give rise to all adult blood cell lineages throughout life. The shared origin of arterial endothelial cells (ECs) and HSCs means these cells share common mechanisms which regulate their formation. Many pioneering studies have shed light on the importance of different signalling pathways which regulate these complicated processes during embryonic development, however, much less is understood about how these signalling pathways are regulated at the transcriptional level. In this thesis, we investigate the regulatory roles of Foxc1 and Calcrl pathways during blood vessel formation using zebrafish and demonstrate both Foxc1 and Calcrl pathways are important for different aspects of vascular development.

In chapter 3 and chapter 4 we performed detailed characterisation of the *foxc1a*/ *foxc1b* mutants and showed *foxc1a* and *foxc1b* differentially regulate angiogenesis from arteries and veins by modulating VEGF signalling. In the head, the formation of central arteries (CtAs) initiates with sprouting from the primordial hindbrain channels (PHBCs), which are major cranial veins. In *foxc1a* single mutants, the formation of CtAs is significantly reduced. We provide evidences indicating *foxc1a* is required for CtAs formation by positively regulating the expression of *kdrl*, *sox7* and *sox18*. In addition, we reported that *foxc1a* is also required for normal PHBC formation, likely via promoting the expression of *flt4*. In the trunk, reduced secondary angiogenesis from the posterior cardinal vein (PCV) was observed in *foxc1a* single mutants and *foxc1a*; *foxc1b* double mutants, which is in line with our previous conclusion that *foxc1a* promotes venous angiogenesis. However, in the absence of both *foxc1a* and *foxc1b*, ectopic trunk arterial angiogenesis was observed. Our data suggest *foxc1a* and *foxc1b* work co-operatively to antagonise arterial angiogenesis via promoting the Dll4/Notch-mediated suppression of Flt4/ Vegfc signalling. Collectively, *foxc1a* and *foxc1b* control the angiogenic balance during development by regulating competing pro- and anti-angiogenic mechanisms throughout the body (Fig. 4.25). In this thesis, we also demonstrate *foxc1a* and *foxc1b* interact with each other to promote HSC formation via positively regulating Notch signalling cell-autonomously and non-cell- autonomously.

In chapter 5, we describe the generation and characterisation of *calcrla* mutants and *calcrlb* mutants. By performing detailed analysis, we demonstrate that *calcrla* is dispensable for embryonic development, which conflicts with previously published zebrafish studies using morpholinos (Nicoli et al., 2008, Wilkinson et al., 2012). In addition, *calcrlb* fully compensates for loss of *calcrla* function in blood vessels, whereas *calcrla* can only partially compensate for the loss

function of *calcrlb*. This interaction is required for trunk lymphatic formation and to promote vessel integrity.

Also we provide preliminary data showing increased vascular permeability in *calcrlb* mutants with efflux of microvesicles less than 1µm in diameter to facilitate the extravasation of high molecular weight tetramethylrhodamine dye. These microvesicles could potentially reflect activation of the vesiculo-vascuolar organelle (VVO), the main transcellular permeability mechanism within the brain vasculature. There is currently no suitable animal model to study VVO formation *in vivo* (Dvorak and Feng, 2001, Claesson-Welsh, 2015). Our preliminary observations in *calcrlb* mutants suggest these may represent a potential *in vivo* model to study transcellular vascular permeability.

CHAPTER 7

References

ADAMS, J. (2016). How do we make blood cells? Characterising the role of her12 in haematopoietic stem cell formation using zebrafish models. MSc dissertation, University of Sheffield.

ADAMS, R. H. & ALITALO, K. 2007. Molecular regulation of angiogenesis and lymphangiogenesis. *Nat Rev Mol Cell Biol,* 8**,** 464-78.

ADAMS, R. H., WILKINSON, G. A., WEISS, C., DIELLA, F., GALE, N. W., DEUTSCH, U., RISAU, W. & KLEIN, R. 1999. Roles of ephrinB ligands and EphB receptors in cardiovascular development: demarcation of arterial/venous domains, vascular morphogenesis, and sprouting angiogenesis. *Genes Dev,* 13**,** 295-306.

ALDERS, M., HOGAN, B. M., GJINI, E., SALEHI, F., AL-GAZALI, L., HENNEKAM, E. A., HOLMBERG, E. E., MANNENS, M. M., MULDER, M. F., OFFERHAUS, G. J., PRESCOTT, T. E., SCHROOR, E. J., VERHEIJ, J. B., WITTE, M., ZWIJNENBURG, P. J., VIKKULA, M., SCHULTE-MERKER, S. & HENNEKAM, R. C. 2009. Mutations in CCBE1 cause generalized lymph vessel dysplasia in humans. *Nat Genet,* 41**,** 1272-4.

ALLINGHAM, M. J., VAN BUUL, J. D. & BURRIDGE, K. 2007. ICAM-1-mediated, Src- and Pyk2-dependent vascular endothelial cadherin tyrosine phosphorylation is required for leukocyte transendothelial migration. *Journal of Immunology,* 179**,** 4053-4064.

AMBATI, B. K., NOZAKI, M., SINGH, N., TAKEDA, A., JANI, P. D., SUTHAR, T., ALBUQUERQUE, R. J. C., RICHTER, E., SAKURAI, E., NEWCOMB, M. T., KLEINMAN, M. E., CALDWELL, R. B., LIN, Q., OGURA, Y., ORECCHIA, A., SAMUELSON, D. A., AGNEW, D. W., ST LEGER, J., GREEN, W. R., MAHASRESHTI, P. J., CURIEL, D. T., KWAN, D., MARSH, H., IKEDA, S., LEIPER, L. J., COLLINSON, J. M., BOGDANOVICH, S., KHURANA, T. S., SHIBUYA, M., BALDWIN, M. E., FERRARA, N., GERBER, H. P., DE FALCO, S., WITTA, J., BAFFI, J. Z., RAISLER, B. J. & AMBATI, J. 2006. Corneal avascularity is due to soluble VEGF receptor-1. *Nature,* 443**,** 993-997.

ANDO, K., FUKUHARA, S., IZUMI, N., NAKAJIMA, H., FUKUI, H., KELSH, R. N. & MOCHIZUKI, N. 2016. Clarification of mural cell coverage of vascular endothelial cells by live imaging of zebrafish. *Development,* 143**,** 1328-1339.

ARMULIK, A., GENOVE, G., MAE, M., NISANCIOGLU, M. H., WALLGARD, E., NIAUDET, C., HE, L., NORLIN, J., LINDBLOM, P., STRITTMATTER, K., JOHANSSON, B. R. & BETSHOLTZ, C. 2010. Pericytes regulate the blood-brain barrier. *Nature,* 468**,** 557-61.

ASLAM, M., GUNDUZ, D., SCHULER, D., LI, L., SHARIFPANAH, F., SEDDING, D., PIPER, H. M. & NOLL, T. 2011. Intermedin induces loss of coronary microvascular endothelial barrier via derangement of actin cytoskeleton: role of RhoA and Rac1. *Cardiovasc Res,* 92**,** 276-86.

ASTIN, J. W., HAGGERTY, M. J., OKUDA, K. S., LE GUEN, L., MISA, J. P., TROMP, A., HOGAN, B. M., CROSIER, K. E. & CROSIER, P. S. 2014. Vegfd can compensate for loss of Vegfc in zebrafish facial lymphatic sprouting. *Development,* 141**,** 2680-90.

BAHARY, N., GOISHI, K., STUCKENHOLZ, C., WEBER, G., LEBLANC, J., SCHAFER, C. A., BERMAN, S. S., KLAGSBRUN, M. & ZON, L. I. 2007. Duplicate VegfA genes and orthologues of the KDR receptor tyrosine kinase family mediate vascular development in the zebrafish. *Blood,* 110**,** 3627-3636.

BANERJEE, S., HAYER, K., HOGENESCH, J. B. & GRANATO, M. 2015. Zebrafish foxc1a drives appendage-specific neural circuit development. *Development,* 142**,** 753-62.

BELL, D. & MCDERMOTT, B. J. 2008. Intermedin (adrenomedullin-2): a novel counter-regulatory peptide in the cardiovascular and renal systems. *Br J Pharmacol,* 153 Suppl 1**,** S247-62.

BERTRAND, J. Y., CHI, N. C., SANTOSO, B., TENG, S. T., STAINIER, D. Y. R. & TRAVER, D. 2010. Haematopoietic stem cells derive directly from aortic endothelium during development. *Nature,* 464**,** 108-U120.

BIKFALVI, A. 2017. History and conceptual developments in vascular biology and angiogenesis research: a personal view. *Angiogenesis,* 20**,** 463-478.

BOARDMAN, K. C. & SWARTZ, M. A. 2003. Interstitial flow as a guide for lymphangiogenesis. *Circ Res,* 92**,** 801-8.

BOISSET, J. C., VAN CAPPELLEN, W., ANDRIEU-SOLER, C., GALJART, N., DZIERZAK, E. & ROBIN, C. 2010. In vivo imaging of haematopoietic cells emerging from the mouse aortic endothelium. *Nature,* 464**,** 116-20.

BOWER, N. I., VOGRIN, A. J., LE GUEN, L., CHEN, H., STACKER, S. A., ACHEN, M. G. & HOGAN, B. M. 2017. Vegfd modulates both angiogenesis and lymphangiogenesis during zebrafish embryonic development. *Development,* 144**,** 507-518.

BUCHANAN, C. M., SHIH, J. H., ASTIN, J. W., REWCASTLE, G. W., FLANAGAN, J. U., CROSIER, P. S. & SHEPHERD, P. R. 2012. DMXAA (Vadimezan, ASA404) is a multi-kinase inhibitor targeting VEGFR2 in particular. *Clin Sci (Lond),* 122**,** 449-57.

BURNS, C. E., TRAVER, D., MAYHALL, E., SHEPARD, J. L. & ZON, L. I. 2005. Hematopoietic stem cell fate is established by the Notch-Runx pathway. *Genes Dev,* 19**,** 2331-42.

BUSSMANN, J., BAKKERS, J. & SCHULTE-MERKER, S. 2007. Early endocardial morphogenesis requires Scl/Tal1. *PLoS Genet,* 3**,** e140.

BUSSMANN, J., BOS, F. L., URASAKI, A., KAWAKAMI, K., DUCKERS, H. J. & SCHULTE-MERKER, S. 2010. Arteries provide essential guidance cues for lymphatic endothelial cells in the zebrafish trunk. *Development,* 137**,** 2653-7.

BUSSMANN, J., LAWSON, N., ZON, L., SCHULTE-MERKER, S. & ZEBRAFISH NOMENCLATURE, C. 2008. Zebrafish VEGF receptors: a guideline to nomenclature. *PLoS Genet,* 4**,** e1000064.

BUSSMANN, J., WOLFE, S. A. & SIEKMANN, A. F. 2011. Arterial-venous network formation during brain vascularization involves hemodynamic regulation of chemokine signaling. *Development,* 138**,** 1717-1726.

BUTKO, E., DISTEL, M., POUGET, C., WEIJTS, B., KOBAYASHI, I., NG, K., MOSIMANN, C., POULAIN, F. E., MCPHERSON, A., NI, C. W., STACHURA, D. L., DEL CID, N., ESPIN-PALAZON, R., LAWSON, N. D., DORSKY, R., CLEMENTS, W. K. & TRAVER, D. 2015. Gata2b is a restricted early regulator of hemogenic endothelium in the zebrafish embryo. *Development,* 142**,** 1050-1061.

CAOLO, V., MOLIN, D. G. & POST, M. J. 2012. Notch regulation of hematopoiesis, endothelial precursor cells, and blood vessel formation: orchestrating the vasculature. *Stem Cells Int,* 2012**,** 805602.

CARMELIET, P., FERREIRA, V., BREIER, G., POLLEFEYT, S., KIECKENS, L., GERTSENSTEIN, M., FAHRIG, M., VANDENHOECK, A., HARPAL, K., EBERHARDT, C., DECLERCQ, C., PAWLING, J., MOONS, L., COLLEN, D., RISAU, W. & NAGY, A. 1996. Abnormal blood vessel development and lethality in embryos lacking a single VEGF allele. *Nature,* 380**,** 435-9.

CARON, K. M. & SMITHIES, O. 2001. Extreme hydrops fetalis and cardiovascular abnormalities in mice lacking a functional Adrenomedullin gene. *Proc Natl Acad Sci U S A,* 98**,** 615-9.

CARROLL, K. J., ESAIN, V., GARNAAS, M. K., CORTES, M., DOVEY, M. C., NISSIM, S., FRECHETTE, G. M., LIU, S. Y., KWAN, W., CUTTING, C. C., HARRIS, J. M., GORELICK, D. A., HALPERN, M. E., LAWSON, N. D., GOESSLING, W. & NORTH, T. E. 2014. Estrogen Defines the Dorsal-Ventral Limit of VEGF Regulation to Specify the Location of the Hemogenic Endothelial Niche. *Developmental Cell,* 29**,** 437-453.

CASIE CHETTY, S., ROST, M. S., ENRIQUEZ, J. R., SCHUMACHER, J. A., BALTRUNAITE, K., ROSSI, A., STAINIER, D. Y. & SUMANAS, S. 2017. Vegf signaling promotes vascular endothelial differentiation by modulating etv2 expression. *Dev Biol,* 424**,** 147-161.

CERMAK, T., DOYLE, E. L., CHRISTIAN, M., WANG, L., ZHANG, Y., SCHMIDT, C., BALLER, J. A., SOMIA, N. V., BOGDANOVE, A. J. & VOYTAS, D. F. 2011. Efficient design and assembly of custom TALEN and other TAL effector-based constructs for DNA targeting. *Nucleic Acids Res,* 39**,** e82.

CERMENATI, S., MOLERI, S., CIMBRO, S., CORTI, P., DEL GIACCO, L., AMODEO, R., DEJANA, E., KOOPMAN, P., COTELLI, F. & BELTRAME, M. 2008. Sox18 and Sox7 play redundant roles in vascular development. *Blood,* 111**,** 2657-66.

CERMENATI, S., MOLERI, S., NEYT, C., BRESCIANI, E., CARRA, S., GRASSINI, D. R., OMINI, A., GOI, M., COTELLI, F., FRANCOIS, M., HOGAN, B. M. & BELTRAME, M. 2013. Sox18 genetically interacts with VegfC to regulate lymphangiogenesis in zebrafish. *Arterioscler Thromb Vasc Biol,* 33**,** 1238-47.

CHEN, A. T. & ZON, L. I. 2009. Zebrafish blood stem cells. *J Cell Biochem,* 108**,** 35-42.

CHEN, T. T., LUQUE, A., LEE, S., ANDERSON, S. M., SEGURA, T. & IRUELA-ARISPE, M. L. 2010. Anchorage of VEGF to the extracellular matrix conveys differential signaling responses to endothelial cells. *J Cell Biol,* 188**,** 595-609.

CHEN, X., GAYS, D., MILIA, C. & SANTORO, M. M. 2017. Cilia Control Vascular Mural Cell Recruitment in Vertebrates. *Cell Rep,* 18**,** 1033-1047.

CHEN, X., QIN, J., CHENG, C. M., TSAI, M. J. & TSAI, S. Y. 2012. COUP-TFII is a major regulator of cell cycle and Notch signaling pathways. *Mol Endocrinol,* 26**,** 1268-77.

CHIANG, I. K., FRITZSCHE, M., PICHOL-THIEVEND, C., NEAL, A., HOLMES, K., LAGENDIJK, A., OVERMAN, J., D'ANGELO, D., OMINI, A., HERMKENS, D., LESIEUR, E., LIU, K., RATNAYAKA, I., CORADA, M., BOU-GHARIOS, G., CARROLL, J., DEJANA, E., SCHULTE-MERKER, S., HOGAN, B., BELTRAME, M., DE VAL, S. & FRANCOIS, M. 2017. SoxF factors induce Notch1 expression via direct transcriptional regulation during early arterial development. *Development,* 144**,** 2629-2639.

CHOI, Y. & CHAN, A. P. 2015. PROVEAN web server: a tool to predict the functional effect of amino acid substitutions and indels. *Bioinformatics,* 31**,** 2745-2747.

CHOI, Y., SIMS, G. E., MURPHY, S., MILLER, J. R. & CHAN, A. P. 2012. Predicting the Functional Effect of Amino Acid Substitutions and Indels. *Plos One,* 7.

CIAU-UITZ, A. & PATIENT, R. 2016. The embryonic origins and genetic programming of emerging haematopoietic stem cells. *FEBS Lett,* 590**,** 4002-4015.

CLAESSON-WELSH, L. 2015. Vascular permeability--the essentials. *Ups J Med Sci,* 120**,** 135-43.

CLEMENTS, W. K., KIM, A. D., ONG, K. G., MOORE, J. C., LAWSON, N. D. & TRAVER, D. 2011. A somitic Wnt16/Notch pathway specifies haematopoietic stem cells. *Nature,* 474**,** 220-U262.

CORADA, M., MARIOTTI, M., THURSTON, G., SMITH, K., KUNKEL, R., BROCKHAUS, M., LAMPUGNANI, M. G., MARTIN-PADURA, I., STOPPACCIARO, A., RUCO, L., MCDONALD, D. M., WARD, P. A. & DEJANA, E. 1999. Vascular endothelial-cadherin is an important determinant of microvascular integrity in vivo. *Proceedings of the National Academy of Sciences of the United States of America,* 96**,** 9815-9820.

CORMIER-REGARD, S., NGUYEN, S. V. & CLAYCOMB, W. C. 1998. Adrenomedullin gene expression is developmentally regulated and induced by hypoxia in rat ventricular cardiac myocytes. *J Biol Chem,* 273**,** 17787-92.

COULTAS, L., NIEUWENHUIS, E., ANDERSON, G. A., CABEZAS, J., NAGY, A., HENKELMAN, R. M., HUI, C. C. & ROSSANT, J. 2010. Hedgehog regulates distinct vascular patterning events through VEGF-dependent and -independent mechanisms. *Blood,* 116**,** 653-660.

COVASSIN, L. D., VILLEFRANC, J. A., KACERGIS, M. C., WEINSTEIN, B. M. & LAWSON, N. D. 2006. Distinct genetic interactions between multiple Vegf receptors are required for development of different blood vessel types in zebrafish. *Proc Natl Acad Sci U S A,* 103**,** 6554-9.

CUMANO, A. & GODIN, I. 2007. Ontogeny of the hematopoietic system. *Annual Review of Immunology,* 25**,** 745-785.

DACKOR, R., FRITZ-SIX, K., SMITHIES, O. & CARON, K. 2007. Receptor activity-modifying proteins 2 and 3 have distinct physiological functions from embryogenesis to old age. *J Biol Chem,* 282**,** 18094-9.

DACKOR, R. T., FRITZ-SIX, K., DUNWORTH, W. P., GIBBONS, C. L., SMITHIES, O. & CARON, K. M. 2006. Hydrops fetalis, cardiovascular defects, and embryonic lethality in mice lacking

the Calcitonin receptor-like receptor gene. *Molecular and Cellular Biology,* 26**,** 2511-2518.

DAHM, R. & GEISLER, R. 2006. Learning from small fry: the zebrafish as a genetic model organism for aquaculture fish species. *Mar Biotechnol (NY),* 8**,** 329-45.

DAVIS, R. B., KECHELE, D. O., BLAKENEY, E. S., PAWLAK, J. B. & CARON, K. M. 2017. Lymphatic deletion of calcitonin receptor-like receptor exacerbates intestinal inflammation. *JCI Insight,* 2**,** e92465.

DE PATER, E., KAIMAKIS, P., VINK, C. S., YOKOMIZO, T., YAMADA-INAGAWA, T., VAN DER LINDEN, R., KARTALAEI, P. S., CAMPER, S. A., SPECK, N. & DZIERZAK, E. 2013. Gata2 is required for HSC generation and survival. *Journal of Experimental Medicine,* 210**,** 2843-2850.

DE VAL, S., CHI, N. C., MEADOWS, S. M., MINOVITSKY, S., ANDERSON, J. P., HARRIS, I. S., EHLERS, M. L., AGARWAL, P., VISEL, A., XU, S. M., PENNACCHIO, L. A., DUBCHAK, I., KRIEG, P. A., STAINIER, D. Y. & BLACK, B. L. 2008. Combinatorial regulation of endothelial gene expression by ets and forkhead transcription factors. *Cell,* 135**,** 1053-64.

DEJANA, E. 1997. Endothelial adherens junctions: implications in the control of vascular permeability and angiogenesis. *J Clin Invest,* 100**,** S7-10.

DEJANA, E. 2012. Endothelial cell to cell junctions and the control of vascular permeability. *Vascular Pharmacology,* 56**,** 307-307.

DEJANA, E., TOURNIER-LASSERVE, E. & WEINSTEIN, B. M. 2009. The control of vascular integrity by endothelial cell junctions: molecular basis and pathological implications. *Dev Cell,* 16**,** 209-21.

DEJANA, E., VALIRON, O., NAVARRO, P. & LAMPUGNANI, M. G. 1997. Intercellular junctions in the endothelium and the control of vascular permeability. *Ann N Y Acad Sci,* 811**,** 36-43; discussion 43-4.

DIETERLEN-LIEVRE, F. 1975. On the origin of haemopoietic stem cells in the avian embryo: an experimental approach. *J Embryol Exp Morphol,* 33**,** 607-19.

DRIEVER, W., SOLNICA-KREZEL, L., SCHIER, A. F., NEUHAUSS, S. C., MALICKI, J., STEMPLE, D. L., STAINIER, D. Y., ZWARTKRUIS, F., ABDELILAH, S., RANGINI, Z., BELAK, J. & BOGGS, C. 1996. A genetic screen for mutations affecting embryogenesis in zebrafish. *Development,* 123**,** 37-46.

DSCHIETZIG, T., AZAD, H. A., ASSWAD, L., BOHME, C., BARTSCH, C., BAUMANN, G. & STANGL, K. 2002. The adrenomedullin receptor acts as clearance receptor in pulmonary circulation. *Biochemical and Biophysical Research Communications,* 294**,** 315-318.

DUARTE, A., HIRASHIMA, M., BENEDITO, R., TRINDADE, A., DINIZ, P., BEKMAN, E., COSTA, L., HENRIQUE, D. & ROSSANT, J. 2004. Dosage-sensitive requirement for mouse Dll4 in artery development. *Genes Dev,* 18**,** 2474-8.

DUNWORTH, W. P. & CARON, K. M. 2009. G protein-coupled receptors as potential drug targets for lymphangiogenesis and lymphatic vascular diseases. *Arterioscler Thromb Vasc Biol,* 29**,** 650-6.

DUONG, T., KOLTOWSKA, K., PICHOL-THIEVEND, C., LE GUEN, L., FONTAINE, F., SMITH, K. A., TRUONG, V., SKOCZYLAS, R., STACKER, S. A., ACHEN, M. G., KOOPMAN, P., HOGAN, B. M. & FRANCOIS, M. 2014. VEGFD regulates blood vascular development by modulating SOX18 activity. *Blood,* 123**,** 1102-12.

DVORAK, A. M. & FENG, D. 2001. The vesiculo-vacuolar organelle (VVO): A new endothelial cell permeability organelle. *Journal of Histochemistry & Cytochemistry,* 49**,** 419-431.

EGAWA, G., NAKAMIZO, S., NATSUAKI, Y., DOI, H., MIYACHI, Y. & KABASHIMA, K. 2013. Intravital analysis of vascular permeability in mice using two-photon microscopy. *Sci Rep,* 3**,** 1932.

EL-BROLOSY, M. A. & STAINIER, D. Y. R. 2017. Genetic compensation: A phenomenon in search of mechanisms. *PLoS Genet,* 13**,** e1006780.

ESKENS, F. A. L. M., DE JONGE, M. J. A., BHARGAVA, P., ISOE, T., COTREAU, M. M., ESTEVES, B., HAYASHI, K., BURGER, H., THOMEER, M., VAN DOORN, L. & VERWEIJ, J. 2011. Biologic

and Clinical Activity of Tivozanib (AV-951, KRN-951), a Selective Inhibitor of VEGF Receptor-1,-2, and -3 Tyrosine Kinases, in a 4-Week-On, 2-Week-Off Schedule in Patients with Advanced Solid Tumors. *Clinical Cancer Research,* 17**,** 7156-7163.

ESSER, S., LAMPUGNANI, M. G., CORADA, M., DEJANA, E. & RISAU, W. 1998. Vascular endothelial growth factor induces VE-cadherin tyrosine phosphorylation in endothelial cells. *Journal of Cell Science,* 111**,** 1853-1865.

EVANS, D. H., PIERMARINI, P. M. & CHOE, K. P. 2005. The multifunctional fish gill: Dominant site of gas exchange, osmoregulation, acid-base regulation, and excretion of nitrogenous waste. *Physiological Reviews,* 85**,** 97-177.

FATIMA, A., WANG, Y., UCHIDA, Y., NORDEN, P., LIU, T., CULVER, A., DIETZ, W. H., CULVER, F., MILLAY, M., MUKOUYAMA, Y. S. & KUME, T. 2016. Foxc1 and Foxc2 deletion causes abnormal lymphangiogenesis and correlates with ERK hyperactivation. *J Clin Invest,* 126**,** 2437-51.

FERDOUS, A., CAPRIOLI, A., IACOVINO, M., MARTIN, C. M., MORRIS, J., RICHARDSON, J. A., LATIF, S., HAMMER, R. E., HARVEY, R. P., OLSON, E. N., KYBA, M. & GARRY, D. J. 2009. Nkx2-5 transactivates the Ets-related protein 71 gene and specifies an endothelial/endocardial fate in the developing embryo. *Proc Natl Acad Sci U S A,* 106**,** 814-9.

FERNANDEZ-SAUZE, S., DELFINO, C., MABROUK, K., DUSSERT, C., CHINOT, O., MARTIN, P. M., GRISOLI, F., OUAFIK, L. & BOUDOURESQUE, F. 2004. Effects of adrenomedullin on endothelial cells in the multistep process of angiogenesis: involvement of CRLR/RAMP2 and CRLR/RAMP3 receptors. *Int J Cancer,* 108**,** 797-804.

FERRARA, N., CARVER-MOORE, K., CHEN, H., DOWD, M., LU, L., O'SHEA, K. S., POWELL-BRAXTON, L., HILLAN, K. J. & MOORE, M. W. 1996. Heterozygous embryonic lethality induced by targeted inactivation of the VEGF gene. *Nature,* 380**,** 439-42.

FOLKMAN, J. 1995. Angiogenesis in cancer, vascular, rheumatoid and other disease. *Nat Med,* 1**,** 27-31.

FONG, G. H., ZHANG, L., BRYCE, D. M. & PENG, J. 1999. Increased hemangioblast commitment, not vascular disorganization, is the primary defect in flt-1 knock-out mice. *Development,* 126**,** 3015-25.

FOUQUET, B., WEINSTEIN, B. M., SERLUCA, F. C. & FISHMAN, M. C. 1997. Vessel patterning in the embryo of the zebrafish: guidance by notochord. *Dev Biol,* 183**,** 37-48.

FRANCOIS, M., CAPRINI, A., HOSKING, B., ORSENIGO, F., WILHELM, D., BROWNE, C., PAAVONEN, K., KARNEZIS, T., SHAYAN, R., DOWNES, M., DAVIDSON, T., TUTT, D., CHEAH, K. S., STACKER, S. A., MUSCAT, G. E., ACHEN, M. G., DEJANA, E. & KOOPMAN, P. 2008. Sox18 induces development of the lymphatic vasculature in mice. *Nature,* 456**,** 643-7.

FRENCH, C. R., SESHADRI, S., DESTEFANO, A. L., FORNAGE, M., ARNOLD, C. R., GAGE, P. J., SKARIE, J. M., DOBYNS, W. B., MILLEN, K. J., LIU, T., DIETZ, W., KUME, T., HOFKER, M., EMERY, D. J., CHILDS, S. J., WASKIEWICZ, A. J. & LEHMANN, O. J. 2014. Mutation of FOXC1 and PITX2 induces cerebral small-vessel disease. *J Clin Invest,* 124**,** 4877-81.

FRITZ-SIX, K. L., DUNWORTH, W. P., LI, M. & CARON, K. M. 2008. Adrenomedullin signaling is necessary for murine lymphatic vascular development. *J Clin Invest,* 118**,** 40-50.

FUJITA, M., CHA, Y. R., PHAM, V. N., SAKURAI, A., ROMAN, B. L., GUTKIND, J. S. & WEINSTEIN, B. M. 2011. Assembly and patterning of the vascular network of the vertebrate hindbrain. *Development,* 138**,** 1705-1715.

GAENGEL, K., GENOVE, G., ARMULIK, A. & BETSHOLTZ, C. 2009. Endothelial-mural cell signaling in vascular development and angiogenesis. *Arterioscler Thromb Vasc Biol,* 29**,** 630-8.

GALE, N. W., DOMINGUEZ, M. G., NOGUERA, I., PAN, L., HUGHES, V., VALENZUELA, D. M., MURPHY, A. J., ADAMS, N. C., LIN, H. C., HOLASH, J., THURSTON, G. & YANCOPOULOS, D. 2004. Haploinsufficiency of delta-like 4 ligand results in embryonic lethality due to major defects in arterial and vascular development. *Proceedings of the National Academy of Sciences of the United States of America,* 101**,** 15949-15954.

GAMA-NORTON, L., FERRANDO, E., RUIZ-HERGUIDO, C., LIU, Z., GUIU, J., ISLAM, A. B., LEE, S. U., YAN, M., GUIDOS, C. J., LOPEZ-BIGAS, N., MAEDA, T., ESPINOSA, L., KOPAN, R. & BIGAS, A. 2015. Notch signal strength controls cell fate in the haemogenic endothelium. *Nat Commun,* 6**,** 8510.

GARAYOA, M., BODEGAS, E., CUTTITTA, F. & MONTUENGA, L. M. 2002. Adrenomedullin in mammalian embryogenesis. *Microsc Res Tech,* 57**,** 40-54.

GEKAS, C., DIETERLEN-LIEVRE, F., ORKIN, S. H. & MIKKOLA, H. K. 2005. The placenta is a niche for hematopoietic stem cells. *Dev Cell,* 8**,** 365-75.

GENTHE, J. R. & CLEMENTS, W. K. 2017. R-spondin 1 is required for specification of hematopoietic stem cells through Wnt16 and Vegfa signaling pathways. *Development,* 144**,** 590-600.

GERHARDT, H., GOLDING, M., FRUTTIGER, M., RUHRBERG, C., LUNDKVIST, A., ABRAMSSON, A., JELTSCH, M., MITCHELL, C., ALITALO, K., SHIMA, D. & BETSHOLTZ, C. 2003. VEGF guides angiogenic sprouting utilizing endothelial tip cell filopodia. *J Cell Biol,* 161**,** 1163-77.

GERHARDT, H., RUHRBERG, C., ABRAMSSON, A., FUJISAWA, H., SHIMA, D. & BETSHOLTZ, C. 2004. Neuropilin-1 is required for endothelial tip cell guidance in the developing central nervous system. *Dev Dyn,* 231**,** 503-9.

GERING, M. & PATIENT, R. 2005. Hedgehog signaling is required for adult blood stem cell formation in zebrafish embryos. *Developmental Cell,* 8**,** 389-400.

GEUDENS, I., HERPERS, R., HERMANS, K., SEGURA, I., DE ALMODOVAR, C. R., BUSSMANN, J., DE SMET, F., VANDEVELDE, W., HOGAN, B. M., SIEKMANN, A., CLAES, F., MOORE, J. C., PISTOCCHI, A. S., LOGES, S., MAZZONE, M., MARIGGI, G., BRUYERE, F., COTELLI, F., KERJASCHKI, D., NOEL, A., FOIDART, J. M., GERHARDT, H., NY, A., LANGENBERG, T., LAWSON, N. D., DUCKERS, H. J., SCHULTE-MERKER, S., CARMELIET, P. & DEWERCHIN, M. 2010. Role of Delta-like-4/Notch in the Formation and Wiring of the Lymphatic Network in Zebrafish. *Arteriosclerosis Thrombosis and Vascular Biology,* 30**,** 1695-1702.

GIANNOTTA, M., TRANI, M. & DEJANA, E. 2013. VE-Cadherin and Endothelial Adherens Junctions: Active Guardians of Vascular Integrity. *Developmental Cell,* 26**,** 441-454.

GIBBONS, C., DACKOR, R., DUNWORTH, W., FRITZ-SIX, K. & CARON, K. M. 2007. Receptor activity-modifying proteins: RAMPing up adrenomedullin signaling. *Mol Endocrinol,* 21**,** 783-96.

GILLIS, W. Q., ST JOHN, J., BOWERMAN, B. & SCHNEIDER, S. Q. 2009. Whole genome duplications and expansion of the vertebrate GATA transcription factor gene family. *Bmc Evolutionary Biology,* 9.

GOESSLING, W. & NORTH, T. E. 2011. Hematopoietic stem cell development: using the zebrafish to identify the signaling networks and physical forces regulating hematopoiesis. *Methods Cell Biol,* 105**,** 117-36.

GORDON, K., SCHULTE, D., BRICE, G., SIMPSON, M. A., ROUKENS, M. G., VAN IMPEL, A., CONNELL, F., KALIDAS, K., JEFFERY, S., MORTIMER, P. S., MANSOUR, S., SCHULTE-MERKER, S. & OSTERGAARD, P. 2013. Mutation in vascular endothelial growth factor-C, a ligand for vascular endothelial growth factor receptor-3, is associated with autosomal dominant milroy-like primary lymphedema. *Circ Res,* 112**,** 956-60.

GORE, A. V., MONZO, K., CHA, Y. R., PAN, W. J. & WEINSTEIN, B. M. 2012. Vascular Development in the Zebrafish. *Cold Spring Harbor Perspectives in Medicine,* 2.

GOULD, D. B., PHALAN, F. C., BREEDVELD, G. J., VAN MIL, S. E., SMITH, R. S., SCHIMENTI, J. C., AGUGLIA, U., VAN DER KNAAP, M. S., HEUTINK, P. & JOHN, S. W. 2005. Mutations in Col4a1 cause perinatal cerebral hemorrhage and porencephaly. *Science,* 308**,** 1167-71.

GUIU, J., SHIMIZU, R., D'ALTRI, T., FRASER, S. T., HATAKEYAMA, J., BRESNICK, E. H., KAGEYAMA, R., DZIERZAK, E., YAMAMOTO, M., ESPINOSA, L. & BIGAS, A. 2013. Hes repressors are essential regulators of hematopoietic stem cell development downstream of Notch signaling. *Journal of Experimental Medicine,* 210**,** 71-84.

GUSTAFSSON, E., ALMONTE-BECERRIL, M., BLOCH, W. & COSTELL, M. 2013. Perlecan maintains microvessel integrity in vivo and modulates their formation in vitro. *PLoS One,* 8**,** e53715.

HABECK, H., ODENTHAL, J., WALDERICH, B., MAISCHIEN, H. M., SCHULTE-MERKER, S. & CONSORTIUM, T. S. 2002. Analysis of a zebrafish VEGF receptor mutant reveals specific disruption of angiogenesis. *Current Biology,* 12**,** 1405-1412.

HADLAND, B. K., HUPPERT, S. S., KANUNGO, J., XUE, Y. Z., JIANG, R. L., GRIDLEY, T., CONLON, R. A., CHENG, A. M., KOPAN, R. & LONGMORE, G. D. 2004. A requirement for Notch1 distinguishes 2 phases of definitive hematopoiesis during development. *Blood,* 104**,** 3097-3105.

HAFFTER, P., GRANATO, M., BRAND, M., MULLINS, M. C., HAMMERSCHMIDT, M., KANE, D. A., ODENTHAL, J., VAN EEDEN, F. J., JIANG, Y. J., HEISENBERG, C. P., KELSH, R. N., FURUTANI-SEIKI, M., VOGELSANG, E., BEUCHLE, D., SCHACH, U., FABIAN, C. & NUSSLEIN-VOLHARD, C. 1996. The identification of genes with unique and essential functions in the development of the zebrafish, Danio rerio. *Development,* 123**,** 1-36.

HALDIPUR, P., GILLIES, G. S., JANSON, O. K., CHIZHIKOV, V. V., MITHAL, D. S., MILLER, R. J. & MILLEN, K. J. 2014. Foxc1 dependent mesenchymal signalling drives embryonic cerebellar growth. *Elife,* 3.

HAMM, M. J., KIRCHMAIER, B. C. & HERZOG, W. 2016. Sema3d controls collective endothelial cell migration by distinct mechanisms via Nrp1 and PlxnD1. *J Cell Biol,* 215**,** 415-430.

HAN, B., BHOWMICK, N., QU, Y., CHUNG, S., GIULIANO, A. E. & CUI, X. 2017. FOXC1: an emerging marker and therapeutic target for cancer. *Oncogene,* 36**,** 3957-3963.

HAN, B., QU, Y., JIN, Y., YU, Y., DENG, N., WAWROWSKY, K., ZHANG, X., LI, N., BOSE, S., WANG, Q., SAKKIAH, S., ABROL, R., JENSEN, T. W., BERMAN, B. P., TANAKA, H., JOHNSON, J., GAO, B., HAO, J., LIU, Z., BUTTYAN, R., RAY, P. S., HUNG, M. C., GIULIANO, A. E. & CUI, X. 2015. FOXC1 Activates Smoothened-Independent Hedgehog Signaling in Basal-like Breast Cancer. *Cell Rep,* 13**,** 1046-58.

HASSO, S. & CHAN, J. 2011. Chemical approaches to angiogenesis in development and regeneration. *Methods Cell Biol,* 101**,** 181-95.

HAYASHI, H. & KUME, T. 2008a. Forkhead transcription factors regulate expression of the chemokine receptor CXCR4 in endothelial cells and CXCL12-induced cell migration. *Biochem Biophys Res Commun,* 367**,** 584-9.

HAYASHI, H. & KUME, T. 2008b. Foxc transcription factors directly regulate Dll4 and Hey2 expression by interacting with the VEGF-Notch signaling pathways in endothelial cells. *PLoS One,* 3**,** e2401.

HEATON, J., LIN, B., CHANG, J. K., STEINBERG, S., HYMAN, A. & LIPPTON, H. 1995. Pulmonary Vasodilation to Adrenomedullin - a Novel Peptide in Humans. *American Journal of Physiology-Heart and Circulatory Physiology,* 268**,** H2211-H2215.

HELKER, C. S., SCHUERMANN, A., KARPANEN, T., ZEUSCHNER, D., BELTING, H. G., AFFOLTER, M., SCHULTE-MERKER, S. & HERZOG, W. 2013. The zebrafish common cardinal veins develop by a novel mechanism: lumen ensheathment. *Development,* 140**,** 2776-86.

HELKER, C. S., SCHUERMANN, A., POLLMANN, C., CHNG, S. C., KIEFER, F., REVERSADE, B. & HERZOG, W. 2015. The hormonal peptide Elabela guides angioblasts to the midline during vasculogenesis. *Elife,* 4.

HELLSTROM, M., PHNG, L. K., HOFMANN, J. J., WALLGARD, E., COULTAS, L., LINDBLOM, P., ALVA, J., NILSSON, A. K., KARLSSON, L., GAIANO, N., YOON, K., ROSSANT, J., IRUELA-ARISPE, M. L., KALEN, M., GERHARDT, H. & BETSHOLTZ, C. 2007. Dll4 signalling through Notch1 regulates formation of tip cells during angiogenesis. *Nature,* 445**,** 776-80.

HERBERT, S. P. & STAINIER, D. Y. 2011. Molecular control of endothelial cell behaviour during blood vessel morphogenesis. *Nat Rev Mol Cell Biol,* 12**,** 551-64.

HERMKENS, D. M., VAN IMPEL, A., URASAKI, A., BUSSMANN, J., DUCKERS, H. J. & SCHULTE-MERKER, S. 2015. Sox7 controls arterial specification in conjunction with hey2 and efnb2 function. *Development,* 142**,** 1695-704.

HIPPENSTIEL, S., WITZENRATH, M., SCHMECK, B., HOCKE, A., KRISP, M., KRULL, M., SEYBOLD, J., SEEGER, W., RASCHER, W., SCHUTTE, H. & SUTTORP, N. 2002. Adrenomedullin reduces endothelial hyperpermeability. *Circulation Research,* 91**,** 618-625.

HIRATSUKA, S., NAKAO, K., NAKAMURA, K., KATSUKI, M., MARU, Y. & SHIBUYA, M. 2005. Membrane fixation of vascular endothelial growth factor receptor 1 ligand-binding domain is important for vasculogenesis and angiogenesis in mice. *Mol Cell Biol,* 25**,** 346-54.

HOGAN, B. M., BOS, F. L., BUSSMANN, J., WITTE, M., CHI, N. C., DUCKERS, H. J. & SCHULTE-MERKER, S. 2009a. Ccbe1 is required for embryonic lymphangiogenesis and venous sprouting. *Nat Genet,* 41**,** 396-8.

HOGAN, B. M., HERPERS, R., WITTE, M., HELOTERA, H., ALITALO, K., DUCKERS, H. J. & SCHULTE-MERKER, S. 2009b. Vegfc/Flt4 signalling is suppressed by Dll4 in developing zebrafish intersegmental arteries. *Development,* 136**,** 4001-9.

HONG, C. C., PETERSON, Q. P., HONG, J. Y. & PETERSON, R. T. 2006. Artery/vein specification is governed by opposing phosphatidylinositol-3 kinase and MAP kinase/ERK signaling. *Current Biology,* 16**,** 1366-1372.

HOWE, K., CLARK, M. D., TORROJA, C. F., TORRANCE, J., BERTHELOT, C., MUFFATO, M., COLLINS, J. E., HUMPHRAY, S., MCLAREN, K., MATTHEWS, L., MCLAREN, S., SEALY, I., CACCAMO, M., CHURCHER, C., SCOTT, C., BARRETT, J. C., KOCH, R., RAUCH, G. J., WHITE, S., CHOW, W., KILIAN, B., QUINTAIS, L. T., GUERRA-ASSUNCAO, J. A., ZHOU, Y., GU, Y., YEN, J., VOGEL, J. H., EYRE, T., REDMOND, S., BANERJEE, R., CHI, J., FU, B., LANGLEY, E., MAGUIRE, S. F., LAIRD, G. K., LLOYD, D., KENYON, E., DONALDSON, S., SEHRA, H., ALMEIDA-KING, J., LOVELAND, J., TREVANION, S., JONES, M., QUAIL, M., WILLEY, D., HUNT, A., BURTON, J., SIMS, S., MCLAY, K., PLUMB, B., DAVIS, J., CLEE, C., OLIVER, K., CLARK, R., RIDDLE, C., ELLIOT, D., THREADGOLD, G., HARDEN, G., WARE, D., BEGUM, S., MORTIMORE, B., KERRY, G., HEATH, P., PHILLIMORE, B., TRACEY, A., CORBY, N., DUNN, M., JOHNSON, C., WOOD, J., CLARK, S., PELAN, S., GRIFFITHS, G., SMITH, M., GLITHERO, R., HOWDEN, P., BARKER, N., LLOYD, C., STEVENS, C., HARLEY, J., HOLT, K., PANAGIOTIDIS, G., LOVELL, J., BEASLEY, H., HENDERSON, C., GORDON, D., AUGER, K., WRIGHT, D., COLLINS, J., RAISEN, C., DYER, L., LEUNG, K., ROBERTSON, L., AMBRIDGE, K., LEONGAMORNLERT, D., MCGUIRE, S., GILDERTHORP, R., GRIFFITHS, C., MANTHRAVADI, D., NICHOL, S., BARKER, G., et al. 2013. The zebrafish reference genome sequence and its relationship to the human genome. *Nature,* 496**,** 498-503.

HRUSCHA, A., KRAWITZ, P., RECHENBERG, A., HEINRICH, V., HECHT, J., HAASS, C. & SCHMID, B. 2013. Efficient CRISPR/Cas9 genome editing with low off-target effects in zebrafish. *Development,* 140**,** 4982-4987.

HSU, C. H., LIN, J. S., PO LAI, K., LI, J. W., CHAN, T. F., YOU, M. S., TSE, W. K. & JIANG, Y. J. 2015. A new mib allele with a chromosomal deletion covering foxc1a exhibits anterior somite specification defect. *Sci Rep,* 5**,** 10673.

HWANG, W. Y., FU, Y., REYON, D., MAEDER, M. L., TSAI, S. Q., SANDER, J. D., PETERSON, R. T., YEH, J. R. & JOUNG, J. K. 2013. Efficient genome editing in zebrafish using a CRISPR-Cas system. *Nat Biotechnol,* 31**,** 227-9.

ICHIKAWA-SHINDO, Y., SAKURAI, T., KAMIYOSHI, A., KAWATE, H., LINURNA, N., YOSHIZAWA, T., KOYAMA, T., FUKUCHI, J., LIMURO, S., MORIYAMA, N., KAWAKAMI, H., MURATA, T., KANGAWA, K., NAGAI, R. & SHINDO, T. 2008. The GPCR modulator protein RAMP2 is essential for angiogenesis and vascular integrity. *Journal of Clinical Investigation,* 118**,** 29-39.

IIDA, K., KOSEKI, H., KAKINUMA, H., KATO, N., MIZUTANI-KOSEKI, Y., OHUCHI, H., YOSHIOKA, H., NOJI, S., KAWAMURA, K., KATAOKA, Y., UENO, F., TANIGUCHI, M., YOSHIDA, N., SUGIYAMA, T. & MIURA, N. 1997. Essential roles of the winged helix transcription factor MFH-1 in aortic arch patterning and skeletogenesis. *Development,* 124**,** 4627-38.

IIMURO, S., SHINDO, T., MORIYAMA, N., AMAKI, T., NIU, P., TAKEDA, N., IWATA, H., ZHANG, Y., EBIHARA, A. & NAGAI, R. 2004. Angiogenic effects of adrenomedullin in ischemia and tumor growth. *Circ Res,* 95**,** 415-23.

IRRTHUM, A., DEVRIENDT, K., CHITAYAT, D., MATTHIJS, G., GLADE, C., STEIJLEN, P. M., FRYNS, J. P., VAN STEENSEL, M. A. & VIKKULA, M. 2003. Mutations in the transcription factor gene SOX18 underlie recessive and dominant forms of hypotrichosis-lymphedema-telangiectasia. *Am J Hum Genet,* 72**,** 1470-8.

ISOGAI, S., HORIGUCHI, M. & WEINSTEIN, B. M. 2001. The vascular anatomy of the developing zebrafish: an atlas of embryonic and early larval development. *Dev Biol,* 230**,** 278-301.

ISOGAI, S., LAWSON, N. D., TORREALDAY, S., HORIGUCHI, M. & WEINSTEIN, B. M. 2003. Angiogenic network formation in the developing vertebrate trunk. *Development,* 130**,** 5281-90.

IVANOV, K. I., AGALAROV, Y., VALMU, L., SAMUILOVA, O., LIEBL, J., HOUHOU, N., MABY-EL HAJJAMI, H., NORRMEN, C., JAQUET, M., MIURA, N., ZANGGER, N., YLA-HERTTUALA, S., DELORENZI, M. & PETROVA, T. V. 2013. Phosphorylation regulates FOXC2-mediated transcription in lymphatic endothelial cells. *Mol Cell Biol,* 33**,** 3749-61.

JACOB, A., WU, R. & WANG, P. 2012. Regulation of RAMP expression in diseases. *Adv Exp Med Biol,* 744**,** 87-103.

JAIN, R. K. 2003. Molecular regulation of vessel maturation. *Nat Med,* 9**,** 685-93.

JANG, I. H., LU, Y. F., ZHAO, L., WENZEL, P. L., KUME, T., DATTA, S. M., ARORA, N., GUIU, J., LAGHA, M., KIM, P. G., DO, E. K., KIM, J. H., SCHLAEGER, T. M., ZON, L. I., BIGAS, A., BURNS, C. E. & DALEY, G. Q. 2015. Notch1 acts via Foxc2 to promote definitive hematopoiesis via effects on hemogenic endothelium. *Blood,* 125**,** 1418-26.

JELTSCH, M., TAMMELA, T., ALITALO, K. & WILTING, J. 2003. Genesis and pathogenesis of lymphatic vessels. *Cell Tissue Res,* 314**,** 69-84.

JIA, H., BAGHERZADEH, A., BICKNELL, R., DUCHEN, M. R., LIU, D. & ZACHARY, I. 2004a. Vascular endothelial growth factor (VEGF)-D and VEGF-A differentially regulate KDR-mediated signaling and biological function in vascular endothelial cells. *J Biol Chem,* 279**,** 36148-57.

JIA, J., TONG, C., WANG, B., LUO, L. & JIANG, J. 2004b. Hedgehog signalling activity of Smoothened requires phosphorylation by protein kinase A and casein kinase I. *Nature,* 432**,** 1045-50.

JIN, D., HARADA, K., OHNISHI, S., YAMAHARA, K., KANGAWA, K. & NAGAYA, N. 2008. Adrenomedullin induces lymphangiogenesis and ameliorates secondary lymphoedema. *Cardiovasc Res,* 80**,** 339-45.

JOHNSON, B. D., MATHER, K. J. & WALLACE, J. P. 2011. Mechanotransduction of shear in the endothelium: Basic studies and clinical implications. *Vascular Medicine,* 16**,** 365-377.

JULICH, D., HWEE LIM, C., ROUND, J., NICOLAIJE, C., SCHROEDER, J., DAVIES, A., GEISLER, R., LEWIS, J., JIANG, Y. J., HOLLEY, S. A. & TUBINGEN SCREEN, C. 2005. beamter/deltaC and the role of Notch ligands in the zebrafish somite segmentation, hindbrain neurogenesis and hypochord differentiation. *Dev Biol,* 286**,** 391-404.

KADMIEL, M., FRITZ-SIX, K. L. & CARON, K. M. 2012. Understanding RAMPs through genetically engineered mouse models. *Adv Exp Med Biol,* 744**,** 49-60.

KAESTNER, K. H., BLECKMANN, S. C., MONAGHAN, A. P., SCHLONDORFF, J., MINCHEVA, A., LICHTER, P. & SCHUTZ, G. 1996. Clustered arrangement of winged helix genes fkh-6 and MFH-1: Possible implications for mesoderm development. *Development,* 122**,** 1751-1758.

KALEV-ZYLINSKA, M. L., HORSFIELD, J. A., FLORES, M. V. C., POSTLETHWAIT, J. H., VITAS, M. R., BAAS, A. M., CROSIER, P. S. & CROSIER, K. E. 2002. Runx1 is required for zebrafish blood and vessel development and expression of a human RUNX1-CBF2T1 transgene advances a model for studies of leukemogenesis. *Development,* 129**,** 2015-2030.

KAMITANI, S., ASAKAWA, M., SHIMEKAKE, Y., KUWASAKO, K., NAKAHARA, K. & SAKATA, T. 1999. The RAMP2/CRLR complex is a functional adrenomedullin receptor in human endothelial and vascular smooth muscle cells. *Febs Letters,* 448**,** 111-114.

KARKKAINEN, M. J., HAIKO, P., SAINIO, K., PARTANEN, J., TAIPALE, J., PETROVA, T. V., JELTSCH, M., JACKSON, D. G., TALIKKA, M., RAUVALA, H., BETSHOLTZ, C. & ALITALO, K. 2004. Vascular endothelial growth factor C is required for sprouting of the first lymphatic vessels from embryonic veins. *Nat Immunol,* 5**,** 74-80.

KARPANEN, T. & SCHULTE-MERKER, S. 2011. Zebrafish Provides a Novel Model for Lymphatic Vascular Research. *Zebrafish: Disease Models and Chemical Screens, 3rd Edition,* 105**,** 223-238.

KAUFMANN, E. & KNOCHEL, W. 1996. Five years on the wings of fork head. *Mech Dev,* 57**,** 3-20.

KENNEDY, M., FIRPO, M., CHOL, K., WALL, C., ROBERTSON, S., KABRUN, N. & KELLER, G. 1997. A common precursor for primitive erythropoiesis and definitive haematopoiesis. *Nature,* 386**,** 488-493.

KIM, A. D., MELICK, C. H., CLEMENTS, W. K., STACHURA, D. L., DISTEL, M., PANAKOVA, D., MACRAE, C., MORK, L. A., CRUMP, J. G. & TRAVER, D. 2014. Discrete Notch signaling requirements in the specification of hematopoietic stem cells. *EMBO J,* 33**,** 2363-73.

KIM, W., MOON, S. O., SUNG, M. J., KIM, S. H., LEE, S., SO, J. N. & PARK, S. K. 2003. Angiogenic role of adrenomedullin through activation of Akt, mitogen-activated protein kinase, and focal adhesion kinase in endothelial cells. *FASEB J,* 17**,** 1937-9.

KISSA, K. & HERBOMEL, P. 2010. Blood stem cells emerge from aortic endothelium by a novel type of cell transition. *Nature,* 464**,** 112-5.

KOBAYASHI, I., KOBAYASHI-SUN, J., KIM, A. D., POUGET, C., FUJITA, N., SUDA, T. & TRAVER, D. 2014. Jam1a-Jam2a interactions regulate haematopoietic stem cell fate through Notch signalling. *Nature,* 512**,** 319-23.

KOHLI, V., SCHUMACHER, J. A., DESAI, S. P., REHN, K. & SUMANAS, S. 2013. Arterial and venous progenitors of the major axial vessels originate at distinct locations. *Dev Cell,* 25**,** 196-206.

KOHN, S., NAGY, J. A., DVORAK, H. F. & DVORAK, A. M. 1992. Pathways of macromolecular tracer transport across venules and small veins. Structural basis for the hyperpermeability of tumor blood vessels. *Lab Invest,* 67**,** 596-607.

KOLTOWSKA, K., BETTERMAN, K. L., HARVEY, N. L. & HOGAN, B. M. 2013. Getting out and about: the emergence and morphogenesis of the vertebrate lymphatic vasculature. *Development,* 140**,** 1857-70.

KOLTOWSKA, K., LAGENDIJK, A. K., PICHOL-THIEVEND, C., FISCHER, J. C., FRANCOIS, M., OBER, E. A., YAP, A. S. & HOGAN, B. M. 2015. Vegfc Regulates Bipotential Precursor Division and Prox1 Expression to Promote Lymphatic Identity in Zebrafish. *Cell Rep,* 13**,** 1828-41.

KOO, H. Y. & KUME, T. 2013. FoxC1-dependent regulation of vascular endothelial growth factor signaling in corneal avascularity. *Trends Cardiovasc Med,* 23**,** 1-4.

KOYAMA, T., OCHOA-CALLEJERO, L., SAKURAI, T., KAMIYOSHI, A., ICHIKAWA-SHINDO, Y., IINUMA, N., ARAI, T., YOSHIZAWA, T., IESATO, Y., LEI, Y., UETAKE, R., OKIMURA, A., YAMAUCHI, A., TANAKA, M., IGARASHI, K., TORIYAMA, Y., KAWATE, H., ADAMS, R. H., KAWAKAMI, H., MOCHIZUKI, N., MARTINEZ, A. & SHINDO, T. 2013. Vascular endothelial adrenomedullin-RAMP2 system is essential for vascular integrity and organ homeostasis. *Circulation,* 127**,** 842-53.

KREBS, L. T., SHUTTER, J. R., TANIGAKI, K., HONJO, T., STARK, K. L. & GRIDLEY, T. 2004. Haploinsufficient lethality and formation of arteriovenous malformations in Notch pathway mutants. *Genes Dev,* 18**,** 2469-73.

KREBS, L. T., XUE, Y., NORTON, C. R., SHUTTER, J. R., MAGUIRE, M., SUNDBERG, J. P., GALLAHAN, D., CLOSSON, V., KITAJEWSKI, J., CALLAHAN, R., SMITH, G. H., STARK, K. L. & GRIDLEY, T. 2000. Notch signaling is essential for vascular morphogenesis in mice. *Genes Dev,* 14**,** 1343-52.

KRUEGER, J., LIU, D., SCHOLZ, K., ZIMMER, A., SHI, Y., KLEIN, C., SIEKMANN, A., SCHULTE-MERKER, S., CUDMORE, M., AHMED, A. & LE NOBLE, F. 2011. Flt1 acts as a negative regulator of tip cell formation and branching morphogenesis in the zebrafish embryo. *Development,* 138**,** 2111-20.

KRYMSKAYA, V. P., HOFFMAN, R., ESZTERHAS, A., CIOCCA, V. & PANETTIERI, R. A. 1997. TGF-beta 1 modulates EGF-stimulated phosphatidylinositol 3-kinase activity in human airway smooth muscle cells. *American Journal of Physiology-Lung Cellular and Molecular Physiology,* 273**,** L1220-L1227.

KUCHLER, A. M., GJINI, E., PETERSON-MADURO, J., CANCILLA, B., WOLBURG, H. & SCHULTE-MERKER, S. 2006. Development of the zebrafish lymphatic system requires VEGFC signaling. *Curr Biol,* 16**,** 1244-8.

KUHNERT, F., MANCUSO, M. R., SHAMLOO, A., WANG, H. T., CHOKSI, V., FLOREK, M., SU, H., FRUTTIGER, M., YOUNG, W. L., HEILSHORN, S. C. & KUO, C. J. 2010. Essential regulation of CNS angiogenesis by the orphan G protein-coupled receptor GPR124. *Science,* 330**,** 985-9.

KUHNERT, F., TAM, B. Y. Y., SENNINO, B., GRAY, J. T., YUAN, J., JOCSON, A., NAYAK, N. R., MULLIGAN, R. C., MCDONALD, D. M. & KUO, C. J. 2008. Soluble receptor-mediated selective inhibition of VEGFR and PDGFR beta signaling during physiologic and tumor angiogenesis. *Proceedings of the National Academy of Sciences of the United States of America,* 105**,** 10185-10190.

KUMANO, K., CHIBA, S., KUNISATO, A., SATA, M., SAITO, T., NAKAGAMI-YAMAGUCHI, E., YAMAGUCHI, T., MASUDA, S., SHIMIZU, K., TAKAHASHI, T., OGAWA, S., HAMADA, Y. & HIRAI, H. 2003. Notch1 but not Notch2 is essential for generating hematopoietic stem cells from endothelial cells. *Immunity,* 18**,** 699-711.

KUME, T., DENG, K. & HOGAN, B. L. 2000. Murine forkhead/winged helix genes Foxc1 (Mf1) and Foxc2 (Mfh1) are required for the early organogenesis of the kidney and urinary tract. *Development,* 127**,** 1387-95.

KUME, T., DENG, K. Y., WINFREY, V., GOULD, D. B., WALTER, M. A. & HOGAN, B. L. 1998. The forkhead/winged helix gene Mf1 is disrupted in the pleiotropic mouse mutation congenital hydrocephalus. *Cell,* 93**,** 985-96.

KUME, T., JIANG, H., TOPCZEWSKA, J. M. & HOGAN, B. L. 2001. The murine winged helix transcription factors, Foxc1 and Foxc2, are both required for cardiovascular development and somitogenesis. *Genes Dev,* 15**,** 2470-82.

LAFONT, A. G., WANG, Y. F., CHEN, G. D., LIAO, B. K., TSENG, Y. C., HUANG, C. J. & HWANG, P. P. 2011. Involvement of Calcitonin and Its Receptor in the Control of Calcium-Regulating Genes and Calcium Homeostasis in Zebrafish (Danio rerio). *Journal of Bone and Mineral Research,* 26**,** 1072-1083.

LAGERSTROM, M. C. & SCHIOTH, H. B. 2008. Structural diversity of G protein-coupled receptors and significance for drug discovery. *Nat Rev Drug Discov,* 7**,** 339-57.

LAI, E., CLARK, K. L., BURLEY, S. K. & DARNELL, J. E., JR. 1993. Hepatocyte nuclear factor 3/fork head or "winged helix" proteins: a family of transcription factors of diverse biologic function. *Proc Natl Acad Sci U S A,* 90**,** 10421-3.

LANCRIN, C., SROCZYNSKA, P., STEPHENSON, C., ALLEN, T., KOUSKOFF, V. & LACAUD, G. 2009. The haemangioblast generates haematopoietic cells through a haemogenic endothelium stage. *Nature,* 457**,** 892-5.

LAWSON, M., FRIDAY, E., SALLAH, S., GLASS, J. & TURTURRO, F. 2003a. Analysis of cellular constitutive secretion of VEGF(165), expression of alpha nu beta 5 integrin, levels of eukaryotic initiation factor (eIF4E) and response to rapamycin-mediated inhibition of mTOR-proteins in cells derived from ALK(+)-ALCL, acute myeloid leukemia (AML), and multiple myeloma (MM). *Blood,* 102**,** 280b-280b.

LAWSON, N. D., MUGFORD, J. W., DIAMOND, B. A. & WEINSTEIN, B. M. 2003b. phospholipase C gamma-1 is require downstream of vascular endothelial growth factor during arterial development. *Genes & Development,* 17**,** 1346-1351.

LAWSON, N. D., SCHEER, N., PHAM, V. N., KIM, C. H., CHITNIS, A. B., CAMPOS-ORTEGA, J. A. & WEINSTEIN, B. M. 2001. Notch signaling is required for arterial-venous differentiation during embryonic vascular development. *Development,* 128**,** 3675-3683.

LAWSON, N. D., VOGEL, A. M. & WEINSTEIN, B. M. 2002. sonic hedgehog and vascular endothelial growth factor act upstream of the Notch pathway during arterial endothelial differentiation. *Dev Cell,* 3**,** 127-36.

LAWSON, N. D. & WEINSTEIN, B. M. 2002a. Arteries and veins: making a difference with zebrafish. *Nat Rev Genet,* 3**,** 674-82.

LAWSON, N. D. & WEINSTEIN, B. M. 2002b. In vivo imaging of embryonic vascular development using transgenic zebrafish. *Dev Biol,* 248**,** 307-18.

LE BRAS, A., VIJAYARAJ, P. & OETTGEN, P. 2010. Molecular mechanisms of endothelial differentiation. *Vasc Med,* 15**,** 321-31.

LE GUEN, L., KARPANEN, T., SCHULTE, D., HARRIS, N. C., KOLTOWSKA, K., ROUKENS, G., BOWER, N. I., VAN IMPEL, A., STACKER, S. A., ACHEN, M. G., SCHULTE-MERKER, S. & HOGAN, B. M. 2014. Ccbe1 regulates Vegfc-mediated induction of Vegfr3 signaling during embryonic lymphangiogenesis. *Development,* 141**,** 1239-U123.

LEE, D., PARK, C., LEE, H., LUGUS, J. J., KIM, S. H., ARENTSON, E., CHUNG, Y. S., GOMEZ, G., KYBA, M., LIN, S., JANKNECHT, R., LIM, D. S. & CHOI, K. 2008. ER71 acts downstream of BMP, Notch, and Wnt signaling in blood and vessel progenitor specification. *Cell Stem Cell,* 2**,** 497-507.

LEE, P., GOISHI, K., DAVIDSON, A. J., MANNIX, R., ZON, L. & KLAGSBRUN, M. 2002. Neuropilin-1 is required for vascular development and is a mediator of VEGF-dependent angiogenesis in zebrafish. *Proc Natl Acad Sci U S A,* 99**,** 10470-5.

LEE, S., KANG, J., YOO, J., GANESAN, S. K., COOK, S. C., AGUILAR, B., RAMU, S., LEE, J. & HONG, Y. K. 2009. Prox1 physically and functionally interacts with COUP-TFII to specify lymphatic endothelial cell fate. *Blood,* 113**,** 1856-9.

LESLIE, J. D., ARIZA-MCNAUGHTON, L., BERMANGE, A. L., MCADOW, R., JOHNSON, S. L. & LEWIS, J. 2007. Endothelial signalling by the Notch ligand Delta-like 4 restricts angiogenesis. *Development,* 134**,** 839-44.

LEVESQUE, M. J., NEREM, R. M. & SPRAGUE, E. A. 1990. Vascular Endothelial-Cell Proliferation in Culture and the Influence of Flow. *Biomaterials,* 11**,** 702-707.

LI, J., YUE, Y., DONG, X., JIA, W., LI, K., LIANG, D., DONG, Z., WANG, X., NAN, X., ZHANG, Q. & ZHAO, Q. 2015. Zebrafish foxc1a plays a crucial role in early somitogenesis by restricting the expression of aldh1a2 directly. *J Biol Chem,* 290**,** 10216-28.

LIANG, D., XU, X. Z., CHIN, A. J., BALASUBRAMANIYAN, N. V., TEO, M. A. L., LAM, T. J., WEINBERG, E. S. & GE, R. W. 1998. Cloning and characterization of vascular endothelial growth factor (VEGF) from zebrafish, Danio rerio. *Biochimica Et Biophysica Acta-Gene Structure and Expression,* 1397**,** 14-20.

LIAO, B. K. & OATES, A. C. 2017. Delta-Notch signalling in segmentation. *Arthropod Struct Dev,* 46**,** 429-447.

LIEBL, J., ZHANG, S., MOSER, M., AGALAROV, Y., DEMIR, C. S., HAGER, B., BIBB, J. A., ADAMS, R. H., KIEFER, F., MIURA, N., PETROVA, T. V., VOLLMAR, A. M. & ZAHLER, S. 2015. Cdk5 controls lymphatic vessel development and function by phosphorylation of Foxc2. *Nat Commun,* 6**,** 7274.

LIESCHKE, G. J., OATES, A. C., PAW, B. H., THOMPSON, M. A., HALL, N. E., WARD, A. C., HO, R. K., ZON, L. I. & LAYTON, J. E. 2002. Zebrafish SPI-1 (PU.1) marks a site of myeloid development independent of primitive erythropoiesis: implications for axial patterning. *Dev Biol,* 246**,** 274-95.

LIU, F., KANG, I., PARK, C., CHANG, W., WANG, W., LEE, D., LIM, D. S., VITTET, D., NERBONNE, J. M. & CHOI, K. 2012. ER71 specifies Flk-1(+) hemangiogenic mesoderm by inhibiting cardiac mesoderm and Wnt signaling. *Blood,* 119**,** 3295-3305.

LIU, F., LI, D. F., YU, Y. Y. L., KANG, I., CHA, M. J., KIM, J. Y., PARK, C., WATSON, D. K., WANG, T. & CHOI, K. 2015. Induction of hematopoietic and endothelial cell program orchestrated by ETS transcription factor ER71/ETV2. *Embo Reports,* 16**,** 654-669.

LOBOV, I. B., RENARD, R. A., PAPADOPOULOS, N., GALE, N. W., THURSTON, G., YANCOPOULOS, G. D. & WIEGAND, S. J. 2007. Delta-like ligand 4 (Dll4) is induced by VEGF as a negative regulator of angiogenic sprouting. *Proc Natl Acad Sci U S A,* 104**,** 3219-24.

LUGUS, J. J., CHUNG, Y. S., MILLS, J. C., KIM, S. I., GRASS, J., KYBA, M., DOHERTY, J. M., BRESNICK, E. H. & CHOI, K. 2007. GATA2 functions at multiple steps in hemangioblast development and differentiation. *Development,* 134**,** 393-405.

MAISONPIERRE, P. C., SURI, C., JONES, P. F., BARTUNKOVA, S., WIEGAND, S., RADZIEJEWSKI, C., COMPTON, D., MCCLAIN, J., ALDRICH, T. H., PAPADOPOULOS, N., DALY, T. J., DAVIS, S., SATO, T. N. & YANCOPOULOS, G. D. 1997. Angiopoietin-2, a natural antagonist for Tie2 that disrupts in vivo angiogenesis. *Science,* 277**,** 55-60.

MAJESKY, M. W. 2007. Developmental basis of vascular smooth muscle diversity. *Arteriosclerosis Thrombosis and Vascular Biology,* 27**,** 1248-1258.

MAKINEN, T., JUSSILA, L., VEIKKOLA, T., KARPANEN, T., KETTUNEN, M. I., PULKKANEN, K. J., KAUPPINEN, R., JACKSON, D. G., KUBO, H., NISHIKAWA, S., YLA-HERTTUALA, S. & ALITALO, K. 2001. Inhibition of lymphangiogenesis with resulting lymphedema in transgenic mice expressing soluble VEGF receptor-3. *Nat Med,* 7**,** 199-205.

MAMLUK, R., GECHTMAN, Z., KUTCHER, M. E., GASIUNAS, N., GALLAGHER, J. & KLAGSBRUN, M. 2002. Neuropilin-1 binds vascular endothelial growth factor 165, placenta growth factor-2, and heparin via its b1b2 domain. *J Biol Chem,* 277**,** 24818-25.

MATSUOKA, R. L., MARASS, M., AVDESH, A., HELKER, C. S., MAISCHEIN, H. M., GROSSE, A. S., KAUR, H., LAWSON, N. D., HERZOG, W. & STAINIER, D. Y. 2016. Radial glia regulate vascular patterning around the developing spinal cord. *Elife,* 5.

MCLATCHIE, L. M., FRASER, N. J., MAIN, M. J., WISE, A., BROWN, J., THOMPSON, N., SOLARI, R., LEE, M. G. & FOORD, S. M. 1998. RAMPs regulate the transport and ligand specificity of the calcitonin-receptor-like receptor. *Nature,* 393**,** 333-9.

MEAD, T. J. & YUTZEY, K. E. 2012. Notch signaling and the developing skeleton. *Adv Exp Med Biol,* 727**,** 114-30.

MEARS, A. J., MIRZAYANS, F., GOULD, D. B., PEARCE, W. G. & WALTER, M. A. 1996. Autosomal dominant iridogoniodysgenesis anomaly maps to 6p25. *American Journal of Human Genetics,* 59**,** 1321-1327.

MEDVINSKY, A. & DZIERZAK, E. 1996. Definitive hematopoiesis is autonomously initiated by the AGM region. *Cell,* 86**,** 897-906.

MEDVINSKY, A., RYBTSOV, S. & TAOUDI, S. 2011. Embryonic origin of the adult hematopoietic system: advances and questions. *Development,* 138**,** 1017-31.

MELLOR, R. H., TATE, N., STANTON, A. W., HUBERT, C., MAKINEN, T., SMITH, A., BURNAND, K. G., JEFFERY, S., LEVICK, J. R. & MORTIMER, P. S. 2011. Mutations in FOXC2 in humans

(lymphoedema distichiasis syndrome) cause lymphatic dysfunction on dependency. *J Vasc Res,* 48**,** 397-407.

MISHRA, S., CHOE, Y., PLEASURE, S. J. & SIEGENTHALER, J. A. 2016. Cerebrovascular defects in Foxc1 mutants correlate with aberrant WNT and VEGF-A pathways downstream of retinoic acid from the meninges. *Dev Biol,* 420**,** 148-165.

MIURA, N., IIDA, K., KAKINUMA, H., YANG, X. L. & SUGIYAMA, T. 1997. Isolation of the mouse (MFH-1) and human (FKHL14) mesenchyme fork head-1 genes reveals conservation of their gene and protein structures. *Genomics,* 41**,** 489-492.

MIURA, N., WANAKA, A., TOHYAMA, M. & TANAKA, K. 1993. Mfh-1, a New Member of the Fork Head Domain Family, Is Expressed in Developing Mesenchyme. *Febs Letters,* 326**,** 171-176.

MONTEIRO, R., PINHEIRO, P., JOSEPH, N., PETERKIN, T., KOTH, J., REPAPI, E., BONKHOFER, F., KIRMIZITAS, A. & PATIENT, R. 2016. Transforming Growth Factor beta Drives Hemogenic Endothelium Programming and the Transition to Hematopoietic Stem Cells. *Dev Cell,* 38**,** 358-70.

MOORE, M. A. & METCALF, D. 1970. Ontogeny of the haemopoietic system: yolk sac origin of in vivo and in vitro colony forming cells in the developing mouse embryo. *Br J Haematol,* 18**,** 279-96.

MOYON, D., PARDANAUD, L., YUAN, L., BREANT, C. & EICHMANN, A. 2001. Plasticity of endothelial cells during arterial-venous differentiation in the avian embryo. *Development,* 128**,** 3359-3370.

MUKOUYAMA, Y. S., GERBER, H. P., FERRARA, N., GU, C. & ANDERSON, D. J. 2005. Peripheral nerve-derived VEGF promotes arterial differentiation via neuropilin 1-mediated positive feedback. *Development,* 132**,** 941-52.

MULLER, A. M., MEDVINSKY, A., STROUBOULIS, J., GROSVELD, F. & DZIERZAK, E. 1994. Development of Hematopoietic Stem-Cell Activity in the Mouse Embryo. *Immunity,* 1**,** 291-301.

MURAYAMA, E., KISSA, K., ZAPATA, A., MORDELET, E., BRIOLAT, V., LIN, H. F., HANDIN, R. I. & HERBOMEL, P. 2006. Tracing hematopoietic precursor migration to successive hematopoietic organs during zebrafish development. *Immunity,* 25**,** 963-975.

NAG, K., KATO, A., NAKADA, T., HOSHIJIMA, K., MISTRY, A. C., TAKEI, Y. & HIROSE, S. 2006. Molecular and functional characterization of adrenomedullin receptors in pufferfish. *Am J Physiol Regul Integr Comp Physiol,* 290**,** R467-78.

NAKAYAMA, M., TAKAHASHI, K., MURAKAMI, O., SHIRATO, K. & SHIBAHARA, S. 1998. Induction of adrenomedullin by hypoxia and cobalt chloride in human colorectal carcinoma cells. *Biochem Biophys Res Commun,* 243**,** 514-7.

NAOT, D., REID, I. R. & CORNISH, J. 2008. Amylin and Calcitonin Gene-Related Peptide. *Principles of Bone Biology, Vol 1, 3rd Edition***,** 837-853.

NASEVICIUS, A., LARSON, J. & EKKER, S. C. 2000. Distinct requirements for zebrafish angiogenesis revealed by a VEGF-A morphant. *Yeast,* 17**,** 294-301.

NGUYEN, S. V. & CLAYCOMB, W. C. 1999. Hypoxia regulates the expression of the adrenomedullin and HIF-1 genes in cultured HL-1 cardiomyocytes. *Biochem Biophys Res Commun,* 265**,** 382-6.

NICENBOIM, J., MALKINSON, G., LUPO, T., ASAF, L., SELA, Y., MAYSELESS, O., GIBBS-BAR, L., SENDEROVICH, N., HASHIMSHONY, T., SHIN, M., JERAFI-VIDER, A., AVRAHAM-DAVIDI, I., KRUPALNIK, V., HOFI, R., ALMOG, G., ASTIN, J. W., GOLANI, O., BEN-DOR, S., CROSIER, P. S., HERZOG, W., LAWSON, N. D., HANNA, J. H., YANAI, I. & YANIV, K. 2015. Lymphatic vessels arise from specialized angioblasts within a venous niche. *Nature,* 522**,** 56-U100.

NICOLI, S., TOBIA, C., GUALANDI, L., DE SENA, G. & PRESTA, M. 2008. Calcitonin receptor-like receptor guides arterial differentiation in zebrafish. *Blood,* 111**,** 4965-72.

NIKITENKO, L. L., FOX, S. B., KEHOE, S., REES, M. C. & BICKNELL, R. 2006. Adrenomedullin and tumour angiogenesis. *Br J Cancer,* 94**,** 1-7.

NIKITENKO, L. L., MACKENZIE, I. Z., REES, M. C. & BICKNELL, R. 2000. Adrenomedullin is an autocrine regulator of endothelial growth in human endometrium. *Mol Hum Reprod,* 6**,** 811-9.

NIKITENKO, L. L., SMITH, D. M., BICKNELL, R. & REES, M. C. 2003. Transcriptional regulation of the CRLR gene in human microvascular endothelial cells by hypoxia. *FASEB J,* 17**,** 1499-501.

NISHIMURA, D. Y., SWIDERSKI, R. E., ALWARD, W. L. M., SEARBY, C. C., PATIL, S. R., BENNET, S. R., KANIS, A. B., GASTIER, J. M., STONE, E. M. & SHEFFIELD, V. C. 1998. The forkhead transcription factor gene FKHL7 is responsible for glaucoma phenotypes which map to 6p25. *Nature Genetics,* 19**,** 140-147.

NORRMEN, C., IVANOV, K. I., CHENG, J. P., ZANGGER, N., DELORENZI, M., JAQUET, M., MIURA, N., PUOLAKKAINEN, P., HORSLEY, V., HU, J. H., AUGUSTIN, H. G., YLAE-HERTTUALA, S., ALITALO, K. & PETROVA, T. V. 2009. FOXC2 controls formation and maturation of lymphatic collecting vessels through cooperation with NFATc1. *Journal of Cell Biology,* 185**,** 439-457.

O'BRIEN, L. L., GRIMALDI, M., KOSTUN, Z., WINGERT, R. A., SELLECK, R. & DAVIDSON, A. J. 2011. Wt1a, Foxc1a, and the Notch mediator Rbpj physically interact and regulate the formation of podocytes in zebrafish. *Dev Biol,* 358**,** 318-30.

OAKLEY, R. & THARAKAN, B. 2014. Vascular hyperpermeability and aging. *Aging Dis,* 5**,** 114-25.

OBER, E. A., OLOFSSON, B., MAKINEN, T., JIN, S. W., SHOJI, W., KOH, G. Y., ALITALO, K. & STAINIER, D. Y. R. 2004. Vegfc is required for vascular development and endoderm morphogenesis in zebrafish. *Embo Reports,* 5**,** 78-84.

OHLSSON, R., FALCK, P., HELLSTROM, M., LINDAHL, P., BOSTROM, H., FRANKLIN, G., AHRLUND-RICHTER, L., POLLARD, J., SORIANO, P. & BETSHOLTZ, C. 1999. PDGFB regulates the development of the labyrinthine layer of the mouse fetal placenta. *Dev Biol,* 212**,** 124-36.

OKUDA, K. S., ASTIN, J. W., MISA, J. P., FLORES, M. V., CROSIER, K. E. & CROSIER, P. S. 2012. lyve1 expression reveals novel lymphatic vessels and new mechanisms for lymphatic vessel development in zebrafish. *Development,* 139**,** 2381-91.

OLSON, L. E. & SORIANO, P. 2011. PDGFRbeta signaling regulates mural cell plasticity and inhibits fat development. *Dev Cell,* 20**,** 815-26.

ORKIN, S. H. & ZON, L. I. 2008. Hematopoiesis: an evolving paradigm for stem cell biology. *Cell,* 132**,** 631-44.

ORSENIGO, F., GIAMPIETRO, C., FERRARI, A., CORADA, M., GALAUP, A., SIGISMUND, S., RISTAGNO, G., MADDALUNO, L., KOH, G. Y., FRANCO, D., KURTCUOGLU, V., POULIKAKOS, D., BALUK, P., MCDONALD, D., LAMPUGNANI, M. G. & DEJANA, E. 2012. Phosphorylation of VE-cadherin is modulated by haemodynamic forces and contributes to the regulation of vascular permeability in vivo. *Nature Communications,* 3.

OTTEN, C., VAN DER VEN, P. F., LEWRENZ, I., PAUL, S., STEINHAGEN, A., BUSCH-NENTWICH, E., EICHHORST, J., WIESNER, B., STEMPLE, D., STRAHLE, U., FURST, D. O. & ABDELILAH-SEYFRIED, S. 2012. Xirp proteins mark injured skeletal muscle in zebrafish. *PLoS One,* 7**,** e31041.

OTTERSBACH, K. & DZIERZAK, E. 2005. The murine placenta contains hematopoietic stem cells within the vascular labyrinth region. *Dev Cell,* 8**,** 377-87.

PALIS, J., ROBERTSON, S., KENNEDY, M., WALL, C. & KELLER, G. 1999. Development of erythroid and myeloid progenitors in the yolk sac and embryo proper of the mouse. *Development,* 126**,** 5073-84.

PAN, Q., CHANTHERY, Y., LIANG, W. C., STAWICKI, S., MAK, J., RATHORE, N., TONG, R. K., KOWALSKI, J., YEE, S. F., PACHECO, G., ROSS, S., CHENG, Z., LE COUTER, J., PLOWMAN,

G., PEALE, F., KOCH, A. W., WU, Y., BAGRI, A., TESSIER-LAVIGNE, M. & WATTS, R. J. 2007. Blocking neuropilin-1 function has an additive effect with anti-VEGF to inhibit tumor growth. *Cancer Cell,* 11**,** 53-67.

PAOLINELLI, R., CORADA, M., ORSENIGO, F. & DEJANA, E. 2011. The molecular basis of the blood brain barrier differentiation and maintenance. Is it still a mystery? *Pharmacol Res,* 63**,** 165-71.

PARDANAUD, L., YASSINE, F. & DIETERLEN-LIEVRE, F. 1989. Relationship between vasculogenesis, angiogenesis and haemopoiesis during avian ontogeny. *Development,* 105**,** 473-85.

PENDEVILLE, H., WINANDY, M., MANFROID, I., NIVELLES, O., MOTTE, P., PASQUE, V., PEERS, B., STRUMAN, I., MARTIAL, J. A. & VOZ, M. L. 2008. Zebrafish Sox7 and Sox18 function together to control arterial-venous identity. *Dev Biol,* 317**,** 405-16.

PETROVA, T. V., KARPANEN, T., NORRMEN, C., MELLOR, R., TAMAKOSHI, T., FINEGOLD, D., FERRELL, R., KERJASCHKI, D., MORTIMER, P., YLA-HERTTUALA, S., MIURA, N. & ALITALO, K. 2004. Defective valves and abnormal mural cell recruitment underlie lymphatic vascular failure in lymphedema distichiasis. *Nature Medicine,* 10**,** 974-981.

PHAM, V. N., LAWSON, N. D., MUGFORD, J. W., DYE, L., CASTRANOVA, D., LO, B. & WEINSTEIN, B. M. 2007. Combinatorial function of ETS transcription factors in the developing vasculature. *Dev Biol,* 303**,** 772-83.

PILLAY, L. M., MACKOWETZKY, K. J., WIDEN, S. A. & WASKIEWICZ, A. J. 2016. Somite-Derived Retinoic Acid Regulates Zebrafish Hematopoietic Stem Cell Formation. *PLoS One,* 11**,** e0166040.

PIO, R., MARTINEZ, A., UNSWORTH, E. J., KOWALAK, J. A., BENGOECHEA, J. A., ZIPFEL, P. F., ELSASSER, T. H. & CUTTITTA, F. 2001. Complement factor H is a serum-binding protein for adrenomedullin, and the resulting complex modulates the bioactivities of both partners. *J Biol Chem,* 276**,** 12292-300.

PITERA, J. E., WOOLF, A. S., GALE, N. W., YANCOPOULOS, G. D. & YUAN, H. T. 2004. Dysmorphogenesis of kidney cortical peritubular capillaries in angiopoietin-2-deficient mice. *American Journal of Pathology,* 165**,** 1895-1906.

POOLE, T. J. & COFFIN, J. D. 1989. Vasculogenesis and angiogenesis: two distinct morphogenetic mechanisms establish embryonic vascular pattern. *J Exp Zool,* 251**,** 224-31.

PROULX, K., LU, A. & SUMANAS, S. 2010. Cranial vasculature in zebrafish forms by angioblast cluster-derived angiogenesis. *Dev Biol,* 348**,** 34-46.

QUILLIEN, A., MOORE, J. C., SHIN, M., SIEKMANN, A. F., SMITH, T., PAN, L. Y., MOENS, C. B., PARSONS, M. J. & LAWSON, N. D. 2014. Distinct Notch signaling outputs pattern the developing arterial system. *Development,* 141**,** 1544-1552.

RADTKE, F., SCHWEISGUTH, F. & PEAR, W. 2005. The Notch 'gospel'. *EMBO Rep,* 6**,** 1120-5.

REISCHAUER, S., STONE, O. A., VILLASENOR, A., CHI, N., JIN, S. W., MARTIN, M., LEE, M. T., FUKUDA, N., MARASS, M., WITTY, A., FIDDES, I., KUO, T., CHUNG, W. S., SALEK, S., LERRIGO, R., ALSIO, J., LUO, S., TWORUS, D., AUGUSTINE, S. M., MUCENIEKS, S., NYSTEDT, B., GIRALDEZ, A. J., SCHROTH, G. P., ANDERSSON, O. & STAINIER, D. Y. 2016. Cloche is a bHLH-PAS transcription factor that drives haemato-vascular specification. *Nature,* 535**,** 294-8.

RISSANEN, T. T., KORPISALO, P., MARKKANEN, J. E., LIIMATAINEN, T., ORDEN, M. R., KHOLOVA, I., DE GOEDE, A., HEIKURA, T., GROHN, O. H. & YLA-HERTTUALA, S. 2005. Blood flow remodels growing vasculature during vascular endothelial growth factor gene therapy and determines between capillary arterialization and sprouting angiogenesis. *Circulation,* 112**,** 3937-3946.

ROBERT-MORENO, A., ESPINOSA, L., DE LA POMPA, J. L. & BIGAS, A. 2005. RBPj kappa-dependent Notch function regulates Gata2 and is essential for the formation of intra-embryonic hematopoietic cells. *Development,* 132**,** 1117-1126.

ROBERTS, D. M., KEARNEY, J. B., JOHNSON, J. H., ROSENBERG, M. P., KUMAR, R. & BAUTCH, V. L. 2004. The vascular endothelial growth factor (VEGF) receptor Flt-1 (VEGFR-1) modulates Flk-1 (VEGFR-2) signaling during blood vessel formation. *American Journal of Pathology,* 164**,** 1531-1535.

ROBIN, C., BOLLEROT, K., MENDES, S., HAAK, E., CRISAN, M., CERISOLI, F., LAUW, I., KAIMAKIS, P., JORNA, R., VERMEULEN, M., KAYSER, M., VAN DER LINDEN, R., IMANIRAD, P., VERSTEGEN, M., NAWAZ-YOUSAF, H., PAPAZIAN, N., STEEGERS, E., CUPEDO, T. & DZIERZAK, E. 2009. Human placenta is a potent hematopoietic niche containing hematopoietic stem and progenitor cells throughout development. *Cell Stem Cell,* 5**,** 385-95.

ROH, J., CHANG, C. L., BHALLA, A., KLEIN, C. & HSU, S. Y. 2004. Intermedin is a calcitonin/calcitonin gene-related peptide family peptide acting through the calcitonin receptor-like receptor/receptor activity-modifying protein receptor complexes. *J Biol Chem,* 279**,** 7264-74.

ROSSI, A., GAUVRIT, S., MARASS, M., PAN, L., MOENS, C. B. & STAINIER, D. Y. 2016. Regulation of Vegf signaling by natural and synthetic ligands. *Blood*.

ROSSI, A., KONTARAKIS, Z., GERRI, C., NOLTE, H., HOLPER, S., KRUGER, M. & STAINIER, D. Y. R. 2015. Genetic compensation induced by deleterious mutations but not gene knockdowns. *Nature,* 524**,** 230-+.

ROUKENS, M. G., PETERSON-MADURO, J., PADBERG, Y., JELTSCH, M., LEPPANEN, V. M., BOS, F. L., ALITALO, K., SCHULTE-MERKER, S. & SCHULTE, D. 2015. Functional Dissection of the CCBE1 Protein: A Crucial Requirement for the Collagen Repeat Domain. *Circ Res,* 116**,** 1660-9.

ROWLINSON, J. M. & GERING, M. 2010. Hey2 acts upstream of Notch in hematopoietic stem cell specification in zebrafish embryos. *Blood,* 116**,** 2046-56.

RUHRBERG, C., GERHARDT, H., GOLDING, M., WATSON, R., IOANNIDOU, S., FUJISAWA, H., BETSHOLTZ, C. & SHIMA, D. T. 2002. Spatially restricted patterning cues provided by heparin-binding VEGF-A control blood vessel branching morphogenesis. *Genes Dev,* 16**,** 2684-98.

SACILOTTO, N., MONTEIRO, R., FRITZSCHE, M., BECKER, P. W., SANCHEZ-DEL-CAMPO, L., LIU, K., PINHEIRO, P., RATNAYAKA, I., DAVIES, B., GODING, C. R., PATIENT, R., BOU-GHARIOS, G. & DE VAL, S. 2013. Analysis of Dll4 regulation reveals a combinatorial role for Sox and Notch in arterial development. *Proc Natl Acad Sci U S A,* 110**,** 11893-8.

SANDER, J. D., DAHLBORG, E. J., GOODWIN, M. J., CADE, L., ZHANG, F., CIFUENTES, D., CURTIN, S. J., BLACKBURN, J. S., THIBODEAU-BEGANNY, S., QI, Y., PIERICK, C. J., HOFFMAN, E., MAEDER, M. L., KHAYTER, C., REYON, D., DOBBS, D., LANGENAU, D. M., STUPAR, R. M., GIRALDEZ, A. J., VOYTAS, D. F., PETERSON, R. T., YEH, J. R. & JOUNG, J. K. 2011. Selection-free zinc-finger-nuclease engineering by context-dependent assembly (CoDA). *Nat Methods,* 8**,** 67-9.

SANO, H., LEBOEUF, J. P., NOVITSKIY, S. V., SEO, S., ZAJA-MILATOVIC, S., DIKOV, M. M. & KUME, T. 2010. The Foxc2 transcription factor regulates tumor angiogenesis. *Biochem Biophys Res Commun,* 392**,** 201-6.

SANTORO, M. M., PESCE, G. & STAINIER, D. Y. 2009. Characterization of vascular mural cells during zebrafish development. *Mech Dev,* 126**,** 638-49.

SARMAH, S. & MARRS, J. A. 2016. Zebrafish as a Vertebrate Model System to Evaluate Effects of Environmental Toxicants on Cardiac Development and Function. *Int J Mol Sci,* 17.

SASAHIRA, T., UEDA, N., YAMAMOTO, K., KURIHARA, M., MATSUSHIMA, S., BHAWAL, U. K., KIRITA, T. & KUNIYASU, H. 2014. Prox1 and FOXC2 act as regulators of lymphangiogenesis and angiogenesis in oral squamous cell carcinoma. *PLoS One,* 9**,** e92534.

SAXTON, T. M. & PAWSON, T. 1999. Morphogenetic movements at gastrulation require the SH2 tyrosine phosphatase Shp2. *Proc Natl Acad Sci U S A,* 96**,** 3790-5.

SCHEER, N. & CAMPOS-ORTEGA, J. A. 1999. Use of the Gal4-UAS technique for targeted gene expression in the zebrafish. *Mech Dev,* 80**,** 153-8.

SCHOENEBECK, J. J., KEEGAN, B. R. & YELON, D. 2007. Vessel and blood specification override cardiac potential in anterior mesoderm. *Dev Cell,* 13**,** 254-67.

SCHUERMANN, A., HELKER, C. S. & HERZOG, W. 2014. Angiogenesis in zebrafish. *Semin Cell Dev Biol,* 31**,** 106-14.

SCHULTZ, K. M., SASMAN, A., SEO, S., SINGH, H. P., LACAL, P. M., FATIMA, A., LIU, T., LOSORDO, D. W., LEHMANN, O. J. & KUME, T. 2013. Fox transcription factors in corneal angiogenesis. *Angiogenesis,* 16**,** 249-250.

SCHWANN, T. H. 1993. Microscopial researches into the accordance in the structure and growth of animals and plants. 1847. *Obes Res,* 1**,** 408-18.

SEHNERT, A. J., HUQ, A., WEINSTEIN, B. M., WALKER, C., FISHMAN, M. & STAINIER, D. Y. 2002. Cardiac troponin T is essential in sarcomere assembly and cardiac contractility. *Nat Genet,* 31**,** 106-10.

SEHNERT, A. J. & STAINIER, D. Y. 2002. A window to the heart: can zebrafish mutants help us understand heart disease in humans? *Trends Genet,* 18**,** 491-4.

SEILER, C., ABRAMS, J. & PACK, M. 2010. Characterization of Zebrafish Intestinal Smooth Muscle Development Using a Novel sm22 alpha-b Promoter. *Developmental Dynamics,* 239**,** 2806-2812.

SEO, S., FUJITA, H., NAKANO, A., KANG, M., DUARTE, A. & KUME, T. 2006. The forkhead transcription factors, Foxc1 and Foxc2, are required for arterial specification and lymphatic sprouting during vascular development. *Developmental Biology,* 294**,** 458-470.

SEO, S., SINGH, H. P., LACAL, P. M., SASMAN, A., FATIMA, A., LIU, T., SCHULTZ, K. M., LOSORDO, D. W., LEHMANN, O. J. & KUME, T. 2012. Forkhead box transcription factor FoxC1 preserves corneal transparency by regulating vascular growth. *Proceedings of the National Academy of Sciences of the United States of America,* 109**,** 2015-2020.

SEXTON, P. M., MORFIS, M., TILAKARATNE, N., HAY, D. L., UDAWELA, M., CHRISTOPOULOS, G. & CHRISTOPOULOS, A. 2006. Complexing receptor pharmacology: modulation of family B G protein-coupled receptor function by RAMPs. *Ann N Y Acad Sci,* 1070**,** 90-104.

SEXTON, P. M., POYNER, D. R., SIMMS, J., CHRISTOPOULOS, A. & HAY, D. L. 2012. RAMPs as drug targets. *Adv Exp Med Biol,* 744**,** 61-74.

SHALABY, F., ROSSANT, J., YAMAGUCHI, T. P., GERTSENSTEIN, M., WU, X. F., BREITMAN, M. L. & SCHUH, A. C. 1995. Failure of blood-island formation and vasculogenesis in Flk-1-deficient mice. *Nature,* 376**,** 62-6.

SHANKARAN, S. S., SIEGER, D., SCHROTER, C., CZEPE, C., PAULY, M. C., LAPLANTE, M. A., BECKER, T. S., OATES, A. O. & GAJEWSKI, M. 2007. Completing the set of h/E(spl) cyclic genes in zebrafish: her12 and her15 reveal novel modes of expression and contribute to the segmentation clock. *Developmental Biology,* 304**,** 615-632.

SHAW, K. M., CASTRANOVA, D. A., PHAM, V. N., KAMEI, M., KIDD, K. R., LO, B. D., TORRES-VASQUEZ, J., RUBY, A. & WEINSTEIN, B. M. 2006. fused-somites-like mutants exhibit defects in trunk vessel patterning. *Developmental Dynamics,* 235**,** 1753-1760.

SHIN, M., BEANE, T. J., QUILLIEN, A., MALE, I., ZHU, L. J. & LAWSON, N. D. 2016a. Vegfa signals through ERK to promote angiogenesis, but not artery differentiation. *Development,* 143**,** 3796-3805.

SHIN, M., MALE, I., BEANE, T. J., VILLEFRANC, J. A., KOK, F. O., ZHU, L. J. & LAWSON, N. D. 2016b. Vegfc acts through ERK to induce sprouting and differentiation of trunk lymphatic progenitors. *Development,* 143**,** 3785-3795.

SHINDO, A., WADA, H., ISHIKAWA, H., ITO, A., ASAHI, M., II, Y., IKEJIRI, M. & TOMIMOTO, H. 2014. Clinical features and underlying causes of cerebral venous thrombosis in Japanese patients. *Int J Hematol,* 99**,** 437-40.

SHINDO, T., KURIHARA, Y., NISHIMATSU, H., MORIYAMA, N., KAKOKI, M., WANG, Y., IMAI, Y., EBIHARA, A., KUWAKI, T., JU, K. H., MINAMINO, N., KANGAWA, K., ISHIKAWA, T., FUKUDA, M., AKIMOTO, Y., KAWAKAMI, H., IMAI, T., MORITA, H., YAZAKI, Y., NAGAI, R., HIRATA, Y. & KURIHARA, H. 2001. Vascular abnormalities and elevated blood pressure in mice lacking adrenomedullin gene. *Circulation,* 104**,** 1964-71.

SIEGENTHALER, J. A., ASHIQUE, A. M., ZARBALIS, K., PATTERSON, K. P., HECHT, J. H., KANE, M. A., FOLIAS, A. E., CHOE, Y., MAY, S. R., KUME, T., NAPOLI, J. L., PETERSON, A. S. & PLEASURE, S. J. 2009. Retinoic Acid from the Meninges Regulates Cortical Neuron Generation. *Cell,* 139**,** 597-609.

SIEGENTHALER, J. A., CHOE, Y., PATTERSON, K. P., HSIEH, I., LI, D., JAMINET, S. C., DANEMAN, R., KUME, T., HUANG, E. J. & PLEASURE, S. J. 2013. Foxc1 is required by pericytes during fetal brain angiogenesis. *Biol Open,* 2**,** 647-59.

SIEKMANN, A. F. & LAWSON, N. D. 2007. Notch signalling limits angiogenic cell behaviour in developing zebrafish arteries. *Nature,* 445**,** 781-4.

SIEKMANN, A. F., STANDLEY, C., FOGARTY, K. E., WOLFE, S. A. & LAWSON, N. D. 2009. Chemokine signaling guides regional patterning of the first embryonic artery. *Genes Dev,* 23**,** 2272-7.

SKARIE, J. M. & LINK, B. A. 2009. FoxC1 is essential for vascular basement membrane integrity and hyaloid vessel morphogenesis. *Invest Ophthalmol Vis Sci,* 50**,** 5026-34.

SMITH, R. S., ZABALETA, A., KUME, T., SAVINOVA, O. V., KIDSON, S. H., MARTIN, J. E., NISHIMURA, D. Y., ALWARD, W. L., HOGAN, B. L. & JOHN, S. W. 2000. Haploinsufficiency of the transcription factors FOXC1 and FOXC2 results in aberrant ocular development. *Hum Mol Genet,* 9**,** 1021-32.

SONG, M., YANG, H. S., YAO, S. H., MA, F. X., LI, Z., DENG, Y. Q., DENG, H. X., ZHOU, Q., LIN, S. & WEI, Y. Q. 2007. A critical role of vascular endothelial growth factor D in zebrafish embryonic vasculogenesis and angiogenesis. *Biochemical and Biophysical Research Communications,* 357**,** 924-930.

SOUILHOL, C., GONNEAU, C., LENDINEZ, J. G., BATSIVARI, A., RYBTSOV, S., WILSON, H., MORGADO-PALACIN, L., HILLS, D., TAOUDI, S., ANTONCHUK, J., ZHAO, S. L. & MEDVINSKY, A. 2016. Inductive interactions mediated by interplay of asymmetric signalling underlie development of adult haematopoietic stem cells. *Nature Communications,* 7.

SRINIVASAN, R. S., ESCOBEDO, N., YANG, Y., INTERIANO, A., DILLARD, M. E., FINKELSTEIN, D., MUKATIRA, S., GIL, H. J., NURMI, H., ALITALO, K. & OLIVER, G. 2014. The Prox1-Vegfr3 feedback loop maintains the identity and the number of lymphatic endothelial cell progenitors. *Genes Dev,* 28**,** 2175-87.

STAINIER, D. Y., WEINSTEIN, B. M., DETRICH, H. W., 3RD, ZON, L. I. & FISHMAN, M. C. 1995. Cloche, an early acting zebrafish gene, is required by both the endothelial and hematopoietic lineages. *Development,* 121**,** 3141-50.

STRATMAN, A. N., PEZOA, S. A., FARRELLY, O. M., CASTRANOVA, D., DYE, L. E., 3RD, BUTLER, M. G., SIDIK, H., TALBOT, W. S. & WEINSTEIN, B. M. 2017. Interactions between mural cells and endothelial cells stabilize the developing zebrafish dorsal aorta. *Development,* 144**,** 115-127.

SUMANAS, S., GOMEZ, G., ZHAO, Y., PARK, C., CHOI, K. & LIN, S. 2008. Interplay among Etsrp/ER71, Scl, and Alk8 signaling controls endothelial and myeloid cell formation. *Blood,* 111**,** 4500-10.

SUMANAS, S. & LIN, S. 2006. Ets1-related protein is a key regulator of vasculogenesis in zebrafish. *PLoS Biol,* 4**,** e10.

SWIFT, M. R., PHAM, V. N., CASTRANOVA, D., BELL, K., POOLE, R. J. & WEINSTEIN, B. M. 2014. SoxF factors and Notch regulate nr2f2 gene expression during venous differentiation in zebrafish. *Dev Biol,* 390**,** 116-25.

TAKAHASHI, H. & SHIBUYA, M. 2005. The vascular endothelial growth factor (VEGF)/VEGF receptor system and its role under physiological and pathological conditions. *Clin Sci (Lond),* 109**,** 227-41.

TAKAHASHI, T., YAMAGUCHI, S., CHIDA, K. & SHIBUYA, M. 2001. A single autophosphorylation site on KDR/Flk-1 is essential for VEGF-A-dependent activation of PLC-gamma and DNA synthesis in vascular endothelial cells. *Embo Journal,* 20**,** 2768-2778.

TAKAHASHI, Y., KOIZUMI, K., TAKAGI, A., KITAJIMA, S., INOUE, T., KOSEKI, H. & SAGA, Y. 2000. Mesp2 initiates somite segmentation through the Notch signalling pathway. *Nature Genetics,* 25**,** 390-396.

TAKASHIMA, S., KITAKAZE, M., ASAKURA, M., ASANUMA, H., SANADA, S., TASHIRO, F., NIWA, H., MIYAZAKI JI, J., HIROTA, S., KITAMURA, Y., KITSUKAWA, T., FUJISAWA, H., KLAGSBRUN, M. & HORI, M. 2002. Targeting of both mouse neuropilin-1 and neuropilin-2 genes severely impairs developmental yolk sac and embryonic angiogenesis. *Proc Natl Acad Sci U S A,* 99**,** 3657-62.

TAM, P. P. & BEHRINGER, R. R. 1997. Mouse gastrulation: the formation of a mammalian body plan. *Mech Dev,* 68**,** 3-25.

TAMPLIN, O. J., DURAND, E. M., CARR, L. A., CHILDS, S. J., HAGEDORN, E. J., LI, P. L., YZAGUIRRE, A. D., SPECK, N. A. & ZON, L. I. 2015. Hematopoietic Stem Cell Arrival Triggers Dynamic Remodeling of the Perivascular Niche. *Cell,* 160**,** 241-252.

TAO, S., WITTE, M., BRYSON-RICHARDSON, R. J., CURRIE, P. D., HOGAN, B. M. & SCHULTE-MERKER, S. 2011. Zebrafish prox1b mutants develop a lymphatic vasculature, and prox1b does not specifically mark lymphatic endothelial cells. *PLoS One,* 6**,** e28934.

THAMBYRAJAH, R., UCANOK, D., JALALI, M., HOUGH, Y., WILKINSON, R. N., MCMAHON, K., MOORE, C. & GERING, M. 2016. A gene trap transposon eliminates haematopoietic expression of zebrafish Gfi1aa, but does not interfere with haematopoiesis. *Developmental Biology,* 417**,** 25-39.

THOMPSON, M. A., RANSOM, D. G., PRATT, S. J., MACLENNAN, H., KIERAN, M. W., DETRICH, H. W., 3RD, VAIL, B., HUBER, T. L., PAW, B., BROWNLIE, A. J., OATES, A. C., FRITZ, A., GATES, M. A., AMORES, A., BAHARY, N., TALBOT, W. S., HER, H., BEIER, D. R., POSTLETHWAIT, J. H. & ZON, L. I. 1998. The cloche and spadetail genes differentially affect hematopoiesis and vasculogenesis. *Dev Biol,* 197**,** 248-69.

THURSTON, G. & YANCOPOULOS, G. D. 2001. Gridlock in the blood. *Nature,* 414**,** 163-4.

TOPCZEWSKA, J. M., TOPCZEWSKI, J., SHOSTAK, A., KUME, T., SOLNICA-KREZEL, L. & HOGAN, B. L. 2001a. The winged helix transcription factor Foxc1a is essential for somitogenesis in zebrafish. *Genes Dev,* 15**,** 2483-93.

TOPCZEWSKA, J. M., TOPCZEWSKI, J., SOLNICA-KREZEL, L. & HOGAN, B. L. 2001b. Sequence and expression of zebrafish foxc1a and foxc1b, encoding conserved forkhead/winged helix transcription factors. *Mech Dev,* 100**,** 343-7.

TRAVER, D., PAW, B. H., POSS, K. D., PENBERTHY, W. T., LIN, S. & ZON, L. I. 2003. Transplantation and in vivo imaging of multilineage engraftment in zebrafish bloodless mutants. *Nat Immunol,* 4**,** 1238-46.

TSE, D. & STAN, R. V. 2010. Morphological heterogeneity of endothelium. *Semin Thromb Hemost,* 36**,** 236-45.

TSUJIKAWA, K., YAYAMA, K., HAYASHI, T., MATSUSHITA, H., YAMAGUCHI, T., SHIGENO, T., OGITANI, Y., HIRAYAMA, M., KATO, T., FUKADA, S., TAKATORI, S., KAWASAKI, H., OKAMOTO, H., IKAWA, M., OKABE, M. & YAMAMOTO, H. 2007. Hypertension and dysregulated proinflammatory cytokine production in receptor activity-modifying protein 1-deficient mice. *Proc Natl Acad Sci U S A,* 104**,** 16702-7.

TUROWSKI, P., MARTINELLI, R., CRAWFORD, R., WATERIDGE, D., PAPAGEORGIOU, A. P., LAMPUGNANI, M. G., GAMP, A. C., VESTWEBER, D., ADAMSON, P., DEJANA, E. & GREENWOOD, J. 2008. Phosphorylation of vascular endothelial cadherin controls lymphocyte emigration. *J Cell Sci,* 121**,** 29-37.

ULRICH, F., CARRETERO-ORTEGA, J., MENENDEZ, J., NARVAEZ, C., SUN, B., LANCASTER, E., PERSHAD, V., TRZASKA, S., VELIZ, E., KAMEI, M., PRENDERGAST, A., KIDD, K. R., SHAW, K. M., CASTRANOVA, D. A., PHAM, V. N., LO, B. D., MARTIN, B. L., RAIBLE, D. W., WEINSTEIN, B. M. & TORRES-VAZQUEZ, J. 2016. Reck enables cerebrovascular development by promoting canonical Wnt signaling. *Development,* 143**,** 147-59.

ULRICH, F., MA, L. H., BAKER, R. G. & TORRES-VAZQUEZ, J. 2011. Neurovascular development in the embryonic zebrafish hindbrain. *Dev Biol,* 357**,** 134-51.

VAN DONGEN, M. J. P., CEDERBERG, A., CARLSSON, P., ENERBACK, S. & WIKSTROM, M. 2000. Solution structure and dynamics of the DNA-binding domain of the adipocyte-transcription factor FREAC-11. *Journal of Molecular Biology,* 296**,** 351-359.

VAN IMPEL, A., ZHAO, Z. H., HERMKENS, D. M. A., ROUKENS, M. G., FISCHER, J. C., PETERSON-MADURO, J., DUCKERS, H., OBER, E. A., INGHAM, P. W. & SCHULTE-MERKER, S. 2014. Divergence of zebrafish and mouse lymphatic cell fate specification pathways. *Development,* 141**,** 1228-U101.

VAN LESSEN, M., SHIBATA-GERMANOS, S., VAN IMPEL, A., HAWKINS, T. A., RIHEL, J. & SCHULTE-MERKER, S. 2017. Intracellular uptake of macromolecules by brain lymphatic endothelial cells during zebrafish embryonic development. *Elife,* 6.

VAN ROOIJEN, E., VOEST, E. E., LOGISTER, I., BUSSMANN, J., KORVING, J., VAN EEDEN, F. J., GILES, R. H. & SCHULTE-MERKER, S. 2010. von Hippel-Lindau tumor suppressor mutants faithfully model pathological hypoxia-driven angiogenesis and vascular retinopathies in zebrafish. *Dis Model Mech,* 3**,** 343-53.

VANHOLLEBEKE, B., STONE, O. A., BOSTAILLE, N., CHO, C., ZHOU, Y. L., MAQUET, E., GAUQUIER, A., CABOCHETTE, P., FUKUHARA, S., MOCHIZUKI, N., NATHANS, J. & STAINIER, D. Y. R. 2015. Tip cell-specific requirement for an atypical Gpr124-and Reck-dependent Wnt/beta-catenin pathway during brain angiogenesis. *Elife,* 4.

VELDMAN, M. B. & LIN, S. 2012. Etsrp/Etv2 is directly regulated by Foxc1a/b in the zebrafish angioblast. *Circ Res,* 110**,** 220-9.

VENERO GALANTERNIK, M., CASTRANOVA, D., GORE, A. V., BLEWETT, N. H., JUNG, H. M., STRATMAN, A. N., KIRBY, M. R., IBEN, J., MILLER, M. F., KAWAKAMI, K., MARAIA, R. J. & WEINSTEIN, B. M. 2017. A novel perivascular cell population in the zebrafish brain. *Elife,* 6.

VILLEFRANC, J. A., NICOLI, S., BENTLEY, K., JELTSCH, M., ZARKADA, G., MOORE, J. C., GERHARDT, H., ALITALO, K. & LAWSON, N. D. 2013. A truncation allele in vascular endothelial growth factor c reveals distinct modes of signaling during lymphatic and vascular development. *Development,* 140**,** 1497-506.

VOKES, S. A., YATSKIEVYCH, T. A., HEIMARK, R. L., MCMAHON, J., MCMAHON, A. P., ANTIN, P. B. & KRIEG, P. A. 2004. Hedgehog signaling is essential for endothelial tube formation during vasculogenesis. *Development,* 131**,** 4371-80.

WANG, H. U., CHEN, Z. F. & ANDERSON, D. J. 1998. Molecular distinction and angiogenic interaction between embryonic arteries and veins revealed by ephrin-B2 and its receptor Eph-B4. *Cell,* 93**,** 741-53.

WANG, Y. Y., PAN, L. Y., MOENS, C. B. & APPEL, B. 2014. Notch3 establishes brain vascular integrity by regulating pericyte number. *Development,* 141**,** 307-317.

WARGA, R. M., KANE, D. A. & HO, R. K. 2009. Fate mapping embryonic blood in zebrafish: multi- and unipotential lineages are segregated at gastrulation. *Dev Cell,* 16**,** 744-55.

WEIGEL, D., JURGENS, G., KUTTNER, F., SEIFERT, E. & JACKLE, H. 1989. The homeotic gene fork head encodes a nuclear protein and is expressed in the terminal regions of the Drosophila embryo. *Cell,* 57**,** 645-58.

WHITESELL, T. R., KENNEDY, R. M., CARTER, A. D., ROLLINS, E. L., GEORGIJEVIC, S., SANTORO, M. M. & CHILDS, S. J. 2014. An alpha-Smooth Muscle Actin (acta2/alpha sma) Zebrafish Transgenic Line Marking Vascular Mural Cells and Visceral Smooth Muscle Cells. *Plos One,* 9.

WICK, N., SAHARINEN, P., SAHARINEN, J., GURNHOFER, E., STEINER, C. W., RAAB, I., STOKIC, D., GIOVANOLI, P., BUCHSBAUM, S., BURCHARD, A., THURNER, S., ALITALO, K. & KERJASCHKI, D. 2007. Transcriptomal comparison of human dermal lymphatic endothelial cells ex vivo and in vitro. *Physiol Genomics,* 28**,** 179-92.

WIGLE, J. T., HARVEY, N., DETMAR, M., LAGUTINA, I., GROSVELD, G., GUNN, M. D., JACKSON, D. G. & OLIVER, G. 2002. An essential role for Prox1 in the induction of the lymphatic endothelial cell phenotype. *EMBO J,* 21**,** 1505-13.

WIGLE, J. T. & OLIVER, G. 1999. Prox1 function is required for the development of the murine lymphatic system. *Cell,* 98**,** 769-78.

WILD, R., KLEMS, A., TAKAMIYA, M., HAYASHI, Y., STRAHLE, U., ANDO, K., MOCHIZUKI, N., VAN IMPEL, A., SCHULTE-MERKER, S., KRUEGER, J., PREAU, L. & LE NOBLE, F. 2017. Neuronal sFlt1 and Vegfaa determine venous sprouting and spinal cord vascularization. *Nat Commun,* 8**,** 13991.

WILKINSON, R. N., ELWORTHY, S., INGHAM, P. W. & VAN EEDEN, F. J. 2013. A method for high-throughput PCR-based genotyping of larval zebrafish tail biopsies. *Biotechniques,* 55**,** 314-6.

WILKINSON, R. N., KOUDIJS, M. J., PATIENT, R. K., INGHAM, P. W., SCHULTE-MERKER, S. & VAN EEDEN, F. J. M. 2012. Hedgehog signaling via a calcitonin receptor-like receptor can induce arterial differentiation independently of VEGF signaling in zebrafish. *Blood,* 120**,** 477-488.

WILKINSON, R. N., POUGET, C., GERING, M., RUSSELL, A. J., DAVIES, S. G., KIMELMAN, D. & PATIENT, R. 2009. Hedgehog and Bmp polarize hematopoietic stem cell emergence in the zebrafish dorsal aorta. *Dev Cell,* 16**,** 909-16.

WILKINSON, R. N. & VAN EEDEN, F. J. 2014. The zebrafish as a model of vascular development and disease. *Prog Mol Biol Transl Sci,* 124**,** 93-122.

WILSON, J. M. & LAURENT, P. 2002. Fish gill morphology: Inside out. *Journal of Experimental Zoology,* 293**,** 192-213.

WINNIER, G., BLESSING, M., LABOSKY, P. A. & HOGAN, B. L. 1995. Bone morphogenetic protein-4 is required for mesoderm formation and patterning in the mouse. *Genes Dev,* 9**,** 2105-16.

WINNIER, G. E., HARGETT, L. & HOGAN, B. L. 1997. The winged helix transcription factor MFH1 is required for proliferation and patterning of paraxial mesoderm in the mouse embryo. *Genes Dev,* 11**,** 926-40.

WINNIER, G. E., KUME, T., DENG, K., ROGERS, R., BUNDY, J., RAINES, C., WALTER, M. A., HOGAN, B. L. & CONWAY, S. J. 1999. Roles for the winged helix transcription factors MF1 and MFH1 in cardiovascular development revealed by nonallelic noncomplementation of null alleles. *Dev Biol,* 213**,** 418-31.

YAMAGISHI, H., MAEDA, J., HU, T. H., MCANALLY, J., CONWAY, S. J., KUME, T., MEYERS, E. N., YAMAGISHI, C. & SRIVASTAVA, D. 2003. Tbx1 is regulated by tissue-specific Forkhead proteins through a common Sonic hedgehog-responsive enhancer. *Pediatric Research,* 53**,** 35a-35a.

YAMAUCHI, A., SAKURAI, T., KAMIYOSHI, A., ICHIKAWA-SHINDO, Y., KAWATE, H., IGARASHI, K., TORIYAMA, Y., TANAKA, M., LIU, T., XIAN, X., IMAI, A., ZHAI, L., OWA, S., ARAI, T. &

SHINDO, T. 2014. Functional differentiation of RAMP2 and RAMP3 in their regulation of the vascular system. *J Mol Cell Cardiol,* 77**,** 73-85.

YAMAZAKI, T., YOSHIMATSU, Y., MORISHITA, Y., MIYAZONO, K. & WATABE, T. 2009. COUP-TFII regulates the functions of Prox1 in lymphatic endothelial cells through direct interaction. *Genes Cells,* 14**,** 425-34.

YANIV, K., ISOGAI, S., CASTRANOVA, D., DYE, L., HITOMI, J. & WEINSTEIN, B. M. 2006. Live imaging of lymphatic development in the zebrafish. *Nat Med,* 12**,** 711-6.

YELON, D., TICHO, B., HALPERN, M. E., RUVINSKY, I., HO, R. K., SILVER, L. M. & STAINIER, D. Y. 2000. The bHLH transcription factor hand2 plays parallel roles in zebrafish heart and pectoral fin development. *Development,* 127**,** 2573-82.

YOKOYAMA, R., IIHOSHI, S., MIYATA, K., TOYAMA, K., KOMATSU, K., WANIBUCHI, M. & MIKUNI, N. 2016. [Pediatric Iatrogenic Vertebral Arteriovenous Fistula Successfully Treated with Endovascular Treatment:A Case Report]. *No Shinkei Geka,* 44**,** 857-861.

YOON, M. J., KOO, B. K., SONG, R., JEONG, H. W., SHIN, J., KIM, Y. W., KONG, Y. Y. & SUH, P. G. 2008. Mind bomb-1 is essential for intraembryonic hematopoiesis in the aortic endothelium and the subaortic patches. *Mol Cell Biol,* 28**,** 4794-804.

YOSHIDA, M., HATA, K., TAKASHIMA, R., ONO, K., NAKAMURA, E., TAKAHATA, Y., MURAKAMI, T., ISEKI, S., TAKANO-YAMAMOTO, T., NISHIMURA, R. & YONEDA, T. 2015. The transcription factor Foxc1 is necessary for Ihh-Gli2-regulated endochondral ossification. *Nature Communications,* 6.

YOU, L. R., LIN, F. J., LEE, C. T., DEMAYO, F. J., TSAI, M. J. & TSAI, S. Y. 2005. Suppression of Notch signalling by the COUP-TFII transcription factor regulates vein identity. *Nature,* 435**,** 98-104.

YUE, Y., JIANG, M., HE, L., ZHANG, Z., ZHANG, Q., GU, C., LIU, M., LI, N. & ZHAO, Q. 2017. The transcription factor Foxc1a in zebrafish directly regulates expression of nkx2.5, encoding a transcriptional regulator of cardiac progenitor cells. *J Biol Chem*.

YURUGI-KOBAYASHI, T., ITOH, H., SCHROEDER, T., NAKANO, A., NARAZAKI, G., KITA, F., YANAGI, K., HIRAOKA-KANIE, M., INOUE, E., ARA, T., NAGASAWA, T., JUST, U., NAKAO, K., NISHIKAWA, S. I. & YAMASHITA, J. K. 2006. Adrenomedullin/cyclic AMP pathway induces notch activation and differentiation of arterial endothelial cells from vascular progenitors. *Arteriosclerosis Thrombosis and Vascular Biology,* 26**,** 1977-1984.

ZERBINO, D. R., ACHUTHAN, P., AKANNI, W., AMODE, M. R., BARRELL, D., BHAI, J., BILLIS, K., CUMMINS, C., GALL, A., GIRON, C. G., GIL, L., GORDON, L., HAGGERTY, L., HASKELL, E., HOURLIER, T., IZUOGU, O. G., JANACEK, S. H., JUETTEMANN, T., TO, J. K., LAIRD, M. R., LAVIDAS, I., LIU, Z., LOVELAND, J. E., MAUREL, T., MCLAREN, W., MOORE, B., MUDGE, J., MURPHY, D. N., NEWMAN, V., NUHN, M., OGEH, D., ONG, C. K., PARKER, A., PATRICIO, M., RIAT, H. S., SCHUILENBURG, H., SHEPPARD, D., SPARROW, H., TAYLOR, K., THORMANN, A., VULLO, A., WALTS, B., ZADISSA, A., FRANKISH, A., HUNT, S. E., KOSTADIMA, M., LANGRIDGE, N., MARTIN, F. J., MUFFATO, M., PERRY, E., RUFFIER, M., STAINES, D. M., TREVANION, S. J., AKEN, B. L., CUNNINGHAM, F., YATES, A. & FLICEK, P. 2018. Ensembl 2018. *Nucleic Acids Res,* 46**,** D754-D761.

ZHANG, C., LI, Q., LIM, C. H., QIU, X. & JIANG, Y. J. 2007. The characterization of zebrafish antimorphic mib alleles reveals that Mib and Mind bomb-2 (Mib2) function redundantly. *Dev Biol,* 305**,** 14-27.

ZHANG, X. Y. & RODAWAY, A. R. F. 2007. SCL-GFP transgenic zebrafish: In vivo imaging of blood and endothelial development and identification of the initial site of definitive hematopoiesis. *Developmental Biology,* 307**,** 179-194.

ZHAO, Y., HAGUE, S., MANEK, S., ZHANG, L., BICKNELL, R. & REES, M. C. 1998. PCR display identifies tamoxifen induction of the novel angiogenic factor adrenomedullin by a non estrogenic mechanism in the human endometrium. *Oncogene,* 16**,** 409-15.

ZHONG, T. P., CHILDS, S., LEU, J. P. & FISHMAN, M. C. 2001. Gridlock signalling pathway fashions the first embryonic artery. *Nature,* 414**,** 216-20.

ZHONG, T. P., ROSENBERG, M., MOHIDEEN, M. A., WEINSTEIN, B. & FISHMAN, M. C. 2000. gridlock, an HLH gene required for assembly of the aorta in zebrafish. *Science,* 287**,** 1820-4.

ZHOU, Y. & NATHANS, J. 2014. Gpr124 controls CNS angiogenesis and blood-brain barrier integrity by promoting ligand-specific canonical wnt signaling. *Dev Cell,* 31**,** 248-56.

ZOVEIN, A. C., TURLO, K. A., PONEC, R. M., LYNCH, M. R., CHEN, K. C., HOFMANN, J. J., COX, T. C., GASSON, J. C. & IRUELA-ARISPE, M. L. 2010. Vascular remodeling of the vitelline artery initiates extravascular emergence of hematopoietic clusters. *Blood,* 116**,** 3435-44.

ZYGMUNT, T., GAY, C. M., BLONDELLE, J., SINGH, M. K., FLAHERTY, K. M., MEANS, P. C., HERWIG, L., KRUDEWIG, A., BELTING, H. G., AFFOLTER, M., EPSTEIN, J. A. & TORRES-VAZQUEZ, J. 2011. Semaphorin-PlexinD1 signaling limits angiogenic potential via the VEGF decoy receptor sFlt1. *Dev Cell,* 21**,** 301-14.